



Gene therapy approach on Charcot-Marie-Tooth type 1A rats

Hélène Hajjar

► To cite this version:

Hélène Hajjar. Gene therapy approach on Charcot-Marie-Tooth type 1A rats. Neurobiology. Université Montpellier, 2018. English. NNT : 2018MONTT027 . tel-02280148

HAL Id: tel-02280148

<https://theses.hal.science/tel-02280148>

Submitted on 6 Sep 2019

HAL is a multi-disciplinary open access archive for the deposit and dissemination of scientific research documents, whether they are published or not. The documents may come from teaching and research institutions in France or abroad, or from public or private research centers.

L'archive ouverte pluridisciplinaire **HAL**, est destinée au dépôt et à la diffusion de documents scientifiques de niveau recherche, publiés ou non, émanant des établissements d'enseignement et de recherche français ou étrangers, des laboratoires publics ou privés.

THÈSE POUR OBTENIR LE GRADE DE DOCTEUR DE L'UNIVERSITÉ DE MONTPELLIER

En Biologie Santé

École doctorale Sciences Chimiques et Biologiques pour la Santé (CBS2)

Unité de recherche INSERM U1051, Institut des Neurosciences de Montpellier (INM)

Gene therapy approach on Charcot-Marie-Tooth type 1A rats

Présentée par Helene HAJJAR

Le 05 septembre 2018

Sous la direction de Nicolas TRICAUD

Devant le jury composé de

Ana BUJ BELLO, Directrice de recherche, Genethon, France

Robert FLEDERICH, Chargé de recherche, University of Leipzig, Germany

Nathalie CARTIER, Directrice de recherche, MIRCen CEA, INSERM/CEA UMR 1169, France

Marie-Anne COLLE, Professeure, INRA UMR U703, France

Nicolas TRICAUD, Chargé de recherche, INSERM U1051, France

Rapporteuse

Rapporteur

Présidente

Examinatrice

Directeur de thèse



UNIVERSITÉ
DE MONTPELLIER

SUMMARY (FRENCH)

La myéline est une gaine formée par l'enroulement de la membrane plasmique de la cellule de Schwann autour de l'axone dans le nerf périphérique. Lorsque cette gaine est détruite, on parle de démyélinisation, cela provoque de nombreuses maladies, dont les maladies de Charcot Marie Tooth (CMT) de type 1. Les maladies CMT sont héréditaires et atteignent le système nerveux périphérique. Les symptômes communs incluent : une faiblesse musculaire, une démarche maladroite, des troubles de l'équilibre et des pieds très cambrés ou très plats. Le type le plus fréquent est la forme autosomique dominante CMT1A. Une duplication du bras court du chromosome 17 contenant le gène PMP22 (Peripheral Myelin Protein 22) induit la CMT1A. La PMP22, une petite protéine exprimée par les cellules de Schwann, est donc en excès et entraîne une démyélinisation. Il existe un modèle de rats transgéniques PMP22 (ou rats CMT1A) mimant cette pathologie humaine. Les rats CMT1A surexpriment la *pmp22* de souris de façon hétérozygote. Jusqu'à présent, aucun remède n'existe pour les maladies CMT. Un des traitements envisageables est la thérapie génique. Le but de mon projet de thèse était d'étudier la validité et l'efficacité de la thérapie génique chez les rats CMT1A. La stratégie consiste à réduire la surexpression de la protéine PMP22 chez le rat CMT1A à l'aide d'ARNsh anti-PMP22. Pour ne pas être détruits par l'organisme et maintenir une expression longue, ces ARN sh-PMP22 sont transférés chez le rat grâce à des vecteurs viraux dérivés de virus adéno-associés, ou AAV (pour adeno-associated virus). Nous avons donc injecté un des différents sérotypes d'AAV, l'AAV9 exprimant les ARN sh-PMP22 de souris ainsi que la GFP comme marqueur des cellules infectées dans les nerfs sciatiques de rats CMT1A à l'âge de 6 jours ou 7 jours. Nous avons d'abord confirmé que les virus thérapeutiques infectaient une très large proportion de cellules de Schwann dans le nerf sciatique de rat CMT1A et ensuite que l'infection de ces cellules par les virus exprimant les ARN sh-PMP22 induisait une diminution significative de l'expression de la protéine PMP22. L'analyse du phénotype moteur des rats CMT1A traités avec les AAV9 exprimant les ARN sh-PMP22 montre que les rats CMT1A traités ne développent pas la maladie observée dans les contrôles. Egalement, les rats CMT1A présentent une hypoalgésie, un phénotype qui n'apparaît pas dans les CMT1A traités avec les vecteurs thérapeutiques. Le traitement par thérapie génique

empêche la réduction de la vitesse de conduction nerveuse observé dans les rats malades. Concernant la biodistribution des virus, 2,5 mois après le traitement, en dehors des nerfs sciatiques où les virus ont été injectés, le virus était présent dans les muscles qui entourent le nerf et aussi dans quelques ganglions dorsaux. Pour la réponse immunitaire, les rats injectés, à seulement 2 exceptions près, n'ont pas développé de facteurs neutralisants anti-AAV9. Cette thérapie génique pourrait être utilisée dans les essais cliniques. Avant de passer aux études cliniques pour le traitement de la maladie CMT1A à l'aide d'AAV9 exprimant des ARN sh-PMP22 humain, la dose d'expression de ce ARN sh-PMP22 doit être très soigneusement déterminée car si la PMP22 est trop réduite, une autre maladie peut se développer, la neuropathie héréditaire avec hypersensibilité à la pression. Il est aussi important d'avoir un outil bien adapté qui permet d'évaluer l'efficacité du traitement. Aucun existant n'est assez fiable pour mesurer la myéline du nerf périphérique. Pour remédier à ce manque, nous avons testé la technique d'imagerie Coherent Anti-stokes Raman Scattering (CARS) en caractérisant avec succès les défauts de la myéline. Par conséquent, le CARS est une technique prometteuse permettant d'évaluer l'avancement des maladies de la myéline et l'efficacité de nouvelles thérapies pour les neuropathies périphériques démyélinisantes.

SUMMARY (ENGLISH)

Myelin which is synthesized by Schwann cells, covers and protects nerves. If damaged, it causes many demyelinating diseases such as the inherited peripheral nervous system disorder Charcot Marie Tooth or CMT type 1. CMT neuropathies display a large variability from one patient to another. Nevertheless, the most common symptoms include muscle weakness, an awkward way of walking (gait), equilibrium problem and highly arched or very flat feet. The most common subtype of CMT is an autosomal dominant disorder known as CMT1A. CMT1A is caused by the duplication of the *peripheral myelin protein 22 (PMP22)* gene on the short arm of chromosome 17 (17p11.2) resulting in an excess of PMP22. This leads to demyelination. PMP22 is a small protein expressed by Schwann cells. There is still no cure for CMT diseases. One approach for a treatment is gene therapy. The aim of my thesis project was to deliver proof of principle for a gene therapy approach on a CMT1A rat model characterized by extra copies of mouse *pmp22* gene (CMT1A rat). The treatment strategy consisted in reducing PMP22 overexpression in CMT1A rats with shRNA against PMP22. Viral vectors like adeno-associated virus (AAV having serotypes from 1-10) are used to deliver shRNA in vivo so that they won't be destroyed by the organism and for them to be long-lasting. Thus, we injected sciatic nerves of 6-7-day-old CMT1A rats with AAV9 expressing shRNA PMP22 with a GFP marker. We first confirmed that the virus highly transduced Schwann cells and that AAV9 shRNA PMP22 decreased PMP22 protein expression in CMT1A rats' sciatic nerves. CMT1A rats treated with AAV9 shRNA PMP22 showed that they didn't develop the motor phenotype seen in controls. Moreover, hypoalgesia observed in CMT1A rats was alleviated by treatment. In addition, gene therapy increased the reduced nerve conduction velocity found in CMT1A rats. Concerning safety, no viral off-targets were detected except in muscles close to the injection site (sciatic nerve) and in the dorsal root ganglions. Except for 2 rats, there was no immune response against AAV; no anti-AAV9 neutralizing factors. Consequently, this gene therapy could be used in clinical trials. Before moving to clinical studies, the minimal effective dosage should be very carefully defined because if PMP22 is completely deleted, another disease is caused: Hereditary Neuropathy with Pressure Palsies. It is also crucial to have a strong readout to evaluate the outcome of a treatment. However, no tool consistent enough exists for examining the peripheral nerve. Thus, we tested the label-free imaging technique Coherent Anti-stokes Raman Scattering (CARS) and successfully characterized myelination defects.

Consequently, CARS could be used as a consistent outcome measure for developing new therapies for demyelinating peripheral neuropathies.

Acknowledgements

“Nobody said it was easy. No one ever said it would be this hard”.

Those words from a Coldplay song summarize my PhD work.

After three years I spent in the myelin research team at the institute of Neurosciences of Montpellier, I finally reach the end of a journey which would not have been possible without all the people I’m going to mention and thank thereafter.

First, I am very grateful to my thesis director Dr. Nicolas Tricaud for the continuous support of my PhD research, for his big expertise and knowledge. His guidance has helped me through my research and especially through writing of this thesis.

Besides my thesis director I would like to thank the reviewers Dr. Robert Fledrich and Dr. Ana Buj Bello as well as the members of the jury Dr. Nathalie Cartier and Dr. Marie-Anne Colle for their commitment and time. I really appreciate that they agreed to read and assess my thesis work during summer holidays. I look forward for their insightful comments and for the interesting discussions I hope we are going to have during my defense so that I will widen my research perspectives.

My sincere thanks also go to my thesis supervisor Dr. Benoit Gautier for his patience particularly when I ask him tons of questions, for his continuous help in the different stages of research and writing and for teaching me the essence of research. Thank you for pushing me to do my best and test my limits.

I thank my fellow labmates and friends Scarlettte and Graham for all their help during dissections. I also thank Gerben and Mallory for being supportive when I was writing my thesis. I thank everyone in the lab for techniques and tips I learned from them. Thank you for all the laugh and fun we had in the lab and outside and for believing in me when I doubted myself.

Thanks to the members of Tricaud lab who are not part of the team anymore (Jade Berthelot, Marie Deck, Sergio Gonzalez, Eliza Gonzalez). Thanks for all your help, support and advice. It was a real pleasure working with you!

Thanks also to Dr. Jerome Devaux (who lately joined the lab) and to Dr. Florence Apparailly for being part of my thesis committee on my first and second year of thesis and for all their useful comments and suggestions.

I thank Dr. Hassan Boukhaddaoui for the collaboration in the CARS project. Working with him was incredible! It lifted up my spirit when I had some difficulties during my thesis.

I thank our collaborators in Nantes Veronique Blouin, Caroline Le Guiner, Virginie François, Oumeyya Adjali, Célia Couzinié and others in UMR 1089 INSERM for the virus production, the biodistribution test and neutralization factors assay. Also, thanks for welcoming me at UMR1089 research lab for a few days and teaching me the secrets of gene therapy related to viral vectors. Thanks to all the vivid scientific discussions we had!

I thank our collaborators in Germany Michael Sereda, Ruth Stassart and her lab for the CMT1A rat model I used for my thesis project and for teaching me electrophysiology on rats. I learned a lot even if it was during a short period of time!

I also thank Burkhard Gess and Peter Young at the University Hospital Münster, Department of Sleep Medicine and Neuromuscular Diseases, Germany for the shRNA work.

I thank our collaborators from INM team 3 Antoine Jouvenel and Cyril Rivat for the Randall Selitto test. I was lucky to learn from pain and nociception field experts!

I thank all the INM platforms for the amazing job they did for my thesis project:

- Functional analysis platform (INM, Anne-Laure Bonnefont).
- Electron Microscopy platform (INM, Chantal Cazevieille).
- Histology platform (INM, Chantal Ripoll).
- MRI platform (INM, Hassan Boukhaddaoui).

.

I specially thank the animal care facility platform with Jerome Sarniguet and his staff in particular Marie-Line, Christopher, Pascal, Flora and Laura for taking care of my rats. I spent most of my time in the animal care facility and it truly felt like home; like family! The animal care facility staff is extremely helpful!

Last but not least I would like to thank my family and friends outside the research team for always boosting me up throughout my thesis and my life in general. I wouldn't have done it without them!

Table of Contents

Summary (French)	1
Summary (English)	3
Acknowledgements	5
Abbreviations	12
Figures	15
Tables	17
Prolog	18
Introduction	20
I. The myelinated peripheral nerve	20
A. Introduction	20
B. Structure of Myelin	21
C. Molecular composition of myelin	24
D. Regulation of myelin formation	25
1. Transcription factors	25
2. Myelin proteins	26
3. Factors of signaling pathways	26
4. Adhesion proteins	29
5. Polarity proteins	29
II. Peripheral neuropathies	31
A. Acquired neuropathies	31
1. Immune-mediated peripheral neuropathies	31
2. Infectious peripheral neuropathies	31
3. Toxic peripheral neuropathies	32
4. Metabolic peripheral neuropathies	32
B. Inherited peripheral neuropathies	32
III. Charcot Marie Tooth (CMT)	33

A.	Epidemiology	33
B.	Classification	34
C.	CMT1A	35
1.	Epidemiology	35
2.	Genetics	35
3.	Clinical features	36
4.	Electrophysiology	37
5.	Morphology	37
D.	CMT1A animal models	46
1.	Rodent models	46
2.	CMT1A rat	46
E.	Peripheral Myelin Protein (PMP22)	49
1.	PMP22 generalities	49
2.	PMP22 transcript	50
3.	PMP22 protein	50
4.	PMP22 protein synthesis and transport	53
5.	PMP22 Function	53
F.	Pathomechanisms of CMT1A	55
1.	Imbalanced activity of signaling pathways	55
2.	Downregulation of cholesterol genes	55
3.	Downregulation of genes influencing the cytoskeleton and extracellular matrix	56
4.	Upregulation of Schwann cells differentiation and myelination factors	56
5.	Increase in calcium levels	56
6.	PMP22 aggregates formation	57
7.	Axonal loss	57
G.	Clinical features	58
H.	Diagnostic tools	58
1.	Family history	59
2.	Electrophysiological testing	59
3.	Molecular analyses	59
4.	Nerve biopsy	59
5.	Neuroimaging	60
I.	Outcome measures for clinical trials	62
IV.	Treatment for CMT1A	63
A.	Physical therapy and associated rehabilitative measures	63

B.	Treatment at preclinical stages	64
1.	Pharmacological treatments.....	65
2.	Gene therapy.....	67
C.	Clinical trials	68
1.	Ascorbic acid and creatine (vitamin trials).....	68
2.	PXT3003.....	69
3.	ACE-083 for CMT.....	70
4.	Gene therapy approach	70
5.	Other Ongoing clinical trials	71
V.	Gene therapy	75
A.	Types of gene therapy	75
B.	Delivery methods	76
1.	Non-viral vectors (DNA vectors)	76
2.	Viral vectors	77
C.	Safety concerns	85
D.	Clinical trials	85
1.	First trials and drawbacks	85
2.	New trials and successes.....	86
VI.	CMT1A gene therapy approach.....	91
A.	Antisense Oligonucleotides (ASO).....	91
B.	siRNA.....	91
1.	siRNA properties	92
2.	siRNA delivery	92
C.	shRNA.....	92
1.	shRNA properties	93
2.	shRNA life cycle inside of transfected cells.....	93
3.	shRNA delivery	94
D.	Clinical trials	95
1.	ASO	95
2.	siRNA	95
3.	shRNA	96
	Thesis objectives.....	98

Chapter 1 :CMT1A Gene Therapy Project

Material et Methods

I. Therapeutic tools production and validation	100
A. Recombinant AAV (rAAV) manufacturing and purification	100
1. Cell amplification, transfection, harvest and supernatant Polyethylene glycol (PEG)-precipitation	100
2. Vector purification.....	100
3. Vector titration.....	100
B. Animals	101
C. Injected viral solution.....	101
D. Injection of AAV9 CAG eGFP in rodents' sciatic nerves	103
E. Injection of AAV9 CAG eGFP in macaques' sciatic nerves	103
F. Dissections and Immunostaining of sciatic nerve	104
G. In vitro validation of shRNA PMP22.....	105
1. Reverse Transcriptase quantitative real time Polymerase Chain Reaction (RT-qPCR PMP22 mRNA).....	105
2. Western Blot.....	106
II. CMT1A rat model characterization.....	109
A. Animals	109
B. Behavioral Analysis	109
1. Rotarod	109
2. Grip test	110
3. Catwalk.....	110
C. Electrophysiology.....	111
III. Gene therapy approach in CMT1A rats.....	112
A. Animals	112
B. Injected AAV9 viral solution	114
C. Injection of AAV9 shRNA in rats' sciatic nerves (SN).....	114
D. Behavioral Analysis	114
1. Rotarod	114
2. Grip test	114
3. Randall Selitto	114
E. Electrophysiology.....	115
F. Dissections	115
G. Molecular and biochemical techniques	116
1. RT-qPCR.....	116
2. Western Blot.....	117
I. AAV9 Neutralizing factors	118

J.	AAV9 biodistribution.....	119
Results		
I.	Therapeutic tools validation.....	123
A.	Efficiency to transduce myelinating Schwann cells in vivo	123
1.	Efficiency to transduce target cells in rodents.....	123
2.	Transduction rate of myelinating Schwann cells in rodents.....	125
3.	Efficiency of transduction in macaca fascicularis	128
B.	Design, cloning and validation of shRNAs targeting mouse PMP22 mRNA.....	129
II.	CMT1A rat model characterization.....	132
A.	Motor deficits	132
B.	Clumsiness in walking	133
C.	Reduced Nerve Conduction Velocity (NCV).....	134
III.	Experimental design	136
IV.	Efficiency of AAV9 shRNA PMP22 in vivo.....	137
V.	Functional recovery of treated rats	139
A.	Gene therapy improved motor deficits in CMT1A-treated rats	139
B.	Hypoalgesia of CMT1A rats alleviated by gene therapy	140
VI.	Reduced Nerve Conduction Velocity (NCV) corrected by gene therapy.....	141
VII.	Appropriate age of correlation between behavioral analysis, electrophysiological measurements and molecular, biochemical and morphological studies	142
VIII.	Viral biodistribution	145

Discussion

Conclusion and Perspectives

Chapter 2: Label-Free non-linear microscopy Project

Introduction.....	161
Article: “Label-free non-linear microscopy to measure myelin outcome in a rodent model of Charcot-Marie-Tooth diseases”, Journal of Biophotonics	162
Conclusion and Perspectives.....	163
General Conclusion.....	164
Bibliography.....	167

Abbreviations

a.u: arbitrary units	CMTES: CMT Examination Score
AARS: AlAnyl-tRNA Synthetase	CMTNS: CMT Neuropathy Score
AAV: Adeno-Associated Virus	CMTPedS: CMT Pediatric Scale
AAV9: Adeno-Associated Virus serotype 9	CMTSS: CMT Symptom Score
ABC: Active Beta Catenin	CMV: CytoMegaloVirus
AD: Autosomal Dominant	CNS: Central Nervous System
AdV: AdenoVirus	CNTF: Ciliary Neurotrophic Factor
AFO: Ankle-Foot Orthoses	CPV: Center for Production of Vector
Ago2: Argonaute protein 2	CREB: Circular adenosine monophosphate
AIFM1: Apoptosis-Inducing Factor	Response Element Binding
Mitochondrion associated 1	CsCl: Cesium Chloride
Akt: serine-threonine Kinase or protein	CSF: CerebroSpinal Fluid
Kinase B, murine thymoma viral oncogene	Ct: Cycle threshold
homolog 1	CTDP1: CTD Phosphatase subunit 1
AR: Autosomal Recessive	CTSA: CaThepSin A
ARSA: ARylSulfatase A	Cx32: Connexin 32
ASO: AntiSense Oligonucleotides	dHMN: distal Hereditary Motor
ASPA: ASParToAcylose	Neuropathies
ATTR: hereditary TransThyRetin-mediated	DHTKD1: DeHydrogenase E1 and
Amyloidosis	TransKetolase Domain-containing 1
BACE1: Beta secretase beta site Amyloid	DI: Dominant Intermediate
precursor protein Cleaving Enzyme 1	DMEM: Dulbecco's Modified Eagle Medium
BBB: Blood Brain Barrier	DNM2: DyNaMin 2
BCA: Bicinchoninic Acid	DPBS: Dulbecco's Phosphate-Buffered
BCL: BaCLofen	Saline
bp: base pairs	DRG L4 and L5: Lumbar Dorsal Root
BSCL2: Berardinelli-Seip Congenital	Ganglion 4 and 5
Lipodystrophy type 2	DRG: Dorsal Root Ganglion
cAMP: circular Adenosine Monophosphate	DSD: Dejerine-Sottas Disease
CaPO4: Calcium orthophosphate	DSS: Dejerine Sottas Syndrome
CARS: Coherent Anti-Stokes Raman	DTI: Diffusion Tensor imaging
Scattering	DYNC1H1: DYnein Cytoplasmic 1 Heavy
CDA: Cytidine DeAminase	chain 1
cDNA: complementary DeoxyriboNucleic	EGF: Epidermal Growth Factor
Acid	EGR2: Early Growth Response 2; Krox20
CHN: Congenital Hypomyelinating	ENPP1:Ecto-Nucleotide
Neuropathy	Pyrophosphatase/Phosphodiesterase 1
CIDP: Chronic Inflammatory Demyelinating	FAK: Focal Adhesion Kinase
Polyneuropathy	FBLN5: FiBuLiN 5
CMAP: Compound Motor Action Potential	FBS: Fetal Bovine Serum
CMT: Charcot Marie Tooth	GAN: Giant Axonal Neuropathy
CMT1A: Charcot Marie Tooth type 1A	GARS: Glycyl-tRNA Synthetase

GDAP1: Ganglioside-induced Differentiation-Associated Protein
 GJB1: Gap-Junction protein Beta-1
 Gpr: G-protein coupled receptor
 GSTT2: Glutathione S-Transferase Theta-2
 HARS: Histidyl-tRNA Synthetase
 HDACs: Histone DeAcetylases
 HEK: Human Embryonic Kidney
 HK1: HexoKinase 1
 HMSN: Hereditary Motor And Sensory Neuropathy
 HNPP: Hereditary Neuropathy with liability to Pressure Palsies
 HSN or HSAN: Hereditary Sensory/ Autonomic Neuropathies
 HSPB: Heat Shock Protein B
 HSV: Herpes Simplex Virus
 ILK: Integrin-Linked Kinase
 INF2: INverted Formin 2
 ITRs: Inverted Terminal Repeats
 KIF1B: KInesin Family Member 1B
 LAMP1: Lysosome-Associated Membrane Protein 1
 LC3: microtubule-associated protein Light Chain 3
 LF: Left Front
 LH: Left Hind
 LINCL: Late Infantile Neuronal Ceroid Lipofuscinosis
 LITAF: Lipopolysaccharide-Induced Tumor necrosis Factor
 LMNA: LaMiN A/C
 LOD: Limit Of Detection
 LOQ: Limit Of Quantification
 LPLP(D): Lipoprotein Lipase (Deficiency)
 LRSAM1: Leucine-rich Repeats and Sterile Alpha Motif-containing 1
 LSD: Lysosomal Storage Disease
 LTC: Long Term Cohort
 MAG: Myelin-Associated Glycoprotein
 MAPK: Mitogen-Activated Protein Kinase
 MARS: Methionyl-tRNA Synthetase
 MBP: Myelin Basic Protein
 mcDNA: minicircle DNA
 MED25: MEDitor complex subunit 25

Mek-Erk: Mitogen activated protein kinase kinase 1 (Mek) – Extracellular signal-regulated kinase (Erk)
 MFN2: MitoFusiN2
 MLD: Metachromatic LeukoDystrophy
 MPS: MucoPolySaccharidosis
 MPZ : Myelin Protein Zero (P0)
 MRI: Magnetic Resonance Imaging
 MRN: Magnetic Resonance Neurography
 mRNA: messenger RNA
 MT-ATP6: ATP6 subunit of the Mitochondrial Adenosine Triphosphate synthase
 MTMR: MyoTubularin-Related protein
 NAA: N-Acetyl Aspartate
 NAGLU: N-AcetylGLUcosaminidase
 NAION: Non Arteritic Anterior Ischemic Optic Neuropathy
 NCV: Nerve Conduction Velocity
 NDRG1: N-myc Downstream-Regulated Gene 1 protein
 NEFL: NEuroFilament Light chain
 NF: Neutralizing Factors
 NGF: Nerve Growth Factor
 Nmnat1: nicotinamide mononucleotide adenylyl transferase 1
 NRGs: NeuReGulins
 NT-3: NeuroTrophin-3
 NTX: NalTreXone
 P: Postnatal day
 P0: Protein zero
 P2: Protein 2
 PACT: RNA-dependent Protein kinase (PKR) ACTivating protein
 Pals1: Protein associated with lin seven 1
 p-bodies: processing bodies
 PBS: Phosphate Buffer Saline
 PDK3: Pyruvate Dehydrogenase Kinase isoenzyme 3
 pDNA: plasmid DeoxyRiboNucleic Acid
 PEG: PolyEthylene Glycol
 Pen/Strep: Penicillin/Streptomycin
 PFA: ParaFormAldehyde
 PI3K: Phosphatidylinositol-4,5-bisphosphate 3-Kinase
 PMP22: Peripheral Myelin Protein 22

PNS: Peripheral Nervous System
 PolyA : PolyAdenylation
 POU3F1: POU domain class 3 transcription Factor 1; Oct6
 PPARG: Peroxisome Proliferator-Activated Receptor Gamma
 PRPS1: PhosphoRibosyl Pyrophosphate Synthetase 1
 PRX: PeRiaXin
 PTEN: Phosphatase and tensin homolog deleted on chromosome 10
 RT qPCR: Reverse Transcriptase quantitative Polymerase Chain Reaction
 r CMTNS: Rasch analysis-based weighted CMT Neuropathy Score
 rAAV: recombinant AAV
 RAB7: RAS-Associated protein raB7
 RF: Right Front
 RH: Right Hind
 RISC: RNA-Induced Silencing Complex
 RLC: RISC Loading Complex
 r-metHuNT-3: recombinant methionyl Human NT-3
 RNAi: RNA interference
 RQ: Relative Quantities
 RT: Room Temperature
 SBF1: Set Binding Factor
 sc: self-complementary
 SCID-X1: X-linked Severe combined Immunodeficiency type 1
 SCoRe: Spectral Confocal Reflectance microscopy
 scr.sh: scramble shRNA
 SCs: Schwann Cells
 SDS: Sodium Dodecyl Sulfate solution
 SGSH: SulfoGlycosamine SulfoHydrolase
 SH3TC2: SH3 domain and TetratriCopeptides repeats 2

SHG: Second Harmonic Generation
 THG: Third Harmonic Generation
 sh49: shRNA PMP22-49
 sh50: shRNA PMP22-50
 shRNA: short hairpin RiboNucleic Acid
 shRNA: short hairpin RNA
 siRNA: small interfering RNA
 SMA: Spinal Muscular Atrophy
 SMN1: Survival Motor Neuron 1
 SN: Sciatic Nerve
 SOX-10 or 2: SRY (Sex determining Region of Y-Chromosome)-related HMG (Hydroxy Methyl Glutaryl)-bOX-10 or 2
 SRB: D-SoRBitol
 SREB: Sterol Regulatory Element Binding
 STC: Short Term Cohort
 SUMF1: Sulfatase Modifying Factor 1
 SURF1: SURFeit 1
 TACE: alpha secretases Tumor necrosis factor- Alpha Converting Enzyme
 TBS: Tris-Buffered Saline
 TFG: Trk-Fused Gene
 TPP: TriPeptidyl Peptidase
 TRBP: Tat-RNA-Binding Protein
 TrJ: Trembler J
 TRPV4: Transient Receptor Potential cation channel subfamily V member 4
 TTR: TransThyRetin
 UFUS: UltraFast US
 US: UltraSound
 vg: vector genome
 Wlds: Wallerian degeneration slow
 WT: Wild-Type
 YAP: Yes-Associated Protein
 YARS: tYrosyl tRNA Synthetase
 YY1: Ying Yang

Figures

Figure 1 : Peripheral nerve.....	21
Figure 2 : Structure of a myelinated axon	22
Figure 3 : Myelin sheath formation	22
Figure 4 : Compact and uncompacted myelin	23
Figure 5 : Propagation of Action Potentials.....	23
Figure 6 : Myelin junctions.....	24
Figure 7 : Neuregulin 1 (NRG1) isoforms	28
Figure 8 : Signs and symptoms of CMT	38
Figure 9 : PMP22 molecular structure	51
Figure 10 : AFO (Ankle Foot Orthoses).....	64
Figure 11 : AAV infection cycle.....	80
Figure 12 : shRNA life cycle	94
Figure 13 : Summary of tests used.....	98
Figure 14 : AAV CAG GFP cassette	101
Figure 15 : AAV injection in sciatic nerve of macaca fascicularis.....	104
Figure 16 : shRNA	108
Figure 17 : Summary of experimental design.....	113
Figure 18 : Injection procedure in the sciatic nerve of an adult rat	124
Figure 19 : Teasing results of rats and mice injected with AAV9 or 10.	125
Figure 20 : Transduction of myelinating Schwann cells in the sciatic nerve of rats and mice....	127
Figure 21 : Transduction of myelinating Schwann cells in the sciatic nerve of macaques.....	129
Figure 22 : Downregulation of PMP22 by shRNA <i>in vitro</i>	131
Figure 23 : Motor impairments in CMT1A rats.....	133
Figure 24 : Locomotion problems in CMT1A rats.....	134
Figure 25 : Decreased NCV in CMT1A rats.	135
Figure 26 : Summary of experimental design.	137
Figure 27 : Downregulation of PMP22 by AAV9 shRNA in sciatic nerves of rats	138
Figure 28 : Improvement of motor phenotype in treated rats	140
Figure 29 : No more hypoalgesia in treated rats.	141

Figure 30 : Increased of NCV in treated rats.	142
Figure 31 : Comparison between 2 cohorts	143
Figure 32 : AAV9 biodistribution.....	146
Figure 33 : No weight loss observed following injections.....	149
Figure 34 : Action potentials in myelinated versus demyelinated axons.....	153
Figure 35 : Anatomy of a peripheral nerve	154

Tables

Table 1 : CMT types, mode of inheritance and characteristics	39
Table 2 : CMT1A murine models	47
Table 3 : Distribution of PMP22 postnatally/young adults	52
Table 4 : Treatment options for CMT1A. References cited in the text above.	72
Table 5 : Viral vectors characteristics	84
Table 6: Gene silencing tools.....	97
Table 7 : Injection parameters for transduction efficiency: vg=vector genome	102
Table 8 : PCR conditions for in vitro validation of shRNA PMP22.....	106
Table 9 : PCR conditions for in vivo validation of shRNA PMP22	117
Table 10: Summary of behavioral tests.....	121
Table 11: Summary of electrophysiological measurements, molecular and biochemical analysis.....	122
Table 12: Neutralising factors against AAV9.....	144

Prolog

Myelin, a tissue mainly made of lipids and proteins, covers and protects nerves. It increases nerve conduction velocity. If damaged, it causes many neuropathies such as the inherited peripheral nervous system disorder Charcot Marie Tooth or CMT. These diseases have been named after the three physicians Jean-Martin Charcot, Pierre Marie and Howard Henry Tooth who first identified it in 1886. CMT diseases affect 1 in 2 500 people worldwide. They usually start in the first two decades of life.

CMT diseases display a large variability from one patient to another even from one twin brother to another. Nevertheless, the most common symptoms include muscle weakness in the feet, ankles, legs and hands, an awkward way of walking (gait), highly arched or very flat feet and numbness in the feet, arms and hands. In severe cases, patients use a wheelchair. CMT diseases are caused by more than 90 gene mutations. However, the most common subtype of CMT is an autosomal dominant disorder known as CMT1A. This neuropathy is caused by the duplication of the *peripheral myelin protein 22 (PMP22)* gene on the short arm of chromosome 17 (17p11.2) resulting in an excess of PMP22. PMP22 is a membrane protein of myelin in the peripheral nervous system. Its overexpression leads to demyelination. The exact mechanisms are not yet fully known.

There is still no cure for CMT diseases. One approach for a treatment is gene therapy. The aim of my thesis project was to deliver proof of principle for a gene therapy approach on a CMT1A rat model characterized by extra copies of mouse *pmp22* gene. The treatment strategy, designed by Dr. Benoit Gautier (my thesis supervisor) and Dr. Nicolas Tricaud (my thesis director), consisted in injecting Adeno-Associated Virus serotype 9 (AAV9) viral vectors expressing short hairpin ribonucleic acid (shRNA) against mouse PMP22 in the sciatic nerves of transgenic rats in order to reduce PMP22 overexpression and hence prevents the disease.

In this thesis manuscript I will first introduce the myelinated fiber of the peripheral nervous system, then the CMT diseases and in particular CMT1A and the problems generated by PMP22 protein overexpression. I will introduce the different animal models for CMT1A and the therapy approaches that have been tested in preclinical and clinical assays. Then I will introduce the gene

therapy approach, the shRNA tools we proposed to use and the different gene therapies that are clinically developed at the moment.

In the material and methods chapter, I will first develop the techniques used for the gene therapy approach. Then I will describe all the tests and measurements used to assess the effectiveness of the gene therapy. After that, in the results section, I will present our data showing a high transduction rate of the viral vector, downregulation of PMP22 and an almost full recovery of treated rats. Finally, I will discuss the results obtained in terms of possible translation to clinical trials.

Before moving to clinical trials, as there is not any reliable enough tool for examining the peripheral nerve, it is important to find a strong readout to evaluate the outcome of a treatment. Non-linear, label free microscopy seems very promising. This is why at the end of this thesis manuscript I will present another project I have done in collaboration with Hassan Boukhaddaoui, the responsible of the Resource Imaging Platform (RIO) of Montpellier (MRI platform) at the Institute for Neurosciences of Montpellier (INM). In this project, we used label-free non-invasive imaging techniques to study the myelin sheath in the sciatic nerve of rodents.

Introduction

I. The myelinated peripheral nerve

A. Introduction

Charcot- Marie-Tooth type 1A (CMT1A) affects the peripheral nervous system (PNS), in particular myelin. The key roles of myelin are to promote rapid conduction of nerve impulses and to nurture axons through metabolic and neurotrophic support. Myelin wraps around many axons (***Figure 1***) but not all (Lemke, 1988; Ozcelik et al., 2010; Taveggia, Feltri, & Wrabetz, 2010). Indeed, axons can be either myelinated or unmyelinated. In the peripheral nervous system, the fibers are divided into three groups: A, B and C. Group A includes the myelinated motor fibers which are the largest fibers with the fastest conduction. Group B encloses the myelinated pre-ganglionic fibers of the autonomic nervous system (part of the nervous system regulating involuntary processes like breathing and heart rate <https://www.ncbi.nlm.nih.gov/pubmedhealth/PMHT0025455>). Group C contains the unmyelinated and the post-ganglionic autonomic fibers which are the smallest-diameter, slowest-conducting fibers (Chapman & Hall, 1976). In the PNS, Schwann cells (SCs) produce myelin (Chapman & Hall, 1976; Lemke, 1988; Taveggia et al., 2010).

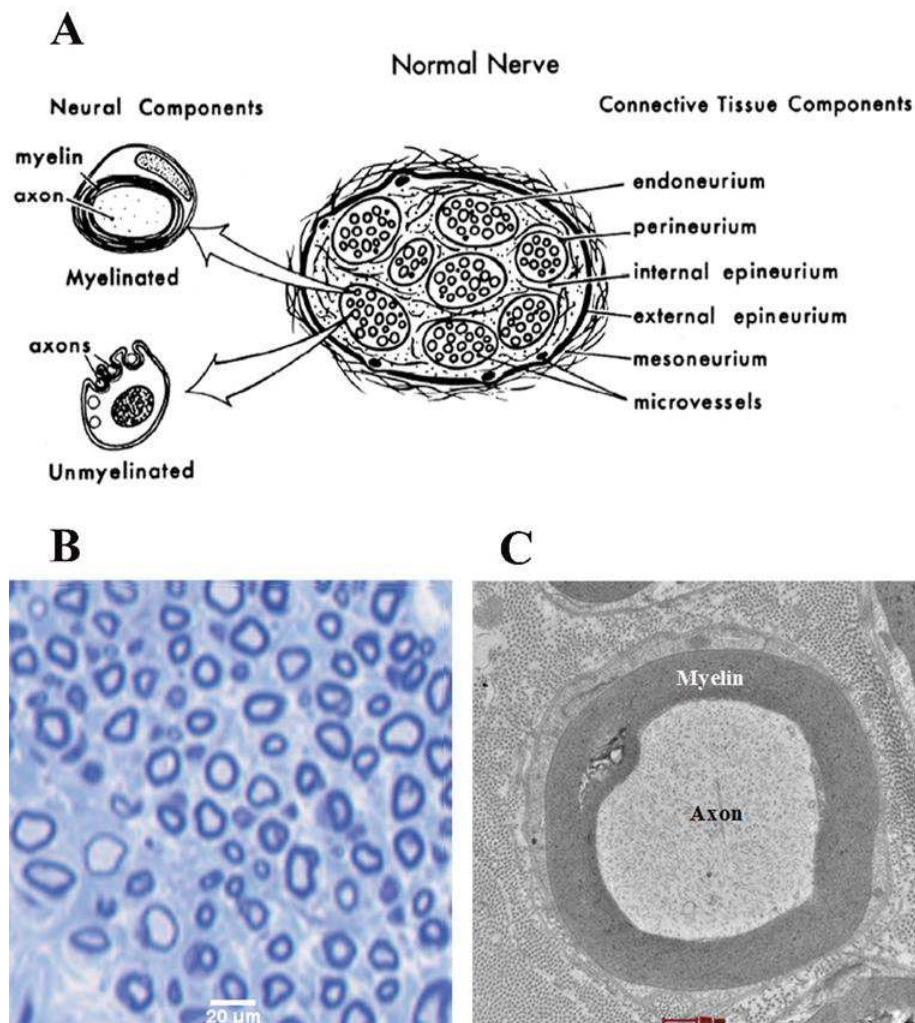


Figure 1: Peripheral nerve: *A: Diagram of nerve's composition. Adapted from nerve.wustl.edu/nd_compression.php. B: Semi-thin section of a 2.5 month-old-rat sciatic nerve stained with Toluidine Blue. Thickly and thinly myelinated fibers are clearly seen with pale areas in the background representing the unmyelinated fibers. Scale bar=20 μ m. C: High power view of a myelinated axon: Myelin wraps around nerve fiber. Electron microscopy ultra-thin section of a 6-month-old rat sciatic nerve. Scale bar= 50nm.*

B. Structure of Myelin

Sheaths enveloping nerve fibers were first seen by Virchow as early as 1854 and were named myelin (Raine, 1977; Snipes & Suter, 1995). Myelin is constituted of several discrete units each separated by a small gap free of myelin. This gap is called Node of Ranvier and the units are named internodal segments (**Figure 2**). Thus, the myelin sheath is not continuous along the axon.

Those internodal segments are each synthesized by a single SC in the PNS (Peters & PALAY SL, 1991; Snipes & Suter, 1995; THOMAS PK, BERTHOLD C-H, 1993).

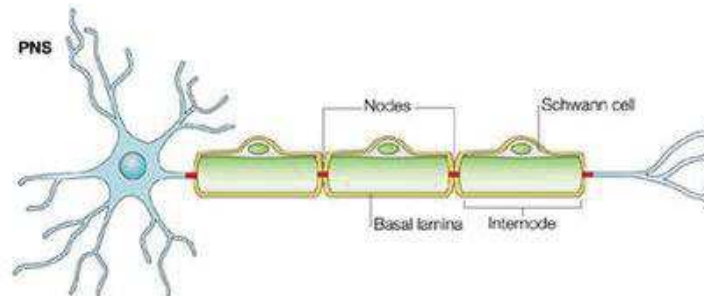


Figure 2 : Structure of a myelinated axon: In the peripheral nervous system (PNS), Schwann cells wrap their membrane many times around the axon creating the myelin sheath. Internodes are spaces in the axon covered by myelin whereas nodes of Ranvier (Nodes in figure) are small gaps free of myelin. Adapted by permission from Springer Nature: Nature Reviews Neuroscience, The local differentiation of myelinated axons at nodes of Ranvier, Poliak and Peles, 2003.

The myelin sheath is formed by successive turns of the Schwann cell plasma membrane that spiral around the axon. The wrappings are then compacted by the exclusion of the cytoplasm and the tight interaction of the membranes in order to make the ‘compact’ myelin (Ghabriel & Allt, 1981; Snipes & Suter, 1995; Tricaud, 2005) (**Figure 3**).

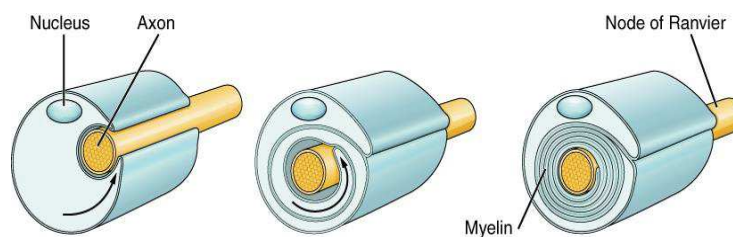


Figure 3 : Myelin sheath formation: A Schwann cell wraps around the axon forming myelin sheath. Adapted from biology dictionary.

Compact myelin is responsible for the electrical insulation of the axon. An ‘uncompacted’ myelin is also generated during myelination. This uncompacted myelin is critical to form and maintain the compact myelin and to nurture axons. It is distributed semiregularly along the myelin sheath generating distinct domains inside the myelinating Schwann cell. Those domains are called Schmidt-Lanterman incisures and paranodal loops (Ghabriel & Allt, 1981; Snipes & Suter, 1995; Tricaud, 2005). Schmidt-Lanterman incisures are crucial in maintaining the myelin sheath

metabolically and in longitudinally extending the sheath (Arroyo & Scherer, 2000; Ghabriel & Allt, 1981; Tricaud, 2005). Those incisures comprise adherens junctions that are mostly composed of E-cadherin (Fannon et al., 1995; Ghabriel & Allt, 1981; Tricaud, 2005). The paranodal loops are located next to the nodes of Ranvier. They constitute the extremities of each turn of compact myelin (Meyer-Franke & Barres, 1994; Snipes & Suter, 1995; Trapp, 1990)(**Figure 4**).

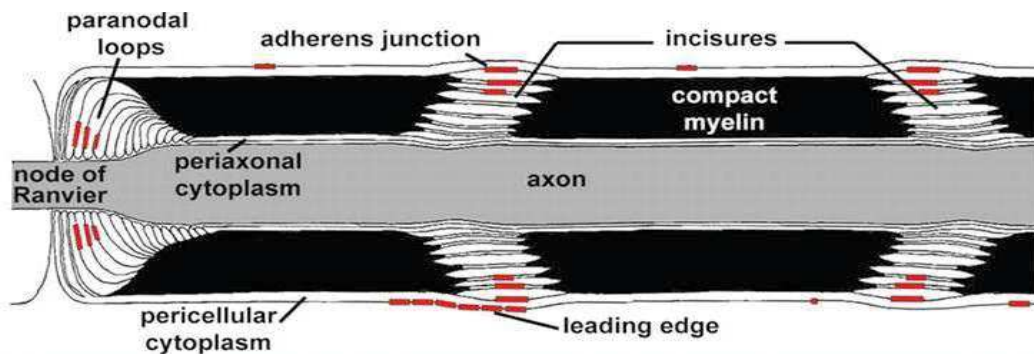


Figure 4: Compact and uncompact myelin: Schematic of a longitudinal view of a myelinated axon depicting the several compartments around the node of Ranvier. Schmidt-Lanterman incisures (incisures in figure) enclose adherens junctions. Adapted from Tricaud et al., 2005.

On the axon the node and paranodes are both actively involved in propagating action potentials along nerve (Sun et al., 2016) (**Figure 5**).

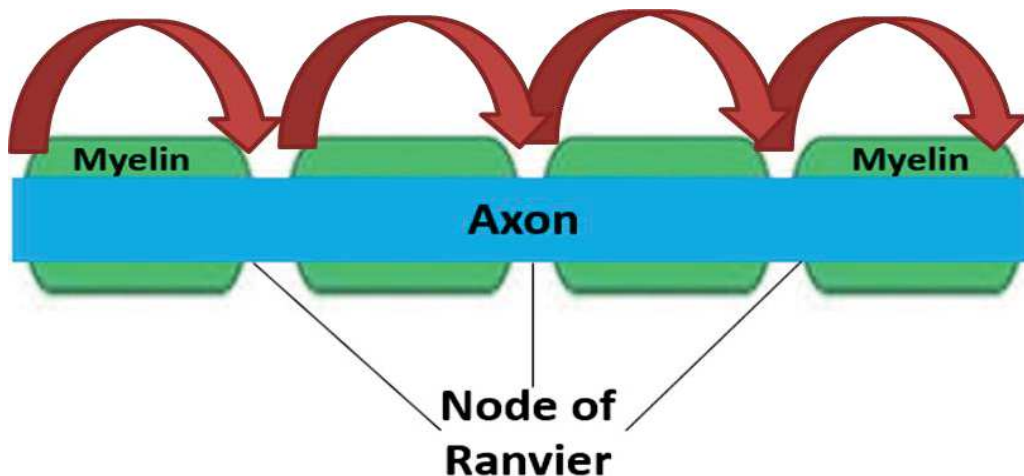


Figure 5: Propagation of Action Potentials: In a myelinated fiber, action potentials (yellow arrows) jump from one Node of Ranvier to the next one. This is known as “Saltatory conduction”.

The structure of a myelinated Schwann cell is complex and well organized. Many junctional complexes such as desmosome-like structures and tight junctions are found inside the

same myelinating Schwann cell (autotypic junctions) between the terminal myelin loops in the paranodal region, at the lateral margins of the Schmidt-Lanterman incisures or in compact myelin (Ghabriel & Allt, 1981; Shinowara, Beutel, & Revel, 1980; Snipes & Suter, 1995). Additionally, intercellular junctions are present between the axon and the paranodal loops, termed axo-glial junctions (**Figure 6**) (Snipes & Suter, 1995; Wiley & Ellisman, 1980).

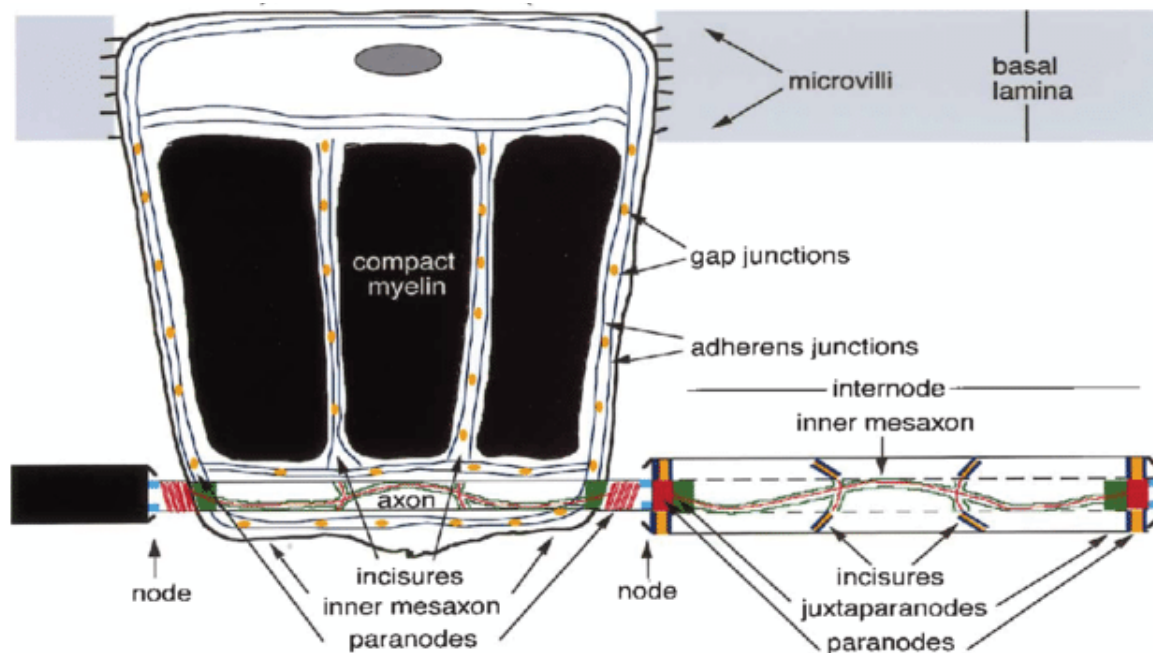


Figure 6 : Myelin junctions: Schematic view of an unrolled Schwann cell showing adherens junctions (2 continuous line) surrounding compact myelin with gap junctions (orange ovals) between their rows. In addition, adherens junctions are found in incisures. Nodes (blue), paranodes (red) and juxtaparanodes (green) are axonal membrane regions. Adapted from Arroyo et al., 1999.

C. Molecular composition of myelin

Myelin is essentially composed of lipids (70-80% of dry weight), water and proteins (Quarles, Macklin, & Morell, 2006; Snipes & Suter, 1995; Suter & Snipes, 1995). Lipids are mainly cholesterol, cerebroside, sulphatide, phosphatidylethanolamines, phosphatidylcholines, phosphatidylserines, spingomyelins, and phosphatidylinositols (Inouye & Kirschner, 1988; Snipes & Suter, 1995). Contrarily to lipids, some PNS myelin proteins such as protein zero (P0 or MPZ), P2 (protein 2), peripheral myelin protein 22 (PMP22), myelin basic protein (MBP), myelin-associated glycoprotein (MAG) and connexin 32 (Cx32) are myelin-specific (Snipes & Suter, 1995). Mutations in genes of those myelin proteins have been associated with many inherited

peripheral neuropathies. For example, *PMP22* gene duplication causes CMT1A (Lupski et al., 1991; Snipes & Suter, 1995; Suter et al., 1992). P0, PMP22, P2 and MBP are distributed in compact myelin while MAG and Cx32 are present in uncompact myelin (Snipes & Suter, 1995).

D. Regulation of myelin formation

The development and the maintenance of the myelin sheath is possible through several types of molecules that promote or inhibit myelination (Taveggia et al., 2010). These molecules include transcription factors and co-factors, myelin proteins, factors of signaling pathways, adhesion proteins and polarity proteins (Arnaud et al., 2009; Fernando et al., 2016; Fields & Stevens, 2000; Hu et al., 2008a; Jacob et al., 2011; Ozcelik et al., 2010; J. A. Pereira et al., 2009; Perrin-Tricaud, Rutishauser, & Tricaud, 2007; Svaren & Meijer, 2008; Taveggia et al., 2010; Tricaud, 2005; Vijay, Chiu, Dacks, & Roberts, 2016; von Boxberg et al., 2014; Willem et al., 2006). I have chosen only a few, mostly the ones that have been studied in our laboratory.

1. Transcription factors

Transcription factors of SCs capable of enhancing myelination include POU3F1 (POU domain class 3 transcription factor 1; Oct6), EGR2 (early growth response protein 2; Krox20) and SOX-10 (Svaren & Meijer, 2008). Dedifferentiation factors such as SOX2 and Notch inhibit EGR2 facilitating myelin regeneration after nerve injury (Mager et al., 2008; Parkinson et al., 2008; Taveggia et al., 2010; Woodhoo et al., 2009).

Other transcription factors comprise Histone deacetylases (HDACs), HDAC1 and HDAC2. Both are chromatin-remodeling proteins and major epigenetic regulators. They promote SC myelination as well as survival in the PNS. While HDAC1 and HDAC2 compensate for each other, they have distinctive functions. HDAC1 decreases active beta catenin (ABC) thus controlling SC survival whereas HDAC2 interacts with Sox10 in order to induce the transcriptional program of myelination (Jacob et al., 2011).

YAP (Yes-Associated protein) is a transcription co-factor involved in myelination, myelin elongation and myelin regeneration (Deng et al., 2017; Fernando et al., 2016; Grove et al., 2017; Poitelon et al., 2016). Extending the myelin sheath is crucial for the conduction of nerve impulses.

Charcot Marie Tooth 4F is an example of a peripheral neurological disorder in which myelin internodal length is decreased (Fernando et al., 2016; Sherman & Brophy, 2018). YAP promotes myelin sheath internodal extension during nerve elongation due to postnatal body growth. YAP regulates myelin sheath elongation by stimulating some myelin gene promoters such as *Egr2* and inhibiting others like P0. The process of myelin sheath extension is carefully controlled in SC as the cell polarity factor Crb3 prevents myelin sheath over elongation through the HIPPO pathway that inhibits YAP activity (Fernando et al., 2016).

2. *Myelin proteins*

P0 and MBP mediate myelin wrapping and compaction whereas MAG mediates the axon interaction with SC (Garbay, Heape, Sargueil, & Cassagne, 2000; Lemke, 1988; Snipes & Suter, 1995). P0 interacts with other similar P0 molecules of the SC plasma membrane to form and maintain the compact myelin sheath (Lemke, 1988; Snipes & Suter, 1995). MBP is a strongly basic protein that plays a role in the synthesis of compact myelin by electrostatic interactions with the membrane's acidic lipids (Garbay et al., 2000). So, they both stably keep the close apposition of lipid bilayers for maintaining a very tight compaction of myelin (Garbay et al., 2000; Han, Myllykoski, Ruskamo, Wang, & Kursula, 2013).

MAG connects with specific gangliosides on the axonal membrane. Those gangliosides are involved in the adhesion of myelinating SC to the axon. Hence, MAG initiates and maintains the structural integrity of the myelin sheath (Garbay et al., 2000).

3. *Factors of signaling pathways*

a) Neuregulins (NRGs)

Neuregulins (NRGs) are a family of growth and differentiation factors encoded by 4 genes. They display in their receptor-interacting sequence a homology with the epidermal growth factor (EGF) receptor. Many distinct NRG isoforms have been identified (Birchmeier & Nave, 2008; Gambarotta, Fregnan, Gnani, & Perroteau, 2013; Gambarotta, Ronchi, Geuna, & Perroteau, 2014). The best-studied member and the prototype of the family is NRG1, which represents one of the largest mammalian genes. NRG1 elicits the activation of signal cascades downstream of the ErbB receptors, such as the activation of ras/ Mitogen-activated protein kinase (MAP) kinase, phosphatidylinositol 4,5-bisphosphate 3 (PI3) kinase/Akt, or focal adhesion kinase (FAK). Those

diverse signal transduction pathways are responsible for the transcription of genes involved in myelination as well as survival, migration, differentiation and proliferation of Schwann cells (Birchmeier & Nave, 2008; Fricker & Bennett, 2011; Gambarotta et al., 2013; Ma et al., 2011). NRG1 isoforms are categorized on the base of their N-terminus and C-terminus domains into many sub-types (Falls, 2003; Mei & Xiong Wen-Cheng, 2008) (**Figure 7.A**).

NRG1 types I, II and III can be cut by the β -secretase β -site amyloid precursor protein cleaving enzyme 1 (BACE1) or by α secretases tumor necrosis factor- α -converting enzyme (TACE) (Gambarotta et al., 2013) (**Figure 7.B**). This proteolysis process is critical to activate NRG1 as BACE1 promotes myelination and remyelination (Hu et al., 2008b; Taveggia et al., 2010; Willem et al., 2006). On the other hand, TACE cleavage impacts negatively on myelination (Marca et al., 2011) (**Figure 7.C**). NRG1 Type I and II are expressed by Schwann cells while type III is expressed by axons (Gambarotta et al., 2014). After cleavage, NRG1 types I and II are released in the extracellular domain and function in a paracrine manner (soluble NRG1) whereas type III stays linked to membrane and undergoes juxtacrine signaling from axons to Schwann cells (Falls, 2003; Gambarotta et al., 2013; Syed & Kim, 2010). NRG1 type I expressed by Schwann cells is dispensable for myelination or myelin maintenance but is critical for nerve regeneration after injury (Stassart et al., 2013). NRG1 type III plays an important role in promoting myelination by SCs (Cotter et al., 2010; Taveggia et al., 2010), in particular in determining how thick the myelin sheath becomes (Birchmeier & Nave, 2008; Gambarotta et al., 2013; Taveggia et al., 2010). Reduced NRG1 type III expression causes hypomyelination (Taveggia et al., 2005; Michailov et al., 2004) while its overexpression increased myelin thickness thus causing hypermyelination (Birchmeier & Nave, 2008; Gambarotta et al., 2013; Michailov et al., 2004).

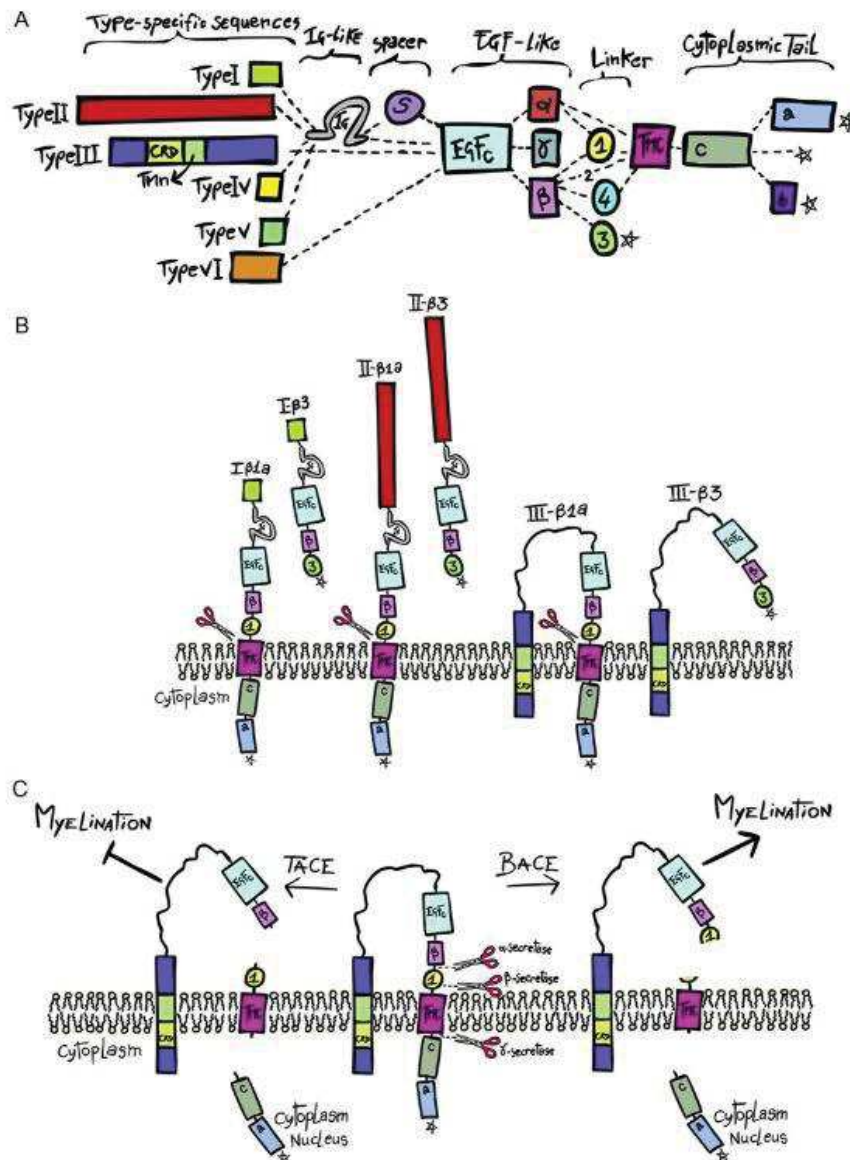


Figure 7 : Neuregulin 1 (NRG1) isoforms: A: 6 isoforms (types I-VI) different in their N-terminal. Ig=Immunoglobulin; CRD=cystein-rich domain; TMn= transmembrane domain; EGF= epidermal growth factor; TMC=transmembrane domain. NRG1 cleavage (B) and effect on myelination (C): BACE has positive effect while TACE has a negative effect. Adapted from Gambarotta et al., 2013

b) Akt

The serine-threonine kinase Akt, or protein kinase B, a downstream effector of the PI3K pathway, is activated by axonal NRG1 type III in myelinating Schwann cells. Akt is involved in increasing myelin protein expression, in promoting myelin sheath formation during regeneration

and in regulating myelin sheath thickness (Cotter et al., 2010; Nave & Salzer, 2006). PI3K-Akt pathway also induces differentiation of SCs most probably from the immature to the promyelinating stage (He et al., 2011; W. Wu, Liu, Liu, Yu, & Wang, 2016; Yamazaki et al., 2009)(Wu et al., 2016, He et al., 2011; Yamazaki et al., 2009).

c) ILK

Integrin-linked kinase (ILK), a 52 kDa protein located in focal adhesion points, stimulates the growth of Schwann cell processes which completely encircle axon and start the segregation of single axons by Schwann cells. Additionally, it plays a crucial role in axonal remyelination most probably through activating Akt that is essential for SC myelination (J. A. Pereira et al., 2009).

4. ***Adhesion proteins***

a) AHNAK

Prerequisites for the myelination process in the PNS include intricate contact of SCs with laminin-containing basement membrane (Cornbrooks, Carey, McDonaldt, Timpl, & Bunge, 1983; McKee et al., 2012). AHNAK, a SC giant scaffold protein (700kDa), impacts the length of myelin segments in vivo (reduced internodal length) through interactions with the transmembrane form of the laminin receptor dystroglycan on Schwann cells (von Boxberg et al., 2014).

b) E-cadherin

E-cadherin constituting the core of SC adherens junction in the uncompacted myelin sheath (Fannon et al., 1995; Tricaud, 2005) is crucial for maintaining Schmidt–Lanterman incisures through recruiting p120 catenin to its juxtamembrane domain (Perrin-Tricaud et al., 2007; Tricaud, 2005). Low levels of p120 catenin inhibit the formation of Schmidt–Lanterman incisures and lead to an important decrease in myelin sheath thickness (Perrin-Tricaud et al., 2007).

5. ***Polarity proteins***

a) Pals1

Protein Associated with Lin Seven 1 (pals1), a cell polarity protein involved in the epithelial cell polarization and in particular in the formation of the apical domain. In myelinating Schwann cells Pals1 is necessary for the distribution of myelin proteins PMP22 and MAG along the plasma membrane. It also plays an important role in the radial and longitudinal growth of the

myelin sheath as Pals-1 silenced cells display a thinner myelin sheath with fewer turns around the axon (Ozcelik et al., 2010).

b) Inhibitors of myelination

PTEN (phosphatase and tensin homolog deleted on chromosome 10) is an inhibitor of Akt pathway, which is critical for myelination. In Schwann cells, PTEN interacts with mammalian disks large homolog 1 (Dlg1), a cell polarity factor involved in the formation of the baso-lateral domain of epithelial cells. Silencing Dlg1 in Schwann cells of mice showed decreased levels of PTEN and Akt hyperactivation. This lead to radial hypermyelination of myelinating Schwann cells. Consequently, Dlg1 role is to negatively regulate myelination and to limit myelin sheath thickness. Interestingly, Dlg1 appears to affect the thickness but not the length of myelin sheath (Cotter et al., 2010).

On the opposite, Crb3, a cell polarity protein involved in the formation of the apical domain of epithelial cells, inhibits myelin sheath elongation without significantly affecting myelin thickness. Crb3 stimulates the HIPPO pathway to phosphorylate and thus inactivate YAP and stop myelination (Fernando et al., 2016).

II. Peripheral neuropathies

Peripheral neuropathies are diseases of the peripheral nervous system. They can affect either the myelin sheath or the peripheral axons. They are subdivided into two main categories, acquired and inherited diseases, depending of the origin of the disease. Since acquired neuropathies have a large number of causes, I will briefly present the most important ones in term of patients: immune-mediated, infectious, toxic and metabolic. I will then focus on inherited diseases, which are mostly known as CMT diseases and in particular on CMT1A, the most common of these CMT diseases (Dimachkie & Barohn, 2015; Lunn & Sheikh, 2014; Saporta & Shy, 2015).

A. Acquired neuropathies

1. *Immune-mediated peripheral neuropathies*

Abnormal humoral and cellular immunological responses against self-antigens in the PNS can be linked to peripheral neuropathies. Those immune-mediated diseases are highly heterogeneous and they are sometimes poorly characterized. The large majority are chronic forms from unknown etiologies, which are generally termed as Chronic Inflammatory Demyelinating Polyneuropathy (CIDP). The acute forms of these diseases are known as Guillain-Barré syndrome (Lunn & Sheikh, 2014; M. A. Saporta & Shy, 2015).

Guillain-Barré syndrome regroup acute, acquired, inflammatory diseases of the peripheral nervous system. High cerebrospinal fluid (CSF) protein levels with low CSF cell counts and a monophasic progression with at least partial recovery are the typical features of this neuropathy. Typical Guillain-Barré syndrome is macrophage-mediated attack on the Schwann cell or the axolemma. Important characteristics of this disease are demyelination and lymphocytic inflammatory lesions in proximal PNS regions (spinal rootlets) (Hughes & Cornblath, 2005; M. A. Saporta & Shy, 2015).

2. *Infectious peripheral neuropathies*

Infectious peripheral neuropathies are caused by the direct effect of microbes or their neurotoxins on peripheral nerves or by the consequences of a crossed immune reaction against peripheral nerve antigens by pathogens such as *Mycobacterium leprae* (Leprosy disease), Human Immunodeficiency Virus, Varicella-Zoster virus, *Borrelia burgdorferi* (Lyme disease) and

Corynebacterium diphtheria (Diphtheria disease) (Brizzi & Lyons, 2014; M. A. Saporta & Shy, 2015).

3. *Toxic peripheral neuropathies*

Toxic neuropathies are caused by environmental exposure to heavy metals such as lead, to chemical compounds such as acrylamide or as a result of medications' side effects mostly cardiac medications, antimicrobial agents and cancer drugs (B. Morrison & Chaudhry, 2012; M. A. Saporta & Shy, 2015).

4. *Metabolic peripheral neuropathies*

Diabetes, a metabolic disease, is the most frequent cause of peripheral neuropathy in the Western world. Symmetrical, predominantly sensory or autonomic neuropathies (or both) and asymmetrical mononeuropathies or plexopathies are the two main groups of diabetic peripheral neuropathies. Chronic forms include demyelinating peripheral neuropathies (B. Morrison & Chaudhry, 2012; M. A. Saporta & Shy, 2015).

B. Inherited peripheral neuropathies

Inherited peripheral neuropathies, a clinically and genetically heterogeneous group of diseases, can be categorized into two groups: the first one affects essentially the peripheral nervous system (CMT diseases) and the second one affects many systems of the human body among which the peripheral nervous system (Pisciotta & Shy, 2018; Rossor et al., 2017). The former group will be discussed in the following chapter.

The latter group is also called complex inherited neuropathy syndromes. It is further divided into many subgroups such as: 1) Hepatic, gastrointestinal and neuropathy syndromes (Rossor et al., 2017; Schmidt et al., 2015) as well as 2) Skin and connective tissue and neuropathy syndromes. Familial visceral amyloidosis constitutes one of the diseases from the first subgroup. It is an autosomal dominant autonomic and sensory axonal neuropathy with adult-onset chronic diarrhea (Rossor et al., 2017; Valleix et al., 2012). Xeroderma pigmentosum is an example from the second subgroup. It is an autosomal recessive sensory-motor axonal peripheral neuropathy with photosensitivity and increased risk of cutaneous malignancy, global developmental delay and deafness (Rossor et al., 2017; Tachi et al., 1988).

III. Charcot Marie Tooth (CMT)

Two French physicians Jean-Martin Charcot and Pierre Marie as well as one English physician Howard Henry Tooth first identified an inherited peripheral neuropathy in 1886 (Brennan, Bai, & Shy, 2015), hence the name Charcot Marie Tooth or CMT given to these group of diseases in 1968 (Magy et al., 2018). CMT diseases are a group of clinically and genetically heterogeneous diseases of the peripheral nervous system (**Table 1**). More than 90 gene mutations can cause CMT diseases (Pisciotta & Shy, 2018). Symptoms are different from one patient to another even from one twin brother to another. CMT diseases have no cure so far (Brennan et al., 2015).

A. Epidemiology

CMT diseases affect 1 in 2500 people worldwide with an estimated prevalence rate of 10-28/ 100 000 in Europe (Braathen, 2012; Brennan et al., 2015; Pareyson, Saveri, & Pisciotta, 2017; Pisciotta & Shy, 2018; Saporta et al., 2011; Schenone et al., 2011). They often overlap with distal hereditary motor neuropathies (dHMN) and hereditary sensory/ autonomic neuropathies (HSN or HSAN). dHMN and HSN or HSAN occur less frequently than CMT disorders and involve predominantly motor nerves (dHMN) or sensory and autonomic nerves (HSN or HSAN). These three groups of inherited peripheral neuropathies are pooled as CMT diseases and related disorders (Pisciotta & Shy, 2018). Although clinical manifestations are very variable from one patient to another, in general signs and symptoms of CMT diseases start in the first two decades of life with a progressive course of gradual weakness and sensory loss (Pisciotta & Shy, 2018; A. S. D. Saporta et al., 2011).

CMT diseases can be inherited as autosomal dominant (AD), X-linked or autosomal recessive (AR) (Pisciotta & Shy, 2018; Saporta et al., 2011). The dominant forms are commonly present in Western Europe, North America and Japan whereas in other countries with an increased dominance of consanguineous marriages like in the Mediterranean basin, between 30 to 50% of all forms is autosomal recessive disorders (Tazir et al., 2014). CMT diseases are globally distributed without any ethnic predisposition (Pisciotta & Shy, 2018).

B. Classification

Based on neuropathology, CMT diseases show two main categories: primary demyelinating and primary axonal neuropathies. The first contain CMT1, CMT3 or Dejerine-Sottas disease (DSD), congenital hypomyelinating neuropathy (CHN), and hereditary neuropathy with liability to pressure palsies (HNPP). The second category includes CMT2 (Schenone et al., 2011).

Neurophysiological analysis and the pattern of inheritance further classify CMT diseases into many subtypes. Regarding the classification based on neurophysiological studies, slow nerve conduction velocities (NCV less than 38 m/s in the upper extremities) and pathological indication of a hypertrophic demyelinating neuropathy characterize CMT1. On the other hand, rather normal nerve conduction velocities and sign of axonal degeneration are typically CMT2 neuropathies. In addition, intermediate nerve conduction velocities (less than and greater than 38 m/s) describe CMT intermediate group. For the classification based on genetics, CMT diseases can be inherited as autosomal dominant (CMT1, CMT2), autosomal recessive (CMT4), and X-linked (CMTX). Letters (A, B...) have been added to include the specific gene triggering the disease. For example, the myelin protein zero (MPZ) gene mutation cause CMT1B (Brennan et al., 2015) (***Table 1***).

There is a new classification proposed by Magy et al (2018). A 3-step approach was used for this purpose: 1) Mention the mode of inheritance as AD for autosomal dominant, AR for autosomal recessive, XL for X-linked and Spo for sporadic cases; 2) Indicate the phenotype (CMT) followed by the neurophysiologic hallmark: 'De' for demyelinating CMT instead of CMT1, 'Ax' for axonal CMT instead of CMT2 or 'In' for intermediate CMT; 3) Naming the gene causing the disease or putting 'UNK' for unknown in case of undiscovered gene or mutation. For example, CMT1A would be 'AD-CMTDe-PMP22'. After conducting an online survey among more than 300 CMT specialists from different background (clinicians and scientists) and from all over the world, responders preferred to start with the phenotype then the transmission mode and finally the gene involved with the precision 'mutation' or 'duplication' or 'deletion'. Consequently, CMT1A would become CMTDe-AD-PMP22 duplication. Responders did not like mentioning 'UNK'; they favored putting nothing when it was the case. This proposal requires further discussions with experts of the scientific and medical communities before modifications and validation (Magy et al., 2018).

Murphy et al. established in their epidemiological study that CMT1 affect around 57% of all CMT patients (Murphy et al., 2012) while Braathen found that CMT1 and CMT2 are equally frequent in the general population (Braathen, 2012). Rearrangements or point mutations of *PMP22* and *MPZ* genes are the most frequent causes of CMT1 (Murphy et al., 2012). CMT1A till CMT1F are the different CMT1 subtypes whereas CMT2A till CMT2Q are the multiple CMT2 subtypes (Tazir et al., 2014) (***Table 1***).

C. CMT1A

1. Epidemiology

CMT1A, identified in 1991, was the first described genetic cause of CMT. It is an autosomal dominant demyelinating disorder with a 10% de novo mutation rate (Brennan et al., 2015). CMT1A is a common subtype of CMT, 70-80% of CMT1 patients or 39.5% of all CMT patients are affected (Murphy et al., 2012).

2. Genetics

CMT1A is commonly caused by the 1.5 Mb tandem duplication of the *peripheral myelin protein 22 (PMP22)* gene on the short arm of chromosome 17 (17p11.2-p12) resulting in an excess of PMP22 (protein with 4 transmembrane domains), peripheral nerve demyelination and secondary axonal loss (Brennan et al., 2015; de Carvalho Alcantara et al., 2015; Schenone et al., 2011). The *PMP22* along with 8 other genes are duplicated (Li, 2017). Six exons (1a, 1b, 2-5) conserved in both human and rodents form the 40-kb PMP22 gene. Exon 1a and 1b encode for two transcripts identical in their coding sequence but different in their 5' untranslated region. This suggests that two promoters - P1 and P2 - control the expression of each transcript. Exon 2 encodes the first transmembrane domain of PMP22, exon 3 the first extracellular loop and exon 4 the second transmembrane domain. The third transmembrane domain is encoded half by exon 4 and the second half by exon 5. Exon-5 also encodes the second extracellular domain, the fourth transmembrane domain, and the 3' untranslated region. P1 and P2 promoters contain a TATA-box-like DNA element with an increased GC island content. Circular adenosine monophosphate (cAMP) response element binding (CREB) protein silence the PMP22 promoter while the sterol regulatory element binding (SREB) protein improves PMP22 transcription in the presence of

steroid hormones. Transcription factors like EGR2, Sox10, and Oct6 regulate myelin protein expression including PMP22. For example, triggering of a G-protein coupled receptor, gpr126, increases cAMP levels and activates the expression of Oct6 which controls genes encoding myelin proteins (Li et al., 2013).

3. *Clinical features*

CMT1A usually starts in the first twenty years of life. Despite phenotypic variability even in monozygotic twins, symptoms include difficulty in walking, a steppage gait, distal weakness, muscular atrophy, sensory loss, hyporeflexia, foot deformity and respiratory problems (Brennan et al., 2015; de Carvalho Alcantara et al., 2015; Fledrich et al., 2017). de Carvalho Alcantara et al study suggested that the high respiratory weakness observed in CMT1A patients could be due to axonal degeneration of nerves directed to muscles of respiration (de Carvalho Alcantara et al., 2015) (***Figure 8***) (de Carvalho Alcantara et al., 2015).

Most patients walk on time. They are usually slow runners and poor at sports during childhood. They develop highly arched feet and hammer toes during their teenage years and need orthotics for ankle support during adulthood. They can also present with foot weakness followed later on by hand weakness. Vibration and proprioception (large modalities) as well as pain and temperature (small modalities) are subject to sensory deficits. Balance problems often result from weak ankles and decreased proprioception. However, most of CMT1A patients stay ambulatory their whole life; their lifespan is not reduced by the disease. Absence of deep tendon reflexes is a main symptom of CMT1A present in almost all the patients. Roussy-Levy syndrome (postural tremor) and muscle cramps might also occur (Li et al., 2013).

In general, CMT1A children progress steadily through early childhood (3–10 years) and adolescence (11–20 years) (Cornett et al., 2017). CMT1A phenotype can be more severe if coupled to diabetes mellitus type II. As a matter of fact, it was previously shown that diabetes mellitus type II worsens electrophysiological features (decreased amplitude of ulnar compound motor action potential i.e. CMAP) and clinical outcomes (more severe motor and sensory impairments). It was hypothesized that diabetes mellitus could impair axonal transport and function of mitochondria (Jerath & Shy, 2017; Sheth et al., 2008). An increased body mass index also worsens lower extremity pinprick loss and lower extremity motor strength on examination but do not alter ulnar NCV (Jerath & Shy, 2017).

4. *Electrophysiology*

Nerve conduction velocity (NCV) depends on many factors including myelinated nerve fiber diameter, myelin thickness and internodal length. NCV was found to be linearly proportional to those factors over certain ranges (Li, 2015; Rushton, 1951). In CMT1A, NCV is usually around 20 m/s much below the normal value of 38m/s. Sensory action potentials are decreased or non-existent. Those two features are observed in the upper extremities median and ulnar nerves of CMT1A patients (Brennan et al., 2015; de Carvalho Alcantara et al., 2015; Fledrich et al., 2017; Li, 2015, 2017). Additionally, the typical feature of CMT1A being the reduced NCV, is generalized among nerves of the same limb or of another limb. This phenomenon of symmetry between limbs and nerves and low NCV is known as a ‘uniform slowing pattern of nerve conduction studies’. A while ago, it was thought that demyelination was responsible for the slow NCV in CMT1A. Highly variable conduction velocities from one case to another along with temporal dispersion and conduction block usually characterize demyelination. Furthermore, demyelination results in a progressive steady decrease in conduction velocities. Yet, these attributes are not or seldom found in CMT1A patients suggesting that CMT1A is not simply due demyelination (Li, 2015, 2017; Manganelli et al., 2016). The investigations of R. Fledrich, R. Stassart and M. Sereda (2014) on a CMT1A rat model suggest that CMT1A is not only a demyelinating disease but also a developmental disease. Indeed a defect in Schwann cell differentiation induces a deficit in myelinated fibers very early on in CMT1A rat pups and this deficit can be corrected by administration of soluble NRG1 in mutant rats (Fledrich et al., 2014).

5. *Morphology*

Nerve biopsy is rarely taken as it is invasive and not mandatory for diagnosing CMT1A. If done, it displays hypomyelination early on, in the first decade of life, onion bulb formation at later ages and a lowered density of myelinated fibers (Brennan et al., 2015; de Carvalho Alcantara et al., 2015; Fledrich et al., 2017; Gabreeels-Festen et al., 1995; Gabreëls-Festen & Van de Wetering, 1999; Li, 2017). Demyelination occurs later on and diseased nerves show onion bulbs over time. It happens when many Schwann cells circle around an axon but fail to form compact myelin. Some SCs make contact with the axon and harvest a thin myelin sheath. In that case active demyelination leads to thin myelin and hence a higher g-ratio. This parameter is measured by dividing the inner fiber diameter over the overall fiber diameter with its myelin sheath. Actually, despite active demyelination, the g-ratio is generally lower in CMT1A as the myelin sheath is thicker. This is

due to the focal myelin deposition which create heavy clump of myelin at paranodal loops in particular. Early on CMT1A patients Schwann cells fail to develop the large myelinated fibers. Consequently, myelinated fibers remain relatively homogeneous in their size with small diameters (Gabreëls-Festen & Van de Wetering, 1999; Li, 2015, 2017). In addition, internodal length is shortened in CMT1A patients (Li, 2015, 2017; M. A. Saporta et al., 2009). Subsequently, CMT1A myelinating Schwann cells do not attain their proper sizes both radially (nerve fiber diameter) and longitudinally (internodal length), suggesting a myelin sheath formation problem. Therefore, since in CMT1A myelin is abnormally developed, this neuropathy would be better termed as a dysmyelinating disease rather than a demyelinating disease (Li, 2017), but this remains controversial.

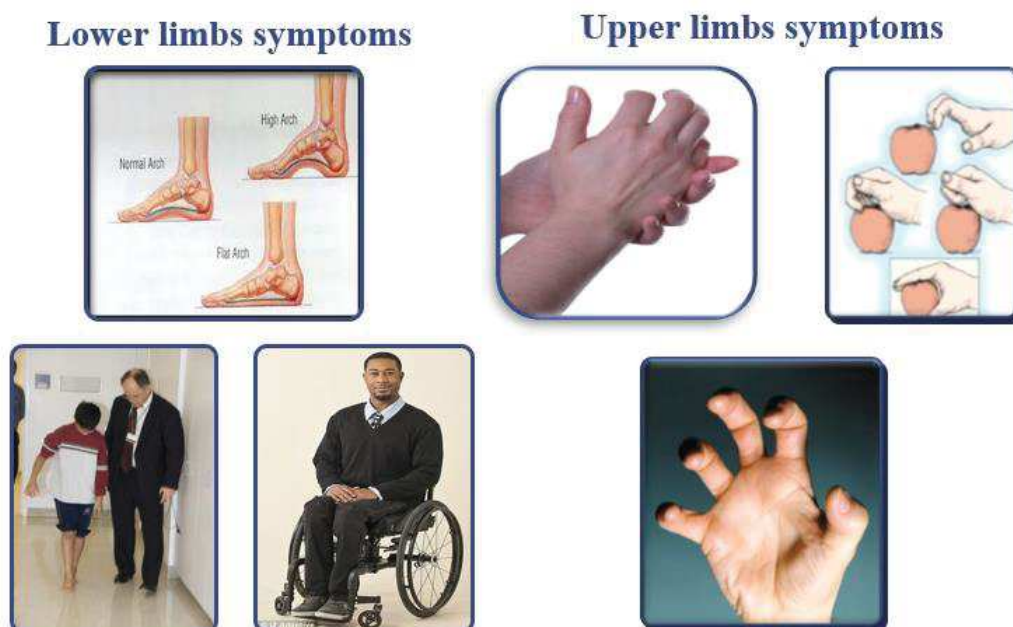


Figure 8 : Signs and symptoms of CMT: Highly arched or very flat foot (Adapted from luckyfeetshoes.com/foot-problems/flat-feet/), steppage gait (Adapted from cmt.org.uk/about-cmt/what-is-cmt/symptoms/), the use of a wheelchair in severe cases (Adapted from www.amsvans.com/blog/designer-is-giving-wheelchair-users-their-personality-back/), numbness and muscle weakness in hands (Adapted from www.handandwristinstitute.com), feet and legs, inability to grasp objects (Adapted and modified from www.slideshare.net/lostpebble/susil-seminar-claw-hand) and claw hand (Adapted from www.gettyimages.fr).

Table 1 : CMT types, mode of inheritance and characteristics

CMT type	Inheritance	Gene	Category	NCV	Onset (years)	Specific characteristics
CMT1A	AD	<i>PMP22</i> duplication 17p11.2-p12	Primary demyelinating neuropathy	<38m/s	All ages	Classic CMT1: steppage gait, balance impairment, distal weakness, atrophy, sensory loss, hyporeflexia, foot deformity, claw hand
CMT1B		<i>MPZ</i>			0 to 20	Clinically more severe than CMT1A
CMT1C		<i>LITAF</i>			Childhood	Unusual gait. Sometimes nerve hypertrophy. Infrequently deafness
CMT1D		<i>EGR2</i>			0 to 10	Classic CMT1/DSN/CHN. Cranial nerve might be involved. Scoliosis
CMT1E		<i>PMP22</i> point mutation			Childhood	Classic CMT1/DSN/CHN. Associated with deafness.
CMT1F		<i>NEFL</i>			1 to 13	Early onset. Severe disease
CMT1		<i>FBLN5</i>			40 to 50	Macular degeneration based on age. Hyperelastic skin
HNPP		<i>PMP22</i> deletion or point mutation		Normal or nearly normal but slowed at entrapment sites	2 to 64	Recurrent entrapment neuropathies. Multifocal neuropathies. Often predominantly length dependent large fiber neuropathy

CMT1X	X-linked	<i>GJB1</i>		Males between 25 and 45m/s, females >35m/s	0 to 20	Classic. Sometimes deafness. Males more severe phenotype than females. Males show the typical 'split hand syndrome'
CMTX dominant/ CMTX6		<i>PDK3</i>		Slow/ intermediate	Childhood	Classic CMT1
CMTX recessive (Cowchock)/ CMTX4		<i>AIFM1</i>		Normal	Early childhood/ infantile	Learning difficulties. Mental retardation. Deafness.
CMTX5	X-linked	<i>PRPS1</i>	Primary axonal neuropathy	Normal	Childhood	Mild-moderate neuropathy Deafness. Late optic atrophy
AR CMT1	AR	<i>PMP22 point mutation</i>	Primary demyelinating neuropathy	<38m/s		Classic CMT1, DSN, CHN, HNPP
AR CMT1-DSN-CH		<i>MPZ</i>				CMT1, DSN, CHN, intermediate, CMT2
CMT 2A1	AD	<i>KIF1B</i>	Primary axonal neuropathies	>38m/s	Childhood	Faster disease progression in early childhood compared to adolescence. Faster progression rate than CMT1A. In CMT2A2, prominent distal weakness, late proximal weakness, optic atrophy and CNS involvement
CMT 2A2		<i>MFN2</i>			6 to 50	
CMT2B		<i>RAB7A</i>			20 to 30	Severe sensory loss. Foot ulcers. Arthropathy and amputations

CMT2B1		<i>LMNA</i>			Childhood	Variable severity, distal muscle weakness and atrophy gradually progressing to the proximal muscles, sometimes sensory deficits, moderate or absent foot deformities, possibly proximal muscle atrophy of the pelvic and scapular girdle later in the disease course.
CMT2B2		<i>MED25</i>			26 to 42	Symmetric moderate to severe weakness of the distal muscles mostly the lower limbs. Important sensory impairments
CMT2C		<i>TRPV4</i>			Birth to 60	More severe in younger patients. Motor predominance. Vocal cord, diaphragm, respiratory involvement/dHMN
CMT2D		<i>GARS</i>			16 to 30	Mostly distal upper limb dHMN
CMT2E		<i>NEFL</i>			10 to 50	Hearing loss. Hyperkeratosis
CMT2F		<i>HSPB1</i>			Adult	Classic/dHMN
CMT2G		<i>12q12-q13.2 chromosome point mutation</i>			20 to 30	Classic

CMT2I/J		<i>MPZ</i>			Late	Classic. Deafness and pupillary abnormalities in CMT2J
CMT2H/K	AD	<i>GDAP1</i>	Primary axonal neuropathies	>38m/s	Variable	Vocal paralysis and pyramidal features
CMT2L		<i>HSPB8</i>			15 to 33	Classic/dHMN
CMT2M		<i>DNM2</i>			0 to 20	Tremor
CMT2N		<i>AARS</i>			15 to 50	Classic
CMT2O		<i>DYNC1H1</i>			Early childhood	Sometimes learning difficulties
CMT2P		<i>LRSAM1</i>			27 to 40	Mild. Sometimes asymmetry
CMT2Q		<i>DHTKD1</i>			13 to 25	Classic
HMSN-P		<i>TFG</i>			17 to 55	Proximal involvement. Tremor. Diabetes mellitus
CMT2		<i>HARS</i>			Late onset	Sensory predominant
CMT2		<i>MARS</i>			Late onset	Motor-sensory
CMT2		<i>MT-ATP6</i>			0 to 20	Motor predominant. Pyramidal signs
ARCMT2A	AR	<i>LMNA</i>	Primary axonal neuropathies	>38m/s	20 to 30	Severe course. Distal and proximal weakness
ARCMT2B		<i>19q13.1–13.3 chromosome point mutation</i>			28 to 42	Classic CMT2
ARCMT2C		<i>NEFL</i>			1 to 10	Severe form
ARCMT2F/dHMN		<i>HSPB1</i>			Variable	Sometimes proximal leg weakness
ARCMT2H		<i>GDAP1</i>			1 to 10	Pyramidal involvement. Vocal cord involvement
ARCMT2K	AR (rarely AD)	<i>GDAP1</i>			Early-onset form	Severe form. Vocal cord paralysis. Skeletal

						deformities. Milder dominant form
ARCMT2P	AR	<i>LRSAM1</i>			30 to 40	Cramps. Erectile dysfunction
CMT3-DS	AD or AR	<i>MPZ, PMP22, EGR2, PRX</i>		<15m/s	Severe early onset	Most severe form of demyelinating CMT, motor delay, increased concentrations of proteins in the cerebrospinal fluid, nerve hypertrophy, and severe dysmyelination at nerve biopsy
CMT 4A	AR	<i>GDAP1</i>	Primary demyelinating neuropathy	Variable	< 2	Severe and progressive, vocal cord and diaphragm paralysis in some cases
CMT 4B1		<i>MTMR2</i>			3	Severe CMT1, facial/bulbar weakness, focally folded myelin, scoliosis
CMT 4B2		<i>MTMR13(SBF2)</i>			4 to 13	Severe CMT1, glaucoma, focally folded myelin
CMT 4B3		<i>MTMR 5 (SBF1)</i>			5 to 11	Severe CMT, scoliosis, syndactyly, focally folded myelin, Pes planus
CMT 4C		<i>KIAA1985 (SH3TC2)</i>			Early onset, 0 to 20	Severe CMT1, scoliosis, cytoplasmic expansions, deafness
CMT 4D/HMSNL		<i>NDRG1</i>			< 10	Severe CMT1, gypsy, deafness, tongue atrophy
CMT 4E		<i>EGR2</i>			Birth	Congenital hypotonia. Respiratory failure. Arthrogryposis

CMT 4F		<i>PRX</i>			Birth to 10	CMT1, more sensory, focally folded myelin
CMT 4G/ HMSN-Russe		<i>HK1</i>			8 to 16	Severe to moderate CMT1
CMT 4H		<i>FGD4</i>			< 2	Delayed milestones. Scoliosis. Severe course
CMT 4J		<i>FIG4</i>			Congenital, childhood or adult	Severe CMT1±ALS (motor neuron disease) phenotype in adulthood
CCFDN		<i>CTDP1</i>			Infancy Neonatal	CMT1, gypsy, cataracts, dysmorphic features
CMT 4		<i>SURF</i>			Childhood	Severe. Associated to cerebellar ataxia, brain MRI abnormalities and lactic acidosis
CMT5-HMSN type V	AD	<i>MFN2 mostly BSCL2 and GJB1 to a lesser extent</i>	Primary axonal neuropathy	>38m/s	Adult	The clinical phenotype is complicated by pyramidal involvement
CMT6-HMSN type VI		<i>MFN2</i>			Early onset	The clinical phenotype is complicated by optic atrophy
DI-CMTA	AD or AR	<i>10q24.1–25.1 chromosome point mutation</i>	Dominant Intermediate (DI)	< and >38m/s	7 to 72	Classic
DI-CMTB		<i>DNM2</i>			0 to 20	Classic with neutropenia and early onset cataract
DI-CMTC		<i>YARS</i>			7 to 59	Classic
DI-CMTD		<i>MPZ</i>			30 to 50	Sensory loss and weakness.

						Deafness/pupil disorders
DI-CMTE		<i>YARS</i>			5 to 28	Glomerulosclerosis and proteinuria
DI-CMTF		<i>YARS</i>			5 to 45	Classic

Adapted from Angelo Schenone et al, 2011; Brennan et al, 2015; Pareyson and Marchesi, 2009; Tazir et al., 2014; Cornett et al, 2017

Abbreviations: AARS, alanyl-tRNA synthetase; AD, autosomal dominant; AIFM1, apoptosis-inducing factor mitochondrion-associated 1; AR, autosomal recessive; BSCL2, Berardinelli-Seip congenital lipodystrophy type 2; CHN, congenital hypomyelinating neuropathy; CNS, central nervous system; CTDP1, CTD phosphatase subunit 1; DHTKD1, dehydrogenase E1 and transketolase domain-containing 1; DI, dominant intermediate; DNM2, dynamin 2; DSS, Dejerine Sottas Syndrome; DYNC1H1, dynein cytoplasmic 1 heavy chain 1; EGR2, early growth response 2; FBLN5, fibulin 5; FGD4, actin filament-binding protein frabin; FIG4, FIG4 homolog SAC1 lipid phosphatase domain containing; GAN, Giant axonal neuropathy; GJB1, gap-junction protein β -1; GARS, glycyl-tRNA synthetase; GDAP1, ganglioside-induced differentiation-associated protein 1; HARS, histidyl-tRNA synthetase; HK1, hexokinase 1; dHMN, distal hereditary motor neuropathy; HMSN, hereditary motor and sensory neuropathy; HNPP, hereditary neuropathy with liability to pressure palsies; HSPB1, heat shock protein B1; HSPB8, heat shock protein B8; KIF1B, Kinesin Family Member 1B; LITAF, lipopolysaccharide-induced tumor necrosis factor; LMNA, lamin A/C; LRSAM1, leucine-rich repeats and sterile alpha motif-containing 1; MARS, methionyl-tRNA synthetase; MED25, mediator complex subunit 25; INF2, inverted formin 2; MFN2, mitofusin 2; MPZ, myelin protein zero; MT-ATP6, ATP6 subunit of the mitochondrial Adenosine Triphosphate synthase; MTMR2, myotubularin-related protein 2; MTMR5, myotubularin-related protein 5; MTMR13, myotubularin-related protein 13; NDRG1, N-myc downstream-regulated gene 1 protein; NEFL, neurofilament light chain; PDK3, pyruvate dehydrogenase kinase isoenzyme 3; PMP22, peripheral myelin protein 22; PRPS1, phosphoribosyl pyrophosphate synthetase 1; PRX, periaxin; RAB7, RAS-associated protein RAB7; SBF1, SET binding factor 1; SBF2, SET binding factor 2; SH3TC2, SH3 domain and tetratricopeptides repeats 2; SURF1, Surfeit 1; TFG, TRK-fused gene; TRPV4, transient receptor potential cation channel subfamily V member 4; YARS, tyrosyl tRNA synthetase.

Split hand syndrome: dissociated muscle weakness in the hands (muscles on the side of the thumb wasted as compared to the muscles on the side of the little finger that are spared).

D. CMT1A animal models

1. Rodent models

Only one rat model and several mouse models were generated to mimic the human CMT1A peripheral neuropathy. All models overexpress the *PMP22* gene (mouse or human). Those models are summarized in **Table 2** : **CMT1A murine models**. Since I used the rat model for my thesis project, further details are exposed right after.

2. CMT1A rat

a) Generation of the model

In 1996, Sereda et al created a rat model for CMT1A, the PMP22-transgenic rat. The rat was specifically chosen as species because it is the favorite model system to test development of SCs *in vivo* and *in vitro*. From a 129SV mouse cosmid genomic library, cloning of the wild-type gene was performed. A restriction fragment of 43 kb with the transcription unit PMP22 was excised along with 7 kb upstream of exon 1A and 4 kb downstream of exon 5. Fertilized Sprague-Dawley rat oocytes were microinjected with DNA. This led to the generation of one founder male which could breed normally. This male was employed to launch a line of PMP22-transgenic rats (M. Sereda et al., 1996) .

b) Genetics

The heterozygous CMT1A rat carries three copies of the mouse *PMP22* gene thus overexpressing the mouse PMP22 protein. They acquire a peripheral neuropathy representing the autosomal-dominant CMT1A human disease (Niemann et al., 1999; M. Sereda et al., 1996). Even before the first demyelination signs, SCs poorly differentiated at time points of early postnatal myelination. From Postnatal day 6 (P6) to P180, mRNA levels of myelination related genes *Hmgcr*, *Prx* and *Mpz* are decreased in CMT1A rats compared to WT. PMP22 mRNA is overexpressed very early on i.e. 2.1x at P1 and 1.2x at P6 and later on, i.e. 1.6x at P18. PMP22 mRNA is reduced during myelination peak i.e. from P28 to P180. Immature and dedifferentiated SCs markers *Pou3f1*, *Ngfr*, *Notch1*, *Jun* and *Sox2* are increased in sciatic nerves (SN) of CMT rats from P18 to P180. From early postnatal development on (from P1on), CMT rat sciatic nerves display an important decrease in PI3K–v-Akt signaling pathway then trigger of the mitogen activated protein kinase kinase 1 (Mek)–mitogen activated protein kinase (Erk) signaling pathway at P6 (Fledrich et al., 2014)

Table 2 : CMT1A murine models

Animal model	Mutation in the animal model	Copy number	Characteristics
CMT1A rat	mouse <i>PMP22</i> cosmid tg	3	Unsteady gait, clumsiness in walking, motor deficits, reduced NCV, hypo-, hyper-, de-, dys-myelination, axonal loss, onion bulb
C22 heterozygotes	human <i>PMP22</i> YAC tg	7	Unsteady gait, severe phenotype, progressive paralysis of the rear legs, very slow NCV and prolong distal motor latencies, Amyelinated or hypomyelinated large caliber axons, demyelination, onion bulbs, difficult to breed
C61 mouse, heterozygotes	human <i>PMP22</i> YAC tg	4	Reduced performance in motor tests, some electrophysiological impairments de-, re-, hyper-myelination, onion bulbs
TgN248	mouse <i>PMP22</i> cosmid tg	16	Severe phenotype (slight shivering, unsteady gait, muscle atrophy and paralysis of the hindlimbs), do not live more than 8 months, poor breeding, high latencies and low CMAP amplitudes with temporal dispersion, low motor NCV. No myelin.
My41	mouse <i>PMP22</i> YAC tg		Severe phenotype (unstable gait since 3 weeks of age and weakness of the rear limbs), do not live long (rarely more than 5 months), breed poorly, a- or hypo-myelinated axons, demyelination.
Double transgenic mice	human, mouse <i>PMP22</i> YAC tg + tetracycline		<i>PMP22</i> overexpression is switched off by tetracycline and on by the absence of tetracycline, slight unsteady gait, little decrease of NCV, demyelination, onion bulbs
C3-PMP mouse	human <i>PMP22</i> YAC tg	3-4	Mild neuromuscular problems, low NCV, hypo- and a-myelinated fibers, hypermyelination of small axons, rare axonal damage
B6C3F1 mice	<i>PMP22</i> gene	High	Muscle weakness and atrophy, sensory loss, amyelinated large and medium axons and few small myelinated fibers, hypomyelinated axons, deficiency of large caliber axons

Adapted from Fledrich, Stassart and Sereda, 2012. tg: transgenic. References: Fledrich et al., 2014; Huxley et al., 1996, 1998; Kobsar et al., 2005; Magyar et al., 1996; Niemann et al., 1999; Norreel et al., 2001; Perea et al., 2001; Robertson, Huxley, King, & Thomas, 1999; Robertson et al., 2002; Sara Sancho, Magyar, Aguzzi, & Suter, 1999; M. Sereda et al., 1996; Verhamme et al., 2011

c) Clinical phenotype and electrophysiology

CMT1A rats have an unsteady gait and they are clumsy when they walk as demonstrated by the outward position of their hind feet seen in footprint analysis. Loss of muscle strength is observed when rats attempt to right up at the cage wall and their hind limbs are unable to support their body weight. Like patients, CMT1A rats present motor deficits and decreased NCV in both motor and sensory nerves (Niemann et al., 1999; M. Sereda et al., 1996). Muscle weakness is more uniformly distributed in CMT1A rats as opposite to the length-dependent fiber loss in CMT1A patients (Zu Horste et al., 2007)

d) Morphology

CMT1A rats display peripheral hypomyelination that is more obvious in large diameter fibers (presumably motor) compared to smaller fibers having normal or even higher thickness sheaths (hypermyelination). Hypomyelination is possibly due to reduced MPZ and MBP. Few SCs showed myelin debris. Endoneurial collagen was amplified. Degradation of axons was rare (less than 1% of fibers). The complicated combination of dysmyelination and superimposed progressive demyelination defines the phenotype of the rat (Niemann et al., 1999; M. Sereda et al., 1996). Hypermyelinated axons are observed at P6, P18 and P180. Amyelinated as well as hypomyelinated (thinly myelinated) axons are seen at P18 and P180. At postnatal day 18 (P18), CMT rats have the same total number of SN axons compared to wild-type (WT) controls. At P90 CMT1A rats show axonal loss (Fledrich et al., 2014). In young rats (5-week-old), amyelinated axons with no sign of myelin disruption as well as hypomyelinated axons and axons with normal myelin thickness were observed. Excessive Schwann cell processes and basal laminae surrounding hypomyelinated or amyelinated axons i.e. onion bulbs increased in number with disease progression. As a matter of fact, electron micrographs of CMT1A rats' sciatic and tibial nerves showed few onion bulbs at 2.5 month and numerous ones at 6 months. Onion bulb formation is more obvious in the ventral roots than in the dorsal roots. This might explain why motor functions are generally more damaged than sensory functions in CMT1A (Niemann et al., 1999; M. Sereda et al., 1996). One limitation of the rat model is that contrarily to what is seen in CMT1A patients, axonal loss in CMT1A rats is not distally pronounced when comparing tibial and sciatic nerves (Zu Horste et al., 2007).

e) Homozygous rat

Homozygous PMP22-Transgenic rats were more harshly affected. In fact, light and electron microscopy analysis revealed an absolute absence of PNS myelin. Highly overexpressed PMP22 Schwann cells do not complete differentiation; they stop at the promyelin stage. Abnormal spasticity,

hind limb paralysis, uncoordinated movements and absence of motor development are displayed by homozygous rats. Hind limb paralysis and spasticity are fatal at 4-6 weeks of age in those rats (Niemann et al., 1999; M. Sereda et al., 1996).

From now on, “CMT1A rat” will refer to the heterozygous PMP22-transgenic rat model created by Sereda in 1996.

f) Biomarkers analysis

Fledrich et al (2012) searched for indicators of disease severity while studying the CMT1A rat. This research team demonstrated that sciatic nerve messenger RNA expression for genes associated with lipid metabolism such as peroxisome proliferator-activated receptor gamma (PPARG) were sometimes downregulated (63-day-old rats) and other times upregulated (7-day-old rats) in severely affected rats compared with mildly affected rats. Consequently, there is inversed proportionality between messenger RNA expression for genes associated with lipid metabolism of the early disease stage and of the late disease stage. Lipid metabolism contributes to the myelination and demyelination process. Nerve conduction velocities determined at 9 weeks of age, were significantly lower in CMT1A rats than in wild-type rats. However, mildly and severely affected rats presented similar results. Hence, axonal loss rather than demyelination might be an indicator of disease severity. Contrarily to nerve conduction velocities, sensorial impairments can be an indicator of disease severity. Indeed, compared to wild-type and mildly affected CMT rats, severely affected animals had an important sensory impairment after testing the response to heat pain with a nociceptive hot plate. Fledrich et al (2012). proposed an important indicator of disease severity while studying rat models: the combination of age and cutaneous messenger RNA levels of glutathione S-transferase theta 2 and cathepsin A (Fledrich, Schlotter-Weigel, et al., 2012).

E. Peripheral Myelin Protein (PMP22)

1. PMP22 generalities

Inherited peripheral neurological disorders including Charcot Marie Tooth disease type 1A (CMT1A), hereditary neuropathy with liability to pressure palsies (HNPP) and severe childhood onset demyelinating neuropathies (Tyson et al., 1997) have been associated with duplications (CMT1A) (Lupski et al., 1991; Pentao et al., 1992; Raeymaekers et al., 1991), deletions (HNPP) (Chance et al., 1993) and point mutations of the *Peripheral Myelin Protein 22 (PMP22)* gene (CMT1E) (Giambonini-

Brugnoli et al., 2005; Gregson et al., 2007). Loss-of-function phenotype is a consequence of deletion whereas gain-of-function phenotypes are consequences of overexpression and point mutations of the *PMP22* gene (Li et al., 2013).

PMP22 is also known as *growth arrest specific gene-3 (gas-3)* due to the fact that it was first discovered as a decreased transcript in mouse NIH-3T3 fibroblasts upon growth arrest (Li et al., 2013; Snipes, Suter, Welcher, & Shooter, 1992). However, so far the exact function of PMP22 protein remains unknown.

2. *PMP22* transcript

In humans, *PMP22* mRNAs are mainly found in Schwann cells of the peripheral nerves. They are also expressed at low level postnatally and in young adults in the central nervous system (brain and brainstem) (Li et al., 2013; Ohsawa et al., 2006). More detailed studies have been done on rats and mice (de Leon, Nahin, Mendoza, & Ruda, 1994; Li et al., 2013; Parmantier, Cabon, Braun, D’Urso, Müller, et al., 1995; Snipes et al., 1992; Welcher, Suter, De Leon, Snipes, & Shooter, 1991; Wulf & Suter, 1999) (***Table 3***).

PMP22 possess 6 Alternative Splicing Variants (ASVs) (variants 1-6). A single gene using alternate exon-intron inclusions and exclusions cause alternative splicing hence creating several messenger RNA (mRNA) isoforms (Taneri, Asilmaz, & Gaasterland, 2012; Visigalli et al., 2016). In both humans and rodents, two alternatively transcribed exons (1a and 1b) results in two different transcripts (refer to Introduction III.C.2 for more details). This might explain the difference in *PMP22* mRNA distribution among tissues. Exon 1b is mostly present in the brainstem, spinal cord, skeletal muscle, heart and SN while exon 1a is mainly found in SN. Those alternatively transcribed exons are the variants 1, 2 and 3 coding for the same PMP22 protein of 18 kDa, the “classical” PMP22. On the other hand, variants 5 and 6 code for a new PMP22 protein isoform of 13 kDa. This smaller isoform is mostly found in the endoplasmic reticulum in opposition to the classical PMP22 protein that is expressed at the plasma membrane. Variant 4 do not code for any PMP22 protein (Visigalli et al., 2016).

3. *PMP22* protein

PMP22 is a membrane-bound 18-kDa polypeptide which is modified by glycosylation after translation to form the mature glycoprotein of 22 kDa (Giambonini-Brugnoli et al., 2005). The peripheral

myelin protein (PMP22) is constituted of 160 amino acid glycoproteins (Hayasaka' et al., 1992) with four hydrophobic regions (Jetten & Suter, 2000).

PMP22 has four transmembrane domains with two extracellular domains and one intracellular domain (**Figure 9**). Transmembrane domain 1 comprising amino acids 1-30 is depicted as a long α -helix, extracellular loop 1 (amino acids 31-57) as a largely unstructured loop, transmembrane domains 2- 4 as a molten globular helical bundle and extracellular loop 2 as a short loop between transmembrane domains 3 and 4. Seven potential metal ion-coordinating sites have been identified in the extracellular loops. Those sites might be involved in the Zinc (Zn) (II) binding ability of PMP22. Extracellular loop 1 is responsible for interactions between two PMP22 proteins while extracellular loop 2 regulates interaction between PMP22 and MPZ (Hasse,et al., 2004; Li et al., 2013).

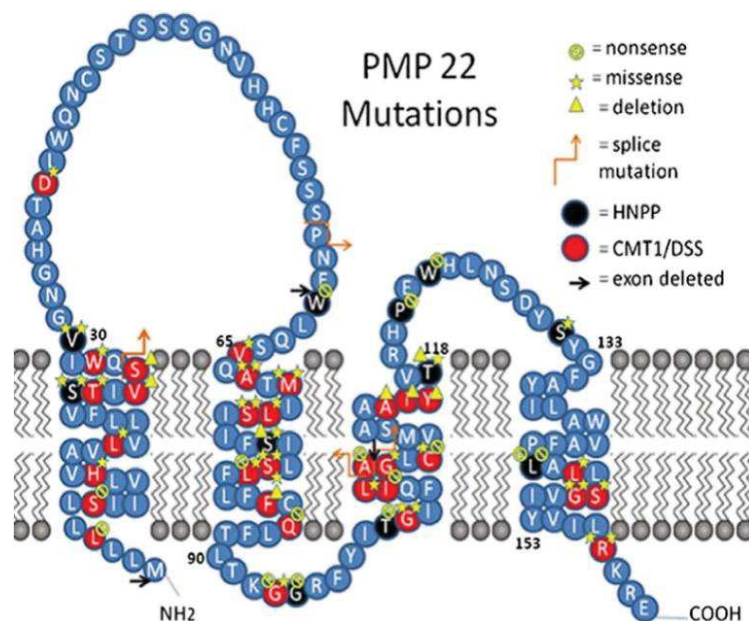


Figure 9 : PMP22 molecular structure: 4 transmembrane domains, 160 amino acids. Mutations sites are represented. Taken from Watila & Balarabe, 2015 who adapted it from Li et al., 2013.

Table 3 : Distribution of PMP22 postnatally/ in young adults

Organ	Human		Rat		Mouse	
	mRNA	Protein	mRNA	Protein	mRNA	Protein
Brain	Low	NA	Low	Low	Low	NA
Brainstem	Low	NA	Medium (motor nuclei). Absent in sensory nuclei	NA	High (motor nuclei). Absent in sensory nuclei	NA
Spinal cord	High	Detected in ventral and dorsal roots, motor neurons and preganglionic sympathetic neurons in spinal cord	Medium in spinal cord's motor neurons and not in sensory counterparts	Medium in dorsal and ventral horn, detected in motor neurons	High in spinal cord motor neuron	High in spinal cord motor neuron
Dorsal Root Ganglion	Detected but not quantified	NA	Absent in neurons but medium in satellite cells	Medium in neurons and satellite cells	Absent	NA
Sciatic Nerve	High	High	High	High	High	High
Cranial nerve	NA	NA	High	Absent	High	Absent
Skeletal muscle	NA	NA	Medium	Undetectable	NA	NA
Heart	NA	NA	Medium	Undetectable	Low	NA
Liver	NA	NA	Detected in bile canaliculi	Low in bile canaliculi	NA	NA
Kidney	NA	NA	Low	Undetectable	NA	NA
Gastro- intestinal tract	NA	NA	High	High	High	NA
Lung	NA	NA	High	Undetectable	High	NA
Testes	NA	NA	Low	NA	NA	NA

NA=Not Applicable. Adapted from : Baechner et al., 1995; de Leon et al., 1994; Li et al., 2013; L. Notterpek et al., 2001; Ohsawa et al., 2006; Parmantier, Cabon, Braun, D'Urso, Muller, et al., 1995; Snipes et al., 1992; Wulf & Suter, 1999

PMP22 is mostly found in the peripheral nervous system of mammals (Gregson et al., 2007) especially in myelinating Schwann cells (Giambonini-Brugnoli et al., 2005) like *PMP22* mRNA (Li et al., 2013). Although *PMP22* mRNA was identified in the cranial nerve motor nuclei of mouse (Parmantier, Cabon, Braun, D'Urso, Muller, et al., 1995) and rat (Snipes et al., 1992), the protein was not expressed in this tissue (Gregson et al., 2007; Parmantier, Cabon, Braun, D'Urso, Muller, et al., 1995; Snipes et al., 1992). Contrarily to Gregson et al (2007) who did not find PMP22 in the central nervous system, Snipes et al (1992) have detected low levels of PMP22 in the central nervous system both in the adult (***Table 3***) and during embryonic development (Giambonini-Brugnoli et al., 2005; Gregson et al., 2007; Snipes et al., 1992). Snipes et al findings correlate with *PMP22* mRNA low levels detected in the brain of humans and rodents (Li et al., 2013; Snipes et al., 1992). In the mammalian peripheral nervous system, this protein is the second most abundant protein after myelin protein zero (P0) (Gregson et al., 2007).

4. *PMP22* protein synthesis and transport

Newly produced PMP22 is transiently retained in the endoplasmic reticulum and Golgi compartments for post-translational modification like glycosylation. Culturing rat Schwann cells or co-culturing rat Schwann cells with neurons results in approximately 70% of newly produced PMP22 to be degraded and only a small portion is transported to the cell surface. Consequently, it has been suggested that PMP22 protein glycosylation stabilize the protein structure preventing protein degradation and allowing transport to the cell surface (Li et al., 2013).

5. *PMP22* Function

The function of PMP22 protein is neither clear nor well-defined. Several hypotheses have been presented including PMP22 involvement in cell proliferation, apoptosis and myelination. However, *PMP22* gene dosage (over-, under-expression and point mutation) has different effects depending of the cell type. In addition, contradictory results have been found between *in vivo* and *in vitro* studies (Li et al., 2013). Since PMP22 is highly relevant in myelinating Schwann cells (Mittendorf et al., 2017), I will only present studies related to its function in the peripheral nervous system.

a) Cell proliferation

The important increase of PMP22 expression during NIH3T3 cell starvation suggested a role of PMP22 in cell proliferation. However, *in vitro* and *in vivo* studies have shown contradictory

effects. Indeed, overexpression of *PMP22* decrease proliferation in Schwann cells (Hanemann et al., 1998; Li et al., 2013; Mittendorf et al., 2017; Zoidl et al., 1995) or fibroblasts (Li et al., 2013; Zoidl et al., 1997) in culture while *in vivo* *PMP22* overexpression in young adult transgenic mice increases Schwann cell proliferation (Li et al., 2013; Sancho et al., 2001). Nonetheless, in CMT1A patients cell proliferation is decreased (S. Lee et al., 2018). In addition, point mutations decrease proliferation of fibroblasts *in vitro* (Zoidl et al., 1997) but increase proliferation of Schwann cells *in vivo* (transgenic mice aged 21-days onward) (Li et al., 2013; Sancho et al., 2001). On the other hand, deficiency of *PMP22* increase proliferation of Schwann cells *in vitro* (Li et al., 2013; Zoidl et al., 1995) and *in vivo* in transgenic (Li et al., 2013; Sancho et al., 2001).

b) Apoptosis

Extensive research has been done on the apoptotic effect of *PMP22* on Schwann cells, but contradictory results were found. Duplication, deletion and point mutation of *PMP22* lead to a higher apoptotic rate of Schwann cells (Sancho et al., 2001) and of cultured fibroblasts (Fabbretti et al., 1995; Sancho et al., 2001) of transgenic mice. However, this rate is decreased in case of several *PMP22* point mutations (L16P, S79C, T118M, and G150D) (Fabbretti et al., 1995; Sancho et al., 2001).

c) Myelination

PMP22 protein is essential for the structure, the development and the maintenance of peripheral nerve myelin (Mittendorf et al., 2017; Suter & Snipes, 1995). Concerning myelin structure, recent studies conducted on an *in vitro* model of lipid bilayers concluded that *PMP22* is involved in organizing the ultrastructure of compact myelin. Indeed, spiral wrapping around a central cylindrical vesicle similar to the wrapping of myelin around an axon was observed in presence of *PMP22* (Mittendorf et al., 2017).

Regarding myelin development and maintenance, the abnormal dosage of *PMP22* impairs different stages of myelination. Over- or under-expressing *PMP22* in Schwann cells *in vitro* indicated that *PMP22* is involved in controlling myelin thickness and stability (Suter & Snipes, 1995). Despite the previously described experiments, the structure of myelin lamellae was similar in over- or under-expressed *PMP22* Schwann cells (D'Urso et al., 1997). Amici et al (2007) demonstrated that *PMP22* plays a role in the initiation of myelination *in vitro* and *in vivo*, in *PMP22* $-/-$ knockout mice (*PMP22* $-/-$ mice). Moreover in the absence of *PMP22*, expression of several

markers of myelination was disturbed (Amici, Dunn, & Notterpek, 2007). Dysmyelination features were also observed in these mutant mice: increased number of promyelinating Schwann cells surrounding axons without wrapping them, hypermyelinated axons, reduced fiber diameter and increased in g-ratio. All of those findings suggested a delayed myelination (S. A. Amici, 2006). Furthermore, histological studies of peripheral nerves from transgenic rodent models harboring extra copies of *PMP22* show amyelinated, hypomyelinated and/or hypermyelinated axons (**Table 2**) (Fledrich, Stassart, & Sereda, 2012) further illustrating PMP22 crucial role in the myelination process.

F. Pathomechanisms of CMT1A

1. Imbalanced activity of signaling pathways

CMT1A is both a dysmyelinating and demyelinating disease, which etiology remains unclear. Many hypotheses have been proposed including imbalanced activity of signaling pathways, dysregulation of critical genes expression, alteration of cholesterol biosynthesis, increase in calcium levels, PMP22 aggregates formation and toxicity toward axons (Fabbretti et al., 1995; Fledrich et al., 2014; Giambonini-Brugnoli et al., 2005; Kinter et al., 2013; Li et al., 2013; Nobbio et al., 2009; S Sancho et al., 2001; Vigo et al., 2005; Visigalli et al., 2016).

Imbalanced activity of the signaling pathways PI3K-Akt and Mek-Erk contributes to CMT1A pathogenesis. Indeed, in the CMT1A rat, there is a decreased signaling of PI3-Akt pathway followed by a stimulation of Mek-Erk pathway. This leads to a persistent differentiation defect of Schwann cells in this rat model, during early postnatal development (Fledrich et al., 2014).

2. Downregulation of cholesterol genes

Studies on PMP22-overexpressing transgenic mice (CMT1A transgenic mice) showed downregulation of genes involved in cholesterol biosynthesis especially the ones encoding the rate-limiting key enzymes HMG-CoA reductase and HMG-CoA synthase. This most probably explains the decreased activity of sterol regulatory element binding protein 2 (SREBP-2) transcription factor. SREBP-2 is a master regulator of the cholesterol pathway genes (Giambonini-Brugnoli et al., 2005; Horton, Goldstein, & Brown, 2002; Sakakura et al., 2001). Cholesterol is an

essential lipid that constitutes a large amount of myelin lipids. It also controls the transferring of major myelin proteins (P0) from the Schwann cell endoplasmic reticulum to myelin membrane. Cholesterol deficiency in Schwann cells disrupts this process leading to the loss of peripheral myelin compaction and the modification in the stoichiometry of myelin membrane components (Li et al., 2013; Saher et al., 2009; Vigo et al., 2005). During myelination genes driving cholesterol biosynthesis are highly expressed in WT while in CMT1A transgenic mice, their expression remains low. This could explain the severe hypomyelination seen early on in CMT1A (Giambonini-Brugnoli et al., 2005).

3. *Downregulation of genes influencing the cytoskeleton and extracellular matrix*

Expressions of genes whose products affect the cytoskeleton such as Ankyrin 3 and the extracellular matrix such as integrins beta 4 and 5 are downregulated in CMT1A transgenic mice. This could be associated with the remodeling of the extracellular matrix seen in CMT1A patients. As the interaction of the myelinating Schwann cell with the basal lamina is critical for myelination (Cornbrooks et al., 1983; McKee et al., 2012) the severity of nerve fiber loss and the duration of the pathology could be linked to these gene expression defects (Giambonini-Brugnoli et al., 2005; Palumbo et al., 2002).

4. *Upregulation of Schwann cells differentiation and myelination factors*

Schwann cells differentiation and myelination require transcription factors such as *Krox20* (refer to Introduction I.D.1). These genes are highly expressed at the start of myelination both in CMT1A transgenic mice and controls. However, at adult age, the expression of some markers of differentiating Schwann cells such as *Oct 6* remains high in CMT1A transgenic mice but not in controls. This suggests a defect in the differentiation program of the Schwann cells in CMT1A disease (Giambonini-Brugnoli et al., 2005; Jaegle & Meijer, 1998).

5. *Increase in calcium levels*

Excess of PMP22 has been shown to increase P2X7, a purinoceptor who lead to extracellular calcium influx into Schwann cells. Increased levels of calcium have been shown to impair myelin synthesis in Schwann cells (Nobbio et al., 2009) and to trigger segmental demyelination (Li et al., 2013; K. J. Smith & Hall, 1988). As high calcium levels are normally present in immature developing Schwann cells (Fields & Stevens, 2000), this mechanism likely

works after development of myelin. Studies have demonstrated that inhibiting P2X7 prevents demyelination in Schwann cell/neuronal co-culture with PMP22 overexpression (Li et al., 2013; Nobbio et al., 2009).

6. PMP22 aggregates formation

Culturing dermal fibroblasts from CMT1A patients and from age-matched controls show fewer mitotic cells as well as a decreased proliferation rate in CMT1A cells compared to controls. This is in line with the hypothesis of inverse relationship between increased PMP22 protein levels and decreased cell proliferation *in vitro* (refer to Introduction III.F.5.a). PMP22 distribution in cultured fibroblasts differs between patients and controls cells. Indeed, PMP22 excess results in perinuclear accumulation of the protein located in aggresomes in Schwann cells (Fortun et al., 2006; Lee et al., 2018; Notterpek et al., 1999; Rangaraju & Notterpek, 2011). As a large amount of PMP22 is misfolded, PMP22 is actively catabolized through protein degradation pathways including the ubiquitin proteasome system and the endosomal-lysosomal compartment (Fortun et al., 2006; Lucia Notterpek et al., 1999). In CMT1A cells there were significantly higher levels of polyubiquitinated molecules compared to controls indicating a deficient proteasome activity in diseased cells. Furthermore, in CMT1A cells there was significantly higher levels of autophagy and lysosomal proteins lysosome-associated membrane protein 1 (LAMP1) and microtubule-associated protein light chain 3 (LC3) compared to controls indicating the activation and recruitment of autophagy lysosomes to clear and process PMP22 aggregates in diseased cells (Fortun et al., 2006; S. Lee et al., 2018; Lucia Notterpek et al., 1999). It can be concluded that PMP22 overexpression leading to the formation of aggregates is a possible mechanism for CMT1A. PMP22 excess overloads the proteasome system hence inducing demyelination (Fortun et al., 2006; S. Lee et al., 2018; Lucia Notterpek et al., 1999).

7. Axonal loss

Axonal loss even at early age is a feature of CMT1A patient and rat model. Why these axons die remains unclear. Many hypotheses have been stated.

First, abnormal mitochondrial transport along the axon is a characteristic of the most frequent forms of CMT in which axonal loss is severe (M. A. Saporta et al., 2009) such as dominant CMT2A and recessive CMT4A (Baxter et al., 2002; Pareyson et al., 2015). High mitochondrial

density was observed in myelinated axons of CMT1A dermal biopsies suggesting a defective mitochondrial transport (M. A. Saporta et al., 2009).

Second, in sciatic nerves of rat overexpressing PMP22 *cntf* (ciliary neurotrophic factor) mRNA expression was dramatically downregulated whereas in CMT1A patients' sural nerve biopsies *cntf* transcript was completely absent. *cntf* is a neurotrophic factor, which is produced and secreted by Schwann cells to support the survival of motor and sensory neurons (Sleeman et al., 2000). CNTF protein levels were also decreased suggesting the deficient support of Schwann cells to axons lead to axonal atrophy in late stages of CMT1A (Vigo et al., 2005).

G. Clinical features

Despite the large variability from one patient to another, the most common symptoms include muscle weakness in the feet, ankles, legs and hands, loss of proprioception and pinprick sensation, amyotrophy of the legs giving an aspect of “jambes de coq” and of the hands leading to the famous “mains en griffes” or claw hand symptom, an awkward way of walking (steppage gait) and highly arched i.e. pes cavus and hammertoes or very flat feet i.e. pes planus. In a study by Ribiere et al (2012) patients with CMT1A appear to feel less pain than other CMT patients (Ribiere et al., 2012). In severe cases, patients use a wheelchair (Brennan et al., 2015; Tazir et al., 2014) (Figure 8)

H. Diagnostic tools

When a patient shows the above clinical features i.e. signs and symptoms of a chronic sensorimotor polyneuropathy, CMT diseases must be seriously considered as one of the differential diagnoses. First, a detailed family history must be taken to identify the mode of inheritance. Then, electrophysiological testing is performed followed by molecular analyses to determine the gene causing the disease and for some cases, nerve biopsy (Murphy et al., 2012; Paasen et al., 2014; Pareyson & Marchesi, 2009; A. S. D. Saporta et al., 2011). New emerging techniques in neuroimaging are also becoming more widely used for the diagnosis of CMT diseases (Padua et al., 2017).

1. Family history

Asking the patient if there are other family members presenting similar signs or symptoms helps the physician in determining the mode of inheritance (AD, AR or X-linked). If one parent is affected, AD or X-linked (in cases of no male-male transmission) inheritance is probable. If many siblings are affected but not the parents or if consanguineous marriages occurred, AR inheritance is considered. Family history can be confusing since symptoms are very variable from one patient to another and some patients may go undiagnosed. Therefore, carefulness is required when taking family history. Clinical as well as electrophysiological examination of first-degree relatives is often necessary to establish the inheritance pattern. Family history gives clues towards the most probable type of CMT. For example, in case of AD inheritance, the disease is likely to be CMT1 and in case of AR, CMT4 (Pareyson & Marchesi, 2009; Pisciotto & Shy, 2018; A. S. D. Saporta et al., 2011).

2. Electrophysiological testing

Nerve conduction velocity (NCV) under 38m/s in upper-limb motor nerves with a diffuse and homogeneous pattern points toward CMT1 and CMT4 (demyelinating CMT). Normal or mildly low NCV (NCV > 38m/s in median or ulnar motor nerves) with decreased amplitudes of compound muscle and sensory action potential indicates CMT2. NCV ranging from 25-45m/s in upper limbs (intermediate NCV) are a bit problematic. Those NCVs hint at the possibility of CMT1X in men or dominant intermediate CMT in both men and women (Murphy et al., 2012; Paasen et al., 2014; Pareyson & Marchesi, 2009).

3. Molecular analyses

Electrophysiological test allows determining the CMT type (1-6 or X) and directs toward subsequent genetic tests required to define the CMT subtype such as A-F for CMT1 (Pareyson & Marchesi, 2009). Around 61% of CMT patients are diagnosed by molecular tests at the moment. Approximately 93% of molecular diagnoses are made based on 4 genes: *PMP22*, *GJB1*, *MFN2* and *MPZ* (Murphy et al., 2012).

4. Nerve biopsy

Neuropathology is seldom examined due to recent advances in genetic testing. Nerve biopsy analysis using electron microscopy is useful in sporadic cases or in inherited cases when the main genetic investigations are negative (Pareyson & Marchesi, 2009).

As an example, nerve biopsies from CMT1A patients display abnormal myelination over the whole nerve length (dysmyelination): onion bulbs occurring usually after the age of six, a reduced g-ratio and a low density of myelinated nerve fibers. In sural nerves of 3 years patients, around 7 000 myelinated fibre/mm² can be found while it is around 13 000 in control. While pathological features were seen in proximal nerves and in roots, the most severe pathological changes occurred distally in nerves (Hanemann, Gabreëls-Festen, Stoll, & Müller, 1997; Jacobs & Love, 1985; Paasen et al., 2014).

5. *Neuroimaging*

Peripheral nerve imaging to diagnose neurological diseases is an evolving research field. It has known many advances in recent years. Many techniques can be used such as ultrasound (US), magnetic resonance imaging (MRI), MR neurography and spectral confocal reflectance microscopy (SCoRe) (Deffieux et al., 2018; Heckel et al., 2015; Noto et al., 2015; Padua et al., 2017; Schain, Hill, & Grutzendler, 2014; Zhang, Guo, & Lee, 2018).

a) Ultrasound (US) imaging

Ultrasound (US) imaging of peripheral nerves is becoming more and more useful in differentiating axonal (CMT2) from demyelinating neuropathies (CMT1). Contrarily to CMT2 patients, CMT1 patients show a significant enlargement in their nerves in US imaging. US imaging can also be used to study the disease progression (Padua et al., 2017). US imaging abnormalities of CMT1A patients' median nerve positively correlated with clinical features and negatively correlated with NCV (Noto et al., 2015).

US imaging is a fast advancing field in neuroscience. New techniques like ultrafast US (UFUS) imaging are being developed. This method is based on replacing image acquisitions of 10 frames per second for US imaging by thousands frames per second for UFUS imaging. At first, image quality, resolution, contrast and signal-noise-ratio were worse than regular US imaging due to the lack of focus of UFUS imaging. Therefore, a new technique was recently added aiming at increasing all the UFUS imaging resolution: cascaded dual-polarity waves relying on a pulse wave with positive and negative polarities. This method did not affect the frame rate. It was tested *in vivo* on human back muscle (Deffieux et al., 2018; Y. Zhang et al., 2018). Unfortunately, UFUS imaging has not yet been applied to CMT diseases diagnostic.

b) Magnetic Resonance Imaging (MRI) and Neurography (MRN)

MRI is a type of medical imaging relying on the magnetic properties of hydrogen atoms (“spin”properties) found in all tissues of the human body (Grover et al., 2015). Patients with peripheral neuropathies can be currently diagnosed by Magnetic Resonance Neurography (MRN), a newly developed MRI technique for peripheral nerves. Nevertheless, the resolution of MRN is not very high compared to other photon-based imaging techniques. It cannot distinguish the axon compartment from the myelin compartment in peripheral nerves making it difficult to differentiate demyelinating from axonal neuropathies. The recent development of diffusion tensor imaging (DTI) technique to complete MRN analysis can solve this problem. DTI relies on the diffusion of water molecules in tissues to depict microstructural modifications. The parameters commonly used in DTI are: Fractional Anisotropy which shows the directional preference of water diffusion, Axial Diffusivity indicating diffusion parallel to fiber orientation and Radial Diffusivity evaluating diffusion perpendicular to fiber orientation. In peripheral nerves, Fractional Anisotropy and Radial Diffusivity can be used as imaging markers of myelin sheath integrity whereas Axial Diffusivity can be used as an imaging marker of axon integrity (Heckel et al., 2015).

c) Spectral confocal reflectance microscopy (SCoRe)

In addition, several *in vivo* imaging procedures are still under research. One of these methods is called spectral confocal reflectance microscopy (SCoRe). It has been tested on mouse brain *in vivo* and on postmortem human cerebral cortex. SCoRe is based on a common laser-scanning confocal system, which is relatively easy to implement for clinical applications. Images results from the reflectance signals of a scanning laser at different wavelengths. The light is reflected by myelin itself so there is no need for an endogenous labeling or staining. Each myelinated fiber show a unique striking color pattern due to the combination of its spatial orientation and of the light wavelength that is reflected. The resolution is high enough to detect nodes of Ranvier and Schmidt-Lanterman incisures. So it is possible to use SCoRe technique for identifying many myelin defects. Indeed, the reflectance signal was found to be decreased in case of reduced myelination in the brain of shiverer mice, a model having a *MPZ* gene mutation resulting in no formation of compact myelin in the CNS (Schain et al., 2014). Further research need to be done to find a suitable imaging technique for *in vivo* diagnosis of neuropathies.

I. Outcome measures for clinical trials

CMT diseases gradually progress and worsen with time. To evaluate therapeutic strategies in clinical trials, finding reliable and strong outcome measures allowing for the detection of relatively small changes over time is crucial. The previously described method for diagnostic can of course be used but several additional methods for outcome measures have been developed.

For adults, simple, consistent and validated standardized assessment tools are the following: the CMT neuropathy score (CMTNS) versions 1 and 2, the most recent Rasch analysis-based weighted version, rCMTNS, and the subscales rCMTES (r CMT examination score) and rCMTSS (r CMT symptom score) (Cornett et al., 2017; Grandis & Shy, 2005; Murphy et al., 2012).

For children only one disease-specific scoring system is available: the CMT Pediatric Scale (CMTPedS). This scale includes 11 items evaluating fine and gross motor function, strength, sensation, and balance in 3 to 20-year-old- children (Burns et al., 2012; Cornett et al., 2017).

Beyond these classical clinical scores several novel outcome measures have been proposed recently. First, biochemical biomarkers found in the patients' skin have been investigated. Cutaneous transcripts of *GSTT2* (*Glutathione S-transferase theta-2*), *CTSA* (*Cathepsin A*), *PPARG*, *CDA* (*Cytidine Deaminase*) and *ENPP1* (*ecto-nucleotide pyrophosphatase/phosphodiesterase 1*) (involved in metabolism, negative regulation of cell growth, regulation of fat cell differentiation, vacuolar/lysosomal membrane and exopeptidase activity) were found not only to characterize patients with CMT1A but also to reliably indicated disease severity and progression. Those transcripts represent a potential tool to speed up the finding of a CMT1A therapy in clinical trials (Fledrich et al., 2017).

Second, gait analysis through the characterization, quantification and following over time of locomotor and postural deficits is promising in CMT diseases (Ferrarin et al., 2013; Kennedy, Carroll, & McGinley, 2016; Lencioni et al., 2014, 2015, 2017; Õunpuu et al., 2013). Spatio-temporal parameter (i.e. walking speed), kinematic, related to joint flexion– extension degree (i.e. flexion–extension of the ankle, linked to the CMT locomotor deficit of foot drop due to anterior tibialis weakness) and kinetic, related to muscle strength (i.e. ankle generated power, linked to push-off deficits of CMT patients due to the weakness of the triceps surae) are the three most important parameters of gait analysis to assess patients with CMT. According to Lencioni et al

(2017), gait analysis including the ability to ascend and descend stairs should be part of the clinical evaluation to better characterize impairment when conducting clinical trials (Tiziana Lencioni et al., 2017).

IV. Treatment for CMT1A

So far, no specific treatment is available for CMT1A disease, but several are being developed at preclinical or clinical stages. Meanwhile, at the moment, physical therapy and rehabilitative measures are the only option to alleviate the symptoms of the patients.

A. Physical therapy and associated rehabilitative measures

Surgery used to be the key choice in the past to correct foot deformities in CMT1A. Nowadays, patients undergo less invasive procedures such as physical therapy and associated rehabilitative measures (Kenis-Coskun & Matthews, 2016; Tazir et al., 2014). CMT1A patients are often prescribed ankle-foot arthrodeses with or without special shoes. In order to prevent osteo-articular problems, patients are advised to exercise moderately (Chetlin, Gutmann, Tarnopolsky, Ullrich, & Yeater, 2004; Tazir et al., 2014) and to do some stretching. In order to enhance quality of life, pain medications, psychological support and counseling are given to patients (Tazir et al., 2014). Mobility, ambulation and upper limb function are enhanced by orthotic devices ideally custom crafted for the needs of patients. Ankle foot orthoses (AFOs) fabricated from thermoplastics, metal, leather or carbon fiber material are examples of orthoses (Kenis-Coskun & Matthews, 2016) (**Figure 10**). Nonetheless, CMT patients think that AFOs are uncomfortable and non-esthetic. Thus, anterior elastic AFOs (A-AFOs) were created to boost comfort in patients. Those AFOs are a “footup splint” consisting of a detachable cuff that can be worn around the ankle and tied into the shoes laces, a “Push brace” made of a preformed foam with three elastic straps and a “Multifit Achilles drop foot orthosis”, comprising a half foot plate, a cut-out heel section and an adjustable back stem reaching the calf (Kenis-Coskun & Matthews, 2016; Ramdharry, Day, Reilly, & Marsden, 2012) (**Figure 10**). CMT1A patients with anterior elastic AFO can walk for a longer time and with less physical effort resulting most probably from decreased steppage gait

(Kenis-Coskun & Matthews, 2016; Menotti et al., 2014). The previously mentioned three types of AFOs can decrease foot drop, one typical feature of CMT1A.

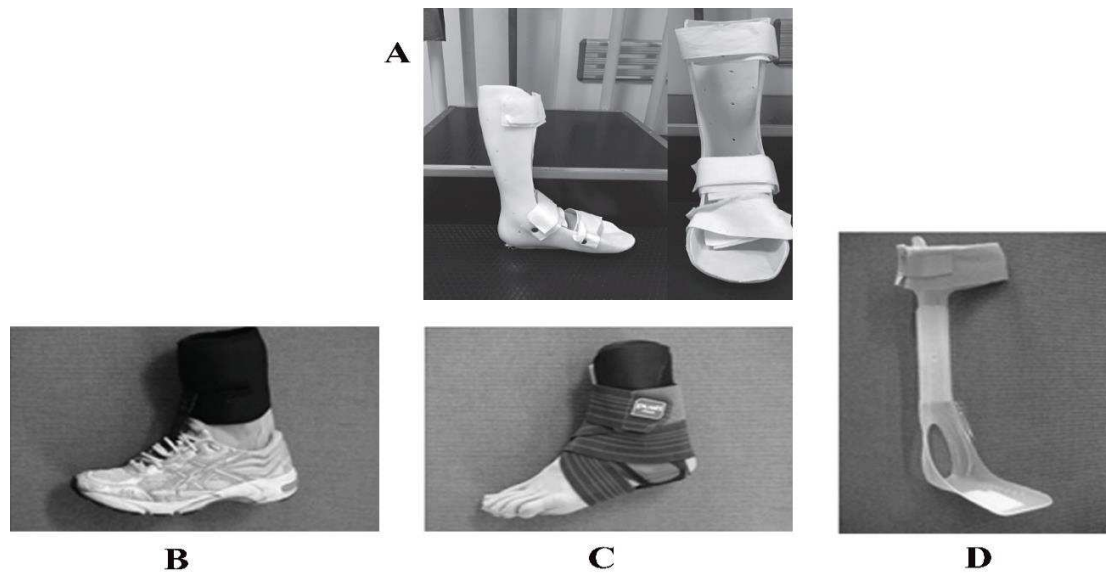


Figure 10 : AFO (Ankle Foot Orthoses): A: Solid; B: Footup splint; C: Push brace; D: Multifit Achilles drop foot orthosis. Adapted from Kenis-Coskun & Matthews, 2016; Ramdharry et al., 2012.

Other than orthotic devices, orthopedic shoes were created to avoid foot drop, to alleviate pain, to enhance gait and to improve walking distance. Those special shoes were produced as weightless as possible (400 g, lighter than regular shoes) (Bensoussan et al., 2016). Furthermore, focal mechanical vibration (fMV) on lower limbs in particular quadriceps and triceps surae improved the balance of CMT1A patients enrolled in the study done by Pazzaglia et al. (Pazzaglia et al., 2016). Upper extremities are often affected in CMT. Their function could be enhanced by a thumb opposition splint. (Kenis-Coskun & Matthews, 2016).

B. Treatment at preclinical stages

Several approaches such as pharmacological and gene therapy have been tested at preclinical level in animal models (**Table 4**).

1. Pharmacological treatments

a) NRG1

According to studies done on transgenic mouse models (Fricker et al., 2011; Michailov et al., 2004; Stassart et al., 2013; Taveggia et al., 2005), soluble NRG1, already used in human trials for heart failure treatment, was suggested as an effective therapeutic candidate to promote nerve regeneration (Gambarotta et al., 2014).

Fledrich et al (2014) tested the efficacy of soluble NRG1 as an experimental therapy in the CMT1A rat and they found that soluble NRG1 was successful in overcoming impaired peripheral nerve development and restoring axon survival into adulthood when dispensed at early age between postnatal days 6 and 18. Therapy enhanced motor performance in a dose-dependent manner; the greatest gain in grip strength without affecting body weight was at the dose of 1 µg/kg. Moreover, soluble NRG1 increased the number of myelinated axons in sciatic nerves reaching wild-type levels and reconstitutes the lowered axonal caliber. In treated rats, CMAP was corrected (increased levels) but NCV did not change. Treatment restored the balance between pro-myelinating Akt pathway and demyelinating MAPK pathway and also lowered the expression of dedifferentiation markers *cJun* and *Sox2*. However, soluble NRG1 therapy neither influenced the differentiation-associated genes nor altered the thickness of myelin sheath in the CMT1A rat. Treatment starting at later ages (from P18 to P90) was not as efficient in CMT1A rats. The clinical phenotype improved but the number of myelinated axons in sciatic nerves and the CMAP showed minor ameliorations and the NCV did not change (Fledrich et al., 2014). Finally, while NRG1 could be used as treatment for human patients, it has serious side effects like an increased risk of cancer (Jabbour et al., 2011).

b) Progesterone antagonist

Progesterone promotes *PMP22* gene expression in Schwann cell cultures and increases *PMP22* mRNA of wild-type rats *in vivo*. In the CMT1A rat, Onapristone, a selective progesterone receptor antagonist originally synthesized for primary breast cancer therapy, was found to decrease *PMP22* mRNA and improve the clinical, electrophysiological and morphological phenotype when injected from 5 days till 7 weeks of age or at a later age (from 5 till 18 weeks of age). Indeed, grip strength as well as CMAP amplitudes were significantly increased in the Onapristone-treated group compared to placebo-treated group. In addition, Onapristone increased the number of mid-

to large caliber myelinated axons (3-4 μm) in the tibial nerve while in the sciatic nerve the number of axons was increased by 7% in the Onapristone-treated group compared to placebo-treated diseased rats after 5 months of treatment. Hence, Onapristone prevented axonal loss. Nevertheless, treatment did not change NCV or myelin thickness. No toxicity signs were observed (M. W. Sereda, Meyer Zu Hörste, Suter, Uzma, & Nave, 2003; Zu Horste et al., 2007).

c) Inhibition of the P2X7 receptor

Intracellular calcium is abnormally increased in Schwann cells from CMT1A rat. Those high concentrations were found to be due to PMP22-associated overexpression of the P2X7 purinoreceptor/channel resulting in extracellular calcium influx into CMT1A Schwann cells (refer to Introduction III.F.5). Pharmacological inhibitors of P2X7 (example KN-62, oxidized ATP) can correct calcium levels in CMT1A Schwann cells, therefore restoring the migration and the secretion of CNTF by Schwann cells. In addition, myelination is improved in co-cultures of CMT1A Schwann cells with dorsal root ganglion sensory neurons (Nobbio et al., 2009). An in vivo study in CMT1A rats showed that 3 mg/kg of the P2X7 receptor pharmacological antagonist A438079 given intraperitoneally every day at the age of one month and for 11 weeks was well tolerated and improved the behavioral as well as the morphological phenotypes. Grip strength was higher in the A438079-treated group compared to vehicle-treated diseased rats. The expression of Schwann cell differentiation markers *Mpz* and *Hmgcr* were significantly increased and de-differentiation markers *c-jun* along with *Ki67* were significantly decreased in A438079-treated CMT1A rats. Macrophage-mediated myelin degeneration and axonal damages were reduced by A438079 treatment. Nevertheless, treatment did not improve the NCV or CMAP (Sociali et al., 2016).

d) Wlds transgene and nicotinamide

Wlds (Wallerian degeneration slow) is a phenotype that spontaneously occurred in a mouse strain in London, UK. After nerve injury these mice showed a delayed axonal degeneration and demyelination due to the recombination of a gene expressed in axons (Coleman et al., 1998). Wlds gene is a chimeric gene between Ubiquitination factor 4B and nicotinamide mononucleotide adenylyl transferase 1 (*Nmnat1*) enzyme (Coleman et al., 1998; T. G. Mack et al., 2001). The mechanism of action is still unknown but the expression of Wlds gene in rat, drosophila and even human neurons in culture preserve axonal degeneration. Meyer zu Horste et al (2011) tested

whether Wlds and nicotinamide prevent axonal loss in CMT1A. CMT1A rat were crossbred with rat expressing Wlds in neurons. A heterozygous double transgenic (PMP22 and Wlds) rat called “CMDS” rat was generated. CMDS rats presented improved clinical impairments (higher grip strength, NCV and CMAP amplitude) and decreased axonal loss of mainly larger caliber axons versus CMT1A rats. However, Wlds transgene did not affect dysmyelination since like in the CMT1A rat, hypermyelination of small caliber axons and hypomyelination of larger ones were observed in tibial nerves’ histological sections (Meyer zu Horste et al., 2011).

The neuroprotective effect of Nicotinamide was observed after nerve crush injury in young adult wild-type rats. However, nicotinamide therapy from 5 till 13 weeks of age didn’t prevent axonal loss and impairment in strength in CMT1A rats (Meyer zu Horste et al., 2011).

2. *Gene therapy*

a) Neurotrophin 3 for CMT1A and CMT1E

Neurotrophin-3 (NT-3) is a neurotrophic factor that preserves axon from generation. Both Schwann cells and muscles express NT-3 (Meier et al., 1999; Sahenk et al., 2014). NT-3 levels decrease following nerve injury and are upregulated during peripheral nerve regeneration (Frostick, Yin, & Kemp, 1998). In addition NT-3 belongs to an autocrine survival loop which contributes to survival and differentiation of SCs without the axon (Meier et al., 1999; Mirsky et al., 2002; Zarife Sahenk et al., 2014). NT-3 administration was shown to enhance axonal regeneration and remyelination process. Nevertheless, NT-3 possesses a short half-life and needs to be continuously administrated. Hence, a more beneficial way of conveying NT-3 is through an adeno-associated virus (AAV) gene transfer. Sahenk et al (2014) tested this possibility first using the trembler J (TrJ) mouse, a naturally occurring animal model of CMT showing a point mutation in the gene PMP22 (Zarife Sahenk et al., 2014). TrJ mice were injected intramuscularly with a single injection of 1×10^{11} vector genome (vg) of AAV1.CMV.NT3. NT-3 was injected in the muscle because the goal of the therapy was to preserve axons and muscle allows for a long-lasting biological systemic effect due to a continuous discharge (CMV: Cytomegalovirus) (Zarife Sahenk et al., 2014). Treated mice showed a significant improvement of grip strength starting around 10 weeks after injection and rotarod performance between 20 and 40 weeks post injection compared to PBS-injected controls. Improved myelin thickness and CMAP amplitude were mostly seen in small and medium sized fibers 20 weeks post injection (Table 4). This NT3 therapeutic strategy

has currently moved to clinical trials (NCT03520751). For further details refer to Introduction IV.C. 4.

b) PMP22 antisense oligonucleotides (ASO)

ASOs are single-stranded synthetic deoxynucleotides that bind target mRNA via Watson-Crick base pairing, resulting in degradation of target mRNA by RNase H, a ubiquitously expressed mammalian enzyme (Rinaldi & A Wood, 2017; Zhao et al., 2017). Zhao et al showed that treating weekly intraperitoneally C22 mice and CMT1A rat (two CMT1A murine models, ***Table 2***) with ASOs after start of disease effectively decreases PMP22 mRNA in affected nerves. NCV and CMAP were increased in both CMT1A rodent models. Moreover, ASO therapy improved rotarod and grip test performance in treated diseased mice (Zhao et al., 2017). However, no effect was shown on behavioral performance of CMT1A rats and the treatment strategy was inconsistent as rats overexpressing mouse PMP22 were treated with an ASO targeting endogenous rat PMP22, while an ASO targeting mouse PMP22 was available. A comparison of my work with the data presented in this article is shown in the discussion part.

C. Clinical trials

1. *Ascorbic acid and creatine (vitamin trials)*

Ascorbic acid and creatinine did not show improvements in treated CMT1A patients (dowling, 2018). Ascorbic Acid is critical to trigger myelination *in vitro* and *in vivo*. Lack of ascorbic acid is associated with femoral peripheral neuropathies. In a preclinical study treatment of the C22 mouse model of CMT1A with high doses of ascorbic acid improved the grip test and rotarod performance, as well as the number of myelinated fibers (Passage et al., 2004). As ascorbic acid relatively easy to produce and is approved for human treatment, a phase 2 clinical trial was organized. Although the treatment was indeed safe and well-tolerated, no significant improvement could be found in treated patients versus placebo treated (Lewis et al., 2013; Mandel et al., 2015; Pareyson et al., 2011) (***Table 4***).

Creatine is a natural substance that plays an important role in the energy metabolism of muscle. Creatine supplements improve repeated maximal exercise performance and recovery from

exercise. It was given orally to a small cohort of 20 patients. No difference was observed between treated CMT1A patients and placebo groups (Chetlin et al., 2004) ([Table 4](#)).

2. **PXT3003**

PXT3003 is a three-drug-combination therapy or what is named as ‘pleotherapy’ by Pharnext. The drugs, baclofen, naltrexone and D-sorbitol are given at a low dose and they are already approved (Tazir et al., 2014). Baclofen (BCL) is an agonist of GABAB receptor. It reduces the activity of adenylate cyclases including intracellular cAMP which positively regulate PMP22 expression. BCL is a safe drug since it is already utilized as spasticity therapy. Naltrexone (NTX) is an opioid receptor antagonist. It also decreases intracellular levels of cAMP. Like BCL, it is safe and currently on the market to treat drug addiction. Finally, D-sorbitol (SRB) plays a role in energy production/storage (polyol pathway). It might improve PMP22 protein folding that is impaired when overexpressed in CMT1A Schwann cells (Chumakov et al., 2014).

In vitro testing proved the efficacy of PXT3003 and the synergy of the three-drug combination. Treating with PXT3003 myelinating co-cultures of dorsal root ganglion (DRG) neurons with Schwann cells derived from CMT1A rats improved myelination. In CMT1A rats, PXT3003 decreased PMP22 mRNA. Treatment also ameliorated the clinical electrophysiological and morphological phenotype of CMT1A rats (Chumakov et al., 2014).

As demonstrated by clinical trial phase 2, PXT3003 therapy is safe and tolerable. Most of treatment-emergent adverse events including gastrointestinal disorders, nausea and nervous system disorders were mild and not dangerous. The highest dose showed the best improvements of the clinical phenotype in the four functional measures done (6MWT=6 Minute Walk Test, Ankle dorsiflexion, Hand Grip and 9HPT=9-Hole Peg Test). Electrophysiological measures suggested a possible improvement of myelin function, but no imaging of myelin has been possible. Distal motor latency was slightly but significantly lower in the high dose group comparing to placebo and motor conduction velocity increased even if it is not statistically significant (Attarian et al., 2016). PXT3003 significantly improved disease progression in CMT1A patients measured with classical clinical scores CMTNS and ONLS (Overall Neuropathy Limitations Scale) (Mandel et al., 2015). PXT3003 is in phase III clinical trial since December 2015 (check the website cited after the bibliography and enter this number [NCT02579759](#)) ([Table 4](#)).

3. *ACE-083 for CMT*

ACE-083 is a therapeutic candidate acting on myostatin (GDF8) and other members of TGF-beta superfamily to improve skeletal muscle growth. When this drug is injected in some muscles, it increases their mass and strength. This was initially demonstrated in a mouse model of neuromuscular diseases, but it is also beneficial in the CMT mouse model Trembler-J. This treatment can be applied to CMT patients displaying a mild-moderate disease phenotype involving specific muscles (Glasser et al., 2018) ([Table 4](#)).

A phase 1 clinical trial study in healthy volunteers resulted in significantly dose-dependent higher muscle volume. However, no significant effect was detected in muscle strength. Furthermore, ACE-083 was safe and well-tolerated (Glasser et al., 2018); [NCT02257489](#)). Adverse events were mild and similar between placebo and treated individuals. The administration route being a local injection in muscles, injection site pain was the most frequent adverse effect. Most of those effects were reported at the time or right after dosing and resolved shortly after. Since 31 July 2017, there is an ongoing phase 2 clinical trial in CMT1A or CMTX patients with the foot drop symptom (mild-moderate ankle dorsiflexion weakness and mild plantar flexion weakness). This trial is expected to end in July 2019 ([NCT03124459](#)) .

4. *Gene therapy approach*

In a pilot clinical trial, recombinant methionyl human NT-3 (r-metHuNT-3) was tested on 8 CMT1A patients. Participants received either placebo or 150 µg/kg r-metHuNT-3 three times a week for 24 weeks. Improvement of motor, reflex and sensory abilities was seen in NT3-treated group versus placebo. Sural nerve biopsies were collected before and after treatment on treated and on placebo patients. Axonal regeneration improved after NT3 treatment (Z. Sahenk et al., 2005).

The following phase I/ IIa clinical trial has been setup using recombinant virus AAV1.tMCK.NT-3 ([NCT03520751](#)). Triple muscle-specific creatine kinase (tMCK) is the promoter controlling the coding sequence (Zarife Sahenk et al., 2014). The goal was to assess a gene therapy approach to treat CMT1A in an open-label (both the researchers and participants know which treatment is being administered), one-time injection ascending dose study. AAV1.tMCK.NTF3 was administered intramuscularly into both legs muscles of 9 CMT1A

subjects aged 15 to 35 years old. The patients are injected with 2×10^{12} vg/kg or 6×10^{12} vg/kg ([NCT03520751](#)) (***Table 4***).

5. *Other Ongoing clinical trials*

The anti-progestin Ulipristal Acetate (EllaOne®) is a drug that antagonizes progesterone activity. It has been developed and tested for long-term safety in the frame of endometrial fibroma treatment. As progesterone promotes PMP22 expression in SCs (Désarnaud et al., 2000; M. W. Sereda et al., 2003; Zu Horste et al., 2007), the anti- progestin EllaOne drug was also evaluated in a clinical trial phase 2 in order to improve the phenotype of CMT1A patients. No results are available yet, but the trial has been terminated prematurely in 2017 because serious hepatic side effects occurred in some patients treated for fibroma ([NCT02600286](#)) (***Table 4***).

MD1003, a high-dose pharmaceutical-grade biotin drug, has been assessed for effect on motor and sensory conduction in demyelinating neuropathies patients including CMT1A. No results for CMT1A are available yet. Biotin is a cofactor for an enzyme involved in fatty acid synthesis, which is critical for the myelin sheath. Biotin treatment had been suggested to be efficient for the treatment of multiple sclerosis. ([NCT02967679](#); Tourbah et al., 2018) (***Table 4***).

Table 4 : Treatment options for CMT1A.

Name	Aim	Design	Animal model	Results
NRG1	Restore axonal survival	<ul style="list-style-type: none"> • P6-P18 IP injection every 2 days. • Different doses: 0; 0.1; 1; 10; 50 µg/ kg 	CMT1A rat	<ul style="list-style-type: none"> • Better motor performance. • Increased number of myelinated axons in sciatic nerves. • CMAP corrected but not NCV. • Restored balance between Akt and MAPK pathway. • No effect on differentiation genes. • No effect on myelination.
Onapristone	Decrease PMP22 excess	<ul style="list-style-type: none"> • Progesterone receptor antagonist • Subcutaneous time-release pellets 5 days - 7 weeks or 5 till 18 weeks • 20mg/kg/day 	CMT1A rat	<ul style="list-style-type: none"> • Increased muscle strength, CMAP, mid-large myelinated axons in tibial and sciatic nerves. • No change in NCV. • No effect on myelination.
A438079	Correct calcium levels	<ul style="list-style-type: none"> • P2X7 receptor antagonist • IP daily injection from 1-2 month of age • 3mg/kg 	CMT1A rat	<ul style="list-style-type: none"> • Increased muscle strength and Schwann cell differentiation markers. • Decrease de-differentiation markers, myelin degradation and axonal loss. • No change in NCV or CMAP.
Wlds transgene	Prevent axonal loss		CMDS (CMT1Ax Wlds)	<ul style="list-style-type: none"> • Higher grip strength, NCV and CMAP amplitude. • Decreased axonal loss of mainly larger caliber axons. • No effect on dysmyelination.

Nicotinamide	Prevent axonal loss	Daily IP injections from 5-10 week of age, 500 mg/kg	CMT1A rat	No effect on axonal loss or on muscle strength.
NT-3	Preserve axon from degeneration	Single intramuscular injection of 1×10^{11} vg of AAV1.CMV.NT3	TrJ mice	Improvement of grip strength and Rotarod performance, thickness of myelin and CMAP amplitude mostly in small and medium sized fibers.
ASO	Decrease PMP22 excess	Intraperitoneal injections	CMT1A rat and C22 mouse	<ul style="list-style-type: none"> Increased NCV and CMAP in both animal models. Improved motor phenotype in treated C22 mice.
Ascorbic acid	Trigger myelination	110 individuals initially, aged 13 to 70 years, randomized, double masked, controlled trial with 4:1 allocation to oral ascorbic acid or matching placebo, 4g/day for 2 years. Not all completed the study (3 withdrawals) due to adverse event	C22 mice (pre-virus studies)	<ul style="list-style-type: none"> In mice, improved motor performance and increased number of myelinated fibers. No effect on patients.
Creatine	Important role in the energy metabolism of muscle.	Double blind trial, 20 patients, daily oral administration, 5g/day, with resistance training during 12 weeks		No difference between treated CMT1A patients and placebo.
PXT3003	Decrease PMP22 excess	323 participants. Randomized triple masking phase 3 clinical trial. Combination of 3 drugs: baclofen, naltrexone and D-sorbitol (NCT02579759).	Preclinical studies in vitro and in CMT1A rats	<ul style="list-style-type: none"> In vitro improvement of myelination Decreased PMP22 and better clinical, electrophysiological and morphological phenotype in rats and in patients except for myelin function, no possible imaging in humans. Safe and tolerable in humans.

ACE-083	Improve skeletal muscle growth	Phase 1 non-randomized, open-label clinical trial (NCT02257489) completed and ongoing randomized, double-blind and placebo-controlled phase 2 (NCT03124459). 42 participants. Bilateral tibialis anterior intramuscular injection of maximum 250 mg/muscle, once every 3 weeks for up to 17 doses.	Pre-clinical studies in TrJ mice and mouse model of neuro-muscular disease	<ul style="list-style-type: none"> • Dose-dependent higher muscle volume in healthy volunteers (phase 1 results). • Safe and well tolerated treatment; mild adverse events mostly related to administration route.
EllaOne (Ulipristal Acetate)	Progesterone antagonist	23 participants, randomized, triple masking phase 2 clinical trial (NCT02600286)		Long term safety tested for endometrial fibroma treatment CMT1A trial terminated due to serious hepatic side effects occurred in some patients treated for fibroma.
MD 1003 (Biotin)	Critical for myelin sheath	15 participants, open label phase 2 for CMT1A and other Peripheral Neuropathy		Efficient for the treatment of multiple sclerosis.
AAV1. tMCK. NT-3	Preserve axon from degeneration	9 CMT1A subjects aged 15 to 35 years old Open-label label, one-time injection phase I/IIa clinical trial. Intramuscular injection into both legs muscles of 2×10^{12} vg/kg or 6×10^{12} vg/kg (NCT03520751).	Refer to above	Improvement in motor, reflex and sensory abilities as well as axonal regeneration.

References cited in the text above.

V. Gene therapy

Gene therapy or the concept of treating an inherited disease with no cure by correcting or replacing a defective gene within the affected cells has long captivated scientists, clinicians and the general public (Naldini, 2015; Piguet, Alves, & Cartier, 2017). However, this approach still raises concerns and fears towards safety and possible consequences (Wirth, Parker, & Ylä-Herttuala, 2013). There are two types of gene therapy (germline and somatic). Gene therapy went through a long and difficult journey from concept to clinical application in several fields of medicine (Dunbar et al., 2018). In order to translate to clinical trial, finding the safest and most efficient delivery method of the therapeutic gene is essential (Naldini, 2015).

A. Types of gene therapy

In germline gene therapy, the therapeutic or modified gene is passed along to the next generation. This category of gene therapy is not allowed by current legislation. In somatic gene therapy, the therapeutic or modified gene is inserted in some target cells without passing along to the next generation (Wirth et al., 2013).

For *ex vivo* somatic gene therapy, diseased human cells are isolated, cultured and genetically altered outside the body through non-viral or viral-mediated gene transfer (Naldini, 2015; Wang & Gao, 2014). In this way, safety and target cell specificity are improved since the body is not directly exposed to gene delivery vectors. Furthermore, the genetically-altered cells are autologous cells from the patient him/herself, hence avoiding the risk of graft-versus-host disease frequently observed in hematopoietic stem cell transplantation between two persons. Stem or progenitor cells with transgene integrated into host genome in addition to integrating viral vectors are most widely used for *ex vivo* gene therapy. For *in vivo* somatic gene therapy, vectors (viral and non-viral) are used to deliver the therapeutic or modified gene to patients (Wang & Gao, 2014). I will develop further the *in vivo* somatic gene therapy in the following paragraphs.

B. Delivery methods

Vectors (gene delivery vehicles) are divided into two main categories: non-viral and viral (Wang & Gao, 2014).

1. *Non-viral vectors (DNA vectors)*

A therapeutic gene expression cassette including a gene transcription promoter, the transcript of interest and a termination signal ending gene transcription can be enclosed in a circularized, double stranded DNA molecule, plasmid DNA (pDNA) serving as a delivery vehicle. Several direct *in vivo* injection techniques exist. The most efficient one is rapidly injecting a large amount of pDNA solution in major organs while temporarily causing pores in cell membrane. This method is known as hydrodynamic injection (D. Wang & Gao, 2014; Wang, et al., 2013). In order to help negatively charged pDNA molecules entering the hydrophobic membranes of cells, pDNA can be compressed into lipoplexes and polyplexes respectively by cationic lipids and cationic polymers. Those cationic lipids and polymers protect pDNA from degradation by nuclease and help penetration into target cells (Jin et al., 2014; Wang & Gao, 2014). To obtain a successful transgene expression, pDNA has to pass through important cellular surveillance mechanism barriers leading for example to a destructive innate immune response when Toll-Like Receptor 9 detects unmethylated CpG dinucleotides in pDNA (Barton, Kagan, & Medzhitov, 2006; D. Wang & Gao, Guangping, 2014). To avoid this, minicircle DNA (mcDNA) that do not possess CpG-rich backbone sequences have been designed (Mayrhofer et al., 2009; Wang & Gao, 2014). This mcDNA also leads to safer, higher and more sustainable transgene expression than classic pDNA (Gill et al., 2009; Wang & Gao, 2014). A part of DNA vector goes to the nucleus and form a non-integrating, episomal DNA leading to transgene expression. Nevertheless, this non-replicable DNA is lost when cells are dividing. Moreover, this DNA tends to be degraded in cells. Consequently, transgene expression is temporary. A scaffold matrix attachment region (S/MAR) might be added to the vector to replicate and retain episomal DNA in daughter cells (Argyros et al., 2011; Wang & Gao, 2014)

The advantages of DNA vectors are an easy production, the large cassette of expression, and the absence of a viral component thus low immunotoxicity. However, DNA vectors are relatively easily degraded and much less effective in gene delivery than viral vectors (D. Wang & Gao, Guangping, 2014).

2. *Viral vectors*

Viruses, naturally evolved microorganisms, have developed many ways to infect cells where they could use the host machinery to replicate their viral genetic material and produce viral proteins. One way for viruses to enter the cell is endocytosis (Vannucci et al., 2013; Wang & Gao, 2014). This concept has encouraged scientists to explore viruses as gene delivery vectors for therapy and in particular viruses that can be manipulated to be non-replicative (they infect but cannot reproduce themselves). A wild-type viral genome is composed of several viral genes and signal sequences that serve for viral life cycle. Viral vectors can be produced in cells in cultures. The majority of viral genes are replaced by a therapeutic cassette in order to limit viral toxicity and pathogenesis, whereas the signal sequences are kept to synthesize a sufficient amount of vector particles. The current most frequently utilized viral vectors for gene therapy are the retrovirus, the herpes simplex virus (HSV), the adenovirus (AdV) and the adeno-associated virus (AAV) (Herzog, Cao, & Srivastava, 2010; Vannucci et al., 2013; Wang & Gao, 2014) (*Table 5*).

a) Retrovirus

Retroviruses include gammaretroviruses and lentiviruses. They are single-stranded RNA viruses. They use virus-derived reverse-transcriptase and integrase enzymes for inserting their proviral complementary DNA into the host genome. Gammaretrovirus only transduce replicating cells whereas lentivirus transduce both replicating and non-replicating cells (Sakuma, Barry, & Ikeda, 2012; D. Wang & Gao, Guangping, 2014). The glycoproteins present on the envelope of those two types of virus could be altered hence allowing specific tissue/cell tropism (Vannucci et al., 2013; D. Wang & Gao, 2014). Retroviral vectors are capable of integrating the host genome. This is not only an advantage of ensuring the stability of transgene and persistence of transgene expression to daughter cells following genome replication and cell division but also a disadvantage: the threat of insertional mutagenesis (Fehse & Roeder, 2008; Wirth et al., 2013) and the risk to cause cancer by possibly disrupting tumor suppressor genes or activating oncogenes (Hacein-Bey-Abina et al., 2010; D. Wang & Gao, Guangping, 2014). To avoid insertional mutagenesis, targeted integration of transgenes to predefined genomic sites has been the topic of many research studies. Zinc finger nucleases, meganucleases or transcription activator-like effector nucleases have been used to cleave genomic DNA at a specific site so that targeted integration occurs (Marcaida et al., 2010; Mussolino & Cathomen, 2012; Urnov et al., 2010). To elude the cancer risk, self-inactivation vectors in addition to modifying the viral integrase have

been created (Lombardo et al., 2007; Provasi et al., 2012; D. Wang & Gao, 2014; Yáñez-Muñoz et al., 2006; Zufferey et al., 1998) (**Table 5**).

b) Herpes simplex virus (HSV)

HSV is a double-stranded DNA virus. Being naturally neurotropic, it is suitable for treating neurological disorders. As HSV is retrogradely transported in neurons; their uptake at sensory nerve terminals following skin or mucous membrane infection, allows gene modifications in neuronal nucleus in the cell body. Some HSV have been designed to produce cell death factor and they are used to treat cancer by inducing oncolysis in transduced tumor cells (Manservigi et al., 2010; D. Wang & Gao, 2014) (**Table 5**).

c) Adenovirus (AdV)

AdV are double stranded DNA viruses. Contrarily to retroviruses, Adv do not integrate the host genome and thus do not cause insertional mutagenesis. AdV form an episomal DNA in the host nucleus. AdV can transduce a large range of cells going from quiescent to proliferating cells and passing by tumor cells. However, the main downside of this vector is its strong immunogenicity in many mammals and in human in particular injection (Lehrman, 1999; D. Wang & Gao, 2014). AdV are still used for infecting and killing tumor cells (oncolysis like HSV) and for vaccination, which requires activation of the immune system (**Table 5**).

d) Adeno-Associated Virus (AAV)

AAV are single stranded DNA viruses. Nowadays, AAV vectors are among the most commonly used viral vectors for gene therapy. Formerly, since it has not been classified as a pathogen, not much was known about this virus. The absence of disease associated with this virus, the persistence of the virus in cells *in vivo*, the ability to transduce non-dividing cells and the diversity of the serotypes have improved the potential of AAV as a delivery tool for gene therapy applications (Daya & Berns, 2008; Grieger & Samulski, 2012; Okada, 2013) (**Table 5**).

i. AAV physical properties

Wild-type AAV is a small (20-26nm), single-stranded encapsulated DNA, non-enveloped parvovirus. Its linear genome is composed of two open reading frames containing the *rep* and *cap* genes bordered by inverted terminal repeats (ITRs) (Grieger & Samulski, 2012). The ITR can pair with themselves through a T-shaped hairpin structure, contain cis elements required for replication

and packaging (Koczot et al., 1973). Four non-structural proteins (Rep78, Rep68, Rep52, and Rep40) and three capsid proteins (Cap: VP1, VP2, and VP3) are encoded by those two genes (Grieger & Samulski, 2012; Okada, 2013; Young et al., 2000).

The large Rep proteins (Rep78 and Rep68) regulate viral replication through the production of DNA binding, site-specific and strand-specific endonuclease activities and DNA-RNA and DNA-DNA helicase activities. Rep78 and Rep68 are essential for facilitating targeted integration into the human genome on chromosome 19 at the AAVS1 designated locus (Grieger & Samulski, 2012; Okada, 2013; Young et al., 2000).

The small Rep proteins (Rep52 and Rep40) play a role in accumulating the single-stranded viral genome in order to package within AAV capsids (Grieger & Samulski, 2012; Okada, 2013). Transcripts utilizing p5, p19 and p40 promoters produce respectively the large Rep proteins (Rep78 and Rep68), the small Rep proteins (Rep52 and Rep40) and capsid proteins (Grieger & Samulski, 2012; Okada, 2013; Qiu & Pintel, 2008; Young et al., 2000).

The three capsid proteins differ in their N-terminus residues. The VP1 protein comprises phospholipidase that is necessary for infectivity while the VP2 and VP3 proteins form the structure of the envelope coat, the capsid (Girod et al., 2002; Grieger & Samulski, 2012).

ii. AAV infection cycle

Wild-type AAV uses the host cell polymerase for its own replication since it does not encode any (K I Berns, 1990). AAV enters the host cell via receptor mediated endocytosis and it is then transported to the nucleus by clathrin coated vesicle (Bartlett et al., 2000). In the nucleus, the virion sheds its capsid and releases its genome (Ding et al., 2005; Srivastava, 2008). The particularity of AAV is that viral genome of wild-type AAV replicates only in the presence of a co-infected helper virus such as an adenovirus. In the absence of this helper virus, AAV integrates into the host cell genome on the specific locus AAVS1 of human chromosome 19. This integration occurs because the Ying Yang 1 (YY1) transcription factor prevents p5 viral promoter to produce viral proteins (Berns & Linden, 1995; Pereira et al., 1997) (**Figure 11**).

Specific genes of the helper adenovirus are required for AAV replication such as: E1A, E2A, E1B 55, E4 (ORF6) and viral associated proteins. E1A associates with the YY1 repressor thus p5 can initiate the expression of large amounts of Rep68/Rep78. E2A promotes AAV

replication *in vitro*. The E1B 55 and E4 (ORF6) proteins stimulate AAV replication and second strand DNA synthesis (Fisher et al., 1996; Samulski & Shenk, 1988; Ward et al., 1998). By blocking the phosphorylation of EIF2 alpha translation factor, the viral associated proteins trigger AAV expression. This factor inhibits AAV gene expression when phosphorylated (Nayak & Pintel, 2007). In addition, UV radiation and hydroxyurea that lead to cell stress naturally intensify AAV replication (Yalkinoglu et al., 1988).

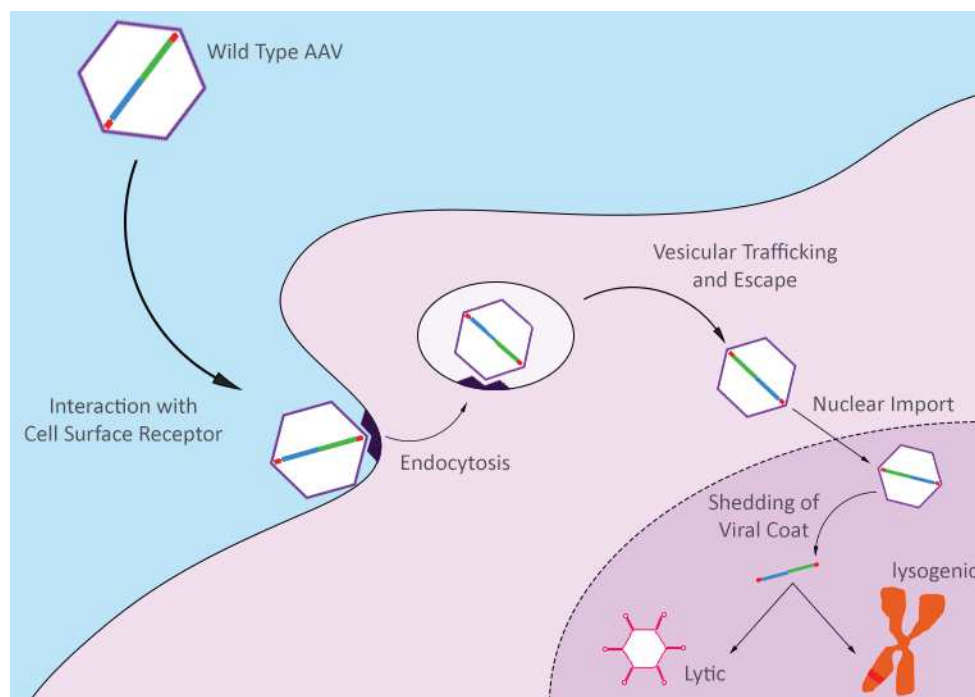


Figure 11 : AAV infection cycle: AAV enters the cell via endocytosis and is transported to the nucleus. In the nucleus it sheds its capsid and releases its genome. It replicates only in the presence of a helper virus (lytic cycle). In the absence of the helper virus, AAV integrates into the host cell genome (lysogenic cycle). Adapted from https://www.abmgood.com/marketing/knowledge_base/Adeno_Associated_Virus_Introduction.php#14

iii. Recombinant AAV (rAAV)

In 1984, some researcher replaced the viral genome of AAV by a simple transgene and transfected it into cells infected with adenovirus. This led to the generation of modern days AAV adaptations: recombinant AAV (rAAV) (Carter, 2004; Grierger & Samulski, 2012).

Modern day rAAV vectors are now produced by substituting the entire AAV viral genome between the ITRs with an expression cassette of approximately 5 kb. Afterwards, the essential

genome of AAV is provided by two plasmids: one delivering the *rep* and *cap* genes in trans (separate from the ITR/Transgene cassette) and the other carrying the adenoviral helper genes. These three plasmids are co-transfected in packaging cells to produce infectious viral particles. These viral particles are non-replicative because they lack the replication gene *rep* (Grieger & Samulski, 2012).

It is now possible to control the rAAV tropism by switching the serotype through the alteration of the *rep* and *cap* genes. It is important to note that since the rAAV does not possess the *rep* gene along with its cis-active intergenic expression element that are both needed for site specific integration, rAAV stays as an extra chromosomal element in the cell, as an episome (Carter, 2004; Daya & Berns, 2008; Grieger & Samulski, 2012).

iv. AAV serotypes and tropisms

At least 10 serotypes of AAV have been characterized each with its own unique traits and tropisms. Tropism is determined based on differences between cell surface receptors of AAV serotypes. It might as well be affected by cellular uptake, intracellular processing, nuclear delivery of the vector genome, uncoating, and second strand DNA synthesis (Wu et al., 2006). AAV1 and AAV5 transduce almost the same cells (vascular endothelial cells). However, AAV5 efficiently transduces astrocytes, whereas AAV1 effectively transduces retina, heart and lung tissue (Chen et al., 2005). AAV 1 and AAV7 transduce efficiently murine skeletal muscle while AAV2, the most widely studied AAV serotype is able to infect various tissues with a preference towards skeletal muscles (Manno et al., 2003), neurons (Bartlett et al., 1998), vascular smooth muscle cells (Richter et al., 2000) and hepatocytes (Koeberl et al., 1997). AAV2 can also kill breast cancer cells without affecting normal mammary epithelial cells (Alam et al., 2011; C. Gao, Zhang, Zheng, & Wang, 2018). AAV3 targets CNS/retina, heart and liver. AAV4 tropism is towards heart and lung cells because it is present mostly in the chest of the host after infection. AAV6 highly transduce airway epithelial cells with a lower immunogenicity compared to AAV2 (G.-P. Gao et al., 2002; Halbert, Allen, & Miller, 2001; Rabinowitz et al., 2004). AAV7 and AAV 8 both transduce hepatocytes with a higher efficiency for AAV8 (Zincarelli et al., 2008). Intravenous injection of AAV8 in dogs transduced most tissues including skeletal muscles, diaphragm, heart and liver but not the brain nor the pancreas nor the thymus cells (Mack et al., 2017). AAV9 targets CNS, heart, lung, liver and skeletal muscle (Armbruster et al., 2016; Zincarelli et al., 2008). AAV9 can cross the blood

brain barrier after intravenous injection (Armbruster et al., 2016; Foust et al., 2009; Gray et al., 2010; Haurigot et al., 2013). After intracerebral injections, AAV10 efficiently transduces the central nervous system (injected hemisphere, cerebellum and cervical spinal cord) but is also detected in other organs such as the liver, the spleen, the lymph nodes and blood but not the gonads (Zerah et al., 2015). AAV viral vector tropism is different depending on animal species. For example, in dogs, AAV8 vector infection of the liver is much lower than in mice and nonhuman primates (Bell et al., 2011; Mack et al., 2017; Nathwani et al., 2007; Nietupski et al., 2011; L. Wang et al., 2011).

v. AAV Pseudotyping

Pseudotyping is defined as the substitution of the capsid of one serotype (usually AAV2) with the capsid of another serotype. This process could lead to different transduction efficiency and tropism profiles (Auricchio, 2003; Balaji et al., 2013). Furthermore, pre-existing immune response against one serotype could be avoided with a capsid from another serotype (Auricchio, 2003). For example, rAAV2/5 designates a virus holding the genome of serotype 2 packaged in the capsid from serotype 5. After brain injections, thanks to the serotype 5 capsid this pseudotyped virus targets neurons that are not transduced by rAAV2; the primary neurons in pyramidal layers of the hippocampal brain area. In addition, rAAV2/5 is more widely distributed in some brain areas than rAAV2. Furthermore, transduction frequencies are higher for rAAV2/5 compared to rAAV2 (Burger et al., 2004). Another example of a more efficient transduction of pseudotyped virus compared to classic one is AAV2/9 after stereotaxic brain surgery for viral injection (Vincent, Gao, & Jacobson, 2014).

vi. AAV advantages and disadvantages:

In comparison to other viral vectors such as lentivirus and adenovirus which both infect most dividing/non-dividing cells with a high transduction rate in particular for adenovirus, AAV serotypes are more cell-specific, while they also infect both dividing and quiescent cells (Vannucci et al., 2013) (**Table 5**).

While 10% of wild-type (WT) AAV may integrate the genome, recombinant AAV (rAAV) usually do not integrate the genome; which prevent the insertional mutagenesis characteristic of lentivirus. Nevertheless, the episomal double-stranded DNA of AAV persist in non-dividing cells for a long time without damaging the host cell (R. H. Smith, 2008).

Furthermore, contrarily to lentivirus and adenovirus which both cause respectively a high or very high immune response, AAV only causes a very mild immune response and an almost negligible pathogenicity. Even though AAV is highly found in the human population and that more than 80% of adults aged 20 years and more have neutralizing antibodies to AAV serotypes 1, 2, 3 and 5, no known illness is linked to AAV (Giacca & Zacchigna, 2012; Vannucci et al., 2013).

On the other hand, the main disadvantage of AAV is its relatively small genome size (5Kb) that restricts the inserted gene size to less than 4.5 kb in length compared to lentivirus (9Kb) and adenovirus (7.5Kb). However, some alternatives have been developed such as an oversized AAV transduction. This is possible via DNA repair pathways using an oversized reporter of 6.2kb and resulting in “fragment” AAV genomes of 5.0, 2.4, and 1.6 kb (Hirsch et al., 2013). This method is efficient as shown in mouse and dog models (Allocca et al., 2008; Monahan et al., 2010).

Another disadvantage for rAAV is being single stranded DNA hence needing to synthesize or recruit the complementary strand before gene expression. After single stranded DNA is converted to double stranded, an important loss of gene expression could occur due to transient instability of the vector genome. This loss affects the overall efficiency of the vector. Consequently, using self-complementary AAV avoid this problem. Self-complementary AAV is generated from packaging two halves of single stranded DNA molecules which fold and base pair to produce a double stranded DNA molecule. Those two halves could be obtained when dimeric inverted repeat genomes are formed during AAV replication cycle. However, self-complementation reduces the inserted gene size of an already small viral vector (McCarthy, 2008).

Table 5 : Viral vectors characteristics. Adapted from Chamcheu et al., 2015; Vannucci et al., 2013; McCarthy, 2008

Vector	Genetic material	Packaging capacity (kb)	Tropism	Vector genome form	Advantages	Disadvantages
Gamma-retrovirus	ssRNA	8	Dividing cells	Integrated	Long-term transgene Expression, low immunogenic	Do not transduce non-dividing cells; random integration into host genome; high risk of insertional mutagenesis.
Lentivirus	ssRNA	9	Dividing/ nondividing cells	Integrated	Long-term transgene expression	Pathogenic; random integration into host genome; complicated production procedure
Herpes Simplex Virus	dsDNA	50	Wide	Non-Integrated	Neurotropic, oncolytic	Transient expression of the transgene, high level of pre-existing immunity, potential remaining cytotoxicity
Adenovirus	dsDNA	7.5	Dividing/ nondividing cells	Non-integrated	Transduce most tissue/cells; oncolytic	Highly immunogenic transient transgene Expression, high levels of pre-existing immunity
Adeno-associated virus	ssDNA	5	Dividing/ nondividing cells	Non-integrated (90%) Integrated Only WT (>10%)	Non-inflammatory; Nonpathogenic, low immunogenic; possible site-specific integration	Possible loss of gene expression, low packaging capacity

C. Safety concerns

The fear and concerns towards gene therapy and its possible consequences have long delayed the clinical translation of this approach. Viral vectors risk of integrating into gene regulatory regions or into transcriptionally active domains have presented a threat of insertional mutagenesis and oncogenesis in patients (Donsante et al., 2001; Fehse & Roeder, 2008; Wirth et al., 2013). To avoid these problems, targeted integration of transgenes to predefined genomic sites has been the topic of many research studies. Immunogenicity of adenoviruses has been another concern. However, many studies demonstrate that those viruses have a safety profile in humans (Hedman et al., 2009; Muona et al., 2012; Wirth et al., 2013). The major concern has been the risk of uncontrolled genetic modifications that could be passed onto next generations in worst case scenario. It is always forgotten that other approved and extensively used agents like radiotherapy also cause genetic changes (Wirth et al., 2013). The ethical aspects and rationality of gene therapy have long been discussed (Beutler, 2001; Friedmann, 2000; Friedmann & Roblin, 1972; Wirth et al., 2013) and attending that the right safety and toxicity studies are done in large animals, gene therapy can reach clinical trials with success (Colle et al., 2009; Le Guiner, Moullier, & Arruda, 2011; Rapti et al., 2012).

D. Clinical trials

As already mentioned, gene therapy faced many difficulties before to be accepted as being a safe way to treat patients (Dunbar et al., 2018). Now several have been successful and many more are under course.

1. *First trials and drawbacks*

a) Retrovirus vector gene therapy for X-linked Severe combined Immunodeficiency (SCID-X1)

Children with SCID-X1 have been treated with Moloney murine leukemia virus–based γ -retrovirus vector expressing interleukin-2 receptor γ -chain complementary DNA. The therapy successfully restored immunity in the majority of patients. However, vector-induced leukemia appeared in 25% of patients. Therefore, a modified γ -retrovirus vector was designed. It was found efficient in treating SCID-X1 and the long-term effect on leukemia genesis is still under

investigation (ClinicalTrials.gov numbers: NCT01410019, NCT01175239, and NCT01129544; Hacein-Bey-Abina et al., 2014).

b) Ornithine transcarbamylase (OTC) deficiency

OTC deficiency safety clinical trial used the human adenovirus type 5 which carried human OTC cDNA. The viral vector was injected into the right hepatic artery. In 1999, one 18-year-old patient died 98 h after gene transfer following an anaphylactic shock due to strong adenovirus infection (Raper et al., 2003). This tragic event led to many interrogations and both the Food and Drug Administration (FDA) and the National Institute of Health (NIH) stopped recommending any policy alterations or clinical holds (Lehrman, 1999).

2. *New trials and successes*

Only a selection of successful trials is presented here.

a) Glybera to treat lipase familial deficiency:

Glybera was the first authorized gene therapy product in the Western marketing world. It is a rAAV1 vector for treating a rare disease called Lipoprotein Lipase (LPL) Deficiency (LPLD) (Wang & Gao, part II, 2014; Ylä-Herttuala, 2012). LPLD causes life threatening pancreatic inflammation (Gaudet, Méthot, & Kastelein, 2012; Wang & Gao, part II, 2014). A single intramuscular injection at different sites is enough for transduced muscular cells to synthesize LPL into blood thus the disease severity is diminished (Gaudet et al., 2012; Stroes et al., 2008; Wang & Gao, part II, 2014). Three days before and twelve weeks after treatment, immune suppression is advised to prevent the viral vector from being attacked or cleared by the host immune defense (Ferreira, Twisk, et al., 2014; Ferreira, Petry, & Salmon, 2014; Wang & Gao, part II, 2014).

b) Gencidine to treat head and neck carcinomas

Gencidine was the first gene therapy approved for human use. It is available on the market in China since 2004. It combines Adenovirus type 5 vector with a p53 expression cassette (Ad-p53). A Chinese clinical trial reported that the majority of patients treated with intratumoral injections of Ad-p53 in combination with radiation therapy (70 Gy/8 weeks) showed complete remission compared to the patients receiving radiation therapy alone. Those results were highly significant, thus the China State Food and Drug Administration approved this product for treating

head and neck cancer (<https://www.inserm.fr/en/health-information/health-and-research-from-z/gene-therapy>; Vattedi & Claudio, 2009).

c) CNS neuropathies gene therapy

CNS neurological diseases are among the hardest to treat for multiple reasons such as the limited diffusion of therapeutics through the blood brain barrier (BBB), the unclear pathomechanisms of neuropathies and the lack of suitable outcome measures after treatment (Piguet et al., 2017). Despite those difficulties, many clinical trials have been done or are ongoing. Some are presented thereafter.

i. Spinal Muscular Atrophy (SMA) type 1

SMA type 1 is a severe, autosomal recessive, progressive motor neuron infancy disease caused by a loss or dysfunction of the gene encoding survival motor neuron 1 (SMN1). The degeneration and loss of lower motor neurons result in muscle atrophy and death. It is the most common genetic cause of death among infants. After successfully testing for viral vector safety, tolerability and effectiveness in preclinical trials in mice and dogs, intravenous injection of self-complementary AAV9 (scAAV9) containing DNA coding for SMN gene therapy approach moved to clinical trials on children of up to 6 months of age (“AveXis” and other funds, NCT02122952). Longer survival, higher achievement of motor milestones and ameliorated motor function were attained after a single dose injected in affected babies. Improved motor behavior milestones included sitting unassisted for a few seconds, roll over, crawl and ability to speak. However, high serum aminotransferase levels without any other liver enzyme abnormalities were found in treated patients. This has been categorized as serious adverse events due to AAV infection in the liver. Liver enzymes increase was decreased by prednisolone treatment (Armbruster et al., 2016; Mendell et al., 2017; Piguet et al., 2017).

ii. Lysosomal storage disease (LSD)

LSD is caused by a lysosomal function deficiency resulting in undigested or partially digested materials in cells. This leads to metabolic dysfunctions, neurodegeneration and neuroinflammation. Twenty eight AAV-based gene therapy clinical trials exist for LSD with the majority based on intraparenchymal injection and some intrathecal (Batten disease) and one intravenous injection (MPSIIIA) (Piguet et al., 2017).

iii. Metachromatic leukodystrophy (MLD)

MLD is a very severe autosomal recessive infantile disease with a survival rate of maximum seven years. It is caused by a deficiency in arylsulfatase A (ARSA) resulting in severe motor and cognitive impairment. This impairment has been linked to demyelination of both the peripheral and the central nervous system (Colle et al., 2010; Piguet et al., 2017; Zerah et al., 2015). Efficacy and toxicology studies in *Macaca fascicularis* nonhuman primates proved that intracerebral injection of AAVrh.10cuARSA (AAV serotype rh10 with human ARSA cDNA coding for Arylsulfatase A enzyme) is safe and well-tolerated except for a few minor lesions attributed to the surgical procedure itself and for a dose-dependent inflammatory response against human ARSA. Inflammation was expected since human ARSA and *Macaca* ARSA differ by 17 amino acids. No significant adverse events neither clinical nor biochemical were detected in *Macaca*. Moreover, ARSA enzyme expression is maintained in the brain (Zerah et al., 2015). Efficacy tests included cognitive, behavioral and neuromotor tests (Ciron et al., 2009), whereas toxicity assessment comprised neutralization antibodies against the viral capsid, neuropathology and pathology of peripheral organs as well as biodistribution of the viral vectors in tissues and fluids (Zerah et al., 2015). This gene therapy approach was translated to clinical trial (NCT01801709) that is still ongoing (Piguet et al., 2017; Zerah et al., 2015).

iv. Sanfillippo syndrome type A

Sanfillippo syndrome type A, also called mucopolysaccharidosis (MPS) type IIIA, is an infantile disease appearing before the age of two with a survival rate of 20-30 years. It is caused by an autosomal recessive mutation in the N-sulfoglycosamine sulfohydrolase (SGSH) enzyme gene. Symptoms are mostly neurological and include a progressive deterioration of cognitive and motor abilities. Furthermore, children progressively develop severe mental retardation. Two clinical trials are ongoing for this disease: one with the intracerebral injection of AAVrh10 encoding both the SGSH and the sulfatase modifying factor 1 (SUMF1) cDNAs (clinical trial NCT02053064) and the second with intravenous injection of a scAAV9.U1A-hSGSH coupled with immunosuppressive therapy (prednisolone) (clinical trial NCT02716246). The first therapy was found to be safe, well tolerated and the neurosurgery was uneventful. Patients displayed improvements in their behavioral disorders and in their hyperactivity and sleep disorders after 1 year. A study with a longer follow-up period (5 years) is ongoing to evaluate the safety and tolerability. Preliminary results 6 months

post treatment showed some improvements in cognitive abilities and nonverbal IQ assessment (Piguet et al., 2017).

v. *San Fillippo syndrome type B*

San Fillippo syndrome type B, also called MPS type IIIB, is caused by the accumulation of partially degraded heparin sulfate oligosaccharides consecutive to the deficiency in alpha-N-acetylglucosaminidase (NAGLU) enzyme. MPSIIIB is characterized by progressive impairments of cognitive capacities after 2-4 years. Two clinical trials are ongoing for this disease: one with the intracerebral injection of AAV5 encoding the NAGLU cDNAs (clinical trial ISRCTN19853672) coupled with an immunosuppressive therapy (tacrolimus and mycophenolate mofetil) and the second with intravenous injection of rAAV9-CMV-NAGLU (NCT03315182). The first therapy was well tolerated and cognitive benefits were clearly seen after a two-year-follow-up study. No details are available yet for the second clinical trial (Piguet et al., 2017).

vi. *Canavan disease*

Canavan disease, a childhood genetic disorder, is caused by a defective aspartoacylase (ASPA) enzyme resulting in higher levels of its substrate N-acetyl aspartate (NAA) in the CNS. Consequently, myelination is disturbed and the brain degenerate in a spongiform way. A gene therapy clinical trial consisting in the intravenous injection of AAV2 expressing ASPA resulted in lower NAA concentrations in the brain after a 10-year-follow-up period. In addition, it was observed an improved myelination, a decreased water content in the splenium of the corpus callosum as suggested by MRI, a stabilization of brain atrophy and relatively fewer seizures in treated patients (Ciron et al., 2009; Janson et al., 2002; McPhee et al., 2006; Piguet et al., 2017).

vii. *Late Infantile neuronal Ceroid Lipofuscinosis (LINCL)*

LINCL also called Batten disease results from a deficiency in tripeptidyl peptidase 1 (TPP-1), a proteolytic enzyme encoded by the *CNL2* gene. Less frequently LINCL is due to mutations in *CLN6* gene, which encodes a transmembrane protein of the endoplasmic reticulum. Symptoms include progressive destruction of retinal pigmented epithelial cells and central nervous system neurons. This results in progressive loss of vision and neurological decline starting at approximately 3 years of age. Other symptoms are cognitive defects, seizures and impaired motor skills causing a vegetative state and death in middle to late childhood (Haltia & Goebel, 2013; Sondhi et al., 2005); AAV2 expressing CNL2 was injected intracranially (NCT00151216) and this

led to a slower decline of neurological symptoms after a 6-month-follow-up period (Crystal et al., 2004). Nevertheless, the progression of the disease could not be stopped. AAVrh.10-CAAG-hCLN2 clinical trial NCT01161576 and NCT01414985 were launched in 2011 with no results available yet. A recent clinical trial (NCT02725580) with intrathecal injection of AAV9-CAG-CLN6 is still ongoing (Piguet et al., 2017).

viii. Alzheimer's disease

Alzheimer's disease, the most common neurodegenerative disease in humans, has unclear causes. However, nerve growth factor (NGF) supply has been shown to be beneficial to prevent neuron degeneration. Thus, a clinical gene therapy trial (NCT00087789) has been initiated based on an AAV2 expressing NGF, which is injected intracerebrally. It was found to be safe and well tolerated 2 years after the injections. The therapy decreased the cognitive decline. A phase II clinical trial (NCT00876863) is ongoing (Piguet et al., 2017).

In Alzheimer's disease, brain cholesterol homeostasis seems to be impaired. Indeed, in normal conditions, cholesterol 24-hydroxylase, an enzyme encoded by the *CYP46A1* gene, convert brain cholesterol into 24S-hydroxycholesterol to allow cholesterol transport through the BBB. This is critical to discard cholesterol excess from the brain. In Alzheimer's disease patients, the level of brain cholesterol is increased while the level of 24S-hydroxycholesterol is decreased (Ayciriex et al., 2017; Burlot et al., 2015). In THY-TAU22 mice, an Alzheimer's disease -like mice model, AAV-CYP46A1 injections in the hippocampus increased the levels of CYP46A1 and restored normal level of 24S-hydroxycholesterol. Consequently, memory capacities, synaptic impairments as well as neuronal morphology and function were improved (Burlot et al., 2015). This gene therapy approach will enter clinical trials soon.

VI. CMT1A gene therapy approach

Considering a gene therapy approach for CMT1A (my thesis project) appears to be an interesting option. Since this disease is caused by an overexpression of the *PMP22* gene, the most logical therapeutic strategy is to decrease this excess. Gene downregulation can be achieved through mRNA downregulation via antisense oligonucleotides (ASO) or RNA interference (RNAi).

A. Antisense Oligonucleotides (ASO)

ASO are short single stranded nucleic acids made of 13-25 nucleotides. They bind to their complementary mRNA either to restore protein synthesis or to inhibit the production of a mutant protein (Mustonen, Palomäki, & Pasanen, 2017; Pirmohamed, 2018). Exon splicing is the mechanism of ASO that results in restoring protein production (Mustonen et al., 2017; Sierakowska, Sambade, Agrawal, & Kole, 1996; van Deutekom, 2001). Stimulating RNase H and thus degrading mRNA as well as inhibiting ribosomes binding and thus stopping translocation of mRNA (steric block) are two mechanisms used by ASO for preventing protein synthesis (Bennett & Swayze, 2010; Evers et al., 2015; Fattal & Bochot, 2006; Mustonen et al., 2017) (Table 6).

Chemical modifications improved the capacity of ASOs to recognize and bind to their target RNA. Those include substituting a nonbridging phosphate oxygen atom with a sulfur atom to be more resistant against nucleolytic degradation (first generation ASO) and altering sugars to enhance binding affinity (Bennett et al., 2017; Monia et al., 1993; Stein et al., 1988).

B. siRNA

RNAi is a strong tool for highly specific and selective gene silencing (Burnett, Rossi, & Tiemann, 2011; Rao, Vorhies, Senzer, & Nemunaitis, 2009). The first experimental study reported in 1998 by Fire et al received the 2006 Nobel Prize in Physiology/Medicine (Pushparaj et al., 2008). It is based on double-stranded RNA designed to be the same as the host sequence it targets for mRNA degradation. Many methods exist such as small interfering RNA (siRNA) and short hairpin RNA (shRNA) (Moore et al., 2010; Pushparaj et al., 2008; Rao et al., 2009). It is possible to directly deliver siRNA into the cytosol. Several cell types are possibly targeted by siRNA but with limited efficiency to only cells that can be transfected (Moore et al., 2010).

1. *siRNA properties*

21-25 base pairs (bp) constitute siRNAs (Pushparaj et al., 2008). Within 15 min after delivery, double stranded siRNAs are present in the nucleus and goes to the cytoplasm during the next 4 hours in both an unmodified form and a dissociated one (Rao et al., 2009). ATP-dependent helicase enzyme converts synthetic siRNAs into single strands (Nykänen et al., 2001). Those strands link to a protein complex called the RNA-induced silencing complex (RISC) (Hammond, et al., 2000) in order to bind the specific target sequence mRNA and degrade it (Grishok et al., 2001; Hutvágner et al., 2004; Pushparaj et al., 2008; Timmons et al., 2003) (***Table 6***).

Usually, siRNA are designed by carefully selecting the coding sequence for regions free of translational or regulatory proteins. Approximately 65-75% of designed siRNAs result in 50-65% gene silencing (Bernstein et al., 2001). This is often not significant biologically or therapeutically. To improve efficiency, siRNAs were chemically altered to increase their stability or several siRNAs can be used in parallel for silencing target genes. More than 80% gene silencing was obtained with multiple siRNAs (Pushparaj et al., 2008; Reynolds et al., 2004).

2. *siRNA delivery*

Non-viral vectors could be used to deliver siRNA in vivo (Pushparaj et al., 2008). Examples include polymer particles and cationic liposomes (Zhang et al., 2007). Normally, the majority of siRNA is degraded 48 hours post injection (Pushparaj et al., 2008; Rao et al., 2009).

C. *shRNA*

Short hairpin RNA (shRNA) is a technological method of gene knockdown with high effectiveness when introduced in a viral vector, sustainable outcomes, low copy numbers and very little off-target effects. shRNAs consist of sense and antisense sequences separated by a loop sequence. shRNAs are transcribed by the RNA polymerase enzyme II or III and cleaved by the dicer enzyme to form double-stranded RNA. One of the two RNA strands is removed (the “passenger” strand) and the second (the “guide” strand) binds to targeted mRNAs resulting in their degradation or sequestration (Rao et al., 2009; Moore et al., 2010).

1. *shRNA properties*

shRNAs are composed of two complementary 19–22 bp RNA sequences linked by a short loop of 4–11 nucleotides (Moore et al., 2010).

shRNA could be used to obtain stable knockdown cell lines without multiple rounds of transfection and with high reproducible results. Nevertheless, this task is time-consuming. Several months are usually needed to prepare the construct and select the shRNA positive cells by drug resistance or fluorescent markers (Moore et al., 2010) (***Table 6***).

To get a successful gene knockdown, it is most crucial to properly choose the target sequence. Minimum two target sequences must be designed for each gene to maximize the chances of obtaining a significant gene knockdown. After selecting the target sites, shRNA vectors are built mainly by oligonucleotide-based cloning or by PCR-based cloning (Moore et al., 2010).

Synthesis of shRNAs occurs in the nucleus of cells. Since they can be continuously produced by the host cell, their effect is durable. After that, they are processed, taken to the cytoplasm and incorporated into the RISC to degrade the targeted mRNA (Rao et al., 2009).

2. *shRNA life cycle inside of transfected cells*

RNA polymerase II or III can transcribe shRNA via promoters of RNA polymerase II or III on the expression cassette. RNA polymerase II promoter produces a primary transcript. This transcript is processed in the nucleus by a complex including the RNase III enzyme Drosha (Lee et al., 2003) and the double-stranded RNA-binding domain protein DGCR8. Pre-shRNA is the processed primary transcript. Exportin 5, a Ran-Guanosine Triphosphate-dependent mechanism, carries the pre-shRNA to the cytoplasm (Rao et al., 2009; Yi et al., 2003). There, it is inserted into another RNase III complex. This complex is formed of the RNase III enzyme Dicer and double-stranded Tat–RNA-binding protein (TRBP) or PACT (RNA-dependent protein kinase (PKR) activating protein). The loop of the hairpin is removed to form a double-stranded siRNA: the mature shRNA (Lee et al., 2003; Rao et al., 2009). Afterwards, mature shRNA/siRNA in the Dicer/TRBP/PACT complex is linked to Argonaute protein 2 (Ago2), the main constituent of RISC. The double-stranded RNA/ Dicer/ TRBP/Ago-2/ RISC form the RISC loading complex (RLC) (Rao et al., 2009) (***Figure 12***).

In the RLC, RNase-H like activity of Ago-2 separates the two strands of the RNA leading to the departure of the passenger strand. Following that, Ago protein complexes loaded with guide strand RNA search for complementary target sites in mRNAs, where Ago-2 cleaves mRNA resulting in mRNA degradation. Other Ago protein containing complexes predominantly associate with partially complementary target sites for translation repression through mRNA sequestration in processing bodies (p-bodies). Finally, the active RNA loaded complex is released for additional rounds of gene silencing activity (Rao et al., 2009) (**Figure 12**).

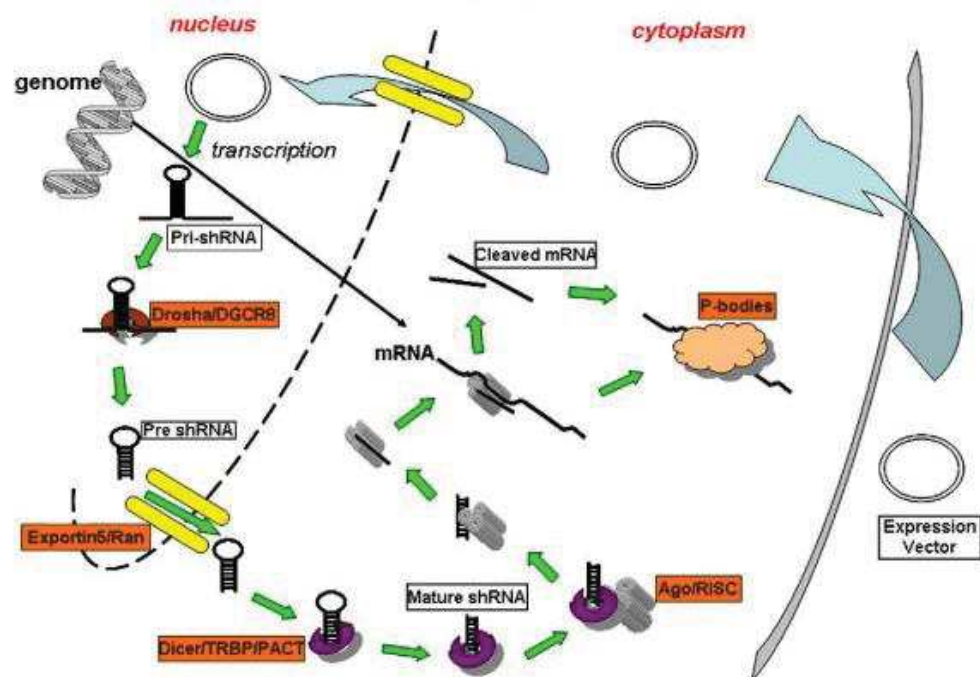


Figure 12 : shRNA life cycle: shRNA is delivered to the cytoplasm. After that, it is transported to the nucleus where it is transcribed to pri-shRNA. It is converted to the primary transcript pre-shRNA by Drosha/DGCR8. Exportin5 carries pre-shRNA to the cytoplasm. There, pre-shRNA is processed into mature shRNA by Dicer/TRBP/PACT complex. This complex and shRNA bind to the Ago protein of the RISC. The double stranded shRNA is then converted to a single strand shRNA. Finally, shRNA complexed with Ago/RISC degrade the targeted mRNA. Other Ago complexes could also sequester mRNA in processing (p-bodies) in order to repress translation. Adapted from Rao et al, 2009.

3. shRNA delivery

Two main methods exist for delivering shRNA: transfection as plasmid vectors transcribed by RNA pol III or modified pol II promoters and infection of cell with viral vectors (Moore et al., 2010).

D. Clinical trials

ASO and RNAi-based therapies are recently widely used in clinical trials for cancer, infections and other inherited diseases (Burnett et al., 2011). Some examples are developed thereafter.

1. ASO

Chemically modified antisense oligonucleotides (ASOs) are being used in clinical trials for Huntington disease (NCT02519036) (Piguet et al., 2017). Safety and tolerability profile has been demonstrated. In addition, ASO gene therapy decreased the toxic huntingtin protein that initiates the pathology (van Roon-Mom, Roos, & de Bot, 2018).

Nusineren is a recently licenced ASO to treat spinal muscular atrophy. This drug targets the *SMN2* gene thus synthesizing a full-length protein. Therapy administered early in life importantly decreased mortality and enhanced motor function (Finkel et al., 2017; Pirmohamed, 2018).

2. siRNA

The long and difficult journey of RNAi-based therapy might have come to an end. Alnylam Pharmaceuticals, pioneer in the field of RNAi, have submitted all regulations to the Food and Drug Administration (FDA) and the European Medicines Agency for the therapy of hereditary transthyretin-mediated amyloidosis (ATTR), patisiran (C. Morrison, 2018). Hereditary Transthyretin Amyloidosis is an autosomal disorder caused by mutations in the gene coding for transthyretin (TTR), a protein produced by the liver. In the disease, this protein form amyloid in peripheral nerves, the heart, kidney and gastrointestinal tract (Adams et al., 2018; Hawkins et al., 2015; Ruberg & Berk, 2012). It is a life-threatening, multisystem disorder. It causes important sensorimotor defects, hypotension, diarrhea, impotence, bladder impairments and cardiac manifestations such as heart failure (Adams et al., 2018; Ando et al., 2013; Conceição et al., 2016). Alnylam published the results of the RNAi-based therapy phase 3 clinical trial (APOLLO ClinicalTrials.gov number: NCT01960348). Patisiran, a double stranded siRNA targeting TTR mRNA, was injected intravenously in lipid nanoparticles for liver delivery. The dose of 0.3 mg/kg was administered for approximately 80 minutes once every 3 weeks for 18 months. Patisiran-treated patients showed an ameliorated quality of life and improvements in walking, in nutritional

status as well as in cardiac manifestations. The only adverse event was mild-to-moderate and related to injections. It diminished with time (Adams et al., 2018).

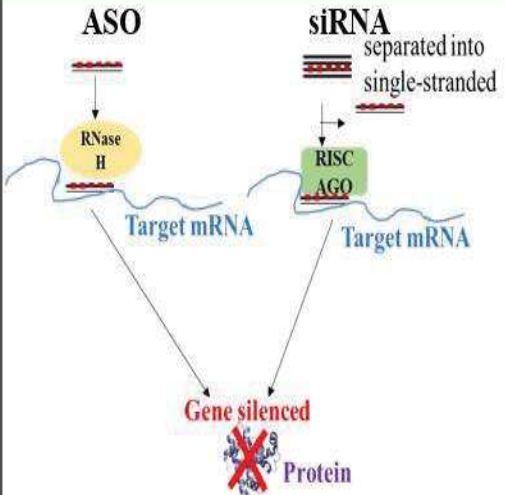
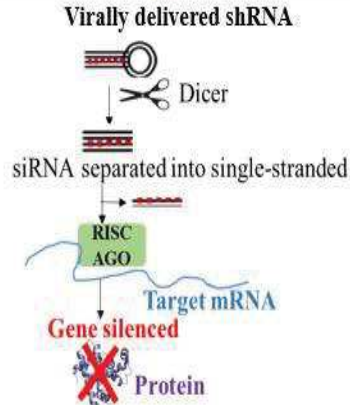
Another pharmaceutical company, Quark, is assessing QPI-1007, a siRNA treatment for NAION in a phase 3 clinical trial (NCT02341560). NAION (Non Arteritic Anterior Ischemic Optic Neuropathy) is caused by damage to the optic nerve with in general painless visual loss evolving over many hours to days as the main symptom (Atkins et al., 2010). 3mg of QPI-1007 are administered as single or multi-dose intravitreally (naked siRNA). The expected completion date is October 2020 (NCT02341560).

3. *shRNA*

Lentiviral-delivered shRNA as a treatment for Human Immunodeficiency Virus (HIV) infection is currently recruiting patients for a phase 1 clinical trial since May 2018 (NCT03517631). Briefly, peripheral blood mononuclear cells are taken from patients, modified by transducing with lentivirus shRNA and reinfused into patient. This is an autologous cell therapy approach aiming at assessing the efficacy and safety of the treatment (NCT03517631; Burnett et al., 2011).

AAV shRNA as a treatment for Hepatitis C (drug TT-034) is currently in a follow-up study to a phase I/II clinical trial until 2022 (NCT01899092; NCT02315638). The strategy consists in delivering 3 sequences of anti-Hepatitis C Virus into the liver of patients with 3 different shRNAs included in an AAV vector. Administration of the drug is by single intravenous injection. 5 dose levels were tested: 4×10^{10} , 1.25×10^{11} , 4×10^{11} , 1.25×10^{12} , and 4×10^{12} vg/kg. Headache was the most common adverse events. Transduction varied from one patient to another with the same dose (Patel et al., 2016).

Table 6: Gene silencing tools

Gene silencing	Advantages	Disadvantages
 <p>The diagram illustrates two gene silencing pathways. On the left, ASO (Antisense Oligonucleotide) is shown binding to Target mRNA, which is then degraded by RNase H. On the right, siRNA (small interfering RNA) is shown being separated into single-stranded form and loaded into the RISC complex with AGO, leading to Target mRNA degradation. Both pathways result in Gene silenced and Protein inhibition.</p>	<ul style="list-style-type: none"> ❖ No need for vector ❖ Increased stability and binding capacities when chemically modified 	<ul style="list-style-type: none"> ❖ Need continuous dosing ❖ Toxic ❖ Important off-target effects ❖ Inflammatory ❖ High doses depending on chemical alterations
 <p>The diagram illustrates the pathway for virally delivered shRNA. shRNA is delivered via a virus, processed by Dicer into siRNA, separated into single-stranded form, and loaded into the RISC complex with AGO, leading to Target mRNA degradation. This results in Gene silenced and Protein inhibition.</p>	<ul style="list-style-type: none"> ❖ Gene silencing never 100% ❖ Long lasting effect ❖ Less inflammatory than siRNA ❖ Less toxic than siRNA ❖ No need for regular dosing 	<ul style="list-style-type: none"> ❖ Off-targets fewer than siRNA ❖ Unspecific promoter

ASO: antisense oligonucleotides; siRNA: small interfering RNA; shRNA: Short hairpin.

Thesis objectives

I just presented the shRNA tools and the different gene therapies that are clinically developed at the moment. Considering a shRNA gene silencing approach for CMT1A (my thesis project) appears to be an interesting option since CMT1A is caused by an overexpression of PMP22. There are several murine models for CMT1A; we have chosen to work on the CMT1A rat because we believe it mimics best the human disease. For my thesis project, I studied the effectiveness of the following gene therapy approach on CMT1A rats: AAV-9 shRNA mouse PMP22 injected bilaterally in sciatic nerves at 6-7 days of age, time at which myelination starts and when first myelination deficits appear in the sciatic nerves of CMT1A rats.

The efficacy of the therapy was assessed by (*Figure 13*):

1. Molecular and biochemical techniques
2. Histological procedures
3. Behavioral analysis

Those methods are presented right after.

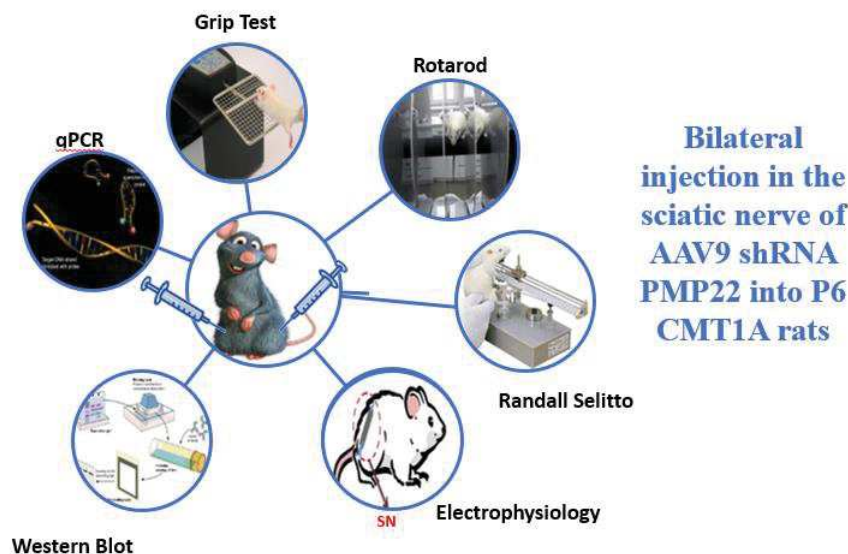
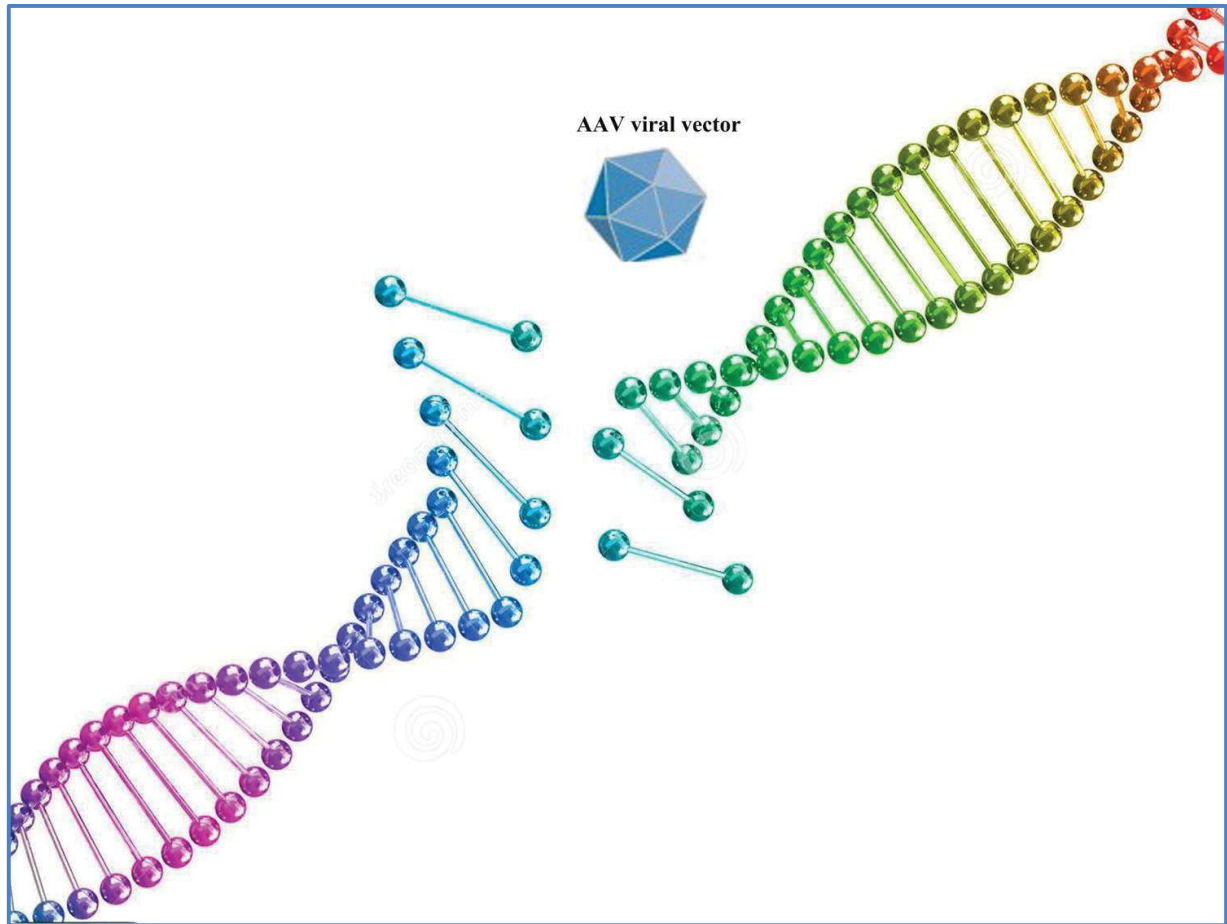


Figure 13 : Summary of tests used

Chapter 1: Gene Therapy Project



Material and Methods

I. Therapeutic tools production and validation

A. Recombinant AAV (rAAV) manufacturing and purification

Done at the Center for production of vector (CPV)-UMR1089, Nantes

1. *Cell amplification, transfection, harvest and supernatant Polyethylene glycol (PEG)-precipitation*

Human embryonic kidney (HEK) 293 cells cultured with Dulbecco's Modified Eagle Medium (DMEM) supplemented with 10% Fetal Bovine Serum (FBS) and 1% Penicillin Streptomycin (Pen/Strep) are co-transfected with the vector plasmid and helper plasmid (containing helper genes from adenovirus and the *rep cap* genes according to the capsid serotype) using the Calcium orthophosphate (CaPO₄) precipitate technique. The cells were incubated 6 to 15 hours at 37 +/- 1°C and 5 +/- 1% CO₂ with only the transfection medium. This medium was then removed and replaced by fresh exchange medium (DMEM, 1% Pen/Strep) prior to a 3 days incubation at 37 +/- 1°C and 5 +/- 1% CO₂. After that, the transfected cells were harvested. The supernatant is precipitated at 5 +/- 3°C overnight with PEG, centrifuged and discarded. The PEG-pellet was resuspended in Tris-buffered saline (TBS) before benzonase digestion.

2. *Vector purification*

The viral suspension is purified by two successive cesium chloride (CsCl)-gradient ultracentrifugation of respectively 24 hours, 28 000 rpm and 48 hours, 38 000 rpm. The viral suspension is then subjected to 4 successive rounds of dialysis against Dulbecco's phosphate-buffered saline (DPBS) 1X. The purified vector is finally collected, sampled for vg titer and purity assay, and stored at <-70°C.

3. *Vector titration*

Quantitative polymerase chain reaction (qPCR) was used to titer the rAAV vector genome. The target amplicons correspond to PolyA (Polyadenylation) or ITR-2.

B. Animals

Sprague Dawley rats and Swiss mice (Janvier) of different ages (pups and adults) as well as non-human primates (NHP, macaca fascicularis) served for transduction efficiency of AAV CAG GFP viral vectors serotypes 9 and rh10 (**Figure 14**, **Table 7**).

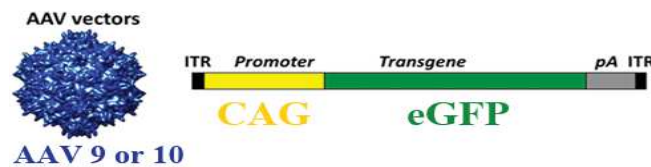


Figure 14 : AAV CAG GFP cassette. ITR= Inverted Terminal Repeat. GFP (Green Fluorescent protein) transgene under the control of a CAG promoter (CMV enhancer fused to chicken beta actin promoter). Adapted and modified from Figure 1 of Masat et al, *Humoral Immunity to AAV Vectors in Gene Therapy: Challenges and Potential Solutions*. *Discovery Medicine*; ISSN: 1539-6509; *Discov Med* 15(85):379-389, June 2013.

C. Injected viral solution

The viral solutions were prepared by diluting virus with sterile phosphate buffer saline (PBS) 1x and filtered 0.05% fast green to inject into sciatic nerves of mice, rats and macaques according to the following criteria (**Table 7**).

Table 7 : Injection parameters for transduction efficiency: vg=vector genome

	Rat		Mice		Non-human primate (NHP) : macaque fascicularis	
	Pups	Adults	Pups	Adults		
Vectors	AAV9_CAG_eGFP		AAV9 and AAVrh10		AAV9_CAG_eGFP	AAVrh10_CAG_eGFP
Injection	Unilateral in the right sciatic nerve				Unilateral in the left sciatic nerve	
Vector Quantity (vg/nerve)	1x10 ¹¹	1.8x10 ¹¹	1.15x10 ¹⁰	4.6x10 ¹⁰	5x10 ¹¹	5x10 ¹²
Volume injected per nerve (µl)	8	30	2	8	40	400
Injection time (min)	15	15	3-4	15	10	30
Number of animals per vector	3	6 (+ 1 PBS-injected control)	6 (+ 1 PBS-injected control)	9 (+ 1 PBS-injected control)	1	
Injection Age	P6-P7	1 month	P3-P4	2 months	2 years	
Sacrifice	1-month post injection					

D. Injection of AAV9 CAG eGFP in rodents' sciatic nerves

Injection needles were pulled using borosilicate glass capillary (GC 100-10, Harvard number 30-0016, 1 mm O. Dx0.58mm I.D) with the “Nichrome Coil Filament P30N4” machine. For the surgery, each rodent was anesthetized using the anesteo anesthesia system: inside an isoflurane box with isoflurane set at 4% and air flow adjusted to 3L/minute. A few minutes later, the animal was placed on the surgery table, under a microscope with inclined and rotatable binocular stereo heads and on a 37° C-heating plate. Its head was introduced inside a mask cone with decreasing isoflurane to 2%, setting O₂ flow to 0.5% and nose cone aspiration flow to around 1.8 LPM (liter per minute). The region of incision was shaved for adult animals and disinfected for both adults and pups with betadine solution and ethanol 70%. Skin was cut at the sciatic nerve location, at the level of the thigh. The connective tissue and fat connecting the two muscles *gluteus superficialis* and *biceps femoris* were carefully torn apart to expose the small cavity containing the sciatic nerve. The nerve was gently lifted out using a spatula. The needle filled with the appropriate volume of viral solution (**Table 7**) was carefully lowered into the nerve using a microinjector (WPI=World Precision Instruments, Europe). Over several minutes (**Table 7**), the viral solution was injected using a pulse generator (GW INSTEK GIG8215A) with a 0.9 frequency and a 50 Ω output, as well as a pneumatic picopump (PV820 WPI) with 100 ms amplitude and a 10 psi pressure. At the end of the injection, the sciatic nerve was replaced inside its cavity and muscles were pushed back around it. The wound was closed by suturing and using histoacryl tissue glue (B/Braun Aesculap, cat. no. 1050060) for pups and surgical clips for adults.

E. Injection of AAV9 CAG eGFP in macaques' sciatic nerves

Local anesthesia was by Ketamine (10mg/kg) + Xylazine (0.5mg/kg) for induction and by Propofol (1ml/kg/h) for maintenance. Injection of AAV into the sciatic nerve of 2 year-old-macaques (*macaca fascicularis*) was done at the MIRCEN facility of the CEA Fontenay aux roses by the neurosurgeon Dr Michel Zerah, with the help of Benoit Gautier and Claire-Maëlle. Macaques were anesthetized and injected using a capillary fiber linked to a 26 G Hamilton syringe (Gastight, PTFE Luer Lock) right above the split of the sciatic nerve into common fibular and tibial nerves. 40μL were injected for AAV9 and 400μL for AAV10 over 10 minutes for AAV9

(5×10^{11} vg/nerve) and 30 minutes for AAV10 (5×10^{12} vg/nerve). There was some viral leak with AAV9 (Table 7, Figure 15).

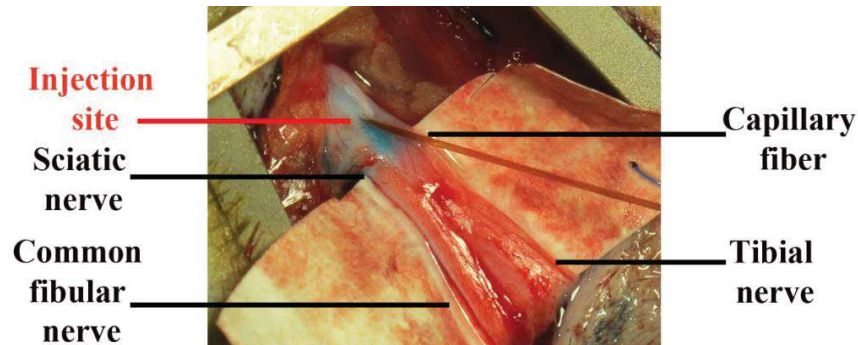


Figure 15 : AAV injection in sciatic nerve of *macaca fascicularis*

F. Dissections and Immunostaining of sciatic nerve

One month after injections, animals were sacrificed by lethal dose of sodium Pentobarbital, and their injected sciatic nerve was dissected to study the virus transduction efficiency. Macaques were perfused first by phosphate buffer saline then by paraformaldehyde (PFA).

Some dissected sciatic nerves of rodents were teased in small fibers bundles in order to determine the type of cells transduced by the viral vector (GFP marker on AAV). The percentage of transduced myelinating Schwann cells, non-myelinating Schwann cells and axons was determined. Minimum 300 cells were counted. Other dissected sciatic nerves of rodents were fixed in PFA 4% for 1.5 h at room temperature and incubated in successive sucrose baths 6 and 30 % for 1-2 days each at 4°C.

Peripheral nerves of macaques (radialis, median, sciatic, common fibular and tibialis) were incubated in successive baths of sucrose 10% for 3-4 days then sucrose 30% for 4 days with changing the medium every 2 days. Rodent sciatic nerves were embedded in OCT and stored at -80°C until coronal sections were cut using the cryostat (Leica cryostat 3050) and placed on Superfrost slides (Thermo scientific, reference J1800AMN2) stored at -20°C. Nerves of macaques were embed in paraffin. Slides were fixed again for 3-4 min in PFA 4%, washed by PBS and

blocked in 5% Normal Donkey Serum (NDS), 0.1% Triton 1x buffer for 45 min at room temperature. Primary antibodies (1/1 000 dilution) against Myelin Basic protein (MBP- SMI-99, Millipore, reference NE1019) and against β -Tubulin III (Tuj1, Sigma reference T2200) were incubated overnight at 4°C. On the next morning, the nerve sections were incubated with corresponding secondary antibodies (1/1 000 dilution) donkey anti-Mouse, Alexa Fluor 594 (Thermofisher, reference A-21203) and donkey anti-rabbit Alexa Fluor 647 (Thermofisher, reference A-31573) and with DAPI (Sigma, reference SI-D9542-5MG) for 1 h at room temperature, in the dark. The sections were mounted in Dako fluorescent Mounting medium (Reference S3023). ‘Nanozoomer Hamamatsu’ slide scanner was used to obtain images.

AAV9-CAG-GFP transduction rate in % was calculated by dividing the number of myelinated SCs that are transfected by the total number of myelinated SCs. A minimum of 1000 cells were counted.

G. In vitro validation of shRNA PMP22

1. Reverse Transcriptase quantitative real time Polymerase Chain Reaction (RT-qPCR PMP22 mRNA)

Done by our collaborators Burkhard Gess and Peter Young at the University Hospital Münster, Department of Sleep Medicine and Neuromuscular Diseases, Germany

After transfecting the mouse Schwann cell line MSC80 with scramble shRNA or shRNA PMP22-49 (Plasmid from Sigma, TRCN0000087949) or shRNA PMP22-50 (Plasmid from Sigma, TRCN0000087950) plasmids, RNA was extracted, and reverse transcribed into cDNA using commercial kits according to common laboratory practice at the Department of Sleep Medicine and Neuromuscular Diseases in Germany. Next, quantitative real-time PCR was performed in triplicate. *Gapdh* was used as the reference gene. Sequences as well as PCR parameters are detailed in the table below (***Table 8***). For quantitation, mRNA of PMP22 was normalized against GAPDH. The relative expression software tool (REST) was used for quantifications. Results were expressed according to the following relative expression equation (Pfaffl, Horgan, & Dempfle, 2002):

$$\text{ratio} = \frac{(E_{\text{target}})^{\Delta CP_{\text{target}} (\text{MEAN control} - \text{MEAN sample})}}{(E_{\text{ref}})^{\Delta CP_{\text{ref}} (\text{MEAN control} - \text{MEAN sample})}}$$

E= real time PCR efficiency; *CP*= crossing point= point at which the fluorescence is significantly higher than the background fluorescence; Δ = difference; control=reference gene (*ref*).

Table 8 : PCR conditions for in vitro validation of shRNA PMP22

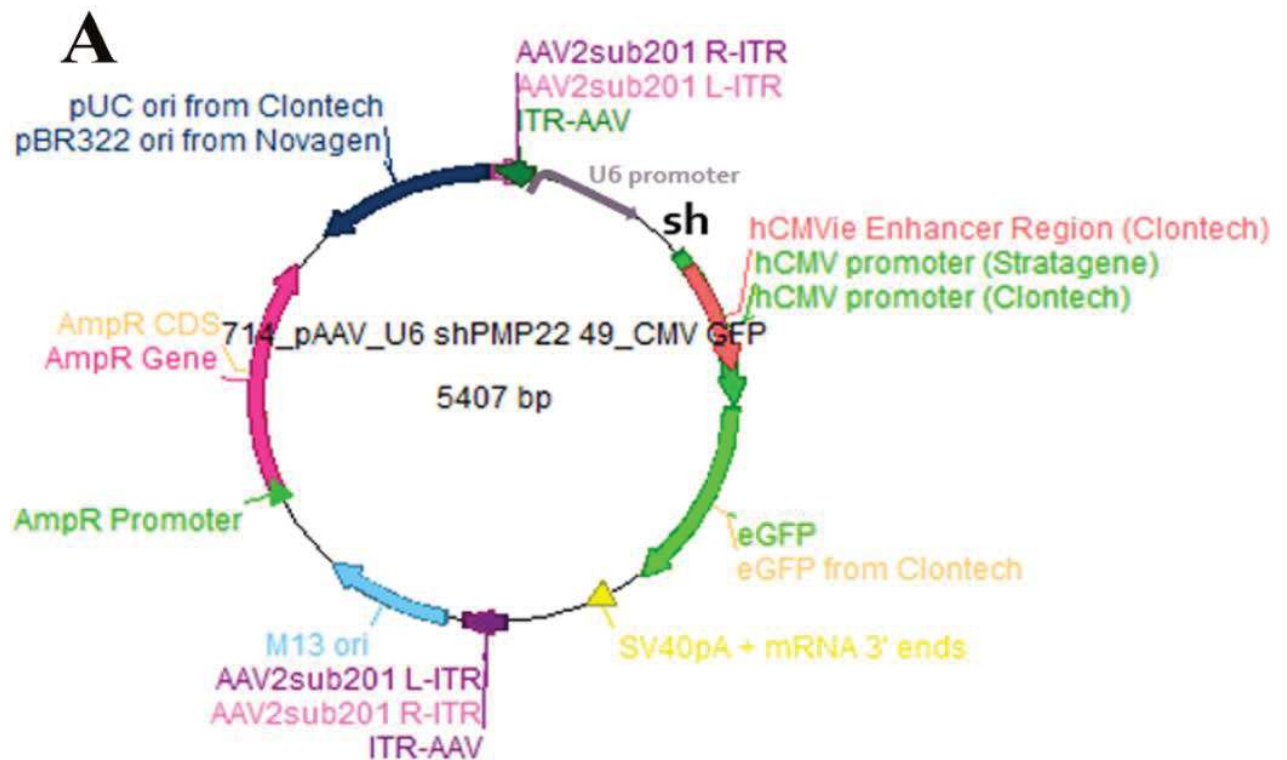
Name of primers	Sequences of primers	Concentrations in qPCR mix (μM)	PCR program
Mouse <i>Pmp22</i> -F	GACAAACCCCAGACAGTTGA	0,4	Sybr Green 10 min at 95°C, 40 cycles of (15s at 95°C, 30 s at 60°C and 30s at 72°C
Mouse <i>Pmp22</i> -R	CAGGAGCCACCAGCTATTACT	0,4	
<i>GAPDH</i> : F	GTCTTCACTACCATGGAGAAGG	0,4	
<i>GAPDH</i> : R	TCATGGATGACCTTGGCCAG	0,4	

F= forward primer, *R*= reverse primer

2. Western Blot

MSC80 cells were seeded in DMEM (Gibco/Thermo Fisher, reference 31966021) with 10% FBS (HyClone reference SV30160.03) and 1% Pen/Strep (HyClone reference SV30010, J160026) until reaching 70-90% confluency (400 000 cells/well in a 6-well-plate). Cells were transfected using Lipofectamine 3000 reagent (Thermo Fisher, reference L3000015) according to manufacturer recommendations with scramble shRNA (*scr.sh*) or shRNA PMP22-49 (*sh49*) or shRNA PMP22-50 (*sh50*) plasmids (2.5 μg of DNA/well in a 6-well-plate, plasmids produced in Nantes-CPV-UMR1089 and containing U6 and CMV promoters as well as a GFP marker) (**Figure 16**). Proteins were extracted with a radioimmunoprecipitation assay (RIPA) lysis buffer (Thermo Scientific reference 89901). Protease (Thermo Scientific Halt Protease Inhibitor Cocktail reference 78430) as well as phosphatase (Thermo Scientific Halt Phosphatase Inhibitor Cocktail reference 78420) inhibitors were added. After that, proteins were quantified using the bicinchoninic acid (BCA) protein assay kit (Thermo Scientific, reference: 23225) based on colorimetric detection. 20 μg of proteins were separated in 10% precast polyacrylamide gels (Bio Rad, reference: 4568034). After that, proteins were transferred to Polyvinylidene difluoride (PVDF) membranes by rapid (7

min), semi-dry blotting process (Bio Rad Trans blot transfer pack, reference: 1704157 and Bio Rad Trans-Blot Turbo system). Membranes were blocked for 1 hour at room temperature using a commercial buffer (Odyssey Blocking buffer (PBS) LI-COR 927-40000). The following primary antibodies were incubated overnight, at 4°C, in blocking buffer, on a shaker: rabbit anti-PMP22 (Sigma, Reference SAB4502217, 1/750 dilution) and mouse anti-Tubulin (Millipore, reference MABT205, 1/7 000 dilution). Following washing with TBS-0.1% Tween (TBST), secondary antibodies were incubated for 1 hour at room temperature at a 1/12 000 dilution: IRDye 800CW donkey anti-rabbit (Li-Cor, green fluorescence, reference 925-32213), IRDye 800CW donkey anti-goat (Li-Cor, green fluorescence, reference 925-32214) and IRDye 680RD donkey anti-mouse (Li-Cor, red fluorescence, reference 925-68072). After washing in TBST, results and quantifications were obtained by the Odyssey CLX Li-Cor Imaging System and its “Image Studio” software. Samples were run in triplicates with the following conditions: non-transfected cells, cells transfected with sh.scr, cells transfected with sh49 and cells transfected with sh50 so that three blots were performed in total.



B

CGCGGTGCTAGTGTTGCTCTT CTCGAG
 GCGCCACGATCACAACGAGAA CTCGAG

sh49

C

CACTGACTACTCCTATGGCTT CTCGAG
 GTGACTGATGAGGATACCGAA CTCGAG

sh50

Figure 16 : shRNA: plasmid map (A) and sequences for sh49 (B) and sh50 (C).

II. CMT1A rat model characterization

A. Animals

PMP22 transgenic rats called CMT1A rats (M. Sereda et al., 1996) were used for this study. Wild-type (WT) littermates served as controls. Genomic DNA was extracted from tail biopsies for genotyping by polymerase chain reaction with mouse transgene-specific primers 5'-GACAAACCCCAGACAGTTG-3' and 5'-CCAGAAAGCCAGGGAAGT-3' previously described (M. Sereda et al., 1996). All experiments were performed based on the French regulations for animal experimentation (French decree 2013-118, Directive 2010/63/EU).

Equal number of males and females served for model functional characterization. Tests were performed every 1-2 months until 6 months of age of rats then at 12 months right before sacrifice except for nerve conduction velocity measurements which was only done at 12 months (***Table 10***, ***Table 11***). 22 WT and 20 CMT1A rats were tested for motor deficits by rotarod and grip test, for locomotion impairments Catwalk and for nerve conduction velocity by electrophysiological measurements. Those tests are detailed thereafter.

B. Behavioral Analysis

All tests were performed by the same investigator who was blinded toward genotype and treatment.

1. Rotarod

The rotarod test (Bioseb) was used to assess motor coordination and balance in rats. The animal is placed on the rotating bar of the apparatus and the timer is started. As soon as the animal drops, the latency to fall (minutes and seconds) and the rotation speed (rpm) are automatically recorded. Rats were first given a one-day training to familiarize them with the rotating bar. Their ability to stay for a minimum of 2 minutes at constant speed (4 rpm) was verified. For the actual measurements, latency to fall and rotation speed of rats were recorded by accelerating the speed from 4 till 40 rpm over a 5 minutes period. Each animal underwent three trials. Data of the latency to fall were averaged for each rat and then averaged for each group.

2. *Grip test*

The grip test (Bioseb) was used to study muscular strength in rats' rear paws. The animal is placed on a grid and pulled by its tail. The measure is done by a sensor connected to an electronic device recording the force in Newtons. Each rat underwent three trials. Data were averaged for each rat and then averaged for each group.

3. *Catwalk*

The Catwalk test was used to analyze gait characteristics in rats. The animal crossed from one side to the other on an enclosed walkway on a glass plate. Green light enters the plate and is scattered at the areas where the animal's paws contact the glass plate. The paws are captured by a video camera located underneath the walkway and connected to a computer with the CatWalk software (Noldus Information Technology , 2015). Minimum three runs having a constant and homogeneous speed of crossing were analyzed per rat. The automatic classification of runs i.e. assigning labels to paws (RF=right front, LF=left front, RH=right hind, LH=left hind) was verified manually. After that, the catwalk software calculated a huge number of parameters related to individual footprints, positions of footprints and time-based relationships between footprints. Data were averaged per animal and per group.

Statistically significant parameters were (Noldus Information Technology , 2015):

- Max contact max intensity (max contact): parameter measuring maximum intensity at maximum contact of a paw. Intensity ranges from 0 to 255 arbitrary units (a.u). The intensity of a print depends on the degree of contact between a paw and the glass plate. It is usually used to assess the effects of neuropathic pain.
- Regularity index: number of normal step sequence patterns relative to the total number of paw placements in percentage (%).
- Phase dispersions: temporal relationship between placements of two paws. It is used as a measure of inter-paw coordination. It ranges from -50 to 75%.
- Couplings: Like the phase dispersions parameter, couplings describe the temporal relationship between placements of two paws within a step cycle. It is used as a measure of inter-paw coordination. The value of Couplings ranges between 0 and 100 %.

- Single Stance: duration (in seconds) of ground contact for a single hind paw (Coulthard et al., 2002). It is used for gait analysis in pain models. In CatWalk, Single Stance is the part in the step cycle of a hind paw where the contralateral hind paw does not touch the glass plate.

C. Electrophysiology

Proximal as well as distal electrophysiological measurements on both sciatic nerves of rats were performed at 12 months in non-injected rats and every 1-3 months starting one month after injection (**Table 11**). Rats were anesthetized with isoflurane (anesteo) and placed on a heating plate at 37°C. On the rat's thigh, along the nerve at the sciatic notch, a pair of 12 mm-steel needle electrodes with 2 mm pin plugs (AD Instruments, MLA1304, Oxford, UK) was positioned subcutaneously for proximal stimulation. Compound muscle action potentials (CMAPs) were recorded from the intrinsic foot muscles using 12 mm-steel electrodes with 1.5 mm safety socket plugs (AD Instruments, MLA1303, Oxford, UK) placed on the rat's paw's muscle, middle toe and the ground electrode on the tail for safety. CMAP is defined as the sum of activity in muscle fibers following motor nerve stimulation. Supramaximal square wave pulses, a biphasic stimulation lasting 0.2ms (200µs) were given using a PowerLab 26T machine connected to the LabChart software (AD Instruments, Oxford, UK). Stimulation was delivered by increasing current intensity beginning with 1mA then higher until no more change in amplitude (maximum 7mA). The highest response measurement was selected. The same process was repeated for distal stimulation. Above the ankle, along the tibial nerve, a pair of electrodes was positioned in addition to the electrodes on the intrinsic foot muscles. Both amplitudes and latencies of CMAP were determined using the LabChart software program. Latency is the time at which there is a change in the baseline meaning there is a stimulation response. The distance between the proximal and distal sites of stimulation was measured with a ruler with the limb as extended as possible. Nerve conduction velocities (NCVs) were calculated from sciatic nerve latency measurements:

$NCV \text{ (m/s)} = \text{distance} / (\text{Proximal Latency} - \text{Distal Latency})$ (**Table 11**).

III. Gene therapy approach in CMT1A rats

A. Animals

CMT1A rats and their WT littermates were injected with AAV9 shRNA at 6-7 days of age (P6-P7) in sciatic nerves. They were divided into 2 cohorts subdivided into 4 groups each. The 2 cohorts are termed “long term cohort or LTC” and “short term cohort or STC”. LTC served to study the efficiency of the gene therapy on the long run (until 1 year of age) while STC was used to correlate behavioral analysis and electrophysiological measurements with biochemical studies. Rats of STC were sacrificed at 2.5 months (**Figure 17**).

The 4 groups are:

- WT injected with AAV9 scramble shRNA (8 animals)
- CMT1A injected with AAV9 scramble shRNA (8 animals)
- CMT1A injected with AAV9 shRNAPMP22-49 (8 animals)
- CMT1A injected with AAV9 shRNAPMP22-50 (8 animals)

The efficiency of the AAV9 shRNA PMP22 gene therapy was assessed by behavioral analysis and biochemical studies as detailed below (**Figure 17**).



Treated gr: Long term cohort (LTC): (Males & females):

- WT shRNA control (n=7)
- CMT1A shRNA control (n=8)
- CMT1A shRNA PMP22-49 (n=8)
- CMT1A shRNA PMP22-50 (n=8)

KEEP UNTIL 12 MONTHS

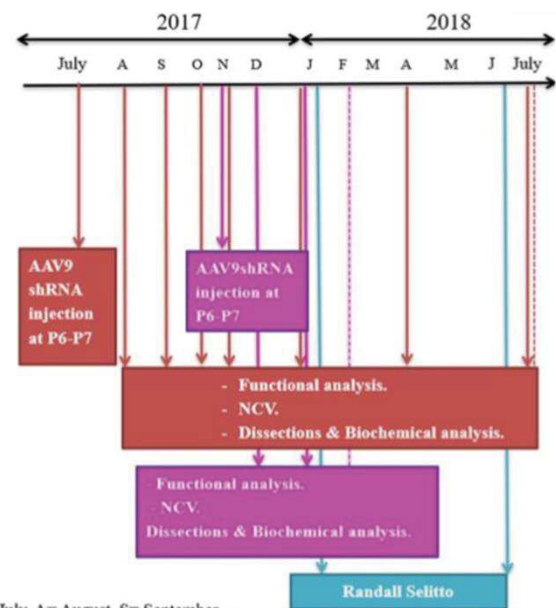
2 rats died one injected with sh49 and the other with sh50

Treated gr: Short term cohort (STC):

(Males & females):

- WT shRNA control (n=8)
- CMT1A shRNA control (n=8)
- CMT1A shRNA PMP22-49 (n=8)
- CMT1A shRNA PMP22-50 (n=8)

Nociceptive test



Legends: ----- date of sacrifice; Months= July, A= August, S= September...
gr= group, WT= Wild type, Functional analysis: Rotarod and grip strength
Biochemical analysis: electron microscopy (EM), Western Blot (WB) and Q-PCR
NCV= Nerve Conduction Velocity

Figure 17: Summary of experimental design

B. Injected AAV9 viral solution

For rat pups, the sequence of scramble shRNA is confidential (CPV-UMR1089, Nantes). The sequences of shRNA PMP22 sense strands are the following: CGCGGTGCTAGTGTGCTCTT (49) and CACTGACTACTCCTATGGCTT (50) (**Figure 16**). The AAV9 viral solutions were prepared by diluting virus with sterile phosphate buffer saline 1x (PBS) and filtered 0.01% fast green to inject 8µl of 1×10^{11} vg/nerve giving a concentration of 1.25×10^{10} vg/µl.

C. Injection of AAV9 shRNA in rats' sciatic nerves (SN)

Refer to Material and Methods I. D. Both sciatic nerves were injected but not successively since it takes a long period of time and pups dye one day later. Pups were first injected in one sciatic nerve, woken up and after a while injected in the second nerve.

D. Behavioral Analysis

The efficacy of AAV9shRNA PMP22 gene therapy was assessed by motor behavioral test in rats each 1-3 month starting one month after injections. Those tests included: rotarod, grip test and Randall Selitto (**Table 10**). All tests were performed by the same investigator who was blinded toward genotype and treatment.

1. Rotarod

Refer to Material and Methods II. B.1.

2. Grip test

Refer to Material and Methods II. B.2.

3. Randall Selitto

Performed by Antoine Jouvenel, PhD student "Pain assessment" team

The Randall Selitto test (Bioseb) was used to assess the nociceptive threshold of 6 and 11-month-old rats. The rat hind paw is placed on a small plinth under a cone-shaped pusher with a rounded tip. An increasing pressure force is applied to the animal paw by the operator who presses a pedal switch initiating the mechanism exerting the force. The maximum force applied to prevent injuring the skin is 600 g. When the rat reacts orally, the operator stops pressing the pedal and

records the force at which the animal felt pain (the nociceptive threshold of the animal). Each rat was first trained to get used to the test and the experimenter for 10 days. The training consisted of handling rats every day, restraining them and carefully immobilizing them to apply the pressure on both of their hind paws.

E. Electrophysiology

Refer to Material and Methods II.C ([Table 11](#)).

F. Dissections

The 32 AAV9 shRNA-injected rats of STC were sacrificed at 2.5 months of age ([Figure 17](#)). First, each rat was administered intraperitoneally with the drug Pentobarbital sodium used for anesthesia and euthanasia (54.7 mg/mL, 100 mg/kg, CEVA Santé animale, reference 6742145). Second, blood (600 µL) was collected by cardiac puncture for neutralization assay (refer to Material and Methods III.I) for 5 WT injected with AAV9 scramble shRNA and 5 CMT1A rats injected with AAV9 scramble shRNA and after centrifugation serum was recuperated and frozen at -80 °C. In addition, whole blood was collected in EDTA tubes for AAV vector biodistribution for 4 WT injected with AAV9 scramble shRNA, 2 CMT1A rats injected with AAV9 scramble shRNA, 1 CMT1A rats injected with AAV9 shRNA PMP22-49 and 1 CMT1A rats injected with AAV9 shRNA PMP22-50. Third, each rat was perfused with around 100 mL of 1x PBS (Gibco, reference 10010023). Finally, the following organs and nerves were dissected: heart, liver, spleen, kidney, muscle closed to sciatic nerve, lumbar (L) spinal cord, dorsal root ganglions (DRG) L4 and L5 as well as brainstem for AAV biodistribution and both sciatic nerves cut in multiple pieces for RT-qPCR (refer to Material and Methods III. G.1), AAV biodistribution (refer to Material and Methods III. J) and Western Blot (refer to material and Methods III. G.2) ([Table 11](#)). Two small pieces of each organs were cut: one was snap frozen in liquid nitrogen then stored at -80°C for biochemical analysis and the second fixed for 24 h in PFA 4% at 4°C then placed in sucrose 6 and 30 % for around 48h at 4°C and embed in Optimal Cutting Temperature (OCT, NEG-50, reference 650-2) for histological studies.

29 out of 31 of AAV9 shRNA-injected rats of LTC (1 rat euthanized due to paw's infection and another one died due to visceral tumor) were sacrificed at 12 months of age (**Figure 17**). First, each rat was administered intraperitoneally with the drug Pentobarbital sodium used for anesthesia and euthanasia (54.7 mg/mL, 100 mg/kg, CEVA Santé animale, reference 6742145). Second, each rat was perfused with around 100 mL of 1x PBS (Gibco, reference 10010023). Third, the following organs and nerves were dissected: lumbar (L) spinal cord, dorsal root ganglions (DRG) L4 and L5 and both sciatic nerves cut in multiple pieces for RT-qPCR (refer to Material and Methods III. G.1), CARS microscopy (refer to Chapter 2: Label-Free non-linear microscopy Project) and Western Blot (refer to material and Methods III. G.2) (**Table 11**). Finally, the spinal cord and DRG from one side of the spinal cord were snap frozen in liquid nitrogen then stored at -80°C for biochemical analysis. DRG from the other side of the spinal cord were fixed for 24 h in PFA 4% at 4°C then placed in sucrose 6 and 30 % for around 48h at 4°C and embed in Optimal Cutting Temperature (OCT, NEG-50, reference 650-2) for histological studies.

In order to avoid contamination, dissection instruments were cleaned between each tissue and each rat. The following reagents were used in this order for the cleaning: tap water to remove the blood, 10% Sodium dodecyl sulfate solution (SDS, Sigma, reference L4522), PBS (2 baths), RNase Away (Thermo Scientific, reference 10666421 and PBS (2 baths).

G. Molecular and biochemical techniques

1. RT-qPCR

Translational gene therapy for genetic diseases- UMR1089, Nantes, France

TRIzol® reagent (Thermo Fisher Scientific, reference 15596026) was used to extract total RNA, according to the manufacturer's instructions. After treating total RNA (150 ng) with RNase-free DNase I (ezDNase, Thermo Fischer Scientific, reference 11766051), random primers, oligo (dT)18 (Thermo Fischer Scientific, reference SO131) and SuperScript IV Vilo Master Mix (Thermo Fischer Scientific, reference 11756050) served to synthesize cDNA from total RNA in a final volume of 20 µL. Afterwards, quantitative PCR (qPCR) analysis was done on 5 µL of cDNA (diluted 1/15) in duplicate using primers for *Pmp22*, *Mpz* and rat *Hprt1*. Sequences as well as PCR parameters are detailed in the table below (**Table 9**). For quantitation, mRNA of PMP22 and MPZ

were normalized against rat HPRT1 mRNA, co-amplified as an endogenous control. "cDNA-like samples" analysis confirmed the absence of DNA contamination for each RNA sample. This was acquired by excluding reverse transcriptase from the reaction mix. Analyzing serial dilutions of cDNA sample (1/10 to 1/100000 for Pmp22 or Mpz and 1/5 to 1/60 for HPRT1) from a sciatic nerve of a transgenic rat injected with AAV9 shRNA scramble defined the efficiency, linearity and absence of qPCR inhibition. Results were expressed in relative quantities (RQ): $RQ = 2^{-\Delta Ct} = 2^{-(\text{Cycle threshold } Ct \text{ target} - Ct \text{ endogenous control})}$. The limit of quantification (LOQ) of our test was for mouse Pmp22 RQ =2.4 and for Mpz RQ=0.5.

Table 9 : PCR conditions for in vivo validation of shRNA PMP22

Name of primers	Sequences of primers	Concentrations in qPCR mix (μM)	PCR program
Mouse Pmp22-F	GACAAACCCCAGACAGTTGA	0,25	Sybr Green 30s at 95°C, 40 cycles of (5s at 95°C and 30s at 64 °C) + melt curve
Mouse Pmp22-R	CAGGAGCCACCAGCTATTACT	0,25	
Mpz: F	TGTTGCTGCTGTTGCTCTTC	0,25	Sybr Green 30s at 95°C, 33 cycles of (5s at 95°C and 30s at 60 °C) + melt curve
Mpz: R	TTGTGAAATTTCCCCTTCTCC	0,25	
Rat HPRT F	GCGAAAGTGGAAGCCAAGT	0,2	Taqman 30s at 95°C, 33 cycles of (5s at 95°C and 30s at 60 °C) + melt curve
Rat HPRT R	GCCACATCAACAGGACTCTTGTAG	0,2	
Rat HPRT P	CAAAGCCTAAAAGACAGCGCAAGTTGAAT	0.2	

F= forward primer, R= reverse primer, P= TaqMan probe

2. Western Blot

Western Blot biochemical technique was used to quantify PMP22 protein in rat sciatic nerves. At the time of dissection, rats were 2.5 months old. Proteins were extracted and quantified using the BCA protein assay kit (Thermo Scientific, reference: 23225) based on colorimetric detection. 20 μg of proteins were separated in 10% precast polyacrylamide gels (Bio Rad,

reference: 4568034). After that, proteins were transferred to Polyvinylidene difluoride (PVDF) membranes by rapid (7 min), semi-dry blotting process (Bio Rad Trans blot transfer pack, reference: 1704157 and Bio Rad Trans-Blot Turbo system). Membranes were blocked for 1 hour at room temperature using a commercial buffer (Odyssey Blocking buffer (PBS) LI-COR 927-40000). The following primary antibodies were incubated overnight, at 4°C, in blocking buffer, on a shaker: Rabbit Anti-PMP22 (Sigma, Reference SAB4502217, 1/500 dilution), goat anti-MPZ (Invitrogen, reference PA5-18773, 1/500 dilution) and mouse anti-alpha tubulin (Millipore, reference MABT205, 1/7 000 dilution). On the next morning, membranes were washed for 3-5x7 min in Tris-buffered saline, 0.1% Tween 20 (TBST). Following the washing, secondary antibodies (Li-Cor) were utilized at a 1/12 000 dilution: IRDye 800CW Donkey anti-rabbit (green fluorescence, reference 925-32213), IRDye 800CW Donkey anti-goat (green fluorescence, reference 925-32214) and IRDye 680RD Donkey anti-mouse (red fluorescence, reference 925-68072). After washing in TBST, results and quantifications were obtained by the Odyssey CLX Li-Cor Imaging System and its “Image Studio” software. Statistical analysis was done using Graphpad Prism 7 software. Three blots were performed with on each, samples from 2 WT rats injected with scramble shRNA, 2 CMT1A rats injected with scramble shRNA, 2 CMT1A rats injected with shRNA PMP22-49 and 2 CMT1A rats injected with shRNA PMP22-50. The first blot was chosen as reference and the other blots were corrected using a factor for each based on the average value of the WT samples. Statistical analysis was done using Graphpad Prism 7 software. Western Blots were reprobbed using different antibodies (rabbit anti-Akt Cell Signaling, reference: 9272, 1/1 000 dilution, mouse anti-Anti-Glyceraldehyde-3-Phosphate Dehydrogenase Antibody, clone 6C5 (GAPDH, Millipore, reference MAB374, 1/1 000 dilution).

H. AAV9 Neutralizing factors

Gene Therapy Immunology (GTI) core - UMR1089, Nantes, France

An inhibition assay was used to detect neutralizing factors (NF) against the viral vector AAV9 (***Table 11***). The aim of this technique is to measure cell transduction efficiency of the viral vector. In practice, serial dilution of serum (1/50, 1/500, 1/5 000, 1/50 000 and 1/500 000) were incubated with cells and AAV9 expressing the reporter gene *Lac Z*. A chemiluminescent method

(Galacto star kit, Life Tech, reference) was used to detect gene expression. Cell number range, AAV9 transduction level in the absence of serum, limit of detection (LOD) and a neutralizing serum positive control constitute some of the acceptance criteria of the neutralization assay. The positive test is equivalent to more than 50% of transduction inhibited in the presence of AAV9 NF in serum; the 100% corresponding to the transduction control with AAV9 alone.

I. AAV9 biodistribution

Virginie François at the Preclinical Analytics core (PAC) - UMR1089, Nantes, France

For AAV biodistribution i.e. the spreading of the viral vector away from the injection site (Le Guiner et al., 2011), DNA was extracted and quantified by qPCR. Analyzed samples enclosed: the injection site (sciatic nerve), the lumbar dorsal root ganglion 4 and 5 (DRG L4 and L5), the lumbar spinal cord, the heart, the liver, the spleen, the kidney, the muscle close to the sciatic nerve, the brainstem and the blood (***Table 11***). Whole blood was collected in tubes containing EDTA as an anticoagulant. All samples were collected in DNA-free, RNase/DNase-free and PCR inhibitors-free certified microtubes and stored at -80°C before DNA extraction.

First DNA was extracted from blood and tissues according to manufacturer's recommendations (Gentra Puregene, Qiagen, reference 1042606). Briefly, red blood cells were discarded from whole blood samples using the "Red Blood Cell Lysis Solution" (Gentra Puregene) and tissues were grinded with TissueLyserII from qiagen. Then, in the presence of the proteinase K enzyme and of a DNA stabilizer to limit the activity of intracellular along with environmental DNases, an anionic detergent lysed tissues and cells. After that, contaminants were removed with an RNA digesting enzyme for RNA and salt precipitation for proteins. Next, precipitation with isopropanol and drying with 70% ethanol recovered the genomic DNA and the hydration solution (1 mM EDTA, 10 mM Tris·Cl pH 7.5) dissolved it (Gentra Puregene, Qiagen handbook, 2014). Lastly, the DNA concentration was measured by a nanospectrophotometer.

Second, a PCR internal control was prepared using a linearized DNA to avoid interference with PCR efficiency from supercoiled DNA. The linearized DNA enclosing one copy of the

sequence to analyze was purified. The following formula was utilized to calculate the weight of one copy of the plasmid:

$$\begin{aligned}\text{Weight of one copy of the plasmid} &= \frac{\text{Weight of 1bp (g/mol)} \times \text{size of the plasmid (bp)}}{\text{Avogadro's number (molecules/mol)}} \\ &= \frac{660 \times \text{size of the plasmid (bp)}}{6,022^{E23}}\end{aligned}$$

A dilution at 10^{11} copies of plasmid in a final volume of 5 μ L was made.

Afterwards, serial dilutions of this linearized DNA plasmid were prepared to get a range from 10^7 to 25 copies for *Gfp* and from 10^6 to 100 copies for reference gene (Le Guiner et al., 2011).

Third, TaqMan qPCR was performed on 50 ng DNA in duplicates for each sample. Primers and probe designed to amplify and match the GFP marker of AAV9 shRNA and an endogenous gene were used to determine vector DNA copy numbers expressed at the end as vector genome per diploid genome (vg/dg). For *Gfp* gene:

Forward: 5'-ACTACAACAGCCACAACGTCTATATCA-3'

Reverse: 5'-GGCGGATCTTGAAGTTCACC-3'

Probe: 5'-FAM-CCGACAAGCAGAAGAACGGCATCA-TAMRA-3'

For rat *Hprt1* gene:

Forward: 5'-GCGAAAGTGGAAAAGCCAAGT-3'

Reverse: 5'-GCCACATCAACAGGACTCTTGTAG-3'

Probe: 5'-JOE-CAAAGCCTAAAAGACAGCGGCAAGTTGAAT-TAMRA-3'

For each sample, Ct values were compared with those obtained with different dilutions of linearized standard plasmids (containing either the *Gfp* expression cassette or the rat *Hprt1* gene). The absence of qPCR inhibition in the presence of gDNA was checked by analyzing 50 ng of gDNA extracted from tissues samples from a control animal, spiked with different dilutions of standard plasmid. The limit of quantification was calculated by dividing 25 copies over the mean of the reference gene. Results were expressed in vector genome per diploid genome (vg/dg). The sensitivity of the test was 0.002vg/dg. The efficiency of the amplification reaction was between 95 and 105% (Le Guiner et al., 2011).

Table 10: Summary of behavioral tests

Cohort	Group	Total initial Number	Rotarod (month)							Grip test (month)							Catwalk (month)					Randall Selitto		Dissection	
			1	2	3	4	6	9	12	1	2	3	4	6	9	12	1	2	4	6	12	6	11	Age	Nb
Non-injected	WT	22	22	20 ¹		19 ²	20 ¹		12	22	22		21 ³	22		12	22	22	21 ³	22	12			6m	10
	CMT1A	20	20	20		20	20		12	20	20		20	20		12	20	20	20	20	12			6m	8
Long term cohort (LTC)	WT sh.scr	7	7	7	7	7	7	7		7	7	7	7	7	7							7	7	12m	8
	CMT1A sh.scr	8	8	8	8	8	8	8		8	8	8	8	8	8							8	8	12m	8
	CMT1A sh49	8	8	8	8	4 ⁴	7 ⁵	7 ⁵		8	8	8	8	7 ⁵	7 ⁵							7 ⁵	7 ⁵	12m	8
	CMT1A sh50	8	8	8	8	8	7 ⁶	7 ⁶		8	8	8	8	7 ⁶	7 ⁶							7 ⁶	7 ⁶	12m	8
Short term cohort (STC)	WT sh.scr	8	8	8						8	8													2.5m	8
	CMT1A sh.scr	8	8	8						8	8													2.5m	8
	CMT1A sh49	8	7 ⁷	7 ⁷						7 ⁷	7 ⁷													2.5m	8
	CMT1A sh50	8	8	8						8	8													2.5m	8

¹: 2WT rats jumped from rotating bar as soon as placed on it; ²: 2WT rats jumped from rotating bar as soon as placed on it + 1 WT with wounded paw; ³: 1 WT rat with wounded paw; ⁴: 1 CMT1A rat euthanized due to paw infection and 3 CMT1A jumped from rotating bar as soon as placed on it; ⁵: 1 CMT1A euthanized due to paw; ⁶: 1 CMT1A rat died from a visceral tumor; ⁷: 1 CMT1A rat drags right hindpaw

Dissections: At 6 months for non-injected rats, 10 WT and 8 CMT1A were dissected, at 12 months all rats of LTC are going to be dissected, at 2.5 months all rats of STC dissected. m=month

Table 11: Summary of electrophysiological measurements, molecular and biochemical analysis

Cohort	Group	Total initial Number	ELECTROPHYSIOLOGY (month)							RT qPCR		NF Serum	qPCR Biodistribution of AAV9+ Histological analysis except for blood										
			1	2	3	4	6	9	12	SN	Skin		SN	Muscle	DRG	Spinal cord	Heart	Liver	Spleen	Kidney	Brainstem	Blood	
Non- injected	WT	22							12			2											
	CMT 1A	20							12			2	1	1	1	1	1	1	1	1	1	1	
Long term cohort (LTC)	WT sh.scr	7	7	7	7	7	7	7															
	CMT1A sh,scr	8	8	8	8	8	8	8															
	CMT1A sh49	8	8	8	8	6 ¹	7 ²	7 ²															
	CMT1A sh50	8	8	8	8	8	7 ³	7 ³															
Short term cohort (STC)	WT sh.scr	8	8	8						8	8	5	8	4	8	8	4	4	4	4	4	4	
	CMT1A sh,scr	8	8	8						8	8	5	4	2	4	4	2	2	2	2	2	2	
	CMT1A sh49	8	8	8						8	8		2	1	2	2	1	1	1	1	1	1	
	CMT1A sh50	8	8	8						8	8		2	1	2	2	1	1	1	1	1	1	

SN= Sciatic Nerve; RT qPCR= Reverse Transcriptase quantitative Polymerase Chain Reaction, it was done for PMP22 mRNA in SN and also for biomarkers analysis in SN and skin for all the rats of the STC; NF= Neutralizing Factors; DRG= Dorsal Rot Ganglion; qPCR= quantitative Polymerase Chain Reaction
¹: 1 CMT1A rat euthanized due to paw infection and a second no signal detected; ²: 1 CMT1A rat euthanized due to paw infection; ³: 1 CMT1A rat died from a visceral tumor

For NF and qPCR, littermates and age-matched non-injected controls were dissected; NOT RATS THAT WERE USED FOR MODEL CHARACTERIZATION

Results

Our goal as described in the introduction was to reduce PMP22 expression. Our collaborators P. Young and B. Gess had attempted to reduce PMP22 expression in CMT1A rats through the intraperitoneal injection of “nude” (not cloned in a plasmid) shRNAs without success. Consequently, we chose a gene therapy approach based on AAV viral vectors expressing shRNA to downregulate PMP22 expression. My thesis project intended to correct the impaired phenotype of the CMT1A rat model (motor deficits, electrophysiological abnormalities, sensorial as well as myelination problems) using the approach previously stated.

I. Therapeutic tools validation

A. Efficiency to transduce myelinating Schwann cells in vivo

1. *Efficiency to transduce target cells in rodents*

In a collaborative work between Nicolas Tricaud's and Patrick Aubourg's lab (INSERM U1169 (EX U986)) laboratories, Benoit Gautier (Aubourg's lab), Claire Perrin-Tricaud, Jade Berthelot, Marie Deck and Sergio Gonzalez (Tricaud's lab) studied the transduction efficiency of single stranded AAV9 and 10 carrying a GFP transgene under the control of a CAG promoter (CMV enhancer fused to chicken beta actin promoter) in the sciatic nerves of mice and rats. (**Figure 14**).

First, 2 month-old-adult mice were injected either with AAV9 (4.6×10^{10} vg/nerve) or AAV10 (4.6×10^{10} vg/nerve) in their sciatic nerve. All injections in this project, except for macaques, were done with a microinjector technique developed in the lab of Nicolas Tricaud (**Figure 18**). Briefly, anesthetized animals were placed on their belly; the skin on the thigh was shaved and cleaned before to be cut; two muscles *biceps femoris* and *gluteus superficialis* were then carefully disjointed and the sciatic nerve under the muscles was hold by a spatula. Then the viral solution stained with Fast Green dye was injected using a fine glass needle linked to a

microinjector controlled by a pulse generator. This system allowed for multiple pulsed injections of small volumes in the hundreds of nanoliters range to almost completely fill the sciatic nerve.

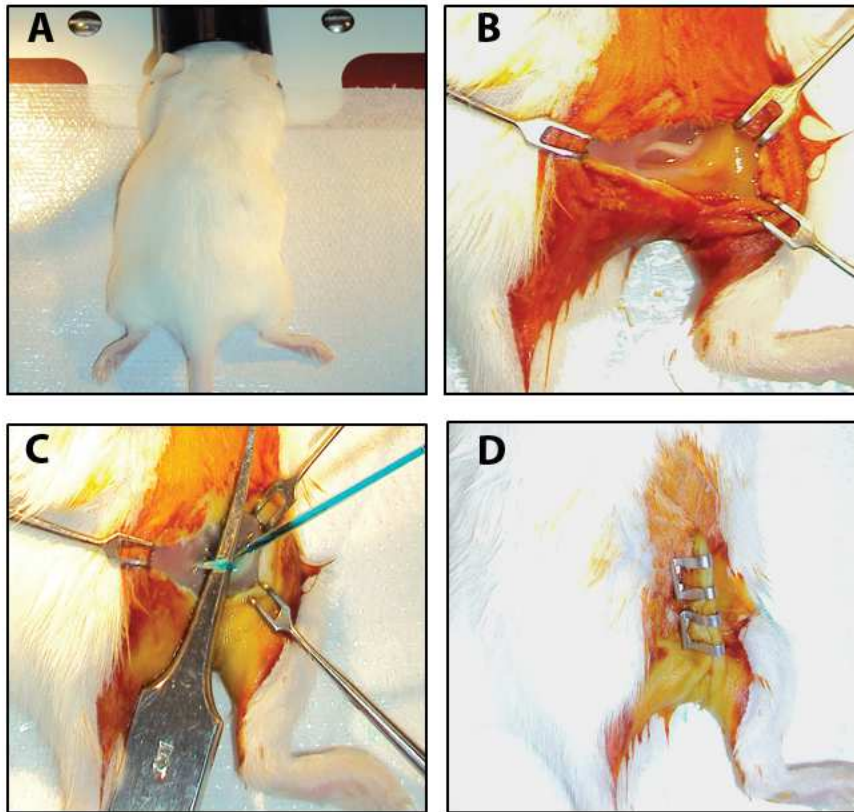


Figure 18 : Injection procedure in the sciatic nerve of an adult rat: A: anesthesia; B: Surgery; C: Injection of virus diluted with Fast Green and PBS; D: Suturing with surgical clips. Adapted and modified from Gonzalez et al, 2014

One month later, sciatic nerves were teased in small fibers bundles to identify the different types of transduced cells based on their morphology: long and large cells were myelinating Schwann cells; fine bipolar cells were non-myelinating Schwann cells; fine never-ending processes were axons (**Figure 19**). Teasing analysis indicated that a very high proportion of transduced cells with both viruses were myelinating Schwann cells. AAV9 remained the most specific one for these cells (**Figure 19**). Few non-myelinating Schwann cells were also transduced. AAV9 did not transduce many axons while AAV10 did infect only a few of them. Thus, AAV9 was selected to carry on testing in 1-month-old adult rats (1.8×10^{11} vg/nerve) with very similar results as in the adult mouse (**Figure 19**). We also tested the transduction of pre-myelinating Schwann cells in the sciatic nerves of mouse and rat pups at postnatal day 3-4 (P3-4) for the mouse

(1.15×10^{10} vg/nerve) and P6-P7 for the rat (1×10^{11} vg/nerve), the ages when myelination starts. Similar results as in adult animals were obtained with AAV9 (**Figure 19**), showing that this virus very specifically targets myelinating Schwann cells when injected directly in the nerve.

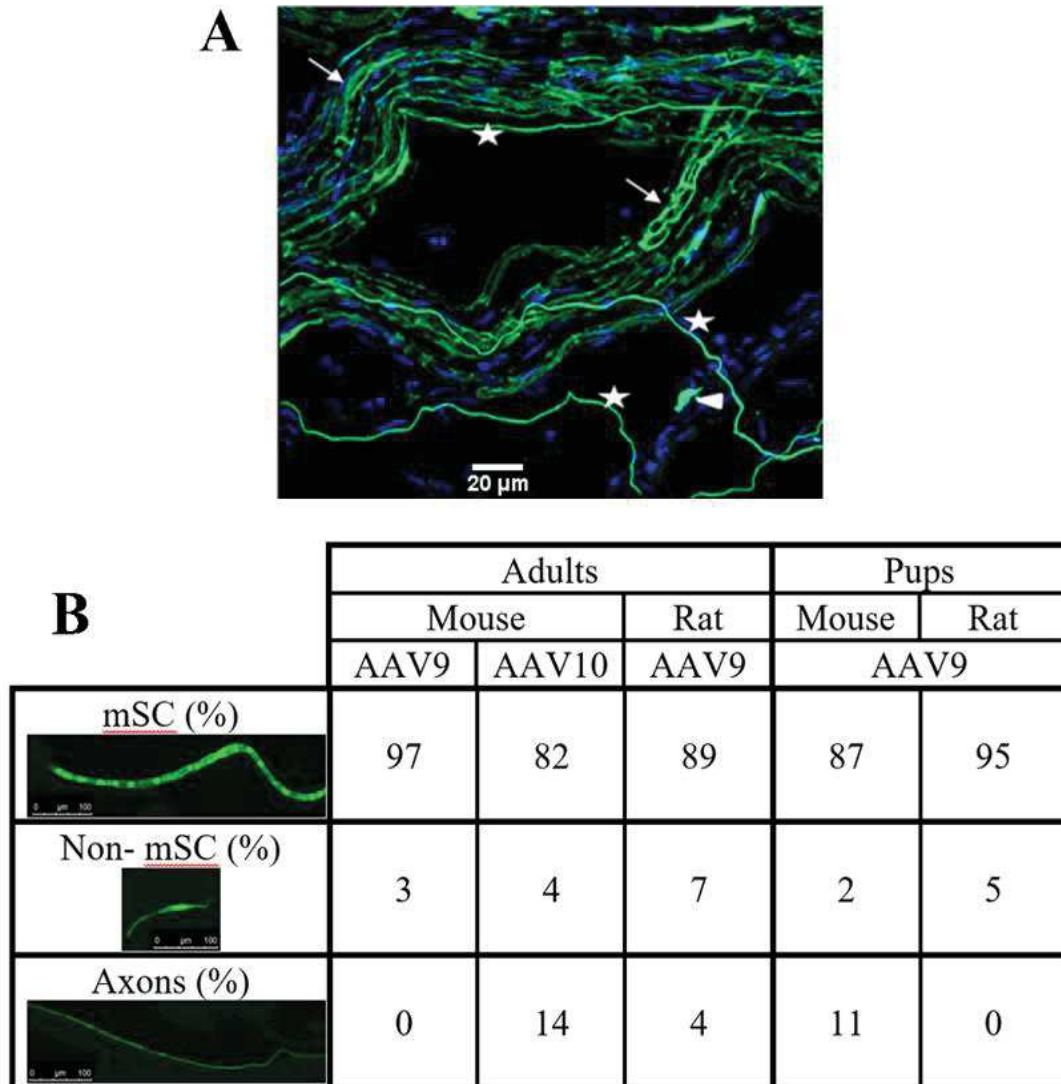


Figure 19 : Teasing results of rats and mice injected with AAV9 or 10: 3 animals per viral vector were injected in the sciatic nerve unilaterally (n=3). **A:** Microscopic image of adult mouse AAV10-injected nerve showing transduced myelinating Schwann cells (white arrows), non-myelinating Schwann cells (white arrowheads) and axons (white star). Scale bar=20 μ m. **B:** Table representing the type of cells transduced in percentage (%): mSC (myelinating Schwann cells), non-mSC= non-myelinating Schwann cells and axons. AAV9 targets almost exclusively mSCs.

2. Transduction rate of myelinating Schwann cells in rodents

We next immunostained cryosections of rat and mouse sciatic nerves injected with AAV9 or 10 to measure the percentage of transduced myelinating Schwann cells. Myelinated fibers were

detected using MBP for the myelin sheath and Tuj1 for myelinated axons. The number of GFP labelled myelinating Schwann cells per myelinated fiber was counted. We found that both viruses transduced a high number of myelinating Schwann cells (***Figure 20***). In adult mice AAV9 transduced more myelinated Schwann cells than AAV10 at the injection site (93% compared to 51 %). In addition, AAV9 diffused more than AAV10 along almost the entire nerve of adult mice (***Figure 20***). In general, for both mice and rats, in adults or pups, a large majority of myelinating Schwann cells were transduced (80-90%) by AAV9 (***Figure 20***).

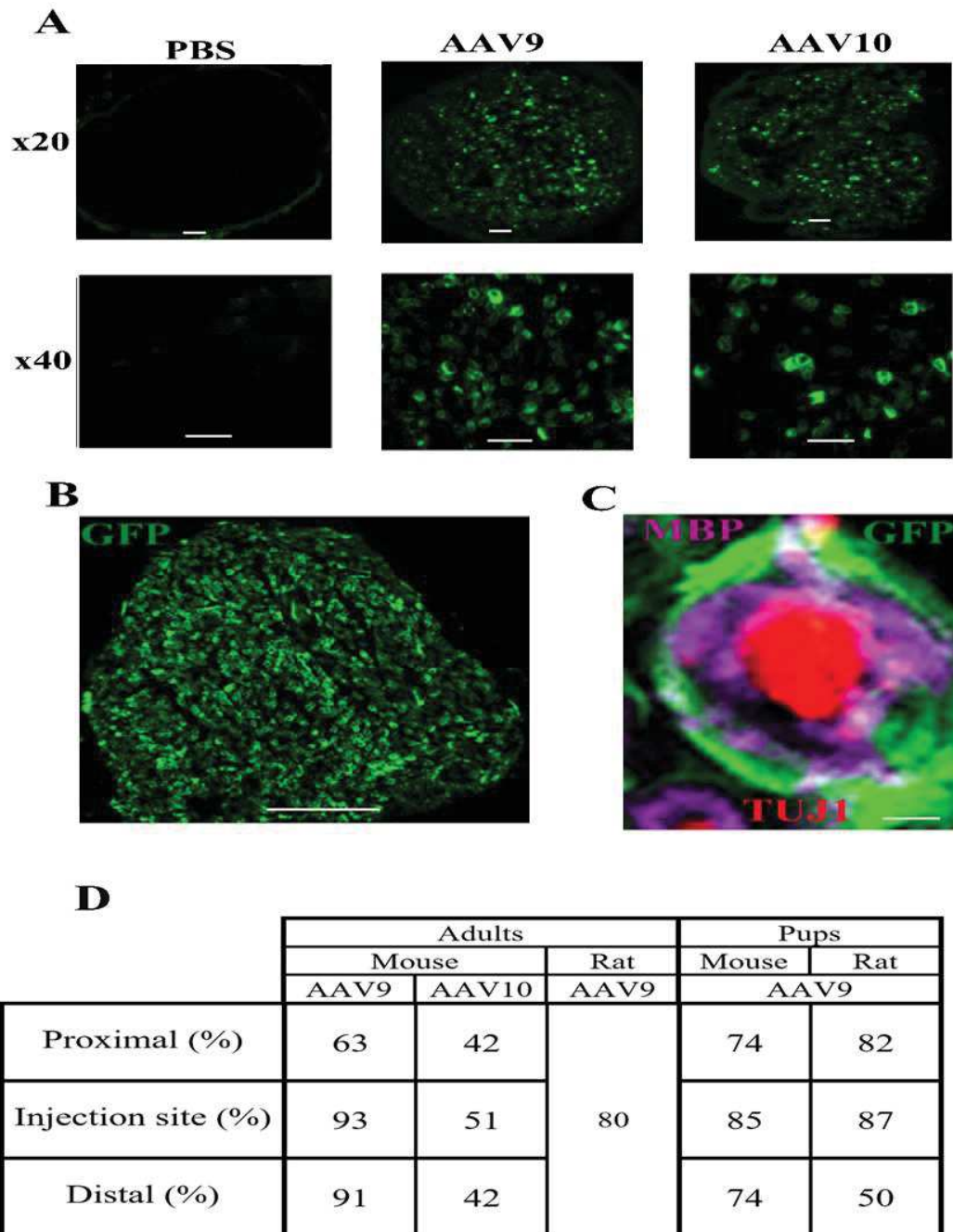


Figure 20 : Transduction of myelinating Schwann cells in the sciatic nerve of rats and mice 3 animals per viral vector (n=3). **A**: Cryosection of an adult mouse sciatic nerve injected with PBS, AAV9 or 10. Scale bar=10 μ m; **B**: Cryosection of a rat pup sciatic nerve injected with AAV9. Scale bar=100 μ m; **C**: Example of an infected cell expressing GFP (green). Myelinating Schwann cells are labelled by Myelin Basic Protein (MBP, purple) and axons by Tubulin β 3 (TUJ1, red). Scale bar=2.5 μ m; **D**: Table representing the percentage of transduced myelinating Schwann cells at the injection site and at different distance of this site (proximal: 1 cm above the injection site, distal: 1 cm below the injection site). AAV9 has a high transduction rate and a good diffusion.

3. *Efficiency of transduction in macaca fascicularis*

Injection of AAV into the sciatic nerve of 2 year-old-macaques (*macaca fascicularis*) was done at the MIRCEN facility of the CEA Fontenay aux roses by the neurosurgeon Dr Michel Zerah, with the help of Benoit Gautier and Claire-Maëlle Fovet. These injections were done using a capillary fiber linked to a Hamilton syringe right above the split of the sciatic nerve into common fibular and tibial nerves. 40 μ L were injected for AAV9 and 400 μ L for AAV10 over 10 minutes for AAV9 (5x10¹¹ vg/nerve) and 30 minutes for AAV10 (5x10¹² vg/nerve). The characteristics of the injected animals are shown in **Table 7**. These animals were sacrificed 30 days after injection and their nerves analyzed by cryosections and immunostaining.

In these animals, we could not detect any transduced cells with AAV10 while AAV9 transduced mostly myelinating Schwann cells. The transduction rate of myelinating SCs was high (70%) at the injection site and the virus showed a relatively good diffusion rate along the nerve as nerve sections located up to 3 cm from the injection site in the proximal direction were infected at a significant rate (**Figure 21**). Overall the diffusion reached up to 5.5 cm.

Taken together these data indicated that AAV9 injected directly in the sciatic nerve was the most specific and the most efficient virus to transduce myelinating Schwann cells *in vivo*. These proves of concept for the use of AAV9 to transduce myelinating Schwann cells *in vivo* was patented by the two labs and INSERM Transfer in 2017 (Patent WO2017005806A1).

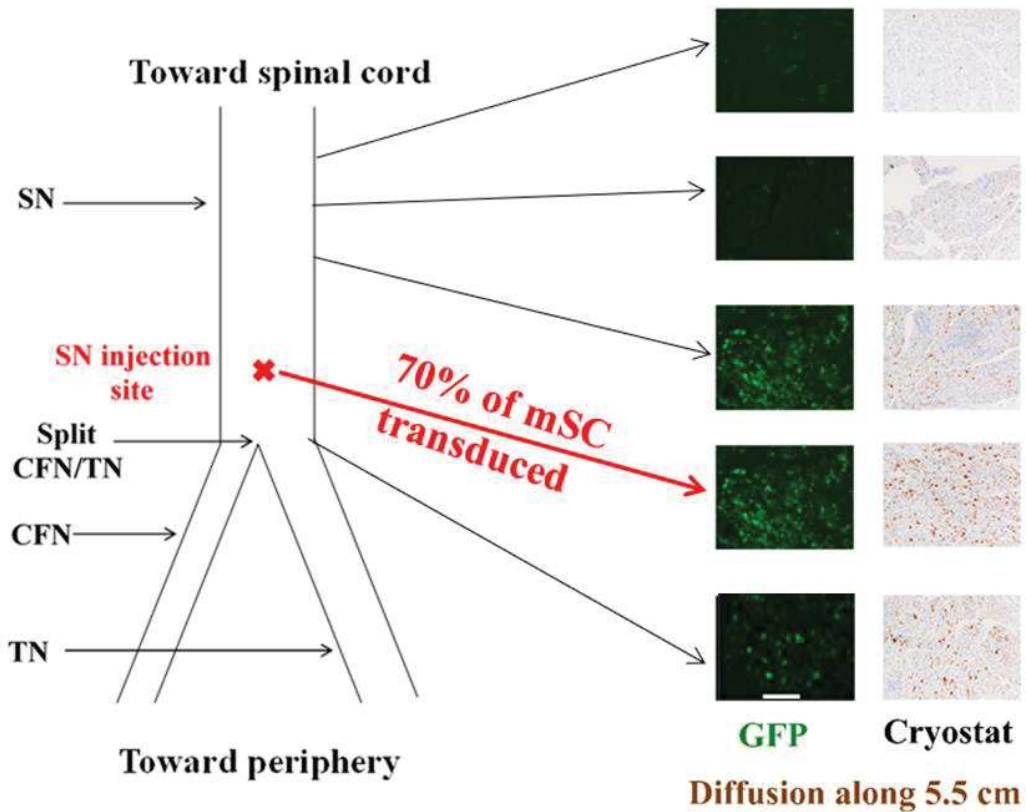


Figure 21 : Transduction of myelinating Schwann cells in the sciatic nerve of macaques: mSC= myelinating Schwann cells; SN= Sciatic Nerve; CFN= Common Fibular Nerve; TN= Tibial Nerve. Good transduction rate of AAV9. Scale bar=50 μ m..

B. Design, cloning and validation of shRNAs targeting mouse PMP22 mRNA

Next, we designed shRNAs targeting mouse PMP22 mRNA, which is overexpressed in CMT1A rats. Our collaborators Burkhard Gess and Peter Young (University Hospital Münster, Department of Sleep Medicine and Neuromuscular Diseases, Germany) had already designed and characterized two shRNAs, shRNA PMP22-49 (sh49) and shRNA PMP22-50 (sh50), to silence mouse PMP22 in CMT1A rats (**Figure 22.A**). These shRNAs target the coding sequence of the mouse PMP22 mRNA (**Figure 22.B and C**). These sequences were homologous of rat but not human or macaque sequences (**Figure 22.B and C**). We chose a control shRNA as a shRNA without any target in mammals. We cloned these shRNA sequences into a recombinant AAV plasmid (pAAV2/9, CPV, UMR1089, Nantes) under the control of a U6 promoter next to the GFP under the control of a CMV promoter. These plasmids were validated by sequencing.

After that, we examined the impact of shRNA therapeutic tool on PMP22 mRNA and protein levels *in vitro*. Mouse Schwann cell line (MSC80) expressing PMP22 and CMT1A rat Schwann cells were transfected with shRNA constructs: scramble shRNA (scr.sh or control sh), shRNA PMP22-49 (sh49) or shRNA PMP22-50 (sh50). PMP22 mRNA expression was then quantified by real-time PCR. We found that MSC80 cells transfected with sh49 and sh50 plasmids showed a significantly decreased expression of PMP22 (**Figure 22.D**). In Schwann cells of the CMT1A rat, *PMP22* mRNA expression was also significantly reduced compared to control shRNA (**Figure 22.E**). In addition, PMP22 protein levels were also downregulated by sh49 and sh50 in MSC80 (**Figure 22.F and G**) and in CMT1A rat Schwann cells (**Figure 22.H and I**), showing that these shRNAs against mouse PMP22 mRNA are effective in reducing mouse PMP22 expression.

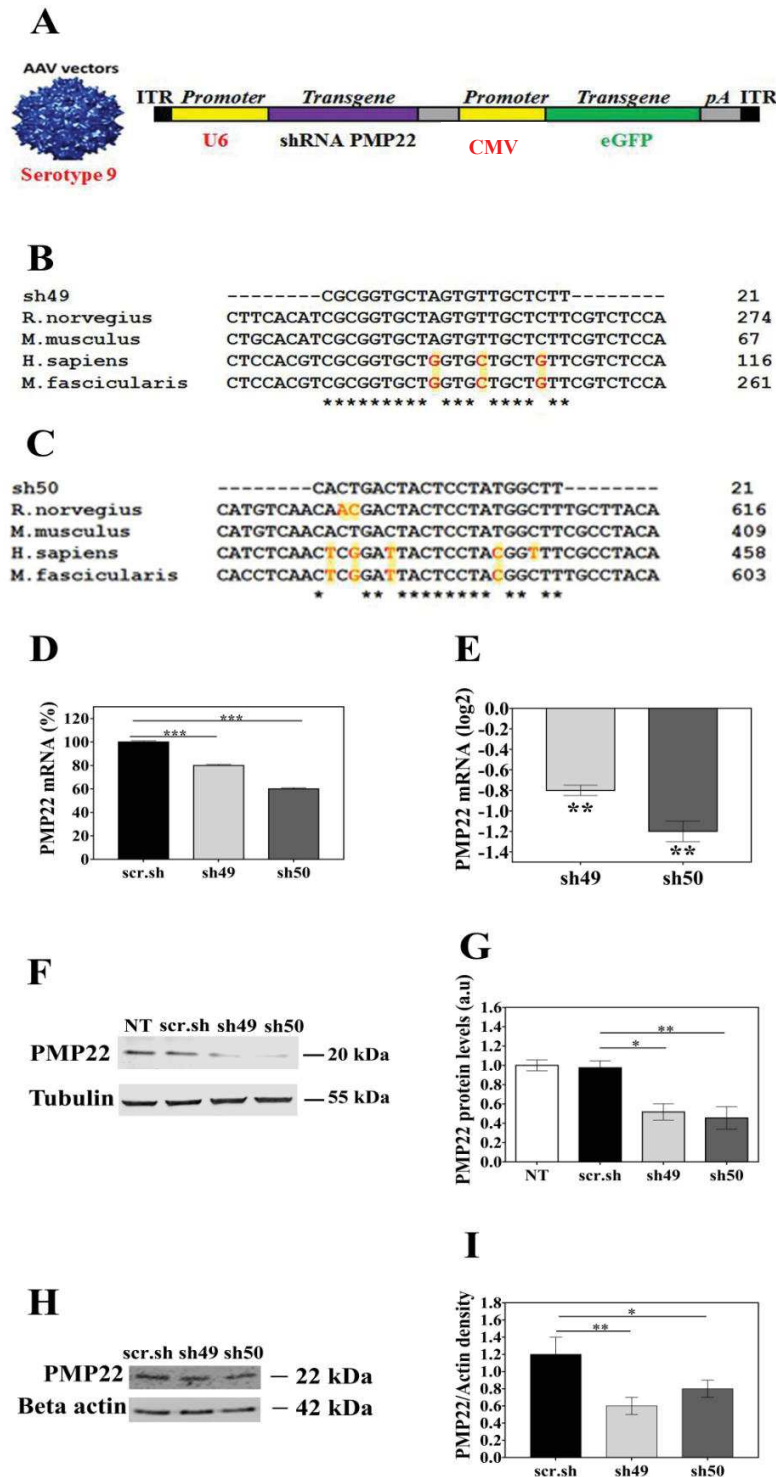


Figure 22: Downregulation of PMP22 by shRNA in vitro: scr.sh= scramble shRNA, sh49 = shRNA PMP22-49, sh50= shRNA PMP22-50. **A:** AAV shRNA cassette diagram. Alignment of sh49 (**B**) and sh50 (**C**) sequences with PMP22 mRNA of rat (*rattus* (*R*)*Norvegicus*), mouse (*Mus* (*M*)*musculus*, human (*homo* (*H*)*Sapiens*) and macaque (*macaca* (*M*)*fascicularis*); **D:** Real-time PCR of PMP22 mRNA extracted from MSC80 cells after transfection with shRNA constructs; scr. sh normalised as 100%; mean +/- standard deviation shown, 4 independent experiments per condition; *** $p < 0.001$ (performed by Gess, B and Young, P). **E:** Real-time PCR of PMP22 mRNA extracted from CMT1A rat Schwann cells after transfection with shRNA constructs; scr.sh not shown but considered 0; mean +/- standard deviation shown; ** $p < 0.01$ (performed by Gess, B and Young, P). **F, G:** Western blots and quantifications in percentage of MSC80 cell lysates after transfection with shRNA plasmids; 3 independent experiments per condition; * $p < 0.05$, ** $p < 0.01$ (performed by Benoit Gautier). **H, I:** Western blots and quantifications in percentage of CMT1A rat Schwann cell lysates after transfection with shRNA plasmids; * $p < 0.05$, ** $p < 0.01$ (performed by Gess, B and Young, P).

Statistical analysis was done using Graphpad Prism 7, Ordinary-One-Way ANOVA followed by Tukey's test. Mean \pm standard deviation shown.

We were then confident for the use of AAV9 viral vector expressing shRNAs 49 and 50 to reduce mouse PMP22 overexpression in myelinating Schwann cells of CMT1A rats.

II. CMT1A rat model characterization

Next, I functionally characterized the CMT1A rat model using different behavioral tests cited in the literature: Rotarod and grip test to study motor impairments seen in CMT1A rats, catwalk to assess the unsteady gait of CMT1A rats and electrophysiological measurements of nerve conduction velocity known to be decreased in CMT1A. I did the behavioral analysis on a regular basis, every 1-2 months until 6 months of age of rats then at 12 months right before sacrifice except for NCV measurements which I only did at 12 months. I used CMT1A rats (20 animals) heterozygous for mouse *pmp22* transgene and control WT animals (22 rats) from the same litter (Table 10, Table 11). The animals utilized to develop our colony were kindly provided by Michael Sereda laboratory in Germany.

A. Motor deficits

Motor deficits cited in the literature (Fledrich et al., 2014; M. Sereda et al., 1996) were confirmed by rotarod (Figure 23.A) for motor coordination and equilibrium and grip test (Figure 23.B) for muscle strength. CMT1A rats fall faster than WT from the rotating bar of the rotarod apparatus. Moreover, they have lower muscle strength as seen by grip test of the rear paws. These deficits start to be statistically significant at 1 month of age for rotarod and 4 months for grip test and are maintained over 12 months.

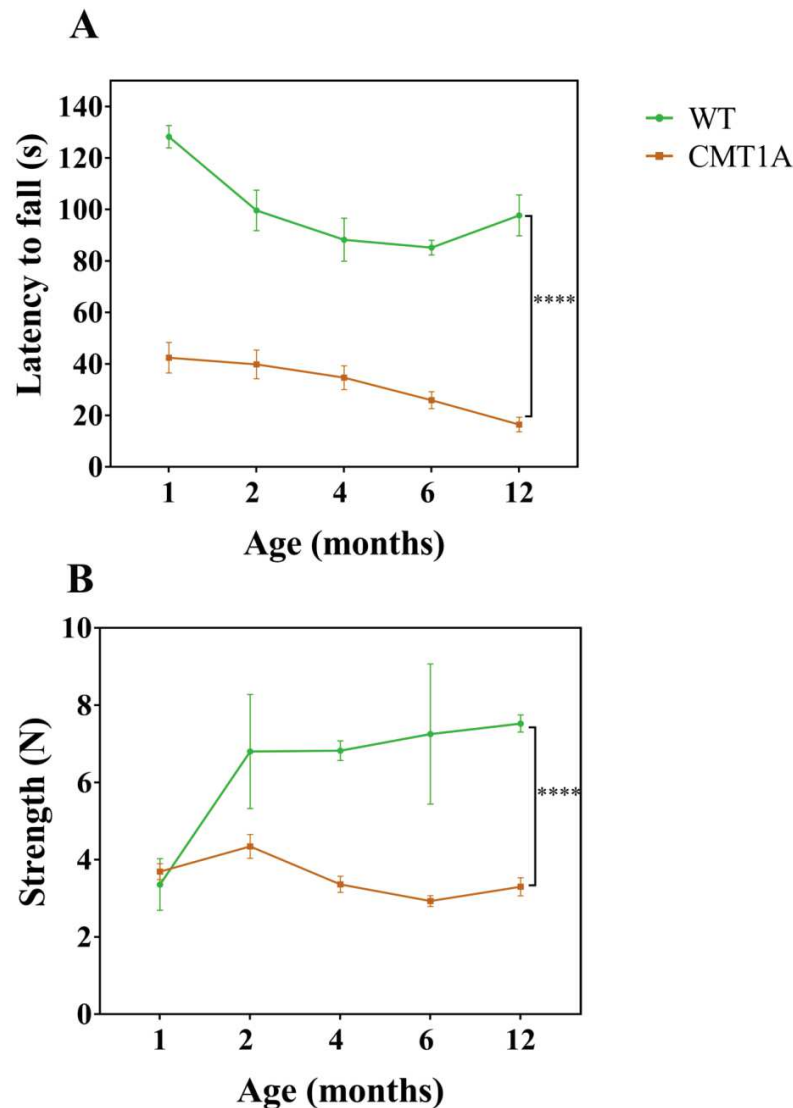


Figure 23: Motor impairments in CMT1A rats:

A: Rotarod, latency to fall in seconds (s).

B: Grip strength test in Newtons (N).

**** $p < 0.0001$.

Statistical analysis was done on Graphpad Prism 7: Two-Way-ANOVA with repeated measures followed by Tukey's test.

Mean \pm SEM per time point.

WT $n=22$ per time point except at 12 months $n=12$.

CMT1A $n=20$ per time point except at 12 months $n=12$.

B. Clumsiness in walking

As far as I know, the Catwalk test was never used to study the gait of CMT1A rats. This test allows for analyzing rat gait while they cross a corridor. It is a modern version of the ink-based trace analysis. Two (**Figure 24.A**) and four (**Figure 24.B**) months-old-CMT1A rats were analyzed for several parameters. The parameters we retained were: “Max contact”, inter-paw coordination parameters “regularity index”, “phase dispersions” and “couplings” as well as “left hind paw single stance”. CMT1A rats of both ages leave their paws on the glass plate of the

apparatus with less intensity than WT (“Max Contact”, **Figure 24.A and B**). Four month-old CMT1A-rats have less inter-paw coordination than WT as seen by the regularity index, phase dispersions and couplings parameters (**Figure 24.C**). CMT1A rats leave one of their hind paws a shorter time on the glass plate compared to WT as indicated by the single stance parameter (**Figure 24.D**). For detailed definition of each parameter refer to the legend of figure 24 and to material and methods chapter.

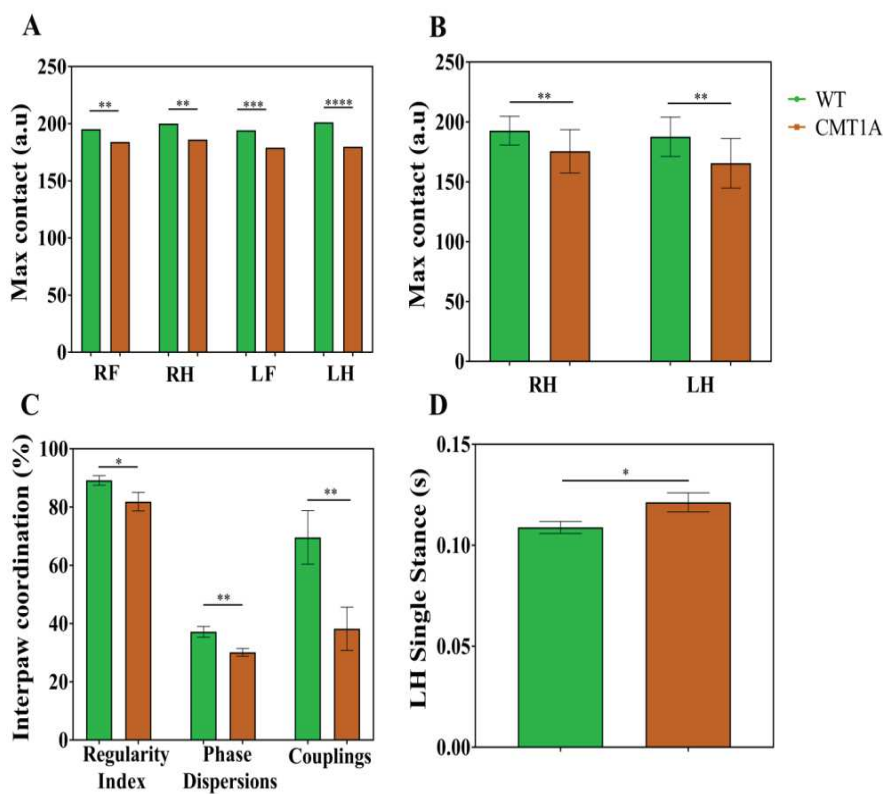


Figure 24: Locomotion problems in CMT1A rats: RF=right front, RH=Right hind, LF= Left front, LH=left hind. **Max contact** in arbitrary units (a.u) for 2- (**A**) and 4-month-old rats (**B**): print intensity of animals when their whole paw is in contact with the glass plate of the Catwalk. **C**: Interpaw coordination parameters in percentage (%), 4-month-old rats: Regularity index expressing the number of normal step sequence patterns relative to the total number of paw placements, phase dispersions describing the temporal relationship between placement of two paws, ranges from -50 to 75% and couplings similar to the phase dispersions parameter but ranges from 0 to 100%. **D**: LH single stance: the duration (in seconds) of ground contact for a single hind paw. It is the part where the contralateral hind paw does not touch the glass plate
* $p < 0.05$, ** $p < 0.01$, *** $p < 0.001$, **** $p < 0.0001$. Graphpad Prism 7: Ordinary One-Way-ANOVA followed by Tukey's test except for Figure 7D: t-test. Mean \pm SEM. WT $n = 22$. CMT1A $n = 20$.

C. Reduced Nerve Conduction Velocity (NCV)

Briefly, after anesthetizing animals with isoflurane, electrodes are placed at both proximal and distal site of the rat's sciatic nerve (refer to material and methods II.C) to stimulate the nerve and record a signal as compound muscle action potentials (CMAP). CMAP is defined as the sum of activity in muscle fibers following motor nerve stimulation. The very start of the CMAP apparition is used as the time measure. The distance between proximal and distal electrodes is also measured and NCV is then calculated based on the classical velocity formula of distance over

duration time. Duration time or latency is the difference between the start of the CMAP response at the proximal and at the distal measure sites:

$$\text{NCV (m/s)} = \frac{\text{distance}}{\text{Proximal Latency} - \text{Distal Latency}}.$$

Using this setup NCV of 12 month-old-CMT1A-rats was significantly lower compared to WT **(Figure 25).**

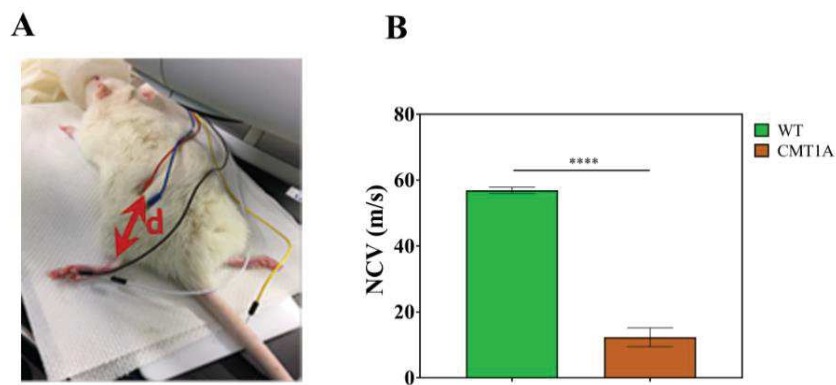


Figure 25: Decreased NCV in CMT1A rats: A: Electrophysiological measurements method; B: NCV= Nerve conduction velocity in meter per second (m/s) * $p < 0.0001$ (t-test). Mean \pm SEM. WT $n=12$. CMT1A $n=12$.***

Taken these data together we concluded that rotarod and grip tests were suitable to study motor deficits seen in diseased animals. In addition, NCV was an essential parameter to measure since reduced values (like I found in CMT1A rats) are a typical feature of CMT1A. We decided to add the measure of the CMAP amplitude to the analysis. However, I noted that Catwalk was time-consuming for analysis with often inconclusive results. Furthermore, since there was a large variability between rats, the sample size had to be increased to observe statistically significant differences. In line with the 3Rs ethic rule (Replacement, Reduction and Refinement, Fenwick, Griffin, & Gauthier, 2009) of animal use in research, we decided not to use the Catwalk for studying the efficiency of the gene therapy approach in rats but only rotarod, grip test and electrophysiological measurements.

III. **Experimental design**

Together with Nicolas Tricaud and Benoit Gautier who joined Nicolas Tricaud's lab in October 2016, we carefully designed the experimental plan. First, we chose to create two cohorts of rat subdivided into 4 groups each. The two cohorts were termed "long term cohort or LTC" and "short term cohort or STC". LTC served to study the efficiency of the gene therapy on the long term (sacrifice at 12 months) while STC was used to correlate behavioral analysis and electrophysiological measurements with biochemical and morphological studies (sacrifice at 2.5 months) (**Figure 26**).

The 4 groups were:

- WT injected with AAV9 scramble shRNA (WT scr.sh) (8 animals)
- CMT1A injected with AAV9 scramble shRNA (CMT1A scr.sh) (8 animals)
- CMT1A injected with AAV9 shRNAPMP22-49 (CMT1A sh49) (8 animals)
- CMT1A injected with AAV9 shRNAPMP22-50 (CMT1A sh50) (8 animals)

In this experimental plan all animals, even WT, are injected in order to detect whether the injection itself affects the animal phenotype, comparing their performance to the previously described non-injected cohort. Then, defects of CMT1A animals in injected conditions only (AAV with control shRNA) can be observed when compared to WT injected animals. Finally, the beneficial effect of shRNA 49 and 50 can be analyzed comparing CMT1A rats injected with AAV control shRNA with mutant animals injected with AAV shRNA 49 and 50.

We chose for assessing motor performance rotarod and grip strength test since I obtained good results with these tests in the preliminary characterization of the animal model. We also decided to add a sensory test, the Randall-Selitto pain test, because a large number of sensory fibers are myelinated and therefore affected in CMT1A. This test had never been used before on CMT1A rats.

At the moment, among all the behavioral and biochemical tests we planned in this experimental plan (**Figure 26**), only the morphological analyses of LTC are still ongoing.

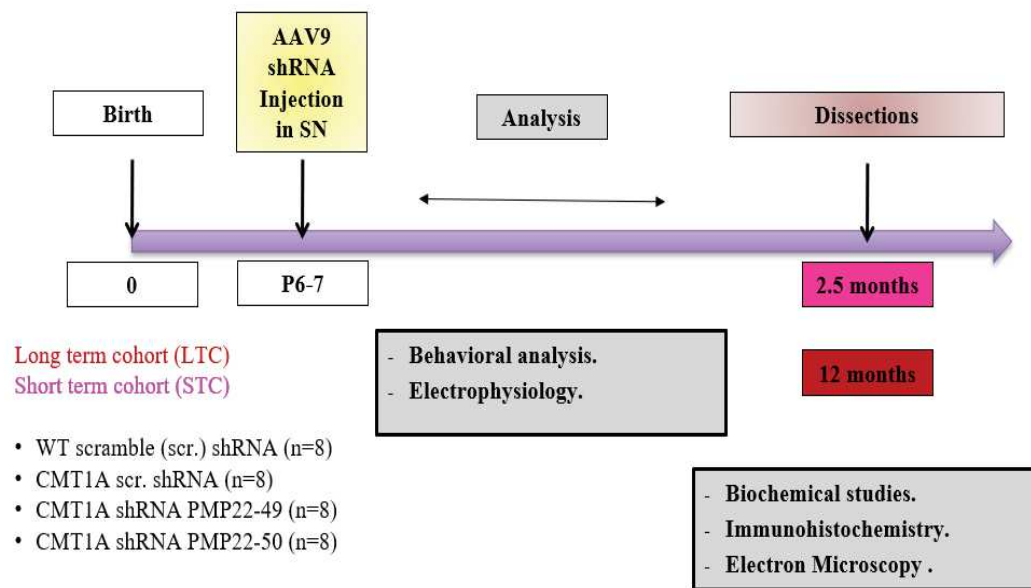


Figure 26: Summary of experimental design.

IV. Efficiency of AAV9 shRNA PMP22 in vivo

We first measured the efficiency of AAV9 expressing shRNAs 49 and 50 to decrease mouse PMP22 in myelinating Schwann cells *in vivo*.

Total mRNA of STC sciatic nerves were collected for each animal. Mouse PMP22 mRNA was quantified by RT qPCR using rat *Hprt* as the reference gene. This work was done in collaboration with Dr. Caroline Le Guiner and Virginie François (Translational gene therapy for genetic diseases-UMR1089, Nantes, France). Results were normalized to values obtained in CMT1A animals expressing control shRNA. Given that WT rats do not possess the mouse *PMP22* gene, the PMP22/HPRT mRNA relative expression is null. Nevertheless, this was not statistically significant (**Figure 27.A**). We plan to reproduce the experiment because the reference gene was weakly expressed in rat sciatic nerve. We will use *Rps9* and *Actb* as reference gene instead.

We also measured the protein expression level of mouse and rat PMP22 in treated or control sciatic nerves. These levels were normalized on rat MPZ protein level because myelin amount is highly heterogeneous in CMT1A rats (Grandis et al., 2004). PMP22 expression increased in CMT1A rats versus WT animals and treatment with PMP22 shRNA 49 and 50

significantly reduced it (**Figure 27.B**). Interestingly, PMP22 expression mouse and rat reached control level in nerve treated with PMP22 shRNAs, suggesting that the downregulation was not sufficient enough to induce deleterious effects such as in animals and patients with PMP22 loss of function.

Thus, taken together these data show that our gene therapy approach is able to restore the correct amount of PMP22 expressed in myelinating Schwann cells of CMT1A rats.

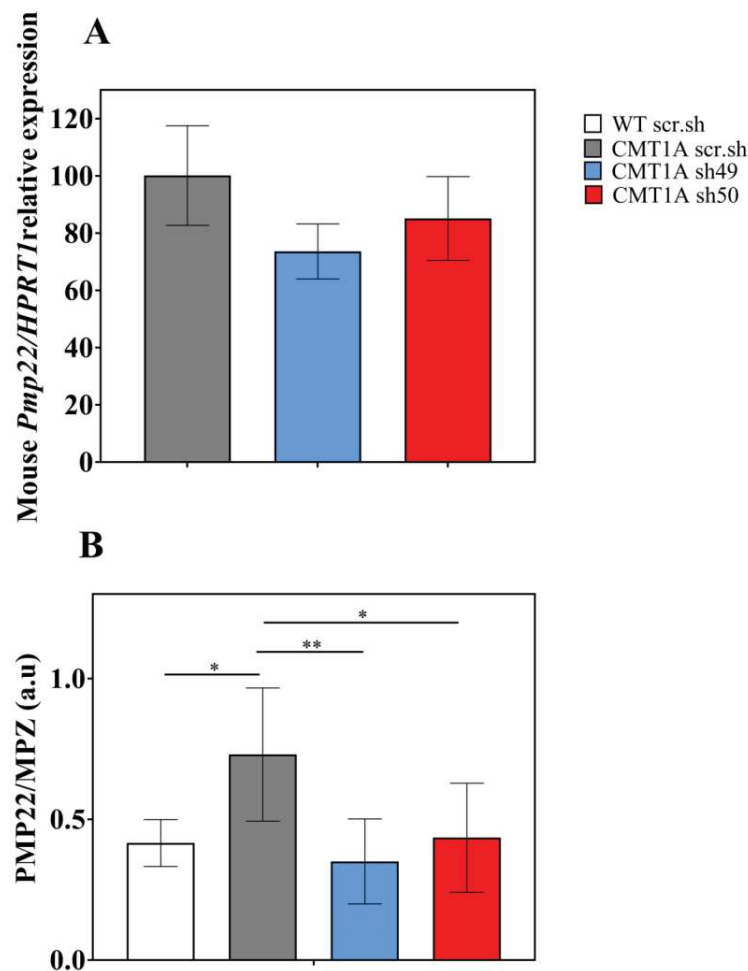


Figure 27: Downregulation of PMP22 by AAV9 shRNA in sciatic nerves of rats: scr.-shRNA= Scramble shRNA, shRNA49 = shRNA PMP22-49, shRNA50= shRNA PMP22-50 Sciatic nerve extracts from 2.5 months-old-rat, n=8 per group.

A: Real-time PCR of MOUSE PMP22 mRNA (performed at the UMR1089, Nantes). Results (still preliminary) are presented as relative expression (% of CMT1A scr.sh).

B: Western blots quantifications of TOTAL PMP22. a.u= arbitrary units.

* $p < 0.05$, ** $p < 0.01$. Statistical analysis was done on Graphpad Prism 7: Ordinary One-Way-ANOVA followed by Tukey's test. Mean \pm SEM.

V. Functional recovery of treated rats

To assess whether a functional recovery was achieved following gene therapy, LTC rats were tested 1, 2, 3, 4, 6, 9 and 12 months post injections. Tests included rotarod for motor coordination and equilibrium, grip test for muscle strength and Randall Selitto (6 and 11 months post injections) for pain sensitivity assessment.

A. Gene therapy improved motor deficits in CMT1A-treated rats

All injected animals of LTC were tested on the rotarod and for the grip test 1, 2, 3, 4, 6, 9 and 12 months post injections. I found that, at the same age, WT and CMT1A rats treated with control shRNA virus had a phenotype like non-injected WT and CMT1A animals respectively (**Figure 28. B and D**). This showed that injection of the virus, infection of myelinating Schwann cells and control shRNA expression had no effect on the phenotypes.

Starting as early as 2 months of age, the latency to fall and the rear limb strength of CMT1A rats treated with both AAV9 shRNA PMP22-49 and 50 were significantly higher than CMT1A rats treated with AAV9 control shRNA (**Figure 28. A and C**). 1-month post-injection, the rotarod and grip test performance of PMP22 shRNA treated CMT1A rats were maintained close to control shRNA treated WT regardless of the time post injection, showing that the treatment with PMP22 shRNA prevent the disease to develop in CMT1A rats. With a single injection at 6-7 days after birth, motor and strength performances could be maintained close to the WT performances for up to 12 months. Performance of CMT1A treated rats reach WT levels in rotarod 4 and 12 months post injections of both sh49 and sh50 while for grip test, 6 and 9 months with both shRNAs injections and 12 months with sh49 only.

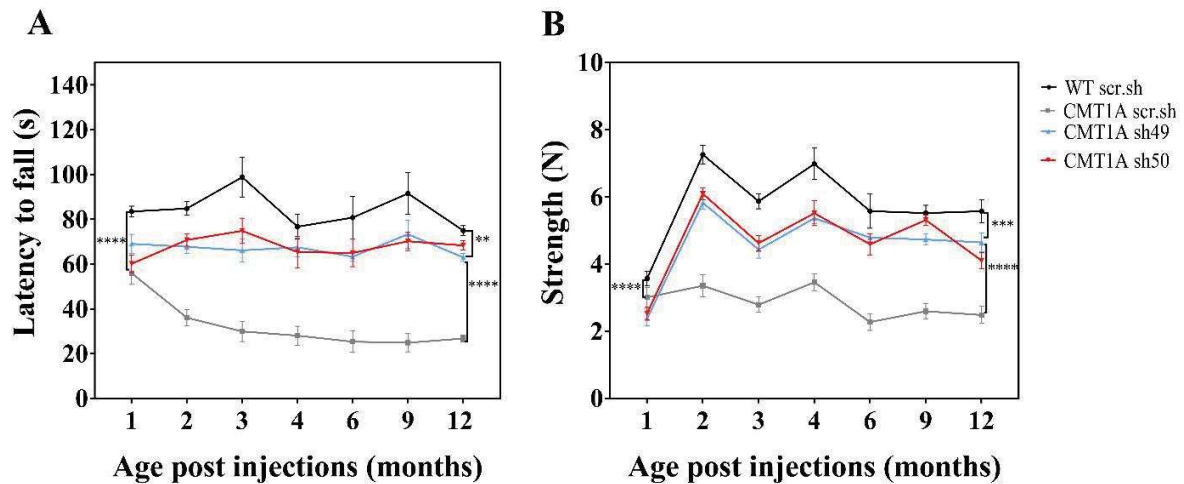


Figure 28: Improvement of motor phenotype in treated rats: Latency to fall in rotarod is expressed in seconds (s) for injected rats (A) and non-injected rats (B). Grip strength of the hind paws is expressed in Newtons (N) for the injected rats (C) and non-injected rats (D). Gene therapy corrected the motor coordination and equilibrium problems as well as increased muscular strength of CMT1A rats. ** $p < 0.01$, *** $p < 0.001$, **** $p < 0.0001$. Statistical analysis was done on Graphpad Prism 7: Two-way ANOVA with repeated measures followed by Tukey's test. Mean \pm SEM and $n=8$ per group and per time point.

B. Hypoalgesia of CMT1A rats alleviated by gene therapy

Randall Selitto measures the nociceptive threshold of rats by applying an increasing pressure on their hind paws using a calibrated weight. This test was done by Antoine Jouvenel (PhD student, INM) on LTC rats 6 and 11 months post injections (**Figure 29**).

We observed hypoalgesia in CMT1A rats treated with control shRNA virus as they can bear a higher pressure applied on their hind paws compared to WT. CMT1A rats treated with PMP22 shRNA viruses had a higher sensibility to pain reaching WT levels even 11 months after the treatment. Consequently, treatment is efficient to maintain the normal response to pain in CMT1A rats (**Figure 29**).

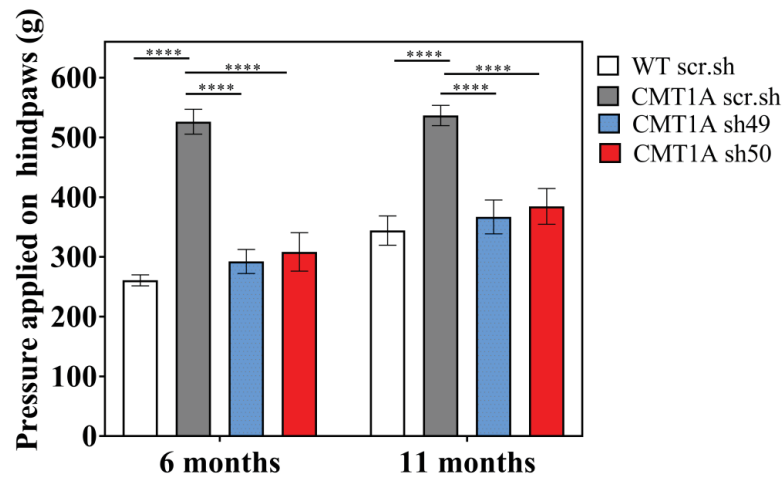


Figure 29: No more hypoalgesia in treated rats: Pressure applied on the hindpaw is represented in grams (g) Gene therapy effectively reduced hypoalgesia**** $p < 0.0001$. Statistical analysis was done on Graphpad Prism 7: Two-way ANOVA with repeated measures followed by Tukey's test. . Mean \pm SEM and $n=8$ per group and per time point.

VI. Reduced Nerve Conduction Velocity (NCV) in CMT1A rats corrected by gene therapy

As a quick reminder of the technique (for further details refer to material and methods II.C or to this chapter section II.C), stimulation electrodes are placed at both proximal and distal site of the rat's sciatic nerve and the recording of the compound of muscle action potentials (CMAP) is done in the hindpaw muscle. Nerve conduction velocity (NCV) is then calculated based on the following formula:

$$\text{NCV (m/s)} = \frac{\text{distance}}{\text{Proximal Latency} - \text{Distal Latency}}.$$

NCV was measured on LTC rats 1, 2, 3, 4, 6, 9 and 12 months post injections. NCV of CMT1A rats treated with control shRNA virus was reduced compared to WT, such as in non-injected CMT1A rats. However, the NCV of CMT1A rats treated with PMP22 shRNA viruses was significantly higher than their genetic CMT1A siblings treated with control shRNA virus. Starting 1 month after treatment with PMP22 shRNA viruses maintained the NCV close to WT animals' values for up to 12 months. However, this therapy had no effect on the amplitude of the compound muscle action potential (CMAP) (**Figure 30**).

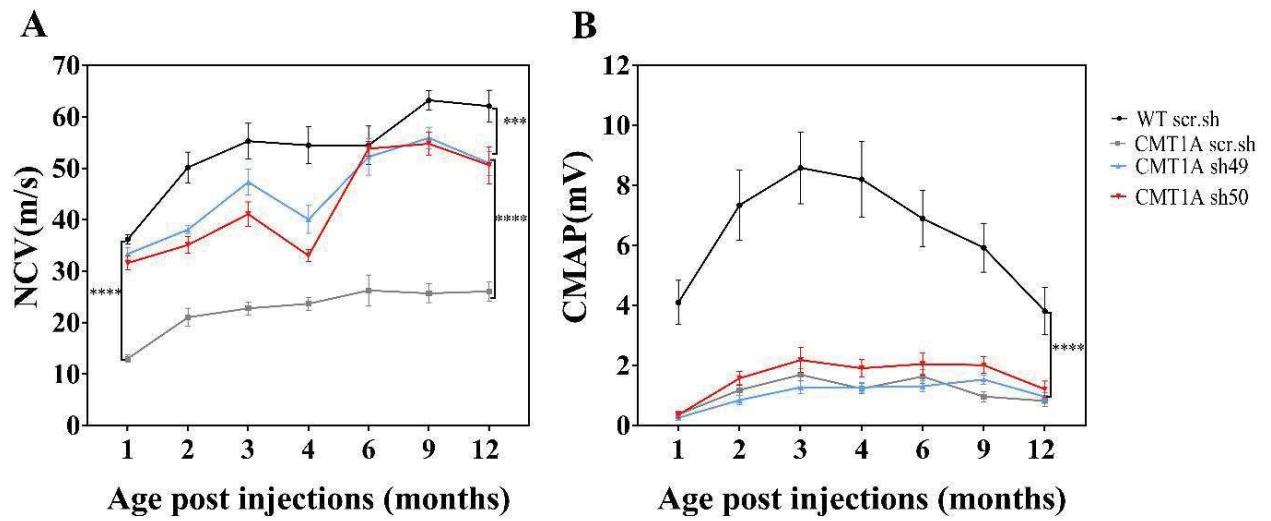


Figure 30: Increased of NCV in treated rats: **A.** NCV (Nerve Conduction Velocity) is denoted in meter per second (m/s) and **B.** CMAP (Compound Muscle Action Potentials) in millivolt (mV). Gene therapy is efficient for NCV but not CMAP. *** $p < 0.001$, **** $p < 0.0001$. Statistical analysis was done on Graphpad Prism 7: Two-way ANOVA with repeated measures followed by Tukey's test. . Mean \pm SEM and $n=8$ per group and per time point.

VII. Appropriate age of correlation between behavioral analysis, electrophysiological measurements and molecular, biochemical and morphological studies

In order to test the homogeneity of experiments I performed, rotarod latency to fall, grip test muscle strength and NCV of injected rats were also measured in the second cohort, STC, at 2 months of age. Similar results were obtained in the STC compared to LTC. A statistically significant difference was only seen in NCV between AAV9 sh49 and sh50 injected groups (**Figure 31**).

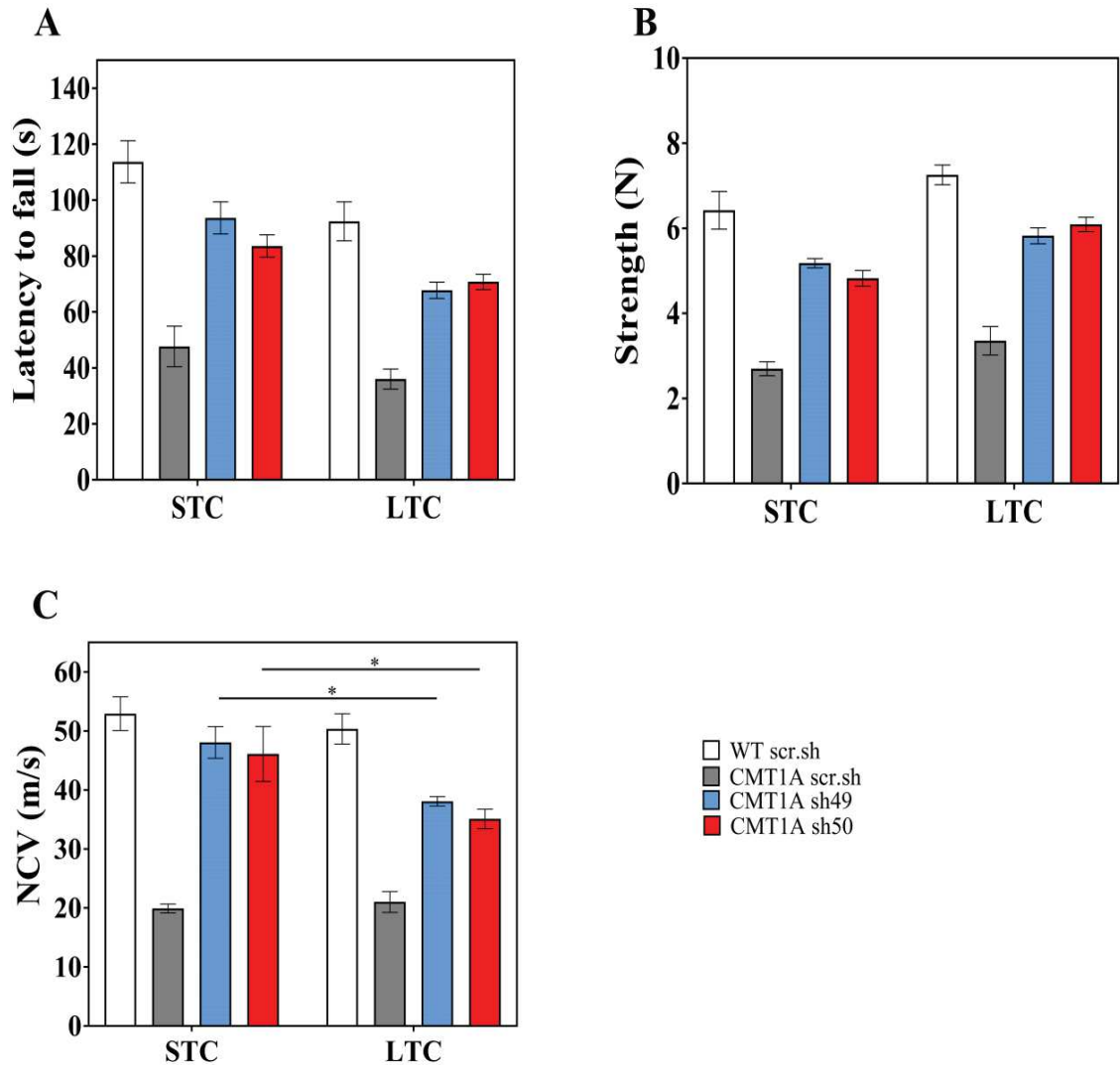


Figure 31: Comparison between 2 cohorts: STC= short term cohort; LTC= long term cohort. No difference was found between LTC and STC except for shRNA 49 and 50 in NCV. **A:** Latency to fall in rotarod expressed in seconds (s). **B:** Grip strength of hind paws expressed in Newtons (N). **C:** NCV expressed in meter per second (m/s). * $p < 0.05$. Statistical analysis was done on Graphpad Prism 7: One-way ANOVA followed by Tukey's test. Mean \pm SEM and $n=8$ per group.

Gene therapy is certainly one of the future treatments proposed to CMT patients. However, several parameters outside the disease symptoms must be assessed in animals before to propose it as a safe clinical treatment. One of these parameters is the immune responses generated against the virus and/or against the transgene in treated animals. We therefore performed a neutralization assay, which measure the immune response against the viral vector. Briefly, cells in culture were

transduced with an AAV9 expressing the reporter gene Lac Z in presence of serial dilutions of the serum of our injected rats. Then a chemiluminescent method was used to detect gene expression. When sera contain anti-AAV9 factors fewer cells are transduced. In this assay more than 50% inhibition of transduction was considered as a positive test for anti-AAV9 factors. This assay was done at the Gene Therapy Immunology core GTI- UMR 1089-Nantes by Célia Couzinié under the supervision of Dr. Oumeya Adjali.

We tested 10 sera of animals injected with different AAVs used in the STC (***Table 12***). Only two of them were positive. In addition, these sera were positive but only at the second lowest dilution tested 1/500, suggesting that anti-AAV9 factors were not abundant. All non-injected control animals' sera were found negative indicating that the test was efficient and that most probably there is no pre-existing immunity against AAV9 in those rats.

Table 12 : Neutralising factors against AAV9

Group	Number of rats tested	AAV9 neutralising factors	
		Conclusion	Titer
WT scr.sh	4	Negative	-
	1	Positive	1/500
CMT1A scr.sh	4	Negative	-
	1	Positive	1/500
Non-injected controls	2 WT	Negative	-
	2 CMT1A	Negative	-

scr.sh= scramble shRNA, WT= Wild-type, CMT1A=Charcot-Marie-Tooth 1A rat model. Positive test means >50% of transduction inhibited in the presence of AAV9 neutralising factors in serum. Assay done at the Gene Therapy Immunology core GTI- UMR 1089-Nantes. Total: n=14 rats.

VIII. Viral biodistribution

Another important parameter to be tested before proposing a clinical trial for gene therapy is biodistribution of viral vectors that were injected in the body. Indeed, viral vectors may well infect the target cells of the therapy, but they may also infect non-target cells in the same organ as target cells but also in other organs when the virus enters the vascular system. This off-target infection depends on the viral tool but also on the delivery route. Viral biodistribution test is based on the detection of the viral DNA in multiple tissues and organs using q-PCR. This test was done in collaboration with Dr. Caroline Le Guiner and Virginie François (Preclinical Analytics core PAC- UMR 1089-Nantes). Results are expressed as vector genome per diploid genome (vg/dg) of cells.

Therefore, we collected and snap froze several organs (sciatic nerve, muscle close to the sciatic nerve, lumbar dorsal root ganglions L4 and L5, lumbar spinal cord, liver, spleen, kidney, brainstem and blood cells) in the sacrificed animals of the STC cohorts at 2.5 months post-injection (**Table 11**). DNA was extracted and the GFP marker of AAV9 gene expression was detected using qPCR together with a linearized DNA plasmid as PCR internal control and *Hprt1* as reference gene. We found viral genome in the sciatic nerve of almost all injected rats. The ratio viral genome on diploid cell genome was 0.56, suggesting that almost half of the cells present in the nerve were infected with at least one virus. As myelinating Schwann cells represent 30% of the Schwann cells present in the rat sciatic nerve (Schmalbruch, 1986), other cells being non-myelinating Schwann cells, fibroblasts, immune cells, this suggests that almost 100% of the myelinating Schwann cells are infected with at least one virus.

The viral genome was also detected in muscles that surround the sciatic nerve because some leak occurs during the injection of the virus into the nerve and AAV9 readily infects muscular cells. 3 out of 16 animals showed AAV9 infection of dorsal root ganglions (DRG), which are in the continuum of the sciatic nerve just before the spinal cord. This indicated that in some animals the injection went so well that the viral solutions reached the DRGs, which are more than 1 cm away from the injection site in rat pups. Only 1 animal out of 8 showed heart infection and 1 out of 8 showed blood infection. No off-target infection was found in spinal cord, liver, spleen, kidney and brainstem (**Figure 32**)

A

Group	Tissues									
	SN	Muscle	DRG	Spinal cord	Heart	Liver	Spleen	Kidney	Brainstem	Blood
WT scr.sh	(+)	(+)	2/8 (+)	(-)	1/4 (+)	(-)	(-)	(-)	(-)	(-)
CMT1A scr. sh	3/4 (+)	(+)	1/4 (+)	(-)	(-)	(-)	(-)	(-)	(-)	1/2 (+)
CMT1A sh49	1/2 (+)	(+)	(-)	(-)	(-)	(-)	(-)	(-)	(-)	(-)
CMT1A sh50	1/2 (+)	(+)	(-)	(-)	(-)	(-)	(-)	(-)	(-)	(-)
Non-injected CMT1A	(-)	(-)	(-)	(-)	(-)	(-)	(-)	(-)	(-)	(-)
Total number of samples	16	8	16	16	8	8	8	8	8	8

B

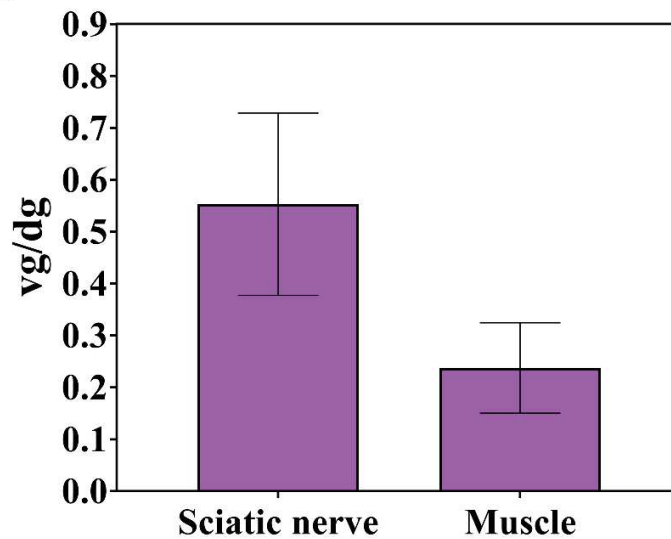


Figure 32: AAV9 biodistribution: scr.sh= scramble shRNA, CMT1A=Charcot-Marie-Tooth 1A rat model. CMT1A sh49 and 50=CMT1A rat injected with AAV9 shRNA PMP22-49 and 50; SN=Sciatic Nerve; DRG= Dorsal Root Ganglion.; (-) = below detection limit so <0.002; vg/dg= vector genome/diploid genome. Mean \pm SEM. Test done at the Preclinical Analytics core PAC- UMR 1089-Nantes.

Discussion

Myelinating Schwann cells highly express PMP22 mRNA as well as protein (Giambonini-Brugnoli et al., 2005; Li et al., 2013; Ohsawa et al., 2006). PMP22 downregulation gene therapy approach for CMT1A would be more efficient if it targets those cells. Many attempts by our laboratory and others, targeting myelinating Schwann cells with viruses were not efficient enough (Gonzalez et al., 2014; Homs et al., 2011). Adenovirus serotype 5 with a cytomegalovirus (CMV) promoter transduces mostly non-myelinating Schwann cells when injected in the sciatic nerve of mice. In addition, adenoviruses are immunogenic and can only be injected in immunodeficient animals (Glatzel et al., 2000; Gonzalez et al., 2014; Perrin-Tricaud et al., 2007; Tricaud, 2005). Lentiviral vectors do not have this problem. Some reported that lentivirus injected intrathecally in adult mice could migrate to peripheral nerves and infect a significant amount of myelinating Schwann cells even as far as the paws (Kagiava et al., 2016). However, in our lab lentivirus infected efficiently only pre-myelinating Schwann cells when injected in the sciatic nerve of P3-P5 mice pups and was not efficient in adults (Gonzalez et al., 2014; Ozcelik et al., 2010). In addition the transduction rate of both adenoviruses and lentiviruses was low: 10% of myelinating Schwann cells in a nerve section (Ozcelik et al., 2010) and neurons. AAV8 transduced more Schwann cells than AAV2 with few infected Schwann cells away from injection site. Furthermore, vector copy number per cell decreased with time (Homs et al., 2011). Thus, we tested AAV9 and AAV10 to obtain a better transduction rate of Schwann cells and an improved diffusion of the viral vector along the nerve. Both AAV9 and AAV10 transduced mostly the targeted myelinating Schwann cells and at a very high transduction rate for AAV9, after injections in the sciatic nerve of adult mice (4.6×10^{10} vector genome/nerve). Moreover, AAV9 diffused along almost the entire nerve more than AAV10. AAV9 high transduction rate of myelinating Schwann cells was also found in rats (1.8×10^{11} vector genome/nerve for adults and 1×10^{11} for pups) and macaques (5×10^{11} vector genome/nerve) after injections in the sciatic nerve. Therefore, we used AAV9 viral vector for PMP22 gene downregulation approach (shRNA) in rat pups' sciatic nerves.

Gene downregulation is possible via RNA interference (RNAi) silencing approaches (Burnett et al., 2011) small interfering siRNA and the cloned form of siRNA, shRNA. Gene silencing by shRNA had been widely used for different purposes such as study on specific molecules or disease mechanism (Djelti et al., 2015) and therapy. Our laboratory used this

approach to define the role of many molecules in the myelination process (Cotter et al., 2010; Ozcelik et al., 2010; Perrin-Tricaud et al., 2007; von Boxberg et al., 2014). Gene silencing by shRNA was tested as a potential treatment for the autosomal dominant neurodegenerative disease Spinocerebellar ataxia type 1 (SCA1) in transgenic mouse models. A polyQ (poly glutamine) expansion in *Ataxin1* (*ATXN1*), which encodes the ATXN1 protein, causes SCA1. Injecting recombinant AAV1 expressing shRNA against human ATXN1 (1×10^{12} vg/mL) into SCA1 mice cerebellar cortices reduced protein levels of ATXN1, enhanced motor coordination as seen by better rotarod performance, cerebellar morphology and cleared the typical ATXN-1 nuclear inclusions seen in SCA1 mice (Ramachandran, Keiser, & Davidson, 2013; Xia et al., 2004). Those studies among other in the literature established that shRNA knockdown is never 100%; so, a significant amount of the target protein is still expressed in cells infected with a virus expressing shRNA. In the TrJ mice model carrying a Leu16Pro *Pmp22* mutation, injecting intraperitoneally an allele-specific siRNA without a viral vector, significantly improved motor function as seen by rotarod. This approach also ameliorated muscle volume as observed in magnetic resonance imaging analysis, increased motor nerve conduction velocity and compound muscle action potentials as well as enhanced myelination as depicted by electron microscopy of the sciatic nerves and by higher levels of myelinating proteins like myelin basic protein and myelin protein zero. Therefore, siRNA is a potential treatment for inherited peripheral neuropathies caused by point mutations (J. S. Lee et al., 2017). Finally, several clinical trials are in course using siRNA such as Patisiran drug for Hereditary Transthyretin Amyloidosis (NCT01960348) and QPI-1007 drug for Non Arteritic Anterior Ischemic Optic Neuropathy (NCT02341560) (Refer to Introduction VI.D.2). Alnylam Pharmaceuticals are about to obtain the first RNAi drug approval (C. Morrison, 2018).

For my thesis project, due to the laboratory strong expertise in viral vectors and shRNA, we opted for the AAV9 shRNA gene therapy approach for CMT1A in the rat model overexpressing mouse PMP22. ShRNA constructs were carefully chosen and tested to decrease PMP22 gene expression without completely deleting this gene and causing another disease, “Hereditary Neuropathy to Pressure Palsies” (HNPP). With our collaborators, we selected two shRNA constructs targeting the mouse and/or rat *PMP22* gene (shRNA PMP22-49 and shRNA PMP22-50) (***Figure 22.B and C***). Two shRNA constructs were used to confirm that the effect of the shRNA is due to its specific silencing of PMP22.

The chosen two constructs downregulate PMP22 mRNA and protein levels *in vitro* and *in vivo*. Mouse PMP22 mRNA is decreased by shRNA as seen by RT-qPCR of MSC80-transfected cells (MSC80 cells express mouse PMP22). Since the antibody we used for PMP22 protein levels reacts with rat and mouse PMP22, we don't know which of rat or mouse PMP22 is decreased; we only know that total PMP22 (mouse and rat) is decreased. We did not differentiate between rat and mouse PMP22 because one of the two shRNA constructs (sh49) we used targeted both. The second shRNA construct (sh50) totally recognizes mouse PMP22 and not rat PMP22. Not distinguishing rat PMP22 from mouse PMP22 is not necessarily important as at the end we anyway reduced the PMP22 protein level to control level. In addition, to translate to clinical trials, human patients possess the *PMP22* gene from only one species, human *PMP22*. Patients do not have *PMP22* genes from two different species like in the CMT1A rat (endogenous rat PMP22 and overexpression of mouse PMP22). The purpose of the therapy was to decrease the excess of PMP22 in CMT1A rat overexpressing mouse PMP22 no matter which species it was. We succeeded in that objective as shown in **Figure 27**.

In addition, it is important to note that by decreasing PMP22, we reduced CMT1A symptoms and we did not cause any other pathology. Indeed, treated CMT1A rats grow normally and did not lose weight (**Figure 33**). In order to rule out concerns about shRNA off-target effects, we had injected both WT and diseased rats with shRNA control/scramble. AAV9 shRNA PMP22 decreased PMP22 mRNA and protein levels. In this way, the cause of the disease (*PMP22* gene overexpression) was corrected.

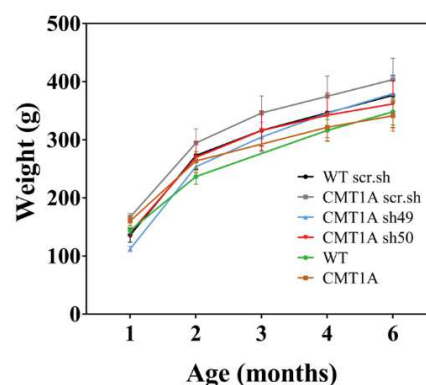


Figure 33: No weight loss observed following injections: AAV9 shRNA did not cause any pathology. No difference in weight with non-injected rats. For each time point: Injected rats: n=8 per group and non-injected rats: WT n=22. CMT1A n=20.

We chose the CMT1A rat because it is one of the best models of the human disease. First, similarly to CMT1A patients, it presents a 1.5-fold increase of the *PMP22* gene expression due to mouse *PMP22* extra gene. This is not the case in other mouse models which possess several fold increases of this gene (Magyar et al., 1996; M. Sereda et al., 1996; Zu Hörste & Nave, 2006). Secondly, the CMT1A rat model mimics the human neuropathy. Based on the behavioural and electrophysiological analysis presented in the results chapter and in literature, CMT1A rats show motor and locomotion deficits and reduced nerve conduction velocity as well as compound muscle action potentials (CMAP) like patients. CMAP is the sum of activity in muscle fibers following motor nerve stimulation. The motor deficits seen in diseased rats were lack of motor coordination and of equilibrium as demonstrated by a poor rotarod performance in addition to muscle weakness as proven by decreased strength in grip test. Clumsiness in walking as deduced from Catwalk analysis of parameters in rats is a common feature of CMT1A rats and patients. I believe that I am the first one to have studied the gait of CMT1A rats using the Catwalk apparatus. In the literature, the footprint analysis with ink is used for this purpose. During the footprint analysis, rats usually overlap their hind paw with previous front paw position thus spreading the inks and impeding analysis (Hamers, Koopmans, & Joosten, 2006). The print intensity of CMT1A rats when their whole paw is in contact with the glass plate of the Catwalk is less than in wild-type (“Max Contact Max Intensity” parameter) (Batka et al., 2014). This intensity parameter indicates weight bearing of paws or paws weight load distribution that could be associated with pain (Masocha & Pavarthy, 2009; Vrinten & Hamers, 2003) or with muscle weakness. The latter is the most plausible for CMT1A rats since they cannot stand their body weight due to muscle weakness (M. Sereda et al., 1996). Moreover, CMT1A rats do not have much inter-paw coordination during walking as shown by the diminished values in the parameters of “Regularity index”, “Phase dispersions” and “Couplings” in CMT1A rats versus WT (Batka et al., 2014; Kloos et al., 2005; Mountney et al., 2013). This could be explained by the fact that diseased rats dragged their paws (dragging resemble the foot drop symptom in human patients). This is suggested by a significant increase in the parameter “left hind paw single stance”, a parameter of the hind paw indicating that the contralateral paw is not in contact with the glass plate. The contralateral paw of the left hind paw being the right hind paw not touching the glass plate as if dragged (Coulthard et al., 2002). As in human patients, there is a reduced nerve conduction velocity in CMT1A rats indicating a demyelinating neuropathy. In comparison, CMT1A mouse models display either a mild clinical

phenotype like C61 heterozygotes and C3-PMP or a very severe phenotype - closer to CMT3- such as C22 and My41 (Magyar et al., 1996; Zu Hörste & Nave, 2006). Histological characteristics of peripheral nerves in CMT1A patients and rats include demyelination, onion bulbs and secondary axonal loss. The important disease variability found in CMT1A patients is also present in the rat model (Fledrich, Stassart, et al., 2012).

The P6-P7 age of rats was specifically chosen for multiple reasons. First, we aimed at a preventive rather than a curative treatment since signs and symptoms appear before 20 years of age, even during childhood (Harding & Thomas, 1980; Yiu et al., 2008). Second, at P6, CMT1A rats overexpress PMP22 (both mRNA and protein) with values higher than at a later age, at the adult stage (2.5-month-old- CMT1A rats) (M. W. Sereda, 1999). Third, by P30, CMT1A rats present the first signs of demyelination and onion bulb formation. Last, by P60 axons are lost, hence myelin recovery is impossible (Fledrich et al., 2014).

In order to target specifically myelinating Schwann cells, we injected the virus directly in the nerve. For that, I used the innovative microinjection technique settled by Dr. Tricaud. This method consists in filling the nerve as much as possible with viral solution at high pressure (Gonzalez et al., 2014). I injected repetitively very small volumes for a total of 8µL over a 15 min period time. The injection took time allowing good spreading of the virus along the nerve to obtain high transduction efficiency. The dose was 1×10^{11} vg/nerve. Both sciatic nerves were injected to obtain a bilateral recovery. It is also important to inject the lower limbs since this is where CMT diseases start before affecting the higher limbs (Tooth, 1886).

Several clinical assays are in course to treat CMT1A (**Table 4**). In addition an ASO approach has been recently proposed at a preclinical stage (Zhao et al., 2017) (refer to Introduction IV.B.2). All these therapeutic proposals require multiple and regular administrations to keep the level of PMP22 lower in the myelinating Schwann cell, which may be cumbersome for patients and costly for the community. With only a single injection of AAV9 shRNA PMP22 in sciatic nerves of rats, we succeeded in obtaining a practically total rescue of the motor and sensory phenotype with a considerably increased nerve conduction velocity. The therapy remained very efficient for a long time (more than 9 months). Precisely, AAV9 shRNA PMP22 gene therapy corrected motor impairments and hypoalgesia in CMT1A rats. As seen by rotarod (**Figure 28.A**) and grip test (**Figure 28.B**), therapy significantly ameliorated motor performance for coordination,

equilibrium and muscle strength. Treated CMT1A rats had an almost total motor functional recovery. In addition, therapy is 100% efficient for hypoalgesia given that treated CMT1A rats have the same behavior of WT rats in Randall Selitto pain assessment test. To my knowledge, no one has ever done the Randall Selitto test on the CMT1A rat model. The sensory phenotype is not much explored in CMT1A rats. Only Fledrich et al (2012) have found that severely affected CMT1A rats are less sensitive to heat pain compared to mildly affected and Wild-type rats. Not feeling pain (hypoalgesia) either by mechanical stimuli (Randall Selitto) or thermal stimuli (hot plate) could be explained by the loss of sensory fibers (Baumgärtner et al., 2002; Fledrich, Schlotter-Weigel, et al., 2012; Zu Horste et al., 2007). Axonal loss is an important feature of CMT1A rats (Fledrich, Schlotter-Weigel, et al., 2012; Fledrich, Stassart, et al., 2012; Zu Horste et al., 2007).

AAV9 shRNA PMP22 gene increased the nerve conduction velocity but not compound muscle action potentials (CMAP) in CMT1A rats. The reason for this is not clear. In the literature, electrophysiological improvements were variable (***Table 4***). Indeed, some treatments could only correct the CMAP with no effect on NCV (Fledrich et al., 2014; Sereda et al., 2003; Zu Horste et al., 2007) or correct both NCV and CMAP (Meyer zu Horste et al., 2011; Zhao et al., 2017) or correct none of NCV and CMAP (Sociali et al., 2016). With our therapeutic strategy, although we had a very high transduction rate and a good diffusion, the whole nerve was not entirely filled with viral vector carrying shRNA PMP22. Thus, we are rectifying myelination mostly around the injection site and not all along the nerve. This may be sufficient to restore a correct nerve conduction velocity but may not be enough to prevent the temporal dispersion of action potentials (***Figure 34***). Temporal dispersion is a typical feature of CMT1A rats since they present a dysmyelinating phenotype (abnormal myelin formation) (M. Sereda et al., 1996). In any case the correction of the NCV but not of CMAP was enough to restore motor and sensory phenotypes.

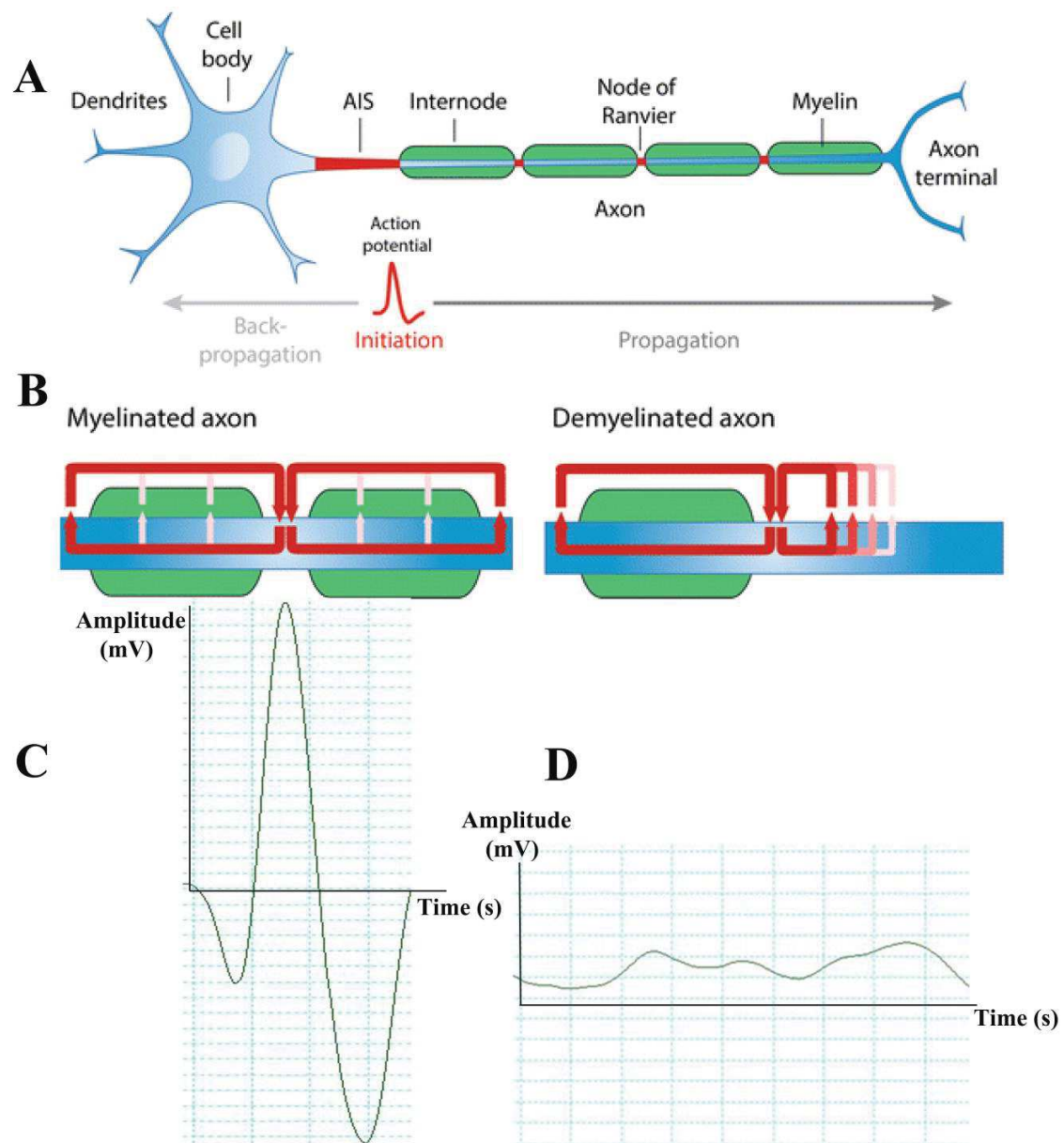


Figure 34: Action potentials in myelinated versus demyelinated axons: *A:* Myelinated neuron with action potential initiation signal (AIS) and propagation. *B* In myelinated fibers, the action potentials jump from one node of Ranvier, to the other. Red arrows indicate high membrane currents. This leads to the generation of single peaks of CMAP as one example is depicted in *C*. In the case of a demyelinated axon, the propagation of action potentials is slowed down or blocked hence temporal dispersion of action potentials occurs as depicted in *D*. Adapted and modified from Freeman, S.A., Desmazières, A., Fricker, D. et al. *Cell. Mol. Life Sci.* (2016) 73: 723.

In order to check for the robustness of my injection protocol in nerves, I have compared the results of motor and electrophysiological tests between the short term cohort and the long term cohort. Actually, both cohorts showed a very similar recovery, implying that the injection technique is reproducible in my hands.

The recent rapid progression of the gene therapy field results in viral vectors with greater titers, higher transduction efficiencies, and frequently with broader tissue/organ tropism. This high efficiency always raises concerns regarding the risk of germ line transmission (Le Guiner et al., 2011). Subsequently, it is crucial to evaluate the safety of those new technologies by analyzing the immune response towards the virus (neutralization assay) and the viral infection in different tissues other than the targeted one(s) (AAV biodistribution).

The high prevalence of neutralizing antibodies against AAV in the human population presents a considerable obstacle to the broad use of AAV vectors in clinical gene therapy (Boutin et al., 2010; Rapti et al., 2012). It was long assumed that preclinical animal research models do not have pre-existing neutralizing factors against AAV except for nonhuman primates (Jiang et al., 2006; L. Wang et al., 2010). Nevertheless, Rapti et al proved that wrong. All of the six animals species tested (mouse, rats, pigs, sheep, dogs and rabbits) had pre-existing neutralizing factors against one or more AAV serotypes 1, 2, 6 or 9 (Rapti et al., 2012). This is why we thought it was important to test for serum factors that can neutralize transduction of AAV9 in the AAV9 shRNA-injected rats. Two out of 10 injected rats were found positive for the neutralization assay but at a very low titer. Thresholds of positivity, prevalence and cut-off values can vary among the different laboratories that perform the analysis because there is no standardized method across laboratories (Vandamme et al., 2017). Depending on the method used, the cut-off is set, and animals are excluded from the study if they display a neutralizing factor titer higher than this value. For example, in certain laboratories where they use serum serial dilutions of 1/2, 1/4 etc...until 1/128 (twofold serial dilution), the cut-off value is 1/2 (Rapti et al., 2012). At the Gene Therapy Immunology (GTI) core (UMR1089, Nantes, France), they do serum serial dilutions of 1/10 starting from 1/50, 1/500 until 1/500 000. Due to high background noise in rats, the minimal dilution is 1/50. The titer of positivity of 1/500 is considered a very low titer based on the method used (personal communication with Célia Couzinié and Oumeya Adjali- GTI core - UMR1089, Nantes, France). Since Rapti et al (2011) observed no inhibition for AAV9 in serum of non-

injected rats prior to injections, they suggested that neutralization factors present in the sera of positive rats were probably caused by injections and not by pre-existing neutralization factors (Rapti et al., 2012). This suggests that in our case a seroconversion occurred in 2/10 rats. AAV can initiate an immune response in animal models (Chirmule et al., 2000; Vandamme et al., 2017) and humans (Flotte et al., 2011; Vandamme et al., 2017) even if they were previously seronegative. Species, vector and injection route do not affect seroconversion. The problem with the seroconversions is that it will inhibit infection after the re-injection of the same AAV vector (Jeune et al., 2013; Vandamme et al., 2017). Usually in adult patients, one single AAV injection is enough since expression of the transgene is long-lasting (Buchlis et al., 2012; Vandamme et al., 2017). This is not the case in pediatric animal models where the expression maybe lost overtime (Vandamme et al., 2017; L. Wang et al., 2011). However, our experiments show long lasting effect after treatment of very young pups P6-P7. In patients we aim at a preventive rather than a curative treatment. Consequently, if our therapeutic approach was translated to clinical trials, children would be injected with AAV. If there was a need for AAV re-injection, this might therefore be possible since only a small minority of tested rats were found positive and at a very low titer. More extensive research needs to be done before passing to clinical trials.

AAV serotypes infect different organs and tissues depending on their administration route (Zincarelli et al., 2008). Focusing on AAV9, intrathecal or intravenous injection in mice led to several off-target effects: colon, ileum, liver and adrenal cortex and central nervous system (Armbruster et al., 2016; Schuster et al., 2014). Intracerebroventricular injection of AAV9 results in infecting the spinal cord, the liver, the heart and hindlimb skeletal muscles (Armbruster et al., 2016; Zincarelli et al., 2008). AAV9 showed the highest viral genome distribution among AAV serotypes 1-9 (Zincarelli et al., 2008). After injection in the sciatic nerve we did not observe AAV9 infection neither in the liver nor in the brainstem. We only detected important amount of AAV9 viral genome at the site of injection (sciatic nerve) and in the muscle that surrounded this site _probably due to leakage of the viral solution during injection or because of the high tropism of AAV9 to hindlimb muscles as demonstrated by Armbruster et al (2016) and Zincarelli et al (2008) (Armbruster et al., 2016; Zincarelli et al., 2008). Furthermore, virus was detected in very few DRGs (3/16) that are in the continuity of the nerve. Two animals showing viral expression in DRGs showed also expression either in the heart (1/8) or in the blood (1/8), suggesting a small leak into the vascular system in very few animals. Three out of sixteen animals showed no viral

expression in the nerve (**Figure 32**). The explanation is that those rats were the ones with which I experienced some technical difficulties during injections, suggesting that not much virus was injected inside the sciatic nerve. One of the two positive rats in the neutralization factors assay showed viral off-target in the DRGs. The presence of anti-AAV9 did not affect the transduction capacity of the virus further supporting that the titer of those factors is very low. To conclude, AAV9 transduced almost exclusively the injection site (sciatic nerves) with only a distribution nearby, in the muscle. There were not important off-target effects of AAV9. Thus, it appears safe. All those results are very promising for moving to clinical trials.

Conclusion and Perspectives

The aim of my thesis project was to test a gene therapy approach using AAV9 virus expressing shRNA PMP22 on a rat model of CMT1A. We found this therapeutic approach very promising since I obtained a high transduction rate, around 90%, in myelinating Schwann cells, a downregulation of PMP22 mRNA back to control levels and a very significant functional recovery with only one single bilateral injection in sciatic nerves of young pups. Furthermore, the treatment efficiency was maintained for at least 9 months post injections, way much longer than the daily or weekly pharmacological treatments proposed up to now in these rats.

In order to translate this gene therapy approach to clinical trials, a bit more research is required. First, the minimal effective dosage should be very carefully defined because if PMP22 expression is too low, another disease is caused. Testing for the dose could be done using two ways: first by transfecting Schwann cells from CMT1A patients with different doses of shRNA targeting human PMP22 and second, by infecting myelinating Schwann cells in the sciatic nerve of non-human primate *macaca fascicularis* with different doses of the therapeutic virus AAV9 expressing human+macaca PMP22 shRNA.

Second, the vector delivery should be optimized to maximize the transduction and diffusion rates in human nerves. In rodents it is easier to target Schwann cells by injecting in the sciatic nerve than in monkeys or humans. This is due to the complex anatomy of peripheral nerves. As a matter of fact, each nerve is made of the epineurium, a connective tissue that surrounds several groups of axon bundles known as fascicles. In these fascicles axons are grouped forming the endoneurium. Each of these fascicles is encircled by a perineurium, a single layer of connective tissue (**Figure 35**). The difficulty is to inject the virus into the endoneurium in order to infect myelinating Schwann cells and to restrict the diffusion. While the epineurium is almost absent in mice and rats, it is really thick in monkey and humans. Crossing the epi- and peri-neurium to reach the endoneurium is therefore a challenge in monkeys and humans. The microinjection technique developed by Dr Tricaud should be adapted to large animals and to humans because it allows such a fine injection at the right place. Preliminary experiments performed in the lab of Prof. Patrick Aubourg (INSERM U1169 and MIRCEN, Fontenay-aux-roses) on macaques were very

encouraging. Nevertheless, they need further enhancements to increase transduction and diffusion rates, such as injecting at different sites and use the appropriate needle size and the right angle for entering the nerve. This requires a large amount of organization and collaboration since usually a neurosurgeon does the injections and veterinarians closely follow-up macaques.

Furthermore, if injection in sciatic nerves is too complicated in humans, another administration method could be tested: intravenous injections. The safeness of this technique should be also assessed by immunological response against the viral capsid (neutralization assay) and AAV biodistribution (off-targets of the virus).

In addition, a curative therapeutic approach might be tested (inject AAV shRNA PMP22 at a later age in CMT1A rats) and compare with the preventive approach which I demonstrated the efficacy during my thesis.

Taken together, these data along with the proposed future studies constitute a strong proof of principle to possibly use AAV9 shRNA PMP22 in clinical trials.

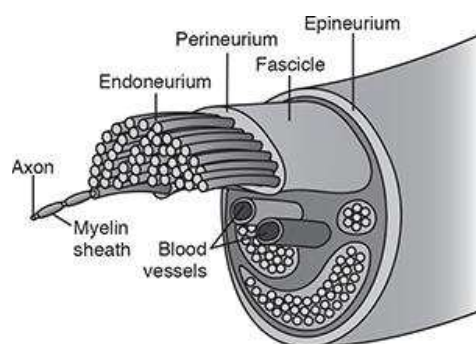
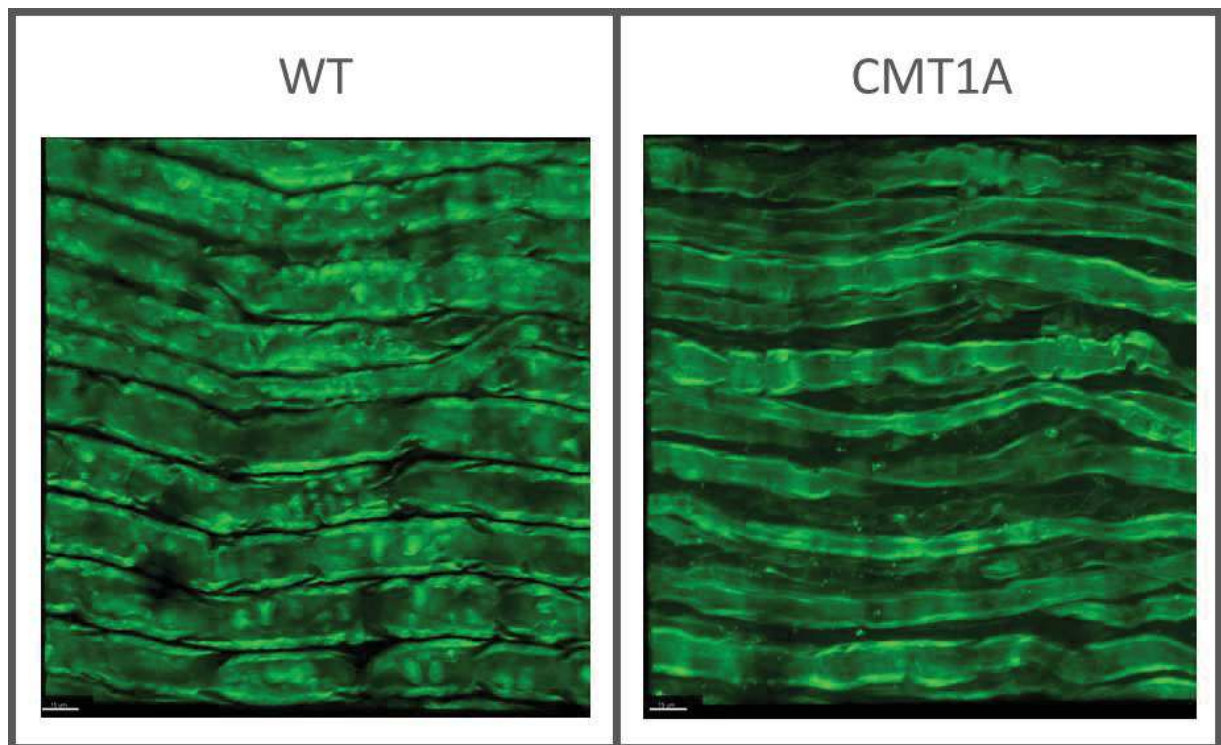


Figure 35: Anatomy of a peripheral nerve: Longitudinal section showing the epi-, peri- and endoneurium as well as a fascicle, myelinated axons and blood vessels

Source: Stephen J. Carp: *Peripheral Nerve Injury: An Anatomical and Physiological Approach for Physical Therapy Intervention*: www.FADavisPTCollection.com
Copyright © F. A. Davis Company. All rights reserved.

Another perspective include studying the inflammatory response in CMT1A rats and check the effectiveness of the gene therapy on that response. As a matter of fact, in CMT1A mouse model C61, high levels of macrophages in peripheral nerves suggest that those cells might partially mediate myelin degeneration (Kobsar et al., 2005; Kohl et al., 2010).

CHAPTER 2: LABEL-FREE NON-LINEAR MICROSCOPY PROJECT

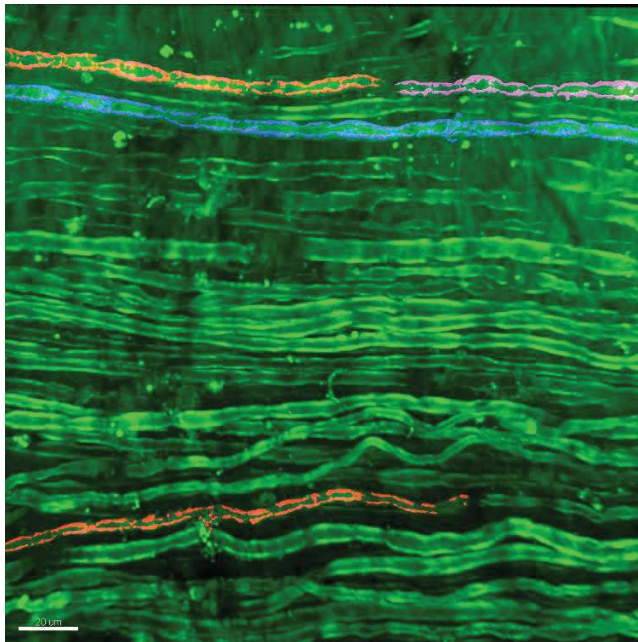


Introduction

Clinical trials evaluating the outcome of a treatment require strong readouts: consistent, reliable and quantitative. In the case of demyelinating diseases such as CMT1A, there is a lack of such readouts to measure outcome of an anti-demyelinating or pro-myelinating therapy. The most straightforward readout is to look directly at peripheral nerves and in particular at the myelin sheath *in vivo* with minimal invasiveness. I have presented some myelin imaging approaches in the introduction among which MRI and SCoRe (Introduction III.H.5). A secondary project in my thesis was to evaluate the use of a novel imaging techniques, non-linear microscopy, to image peripheral myelin sheath in living animals. These techniques are label-free which means they allow imaging of myelin *in vivo* without any labeling at all. We first compared three different non-linear microscopy methods (Second Harmonic Generation: SHG, Third Harmonic Generation: THG and Coherent Anti-Stokes Raman Scattering: CARS) to study peripheral nerve myelin in WT mice and rats *ex vivo* and *in vivo*. We next tested the most promising, CARS, to image and quantify demyelination and dysmyelination in CMT1A rats. Results are presented in the following manuscript under revision at Journal of Biophotonics. This work was done in collaboration with Hassan Boukhaddaoui, research engineer of the Montpellier Ressource Imaging platform of the INM.

Article: “Label-free non-linear microscopy to measure outcome in rodent model of Charcot-Marie-Tooth diseases”, *Journal of Biophotonics*

Abstract Figure:



**Label-free non-linear microscopy to measure myelin outcome in rodent model of
Charcot-Marie-Tooth diseases**

Hajjar H^{1#}, Boukhaddaoui H^{1,3#}, Rizgui A¹, Sar C^{1,3}, Berthelot J¹, Perrin-Tricaud C¹,
Rigneault H² and Tricaud N¹.

1- Institut des Neurosciences de Montpellier, Université de Montpellier, 80 Rue A. Fliche,
34090 Montpellier, France

2- Aix-Marseille Université, CNRS, École Centrale Marseille, Institut Fresnel, UMR 7249,

3- Montpellier Ressources Imaging (MRI)

#these authors contributed equally

Corresponding author: nicolas.tricaud@inserm.fr

Key words: myelin sheath, Schwann cells, peripheral nervous system, demyelinating diseases,
nonlinear optical microscopy

Abstract:

Myelin sheath produced by Schwann cells covers and nurtures axons to speed up nerve conduction in peripheral nerves. Demyelinating peripheral neuropathies result from the loss of this myelin sheath and so far, no treatment exists to prevent Schwann cell demyelination. One major hurdle to design a therapy for demyelination is the lack of reliable measures to evaluate the outcome of the treatment on peripheral myelin in patients but also in living animal models. Non-linear microscopy techniques SHG, THG and CARS were used to image myelin *ex vivo* and *in vivo* in the sciatic nerve of healthy and demyelinating mice and rats. SHG did not label myelin and THG required too much light power to be compatible with live imaging. CARS is the most reliable of these techniques for *in vivo* imaging and it allows for the analysis and quantification of myelin defects in a rat model of CMT1A disease. This microscopic technique therefore constitutes a promising, reliable and robust readout tool in the development of new treatments for demyelinating peripheral neuropathies.

Introduction:

In peripheral nerves of vertebrates, most of the axons are covered by an insulating and nurturing myelin sheath produced by Schwann cells [1,2]. This sheath is critical for fast nerve conduction and long-term survival of motor and some sensory axons of the peripheral nerve. Indeed, numerous human diseases result from the destruction of the myelin, termed demyelination. These demyelinating peripheral neuropathies include acquired diseases such as diabetic demyelinating neuropathy, leprosy, Guillain-Barré syndrome and chronic inflammatory demyelinating neuropathy, and hereditary diseases such as Charcot-Marie-Tooth (CMT) diseases [3]. Together these diseases represent a large spectrum of patients in Europe and worldwide, and while there is no specific treatment, different therapies are being investigated at clinical and preclinical stages.

One major hurdle in the development of these therapies is measuring the outcome of the treatment on peripheral nerve demyelination [2] and eventually on remyelination, the limited regenerative process that occurs spontaneously [4]. None of the methods currently used are really convenient for a longitudinal study for the fate of myelin in a therapy assay. Therefore, one critical step toward the success of a therapy is to design a method that allows imaging peripheral nerve myelin in a live animal without labelling.

Non-linear optic microscopy relies on the absorption of at least two incident photons on molecules, which generates scattered photons with different energy levels [5]. The energy level of the scattered photons is related to both the energy of the incident photons and the structure of the molecules with which the photons collide. Indeed, incident photon wavelengths allows for a resonance effect with particular moieties located on a group of molecules. When two incident photons generate harmonically scattered photons, this is called Second Harmonic Generation (SHG). This is not specific to any molecule, but occurs more efficiently with fairly ordered, large non-centrosymmetric molecules such as collagen helicoid fibrils. When three incident photons generate harmonic scattered photons, this is called Third Generation Harmonic (THG). This also occurs non-specifically but more efficiently at the interface between groups of molecules with different light excitabilities such as between water and lipids or lipid membranes. These two approaches, SHG and THG, have been used to efficiently image biological tissues without any labelling [6].

More recently a novel form of non-linear microscopy has emerged that enables the targeting and imaging of specific molecular bonds. This scheme uses three incident photons where the frequency difference of two of these photons (namely the pump and the Stokes photons) can be made resonant to drive a specific vibrational chemical bond. The interaction of the third photon with this driven vibrational bond generates new wavelengths that can be detected in a way that is similar to fluorescence microscopy. This approach is termed Coherent Anti-Stokes Raman Scattering (CARS) microscopy. While CARS microscopy can be used to image different kinds of molecules, it is particularly efficient in detecting lipids and lipid-enriched myelin has been one of the first biological objects to be imaged by physicists using CARS [7–9].

These different nonlinear optical microscopy techniques have the important advantage of being label-free and are therefore applicable for *in vivo* imaging. However, SHG, THG and CARS techniques are not widely used in the biological and medical communities because the experimental apparatus of the excitation laser and the microscope are complicated, costly and require spatial and temporal synchronization between two independent laser sources [7, 8]. We recently addressed this problem by adapting a commercial setup involving a single laser source duplicated through an optical parametric oscillator (OPO) and by temporally synchronizing the two laser lines through a delay line [10]. In the present work, beyond the described feasibility of using non-linear microscopy for myelin imaging *in vivo*, we addressed the following questions: which exact structures each non-linear microscopy technique are imaging in peripheral nerves, and then, which technique is really compatible with live imaging, for example whether the peripheral myelin could indeed survive the imaging. Finally, we chose a rat model of CMT1A, the most common of the CMT disease, which compiles several characteristics of these diseases such as demyelination but also abnormal myelination (dysmyelination): heterogeneous myelin thickness, focal hypermyelination and short internodal segment [11]. Using this model, we investigated whether the CARS technique, the most adapted for *in vivo* imaging of myelin, could allow for the characterization and the quantification of myelin defects in this disease.

Results

Second, third harmonics and CARS imaging in the sciatic nerve of healthy mice

Using 1097 nm wavelength light to generate SHG we observed a strong signal (548 nm, band-pass filter 500-550) coming from the perineurium, the membrane that collects nerve fibres together, and a weaker signal coming from the endoneurium where there are nerve fibres (Fig. 1A). At higher magnification the strong perineurium signal appeared as the addition of signals coming from many long fibrous structures (Fig. 1B). These structures were likely to be collagen fibrils as SHG at this wavelength is known to emerge from these fibrils [6,12] and electron microscopy shows a high density of these fibrils in the perineurium [13]. The weaker signal, which was better detected when the perineurium was mechanically removed, appeared also at high magnification as collagen fibrils running along myelinated fibres (Fig. 1C). These collagen fibres are easily seen in electron microscopy (Fig. 1D, red overlay). When SHG imaging was performed on sciatic nerve of transgenic mice expressing Yellow Fluorescent Protein (YFP) in axons (Thy-1 mice), SHG signal located distantly from the axon (Fig. 1E). This is consistent with the presence of the myelin sheath between axon and collagen fibrils (see Fig. 1D).

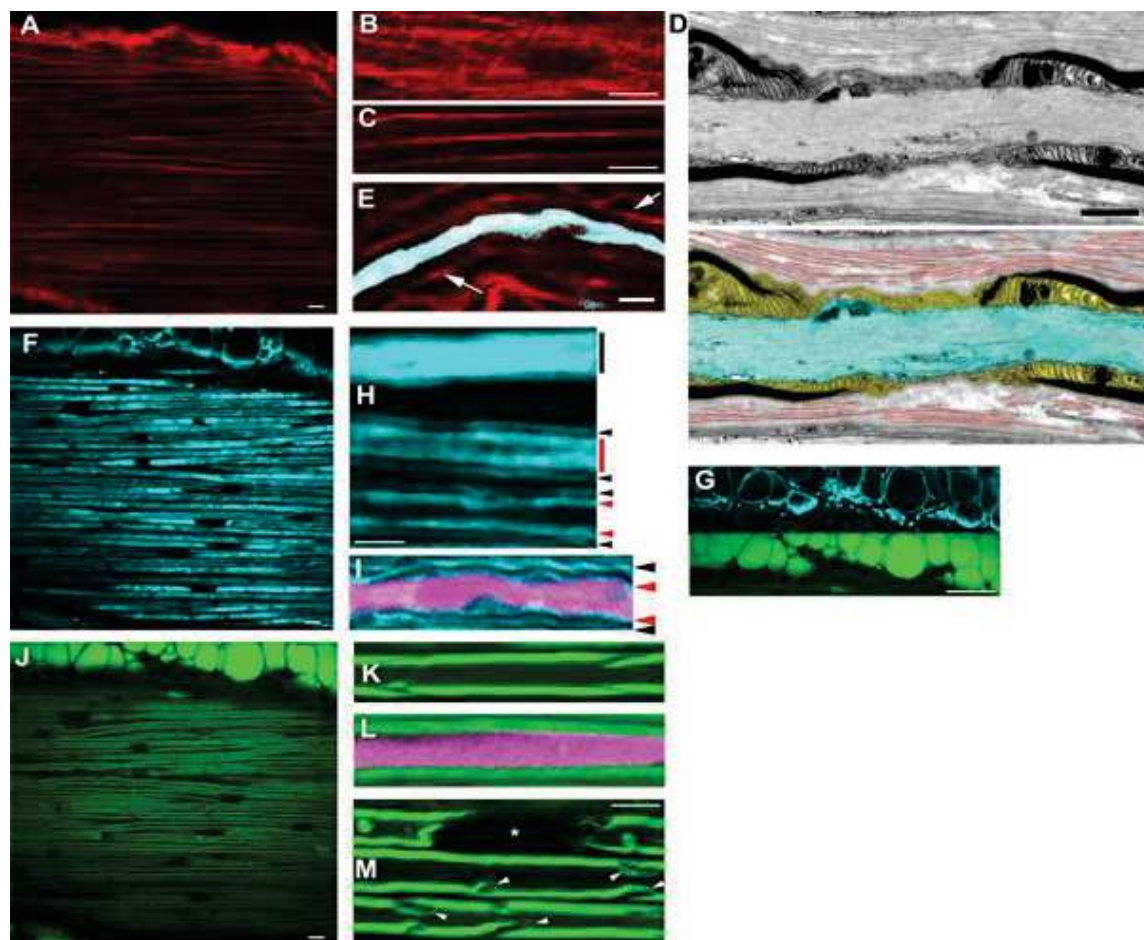


Figure 1: Second, third harmonics and CARS imaging in the sciatic nerve of healthy mice

A- Low magnification longitudinal SHG image of mouse sciatic nerve (scale bar= 50 μ m). B- High magnification SHG image of perineurium (scale bar= 20 μ m). C- High magnification SHG image of endoneurium (scale bar= 20 μ m). D- Upper panel: Electron microscopy image of a myelinated fibre in a mouse sciatic nerve showing a node of Ranvier (scale bar= 500nm). Lower panel: same image colorized for collagen fibrils (red), axon (blue), myelinating Schwann cell (yellow). E- Detail of a myelinated axon labelled with YFP (blue). SHG signal (red) delimitates the unlabelled myelin sheath that surrounds the axon (arrows) (Scale bar= 5 μ m). F- THG image of the nerve area imaged in A. G- Upper panel: THG image of the adipocytes that surrounds the perineurium. Lower panel: same area imaged with CARS (scale bar=20 μ m for both panels). H- Detail of a THG image showing the different bands and their significance: outer interface between compact myelin and extracellular space (black line), inner interface between compact myelin and the axonal space (red line), outer interface seen as optical sections (black arrowheads), inner interface seen as sections (red arrowheads) (scale bar=5 μ m). I- Detail of a myelinated axon labelled with YFP (purple). THG signal (blue) delimitates both the outer interface (black arrowheads) and the inner interface (red arrowheads) with compact myelin. J- CARS image of the nerve area imaged in A and F. K- Detail of a CARS image showing the myelin sheath crossed by two Schmidt-Lanterman incisures. L- Detail of a myelinated axon labelled with YFP (purple) and surrounded by a CARS labelled myelin sheath (green). M- CARS imaging shows different parts of a myelinated fibre: node of Ranvier (asterisk), incisures (white arrowheads) (scale bar=10 μ m).

Using 1300 nm wavelength for THG we observed a strong signal (433 nm, band-pass filter 400-480) coming from the endoneurium and the fat bodies located outside the perineurium (Fig. 1F). Fat bodies did not produce THG signal all over but actually only at their edges (Fig. 1G upper panel). This indicated that lipids themselves did not produce THG signal but this signal was emerging at the interface between lipids and the aqueous environment. In the endoneurium at high magnification this signal appeared as a hatched pattern with lines of different sizes (Fig. 1H). Using YFP axonal labelling, we found that this hatched signal came from a domain outlining the axon (Fig. 1I red arrowheads) and a domain outlining the myelin sheath (Fig. 1I black arrowheads). Taken together these data and previous reports in the literature [14] indicated that THG signal was produced at interfaces of the myelin with the axon (Fig. 1H and I, red arrowheads) and of the myelin and the extracellular environment (Fig. 1H and I, black arrowheads). These THG signals appeared as very large bands when the focus reached the surface of these interfaces (Fig 1H, red and black lines). So, THG can be used to image lipid-enriched myelin but only at its interfaces with the aqueous environment and the THG signal forms therefore a complex pattern.

Using 836nm and 1097 nm wavelengths for pump and stokes photons respectively, we were able to generate a CARS signal coming from lipids. Illuminating the mouse sciatic nerve in these conditions we observed a strong signal (670 nm, band-pass filter 660-685) coming from the endoneurium and fat bodies (Fig. 1J). Fat bodies produced a CARS signal all over (Fig. 1G lower panel) in sharp opposition to THG signal (Fig. 1G upper panel), which confirmed the lipid origin of this signal. At high magnification the endoneurium signal also appeared as a hatched pattern but less complex than with THG (Fig. 1K). When this signal was overlapped with YFP axonal labelling (Fig. 1L) the hatches finely surrounded the axon suggesting CARS signal was derived from the lipid-rich compact myelin. However, unlike the THG signal, emerging CARS signal fully covered the compact myelin sheath, resulting in two large lines flanking the axon (Fig. 1L). CARS signal was robust and discriminating since cytoplasm-filled incisures that cross the myelin could be nicely seen as successive exquisitely delimited “bubbles” opening up in the myelin signal (Fig. 1M white arrowheads). Nodes of Ranvier also appeared devoid of compact myelin (asterisk Fig. 1M, see Fig. 1D).

Ex vivo SHG, THG and CARS imaging of myelin during demyelination and remyelination

As our goal was also to compare non-linear microscopy approaches in demyelinating conditions we next used these approaches in traumatic nerve demyelination conditions. Mouse sciatic nerve was crushed or ligatured and imaged at different time points. In these conditions, axons degenerate distally to the lesion in a few hours; Schwann cells de-differentiate and myelin degenerates distally in 4-5 days forming myelin ovoids that are degraded by the Schwann cells themselves or by macrophages. Then around day 10, Schwann cells remyelinate axons that have grown back from the lesion. The remyelination process is progressive and myelin sheathes are back to normal around two months later (day 60) [2,4].

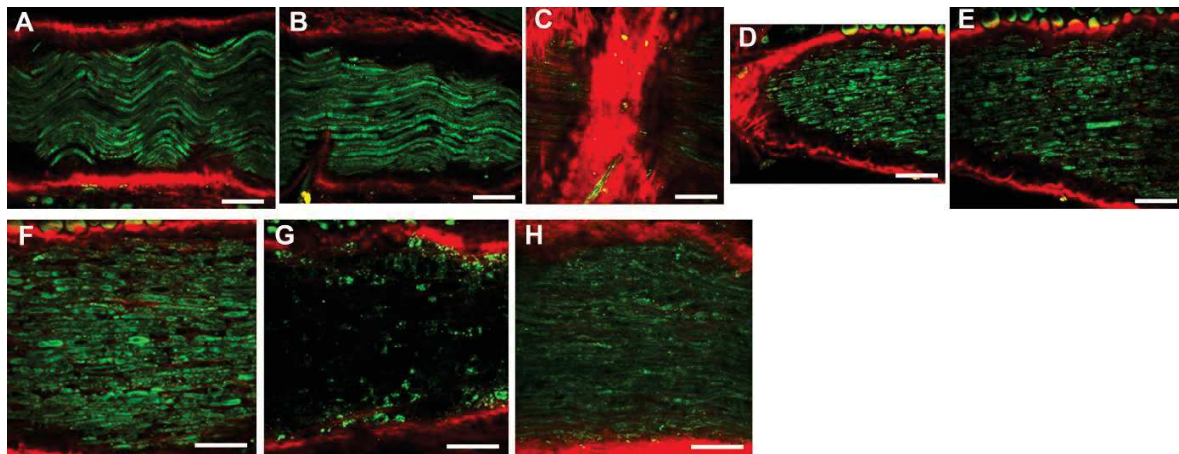


Figure 2: SHG and THG imaging of myelin during demyelination and remyelination

A, B, C, D, E - Successive optical sections from proximal to distal respective to the spinal cord of a crushed mouse sciatic nerve imaged with SHG (red) and THG (green) (scale bars=100μm). F, G, H- SHG (red) and THG (green) imaging of a crushed mouse sciatic nerve distal to the lesion at 4 (F), 15 (G) and 30 (H) days post-crush (scale bars: 100μm).

Using SHG and THG we imaged injured mouse sciatic nerves at the peak of demyelination after dissection and fixation (Fig. 2): at the site of the lesion a scar enriched with transversal collagen fibrils appeared as seen with SHG (Fig. 2C). While upstream of the lesion (Fig 2A, B) the THG signal was similar to the signal detected in non-injured nerves (see Fig. 1A, F), downstream of the lesion (Fig. 2D, E) this signal was fragmented indicating compact myelin fragmentation that characterizes demyelination. The fragmentation of the THG signal at 4 days post injury (Fig. 2F)

was followed by a significant decrease of the signal 15 days post injury (Fig. 2G), illustrating the destruction of the compact myelin. By 30 days post injury this THG signal returned (Fig. 2H), illustrating the remyelination process.

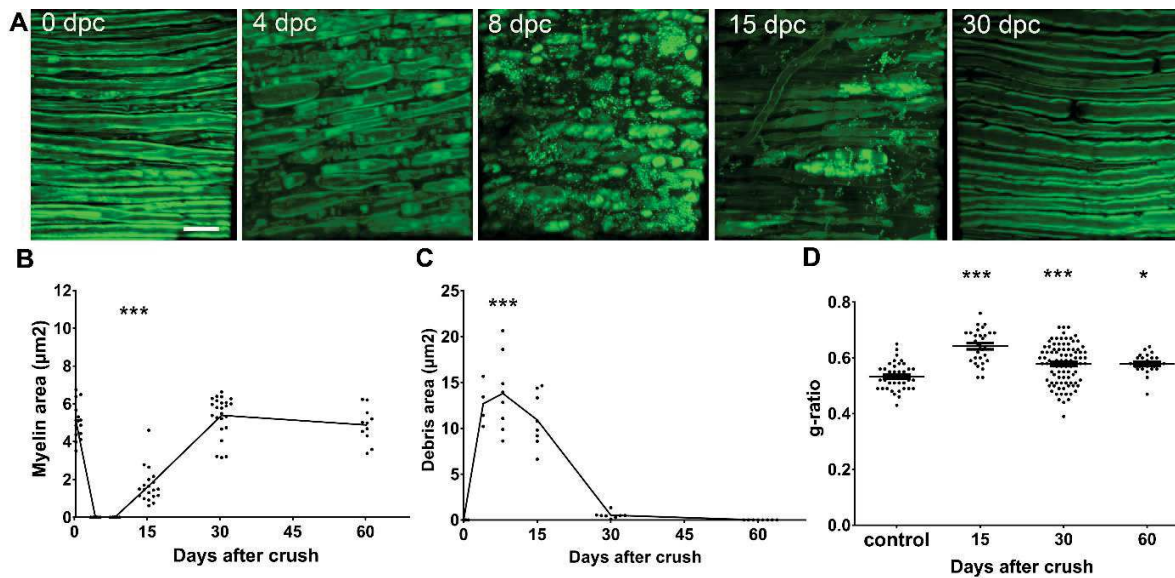


Figure 3: CARS imaging of myelin during demyelination and remyelination

A- CARS imaging of sciatic nerves of mice crushed at day 0 and imaged at different days post-crush (dpc) (same scale bar for all pictures =10μm). B- Graph showing intact myelin area measured with CARS imaging at different days post-crush. C- Graph showing myelin debris area measured with CARS imaging at different days post-crush. D- Graph showing G-ratio measured with CARS imaging at different days post-crush. Statistical analysis uses one-way ANOVA followed by Tukey test. All values were compared to 0 days post crush or to control *, P-value <0.05; **, P-value <0.01; ***, P-value <0.001; P-value >0.05 are non-significant and not shown.

The CARS signal change during demyelination and remyelination was slightly different: 4 days post injury the CARS signal also showed a fragmentation of the compact myelin compared to non-injured nerves (Fig. 3A), however myelin ovoids were more detailed than with THG; 8 days post injury the CARS signal was still very intense but it exclusively constituted myelin debris of all sizes (Fig. 3A). By 15 days post injury, fine myelin sheaths and some large debris could be detected using CARS (Fig. 3A). This was different with the THG signal, which was much lower (Fig. 2G) showing that THG signal results from interfaces between structured myelin and

cytoplasm, which are mostly lost in myelin debris and which are much weaker in very fine myelin. By 30 days, myelin segments were back to their original appearance (Fig. 3A), showing a complete regeneration of the myelin.

CARS imaging of demyelination and remyelination *in vivo*

We next investigated whether THG or CARS imaging could be used to follow quantitatively and longitudinally myelin maintenance, demyelination and remyelination in living mice.

We first anesthetized adult mice and, after a small surgery, gently placed their sciatic nerve under the lens of the multiphoton microscope as previously described [15]. Nerve of control mice were not illuminated while experimental mouse nerves were illuminated for THG or CARS imaging (1 minute at different laser power). Then nerves were placed back, the wound sutured and animals were left to wake up. After 7 or 14 days animals underwent the same *in vivo* imaging and we evaluated the demyelination in illuminated or control nerves using THG or CARS. All our attempts to image myelin *in vivo* using THG induced a significant demyelination of the fibres, indicating that the laser power required to image myelin with THG is deleterious for myelinating Schwann cells. A similar outcome resulted from the illumination of the nerves for CARS imaging at high power (100mW, 50mW, 30mW) but no demyelination could be detected at lower power intensity (20mW and 10mW).

We then used CARS imaging at a safe intensity (10mW) to analyse the myelin of mouse sciatic nerve in living animals after a nerve injury in a longitudinal study. Mice were first imaged before crush (Online supporting information live imaging video 1) and then imaged a second time at different time points distally to the injury (Online supporting information live imaging video 4, 8, 15, 30 days post crush, (dpc)). Qualitatively, demyelination and remyelination could be followed along the same time intervals and with similar images as observed *ex vivo* in Fig. 3A. These processes could also be quantitatively measured by quantifying the relative myelin surface, the relative debris surface and the g-ratio (axon diameter on myelinated fibre diameter). Myelin area decreased sharply 4 days after crush and recovered progressively after 15 days (Fig. 3B), whilst the exact opposite occurred with debris surface as this increased sharply during and after demyelination and decreased when cells remyelinated (Fig. 3C). G-ratio, axon diameter on full

fibre diameter, is a commonly used read-out of the myelin thickness. We measured this ratio using the inner and the outer diameter of the CARS labelled rings. While it could obviously not be measured when cells demyelinated, we found that by 15 days after crush it increased compared to control (Fig. 3D), showing that remyelinating cells had a thin myelin. This ratio remained higher than control even at 60 days post crush, after remyelination was complete (Fig. 3D), suggesting the myelin sheath remained thinner than before crush. This is consistent with previous reports using electron microscopy showing a hypomyelination following demyelination in injured nerves [16].

Qualitative and quantitative imaging of defects in CMT1A rat sciatic nerves myelin using CARS

To go further we investigated whether CARS imaging is sensitive enough to detect myelin defects that occur in a rat model of the hereditary disease Charcot-Marie-Tooth type 1A. Indeed, at the present time, these defects can only be addressed using electron microscopy imaging, which is time and resource consuming. Using this imaging technique, demyelination, focal hypermyelination, short internodal length and onion bulbs are characteristic of the CMT1A nerve in a transgenic rat model of the disease, the CMT1A rat [11]. We anesthetized adult CMT1A rats, exposed their sciatic nerves and imaged them using CARS *in vivo*. Subsequently, we dissected the nerves and imaged them *ex vivo*. *In vivo* imaging revealed the fractioned morphology of the myelin sheath in transgenic rats compared to wild-type. (Fig. 4A, B). *Ex vivo* imaging allowed a more detailed analysis of the morphology. Firstly, some fibres were clearly degenerating, forming beaded structures in a necklace pattern known as myelin ovoids (arrowheads, Fig. 4C). Activated macrophages, clearly seen thanks to their round inclusions (insert Fig. 4C), were abundant. Macrophages participate in the clearance of degenerated myelin. At higher magnification, the main characteristic of transgenic rats' nerves was the high diversity of myelinated fibres phenotypes in the same imaging field. This diversity was also noticed along the same fibre: some fibre parts were clearly hypermyelinated with myelin forming discrete masses along the axon (white arrows, Fig. 4E, F); some fibre parts on the opposite were devoid of detectable myelin or were thinly myelinated (arrowheads, Fig. 4D) and sometimes these thinly myelinated or unmyelinated parts of the fibre were in the continuity of some hypermyelinated parts (red arrowheads, Fig. 4D). In addition, in CMT1A rats, nodes of Ranvier were enlarged (asterisks, Fig. 4G) and myelin sheathes were

completely different from one side of the node to the other (red arrowheads, Fig. 4D, E, G) while wild-type myelin sheath was similar along the same axon (red arrowheads, Fig. 4I). This indicates that on the same axon of a CMT1A rat, some myelin segments are not homogeneous, being hyper- or hypo-myelinated. Furthermore, we observed in many places short myelinated segments between two nodes of Ranvier (Fig. 4G). This shows that myelin defects are not localized in the nerve but occur everywhere leading to a strongly heterogeneous pattern.

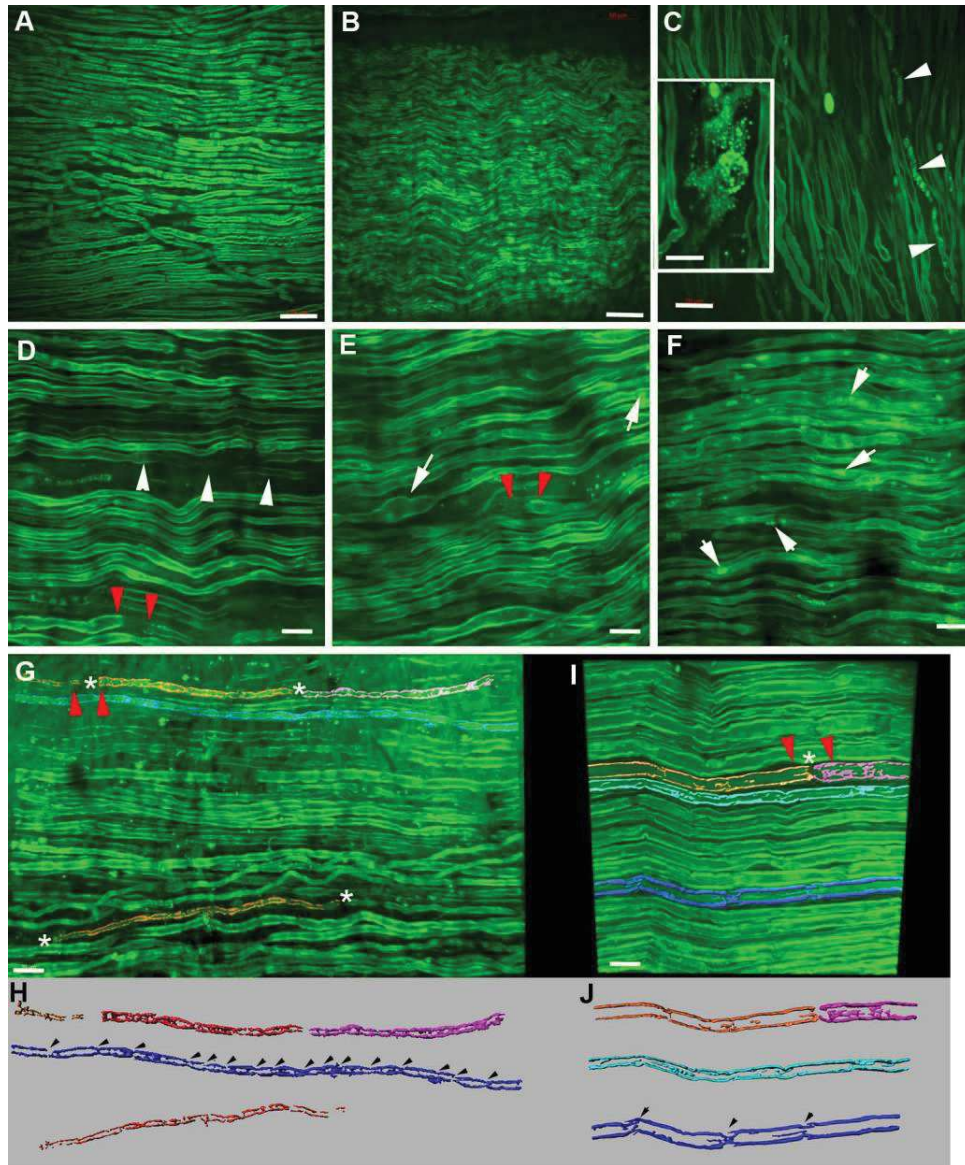


Figure 4: imaging of defects in CMT1A rat sciatic nerves myelin using CARS

A, B- *In vivo* live imaging of wild-type (A) and CMT1A (B) rats sciatic nerves (scale bars= 50 μ m). C- CMT1A rat sciatic nerve imaged *ex vivo* with CARS shows a degenerating fibre displaying fragmentation and myelin ovoid (arrowheads) (scale bar=40 μ m). Insert: detail of a CARS image of CMT1A rat sciatic nerve showing a macrophage with round inclusion (scale bar= 5 μ m). D- CARS image of CMT1A sciatic nerve showing a demyelinated fibre (white arrowheads) and a node of Ranvier separating a hypermyelinated from a hypomyelinated fibres (red arrowheads) (scale bar=10 μ m). E- CARS image of CMT1A sciatic nerve showing focally hypermyelinated regions (white arrows) and a node of Ranvier separating a hypomyelinated from a hypermyelinated fibres (red arrowheads) (scale bar=10 μ m). F- CARS image of CMT1A sciatic nerve showing focally hypermyelinated regions with myelin inclusions (white arrows) (scale bar= 10 μ m). G, I- Z-projection of CARS images of CMT1A (G) and wild-type (I) rat sciatic nerves. Some fibres have been coloured for better clarity. Asterisks show the location of some node of Ranvier and red arrowheads the myelinated fibres flanking nodes of Ranvier (asterisks) (scale bars =10 μ m). H, J- coloured fibres in G and I were extracted and are shown isolated at the same magnification. Black arrowheads show the location of Schmidt-Lanterman incisures.

This heterogeneous pattern hindered the quantitative analysis of the myelin defects with the methods we previously used. Nevertheless, we measured the myelin surface to find less myelin in CMT1A rat nerve (Fig. 5A). G-ratio was difficult to measure because hypermyelinated segments were adjacent to hypomyelinated or demyelinated segments. However, overall we detected a lower G-ratio in CMT1A rat nerves (Fig. 5B), showing a hypermyelination. A significant characteristic of CMT1A rat fibres versus control animal fibres was the shortening of the inter-incisural distance of the remaining myelinated fibres compared to wild-type (black arrowheads, Fig. 4H, J). This feature was the result of the dilatation of the Schmidt-Lanterman incisures that stakes the myelin sheath: in normally myelinated fibre only large and regular incisures are clearly visible while in unstable myelin sheathes all incisures, large and small, dilate resulting in shorter inter-incisural distances [17]. Using this method we could reliably quantify the amount of defective myelin in CMT1A rat sciatic nerves (Fig. 5C). Taken together these data indicated that CARS microscopy allows for imaging and measuring myelin defects in the CMT1A rat model.

Figure 5

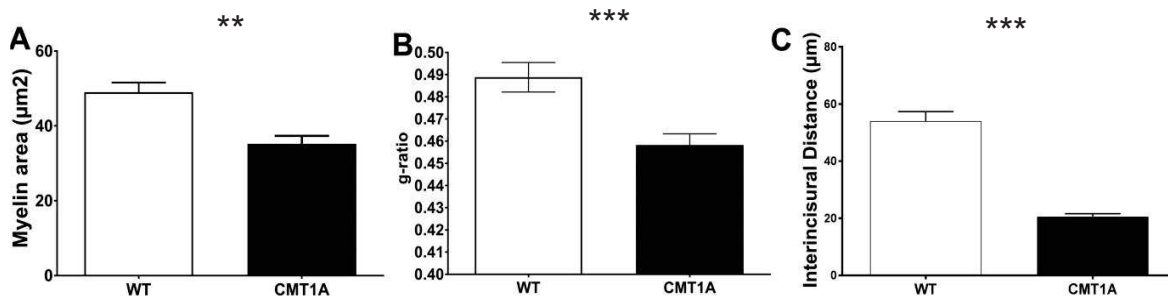


Figure 5: quantitative imaging of defects in CMT1A rat sciatic nerves myelin using CARS

A, B, C- Graphs showing intact myelin area (A), G-ratio (B) and inter-incisural distance (C) measured with CARS imaging in wild-type (WT) and CMT1A (CMT1A) rat sciatic nerves ex vivo. Statistical analysis uses Student T test. *, P-value <0.05; **, P-value <0.01; ***, P-value <0.001.

Discussion

We first compared SHG, THG and CARS in the imaging of mouse and rat peripheral nerves. SHG can be used for imaging collagen fibers both in the perineurium and the endoneurium. THG exposes interfaces between the compact myelin and the surrounding environment, such as axon and extracellular domain resulting in a complex pattern that outlines the myelin sheath without

labelling it directly. Using CARS imaging, the myelin sheath is directly labelled thanks to its rich content in lipids and it appears as a large band surrounding axons. These results are consistent with previous analysis by specialists in optics [18,19] and in peripheral nerve biology [7,14].

We then compared these techniques to analyse demyelination and remyelination in an injury context. SHG signal was increased at the site of the injury but remained relatively weak in the endoneurium during demyelination and remyelination. THG signal decreased sharply after demyelination and resumed during remyelination. However, myelin debris remained mostly undetected. CARS signal changed during demyelination as the linear bands of myelin disappeared to give rise to bright ovoids containing myelin debris. Myelin disappearance and recovery were more precisely measured with CARS because this signal was directly correlated to myelin sheath thickness.

One of the main hurdles to design a therapy for peripheral nerve diseases is the lack of techniques to reliably measure the outcome of therapy on the myelin sheath. Non-linear label-free imaging may therefore represent a significant advance in this domain. However, this kind of imaging requires light to fully penetrate the sample. As nerves are below the skin, this requires at least a skin incision to expose it. Imaging myelin *in vivo* was not trivial due to the breathing movements that change the focus and to the low penetration of the light, which limited the imaging to the nerve surface. In larger animals such as monkeys, and in humans, the epineurium being much larger, it is likely that CARS imaging will be limited by the light penetration through this surrounding tissue. Demyelinating peripheral nerve diseases are complex pathologies because they are mostly chronic diseases. Beyond of the cause of the disease, the complexity of chronicity also results in the heterogeneous appearance of diseased nerves. Indeed, while some cells are normal, some demyelinate and some remyelinate. In addition, extra-nerve cells are also recruited such as macrophages. So, as we saw with the imaging of the CMT1A rat model using CARS, the diseased sciatic nerve shows a complex pattern both on the same axon and between axons. We found that CARS imaging can be used to characterize the loss of myelin (relative myelin surface), the hypo- or hyper-myelination (G-ratio) and also dysmyelination (malformed myelin sheath) using the interincisural distance.

Finally, the interest of CARS imaging probably also resides in the improvements that are being implemented by physicists in the field. Indeed spectral focusing CARS and stimulated Raman scattering microscopy [20] allows for the distinction between several type of lipids, notably

oxidized lipids that are found in lesioned tissues [21,22], but also proteins and ribonucleic acids [23,24]. Another interesting improvement is the use of rotating polarization CARS to detect the spatial orientation of CH₂- moieties on lipids [25]. In “healthy” myelin moieties polarity is much more homogenous than in diseased or ageing myelin [7]. In conclusion, non-linear label free CARS microscopy and potentially endoscopy [26] represents a consistent and strong readout tool in the development of new treatments for demyelinating peripheral neuropathies [27,28].

Material and methods

Animals

PMP22 transgenic CMT1A rats [11] expressing mouse *PMP22* cosmid gene as well as Swiss mice (Janvier, France) were used for this study. Wild-type (WT) littermates of rats served as controls. The genotyping was done with genomic DNA from tail biopsies of rats using polymerase chain reaction with mouse transgene-specific primers as previously described [11]. All experiments were performed accordingly to French regulations for animal experimentation (Comité d'éthique pour l'expérimentation animale Languedoc-Roussillon, #1307).

Sciatic nerve surgery, microscopy set-up and image acquisition

For *in vivo* imaging mice were imaged between 9 and 11 weeks of age and rats between 17 and 21 weeks of age. Animal surgery is described in the supplementary material. The nerve was gently lifted out and a thin and flexible plastic bridge was inserted below the nerve very carefully without damaging it. The nerve was moistened with sterile Phosphate-buffered saline (PBS) in order to prevent the nerve from drying out. Two magnetic brackets were utilized to fix the bridge. The paw was fixed with a scotch tape to minimize movement. A very small and round cover slip was placed on top of the nerve. Then the animal was positioned along with the anaesthesia mask under the multiphoton microscope coupled to a microscope incubator (XL S Examiner Dark, Zeiss) in which the temperature was kept at 37 °C. It was made sure that the coverslip was as flat as possible to get good resolution images. Deionized water was added to immerse a water 20 x objective lens (W Plan-Apochromat 20x/1.0 DIC, Zeiss). After imaging, the sciatic nerve was put back into the cavity, the muscles were readjusted, and the wound was closed using clips. The analgesic Buprenorphine (0.1 mg/kg) was administrated to mice before surgery and after surgery for 48 hours every 12 hours. For longitudinal studies, mice underwent the same surgery after 7 or 14 days to again image the same sciatic nerve *in vivo*.

Animals were then sacrificed and the nerve was dissected to obtain *ex vivo* images. To obtain fixed samples, sciatic nerve was dissected and the epineurium was removed. Nerves were then fixed in 4% paraformaldehyde (PFA) for 2 h at 4°C and kept in PBS at 4°C until imaging (maximum of one week) and then fixed again overnight in 4% PFA and stored in PBS at 4°C.

Non-linear microscopy setup

A multiphoton microscope LSM 7 MP OPO (Zeiss, France) using an upright Axio Examiner Z.1 optical microscope associated with a femtosecond Ti:sapphire laser (680-1080 nm, 80MHz, 140 fs, Chameleon Ultra II, Coherent, France) pumping a tunable optical parametric oscillators (1000-1500 nm, 80MHz, 200 fs, Chameleon Compact OPO, Coherent, France) was utilised to acquire images. Depending on the type of studies (*in vivo* or *ex vivo*), different types of images were obtained: time-lapse images for *in vivo* studies (several images of one single plane across a specific time of around 10s) and z-stack for *ex vivo* studies (several images of multiple planes, approximately 40 μ m depth). A 20x water immersion lens (W Plan Apochromat DIC VIS-IR) was used for images. The characteristics are the following: 1024 pixels frame size, scan speed of 7 (Pixel Dwell 3.15 μ sec/ Scan Time 3.87 sec) and either a zoom x1 or x3.

Four non-linear microscopy techniques were used for images: the two-photon standard fluorescent method, the second harmonic generation (SHG), the third harmonic generation (THG) and Coherent Anti-Stokes Raman Scattering (CARS). The fluorescent method was used for Thy-1 mice with an excitation wavelength of the Ti-sapphire laser of 870 nm and a narrow band pass filter at 500-550 nm in front of one of the detectors. The SHG and THG were utilised for Swiss mice. SHG excitation wavelength of the OPO laser is 1097 nm, the signal detection at half of the excitation wavelength i.e. 548 nm and the filter at 500-550 nm. THG excitation wavelength of OPO laser is 1300 nm, the signal detection at one third of the excitation wavelength i.e. 433 nm and the filter at 400-480 nm. As described by Mytskaniuk V et al, the CARS technique is based on the synchronization of two laser beams: the Ti-sapphire with an excitation wavelength of 836 nm and the OPO with an excitation wavelength of 1097 nm. The signal is detected at 670 nm and the filter ranges from 660-685nm.

Image analysis

Images were analysed by the software Imaris 8.4 (Bitplane, Switzerland). *In vivo* images were cropped due to respiration. The image analysis processes are detailed in supplementary material. Statistics were done using Graphpad Prism 7 software.

Acknowledgments

We thank Freddy Jeanneteau (Institut de Genomic Fonctionnelle, Montpellier, France) for the gift of Thy1-YFP mice. We acknowledge the imaging facility MRI, member of the national infrastructure France-BioImaging supported by the French National Research Agency (ANR-10-INBS-04, «Investments for the future»). This work has been supported by European Research Council grant (FP7-IDEAS-ERC 311610), an INSERM - AVENIR grant to N. Tricaud and by Droguerie Mercury S.A.L through a fellowship to H. Hajjar.

Conflict of Interest

The authors declare no conflict of interest.

References:

- [1] Salzer, J. L., 2015, "Schwann Cell Myelination," *Cold Spring Harb Perspect Biol*, 7(8).
- [2] Tricaud, N., and Park, H. T., 2017, "Wallerian Demyelination: Chronicle of a Cellular Cataclysm," *Cell. Mol. Life Sci.*, 74(22), pp. 4049–4057.
- [3] Katona, I., and Weis, J., 2018, "Chapter 31 - Diseases of the Peripheral Nerves," *Handbook of Clinical Neurology*, G.G. Kovacs, and I. Alafuzoff, eds., Elsevier, pp. 453–474.
- [4] Jessen, K. R., and Mirsky, R., 2016, "The Repair Schwann Cell and Its Function in Regenerating Nerves," *J Physiol*, 594(13), pp. 3521–3531.
- [5] Chung, C.-Y., Boik, J., and Potma, E. O., 2013, "Biomolecular Imaging with Coherent Nonlinear Vibrational Microscopy," *Annu Rev Phys Chem*, 64, pp. 77–99.
- [6] Weigelin, B., Bakker, G.-J., and Friedl, P., 2016, "Third Harmonic Generation Microscopy of Cells and Tissue Organization," *J Cell Sci*, 129(2), pp. 245–255.
- [7] Gasecka, P., Jaouen, A., Bioud, F.-Z., B de Aguiar, H., Duboisset, J., Ferrand, P., Rigneault, H., Balla, N. K., Debarbieux, F., and Brasselet, S., 2017, "Lipid Order Degradation in Autoimmune Demyelination Probed by Polarized Coherent Raman Microscopy," *Biophys. J.*, 113(7), pp. 1520–1530.
- [8] Schie, I. W., Krafft, C., and Popp, J., 2015, "Applications of Coherent Raman Scattering Microscopies to Clinical and Biological Studies," *Analyst*, 140(12), pp. 3897–3909.
- [9] Zumbusch, A., Langbein, W., and Borri, P., 2013, "Nonlinear Vibrational Microscopy Applied to Lipid Biology," *Prog. Lipid Res.*, 52(4), pp. 615–632.
- [10] Mytskaniuk, V., Bardin, F., Boukhaddaoui, H., Rigneault, H., and Tricaud, N., 2016, "Implementation of a Coherent Anti-Stokes Raman Scattering (CARS) System on a Ti:Sapphire and OPO Laser Based Standard Laser Scanning Microscope," *J Vis Exp*, (113).
- [11] Sereda, M., Griffiths, I., Pühlhofer, A., Stewart, H., Rossner, M. J., Zimmerman, F., Magyar, J. P., Schneider, A., Hund, E., Meinck, H. M., Suter, U., and Nave, K. A., 1996, "A Transgenic Rat Model of Charcot-Marie-Tooth Disease," *Neuron*, 16.
- [12] Gluck, M. J., Vijayaraghavan, S., Sinclair, E. B., Ashraf, A., Hausman, M. R., and Cagle, P. J., 2018, "Detecting Structural and Inflammatory Response after in Vivo Stretch Injury in the Rat Median Nerve via Second Harmonic Generation," *J. Neurosci. Methods*, 303, pp. 68–80.
- [13] King, R., 2013, "Chapter 2 - Microscopic Anatomy: Normal Structure," *Handbook of Clinical Neurology*, G. Said, and C. Krarup, eds., Elsevier, pp. 7–27.
- [14] Lim, H., Sharoukhov, D., Kassim, I., Zhang, Y., Salzer, J. L., and Melendez-Vasquez, C. V., 2014, "Label-Free Imaging of Schwann Cell Myelination by Third Harmonic Generation Microscopy," *Proc. Natl. Acad. Sci. U.S.A.*, 111(50), pp. 18025–18030.
- [15] Gonzalez, S., Fernando, R., Berthelot, J., Perrin-Tricaud, C., Sarzi, E., Chrast, R., Lenaers, G., and Tricaud, N., 2015, "In Vivo Time-Lapse Imaging of Mitochondria in Healthy and Diseased Peripheral Myelin Sheath," *Mitochondrion*, 23, pp. 32–41.
- [16] Schröder, J. M., 1972, "Altered Ratio between Axon Diameter and Myelin Sheath Thickness in Regenerated Nerve Fibers," *Brain Res.*, 45(1), pp. 49–65.
- [17] Ghabriel, M. N., and Allt, G., 1981, "Incisions of Schmidt-Lanterman," *Progress in Neurobiology*, 17(1–2), pp. 25–58.
- [18] Bélanger, E., Henry, F. P., Vallée, R., Randolph, M. A., Kochevar, I. E., Winograd, J.

- M., Lin, C. P., and Côté, D., 2011, "In Vivo Evaluation of Demyelination and Remyelination in a Nerve Crush Injury Model," *Biomed Opt Express*, 2(9), pp. 2698–2708.
- [19] HUFF, T. B., and CHENG, J.-X., 2007, "In Vivo Coherent Anti-Stokes Raman Scattering Imaging of Sciatic Nerve Tissue," *J Microsc*, 225(Pt 2), pp. 175–182.
- [20] Folick, A., Min, W., and Wang, M. C., 2011, "Label-Free Imaging of Lipid Dynamics Using Coherent Anti-Stokes Raman Scattering (CARS) and Stimulated Raman Scattering (SRS) Microscopy," *Current Opinion in Genetics & Development*, 21(5), pp. 585–590.
- [21] C. Poon, K. W., Brideau, C., Klaver, R., J. Schenk, G., J. Geurts, J., and K. Stys, P., 2018, "Lipid Biochemical Changes Detected in Normal Appearing White Matter of Chronic Multiple Sclerosis by Spectral Coherent Raman Imaging," *Chemical Science*, 9(6), pp. 1586–1595.
- [22] Ramos, I. R., Lyng, F. M., Rehman, I. U., Sharrack, B., and Woodroffe, M. N., 2017, "The Use of Vibrational Spectroscopy to Study the Pathogenesis Multiple Sclerosis and Other Neurological Conditions," *Applied Spectroscopy Reviews*, 52(10), pp. 868–882.
- [23] Cicerone, M., 2016, "Molecular Imaging with CARS Micro-Spectroscopy," *Current Opinion in Chemical Biology*, 33, pp. 179–185.
- [24] Zhang, X., Roeffaers, M. B. J., Basu, S., Daniele, J. R., Fu, D., Freudiger, C. W., Holtom, G. R., and Xie, X. S., 2012, "Label-Free Live Cell Imaging of Nucleic Acids Using Stimulated Raman Scattering (SRS) Microscopy," *Chemphyschem*, 13(4), pp. 1054–1059.
- [25] Bioud, F.-Z., Gasecka, P., Ferrand, P., Rigneault, H., Duboisset, J., and Brasselet, S., 2014, "Structure of Molecular Packing Probed by Polarization-Resolved Nonlinear Four-Wave Mixing and Coherent Anti-Stokes Raman-Scattering Microscopy," *Phys. Rev. A*, 89(1), p. 013836.
- [26] Lombardini, A., Mytskaniuk, V., Sivankutty, S., Andresen, E. R., Chen, X., Wenger, J., Fabert, M., Joly, N., Louradour, F., Kudlinski, A., and Rigneault, H., 2017, "HighResolution Multimodal Flexible Coherent Raman Endoscope," *arXiv:1708.04149 [physics]*.
- [27] Cialla-May, D., Zheng, X.-S., Weber, K., and Popp, J., 2017, "Recent Progress in Surface-Enhanced Raman Spectroscopy for Biological and Biomedical Applications: From Cells to Clinics," *Chem Soc Rev*, 46(13), pp. 3945–3961.
- [28] Krafft Christoph, von Eggeling Ferdinand, Guntinas- Lichius Orlando, Hartmann Arndt, Waldner Maximilian J., Neurath Markus F., and Popp Jürgen, 2017, "Perspectives, Potentials and Trends of Ex Vivo and in Vivo Optical Molecular Pathology," *Journal of Biophotonics*, 11(1), p. e201700236.

Graphical abstract:

Measuring the treatment outcome of chronic diseases such as the hereditary peripheral neuropathies is not straightforward. It requires specific analyses among which imaging of peripheral nerve myelin. In this article myelin of healthy, injured and diseased small rodents was imaged ex vivo and in vivo using several non-linear microscopy approaches. CARS microscopy allows for the qualitative and quantitative assessment of peripheral nerve myelin defects in living diseased animals.

Supporting information

Label-free non-linear microscopy to measure outcome in rodent model of Charcot-Marie-Tooth diseases

Hajjar H^{1#}, Boukhaddaoui H^{1,3#}, Rizgui A¹, Sar C^{1,3}, Berthelot J¹, Perrin-Tricaud C¹, Rigneault H² and Tricaud N¹.

1- Institut des Neurosciences de Montpellier, Université de Montpellier, 80 Rue A. Fliche, 34090 Montpellier, France

2- Aix-Marseille Université, CNRS, École Centrale Marseille, Institut Fresnel, UMR 7249,

3- Montpellier Ressources Imaging (MRI)

Sciatic nerve surgery

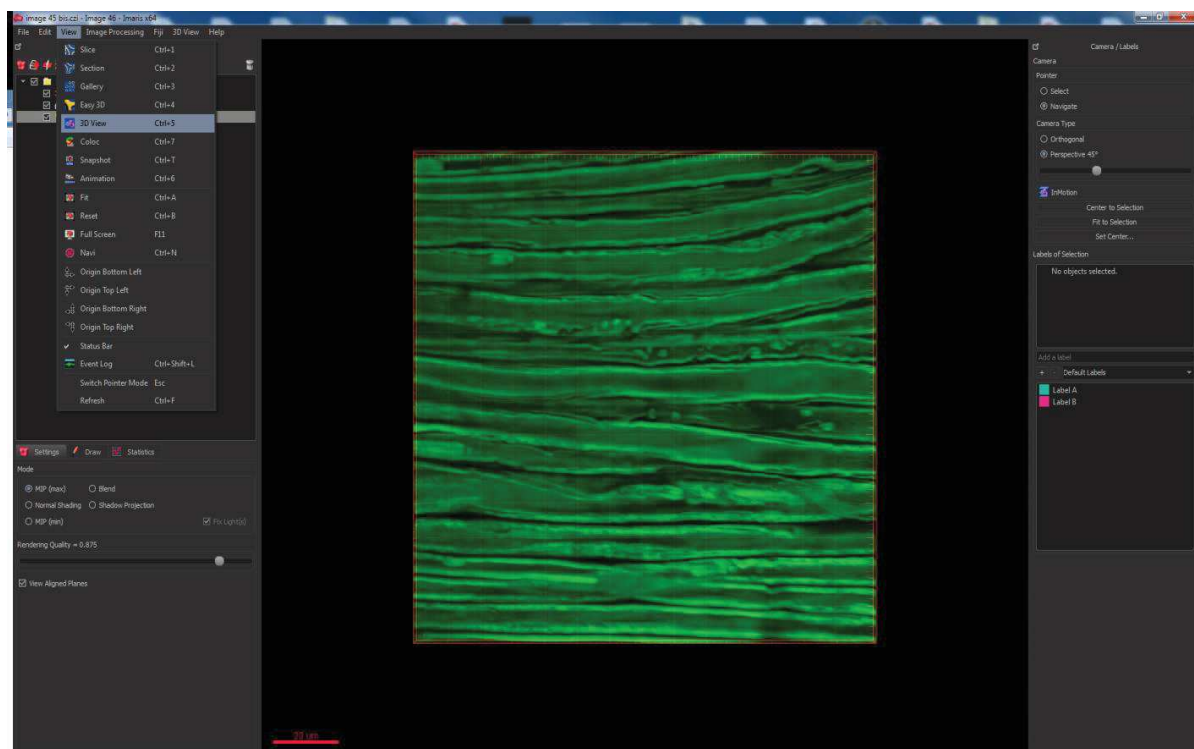
Animals were anesthetized by inhalation of isoflurane (5%) with a constant oxygen flow (1.5 L/min) inside an induction box for around 5 min. Then anesthesia was upheld with a nose cone using 2% isoflurane and 0.8 L/min oxygen flow. Ocry-gel was put on the eyes of animals to avoid ocular dryness. The analgesic Buprenorphine (0.1 mg/kg) was administrated to mice just before surgery and for 48 hours after surgery every twelve hours. Incision area was shaved and cleaned with betadine solution then 70% ethanol and again betadine. Skin was cut at the level of the thigh and the muscles were separated to expose the cavity containing the sciatic nerve. The nerve was gently lift out and a thin and flexible plastic bridge was inserted below the nerve very carefully without damaging it. The nerve was moisten with sterile Phosphate-buffered saline (PBS) for the nerve not to dry. Two magnetic brackets were utilized to fix the bridge. The paw of rat was fixed with a scotch tape to minimize movement. A very small and round cover slip was placed on top of the nerve. Then the animal was positioned along with the anesthesia mask under the multiphoton microscope coupled to a microscope incubator (L S1 Dark, Zeiss) in which the temperature was kept at 37 °C. It was made sure that the coverslip is as flat as possible to get good resolution images. Deionized water was added to immerse the 63x objective lens. After imaging, the sciatic nerve was put back into the cavity, the muscles were readjusted, and the wound was closed using clips.

After 7 or 14 days, mice underwent the same surgery to image again the same sciatic nerve *in vivo*. They were then sacrificed and the nerve was dissected to obtain *ex vivo* images.

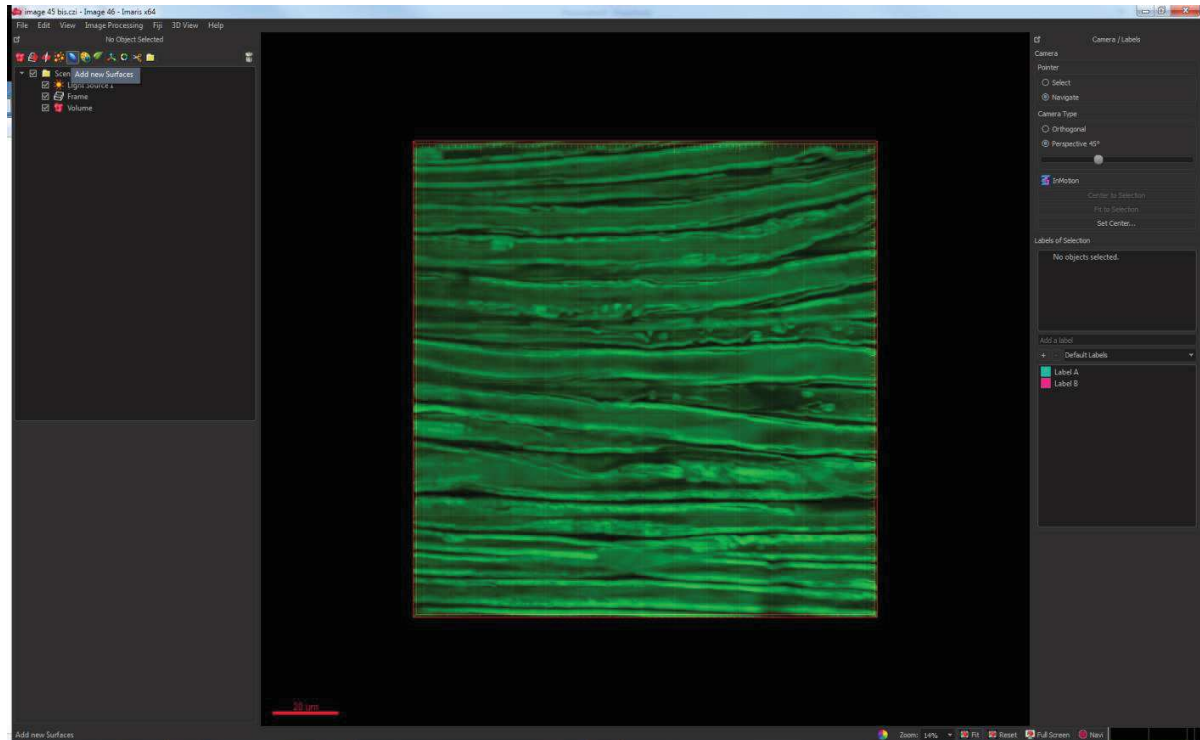
Rats were imaged between 17 and 21 weeks of age. Both *in vivo* and *ex vivo* images were acquired. Nerves were then fixed in 4% paraformaldehyde (PFA) for 2 h at 4°C and kept in PBS at 4°C until imaging (maximum for one week) and then fixed again overnight in 4% PFA and stored in PBS at 4°C.

Image analysis using Imaris

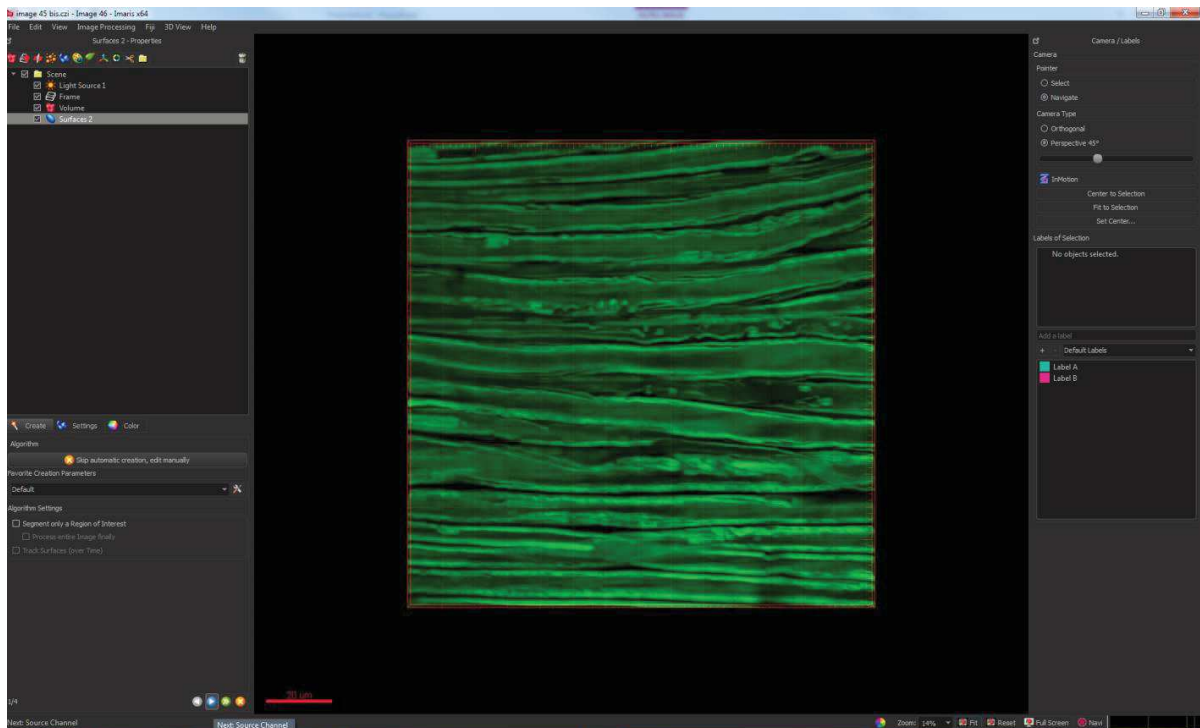
After opening the image with Imaris, we selected in the menu toolbar at the upper left ‘View’ - ‘3D view’



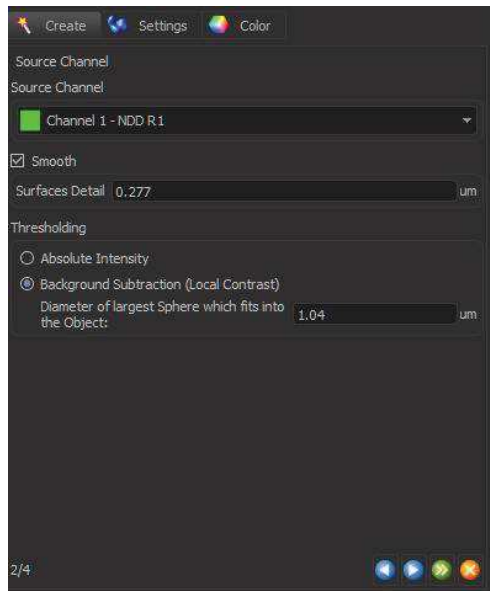
For the quantitation of myelin and debris, we selected the blue ellipsoid icon ‘Add new Surfaces’



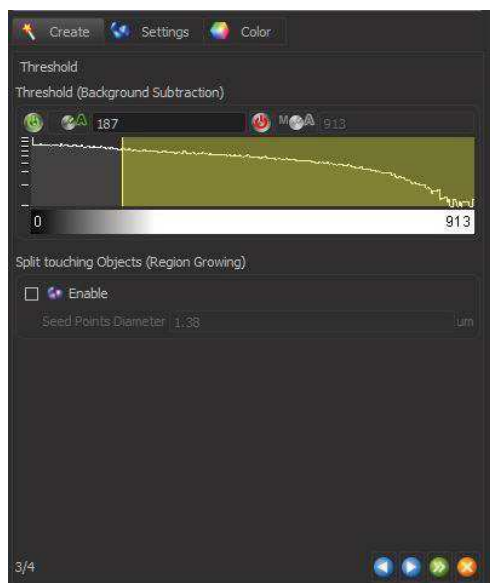
We selected the 'Create' submenu (magic wand icon) and clicked on the 'Next' button



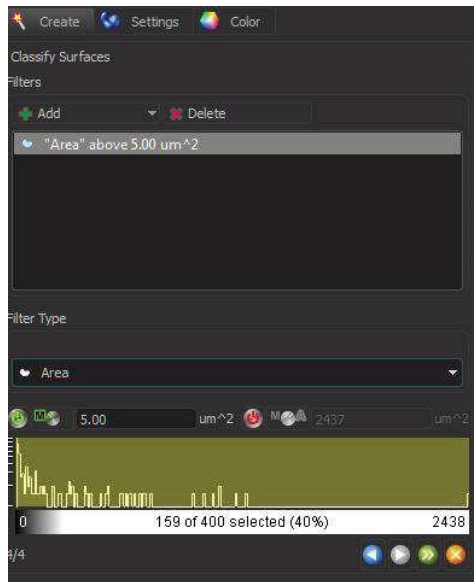
We checked the Smooth option from the Source Channel dropdown menu since smoothing can facilitate object identification in noisy images. In ‘Thresholding’ we chose the ‘Background Subtraction’ option because objects we measure are touching. Then we clicked ‘Next’.



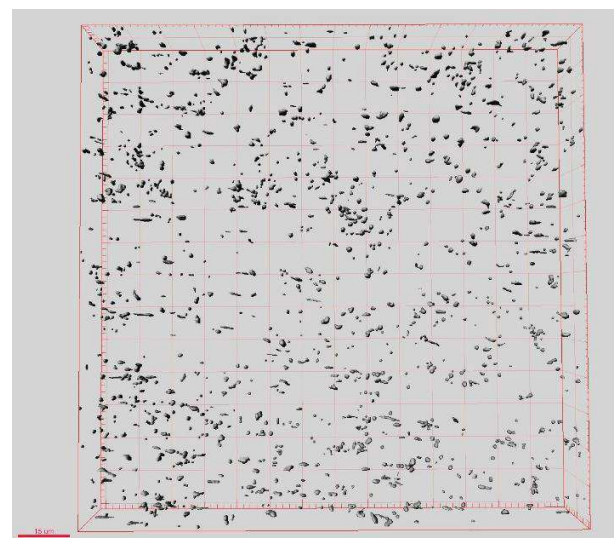
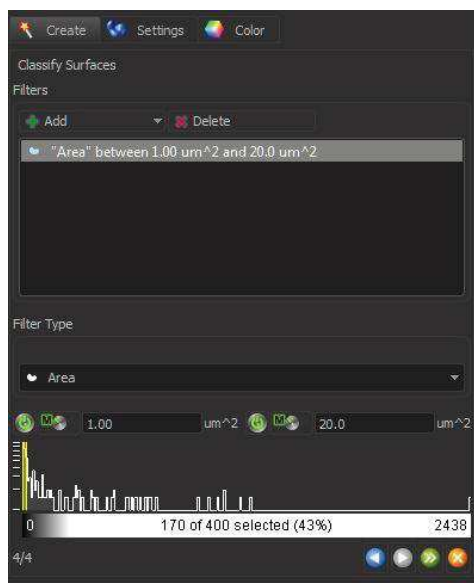
We adjusted the threshold and clicked ‘Next’.



We selected the filter “Area above 5 μm^2 ” for myelin quantitation



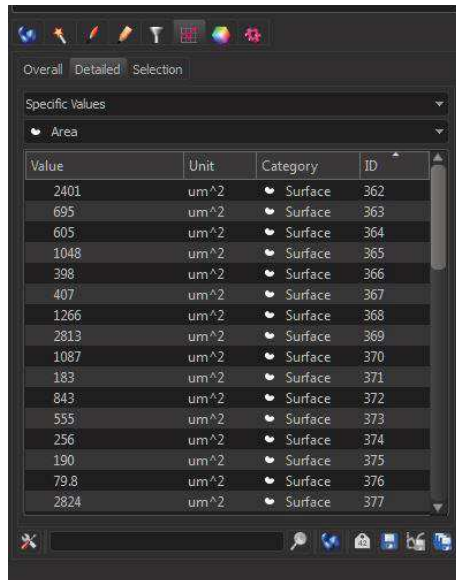
We selected “Area between 1-20 μm^2 ” for debris.



We selected the ‘Finish’ button

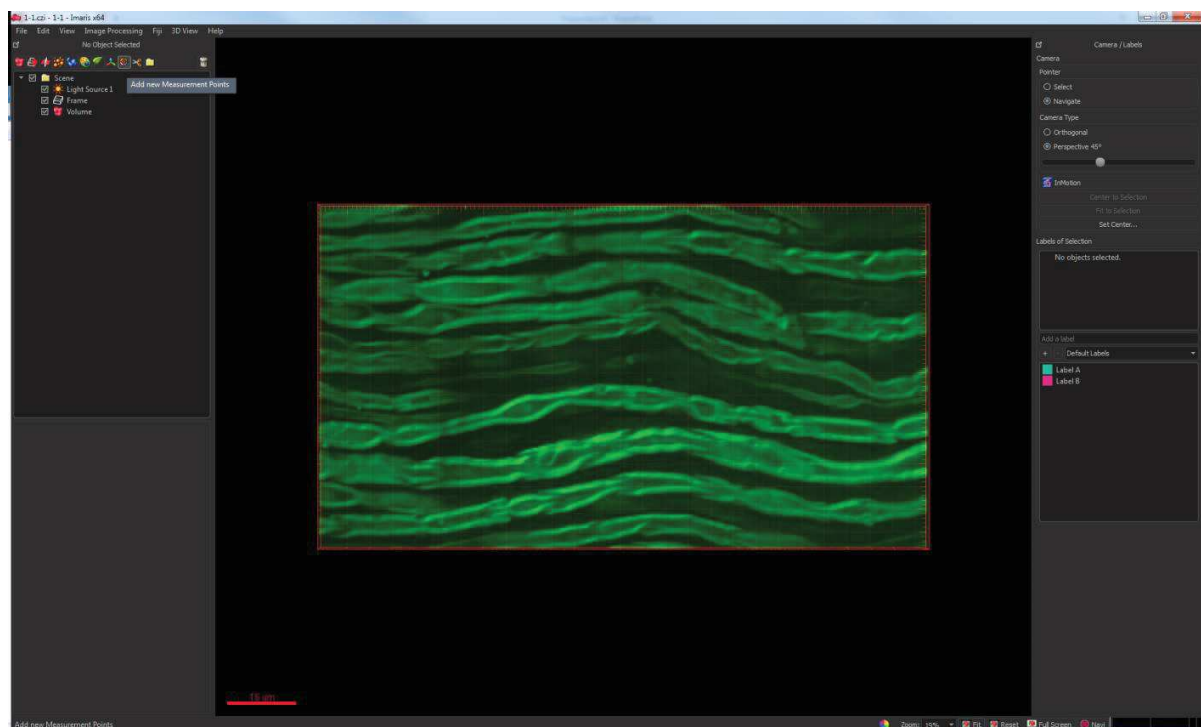


In the 'Statistics' submenu, we selected 'Detailed' and exported data to excel ('Disk' icons at the bottom of the Statistics window)

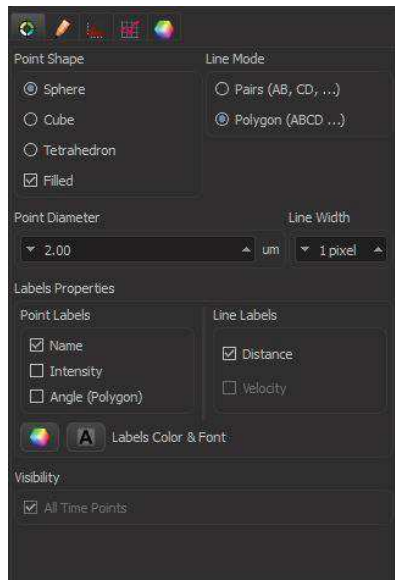


Value	Unit	Category	ID
2401	um^2	Surface	362
695	um^2	Surface	363
605	um^2	Surface	364
1048	um^2	Surface	365
398	um^2	Surface	366
407	um^2	Surface	367
1266	um^2	Surface	368
2813	um^2	Surface	369
1087	um^2	Surface	370
183	um^2	Surface	371
843	um^2	Surface	372
555	um^2	Surface	373
256	um^2	Surface	374
190	um^2	Surface	375
79.8	um^2	Surface	376
2824	um^2	Surface	377

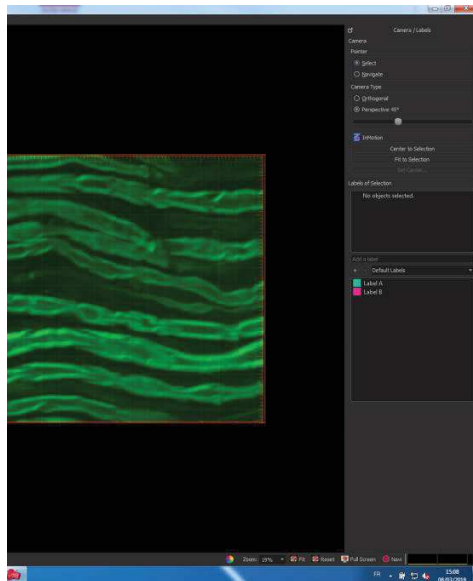
For interincisural distance and g-ratio analysis, we selected the icon “Measurement Points”



We selected the Settings sub-menu of Measurement points, chose the point shape 'Sphere' and in 'Line Mode' polygon points to be drawn for interincisural distance and pairs of points to be drawn for g-ratio.

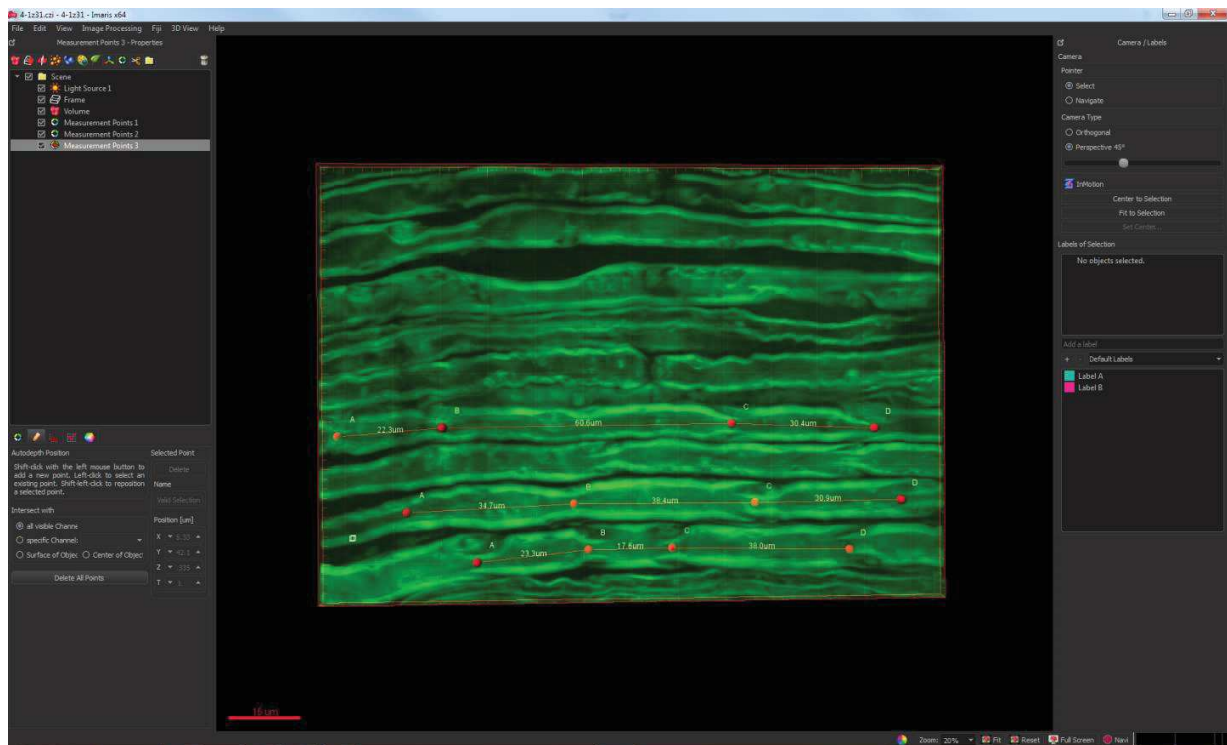


We changed the Mouse Pointer option from 'Navigate' to 'Select' mode

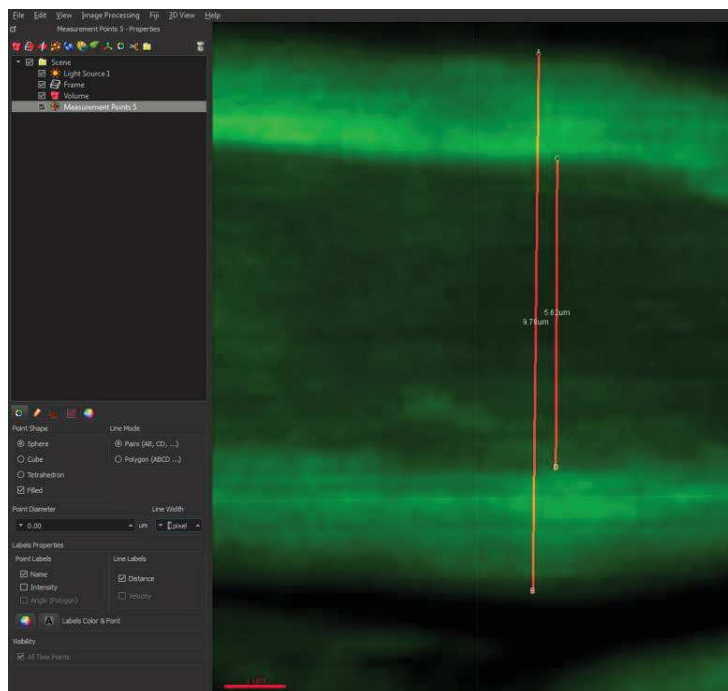


We pressed the pencil icon to add points and followed instructions displayed.

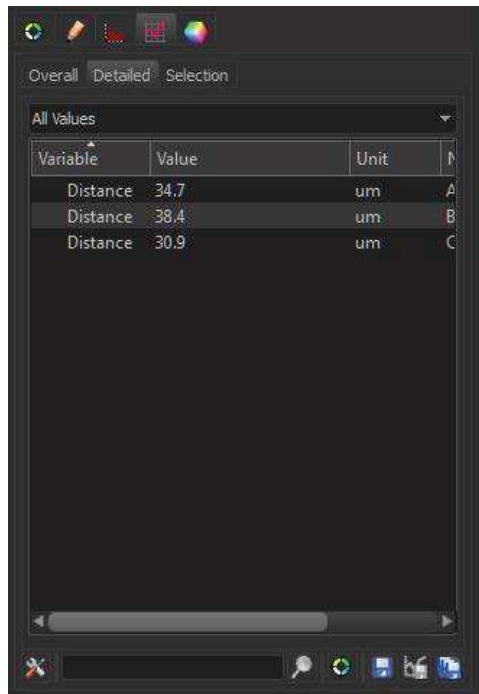
Interincisural distance



g-ratio



In the 'Statistics' submenu, we selected 'Detailed' and exported data to excel ('Disk' icons at the bottom of the Statistics window)



Variable	Value	Unit	N
Distance	34.7	um	A
Distance	38.4	um	B
Distance	30.9	um	C

Conclusion and Perspectives

Imaging myelin in living animals and potentially in humans without using any label is an evolving research field. Many techniques exist including SHG, THG and CARS. In peripheral nerves of mice and rats, SHG can be used for imaging collagen fibers in the perineurium and endoneurium, THG the interfaces of compact myelin with the aqueous environment and CARS the myelin sheath as a large bright band surrounding axon. After comparing those techniques in healthy and injured nerves of mice (demyelination and remyelination), we found out that CARS is the best method of the three since its signal emerges directly from the myelin sheath as clear and strong. Thus, we used CARS for a myelin readout tool in the sciatic nerve of healthy and diseased rats. With CARS imaging, we were able to successfully characterize myelin defects (loss, hypo/hyper- and dysmyelination). Therefore, CARS label-free microscopy is a promising technique as a consistent, reliable and quantitative outcome measure for developing new therapies for demyelinating peripheral neuropathies. However, further research need to be done in order to solve some technical difficulties we encountered during *in vivo* imaging: invasiveness and low light penetration in the tissue. One solution is to use CARS imaging along with technical improvements such as a Bessel beam illumination. This technique allows for the extension of the axial depth of field, which should give a better light penetration: field depth for Bessel Beam is 10 μ m versus 3.5 μ m for the classic Gaussian beam (Masia et al., 2018).

GENERAL CONCLUSION

As part of the myelin team at the Institute of Neurosciences in Montpellier, my thesis research project covered several topics of the myelin translational research. Myelin that wraps axons is essential to protect and nurture them. It also increases nerve conduction velocity to levels that allow large animals and humans to move their bodies fast enough to run at 37 km/h such as Kylian Mbappé in the last football world cup. I had the pleasure to work on a dramatic disease called Charcot Marie Tooth type 1A (CMT1A) and the honour to try to find a cure for it. It is caused by a duplication of the *PMP22* gene on the chromosome 17 of humans resulting in an overexpressed PMP22 protein. There is still no cure for CMT diseases despite extensive research. Gene therapy seems a logical approach since the disease is chronic and inherited. In addition, it is considered as a very innovative treatment compared to classical pharmacological costly and burdensome treatments. Thus, I studied the efficiency of a gene therapy approach which targeted myelinating Schwann cells (highly express PMP22) aiming at reducing the excess of PMP22. The strategy consisted in injecting viral vectors AAV9 carrying the gene silencing therapeutic tool shRNA PMP22 in both sciatic nerves of a rat model of the disease, the CMT1A rat. This model closely mimics the human disease. AAV9 highly transduced the targeted cells, the myelinating Schwann cells and PMP22 mRNA as well as protein levels were downregulated. Therapy corrected the motor deficits seen in diseased rats to almost a full recovery as proved by rotarod and grip test. In addition, treatment alleviated hypoalgesia as seen in Randall Selitto test (the first real pain test realized on this rat CMT1A model so far) and increased nerve conduction velocity as calculated from electrophysiological measurements. This was all achieved with only one single bilateral injection in sciatic nerves. Treatment is still efficient even on the long run; after more than 9 months. Furthermore, safety assessment by testing the immune response against AAV (neutralization assay) as well as off-targets infections of the virus (AAV biodistribution) came out almost completely “clean”. This means that successive injections of the therapeutic vector could safely be performed in order to reach several human nerves. All those results appear very promising and encourage us to translate to clinical trials.

However, no tool consistent enough exists for examining the peripheral nerve. Therefore, it is crucial to find a strong readout to evaluate the outcome of a treatment before moving to clinical trials. Non-linear, label free microscopy seems very appropriate. Among different techniques we found that CARS is the best method to image myelin *in vivo* as its signal comes directly from the myelin sheath as clear and strong. Using CARS imaging on sciatic nerves of rats, we successfully

characterized loss of myelin, hypo-hyper- and dys-myelination in CMT1A rats. Consequently, CARS label-free microscopy could be used as a consistent outcome measure for developing new therapies for demyelinating peripheral neuropathies.

Taken together I realize that the three years of my life I have spent in Montpellier were very useful not only for me as a researcher-student but also, I believe, for all the people suffering with CMT1A. Indeed, I am convinced that in the future an efficient, convenient and well-accepted gene therapy will be available for all these patients around the world.

BIBLIOGRAPHY

- Adams, D., Gonzalez-Duarte, A., O’Riordan, W. D., Yang, C.-C., Ueda, M., Kristen, A. V., ... Suhr, O. B. (2018). Patisiran, an RNAi Therapeutic, for Hereditary Transthyretin Amyloidosis. *New England Journal of Medicine*, 379(1), 11–21. <https://doi.org/10.1056/NEJMoal716153>
- Alam, S., Bowser, B. S., Conway, M. J., Israr, M., Tandon, A., & Meyers, C. (2011). Adeno-associated virus type 2 infection activates caspase dependent and independent apoptosis in multiple breast cancer lines but not in normal mammary epithelial cells. *Molecular Cancer*, 10. <https://doi.org/10.1186/1476-4598-10-97>
- Allocca, M., Doria, M., Petrillo, M., Colella, P., Garcia-hoyos, M., Gibbs, D., ... Auricchio, A. (2008). Serotype-dependent packaging of large genes in adeno-associated viral vectors results in effective gene delivery in mice Mariacarmela. *The Journal of Clinical Investigation*, 118(5). <https://doi.org/10.1172/JCI34316DS1>
- Amici, S. A. (2006). Peripheral Myelin Protein 22 Is in Complex with β 4 Integrin, and Its Absence Alters the Schwann Cell Basal Lamina. *Journal of Neuroscience*, 26(4), 1179–1189. <https://doi.org/10.1523/JNEUROSCI.2618-05.2006>
- Amici, S. A., Dunn, W. A., & Notterpek, L. (2007). Developmental abnormalities in the nerves of peripheral myelin protein 22-deficient mice. *Journal of Neuroscience Research*, 85(2), 238–49. <https://doi.org/10.1002/jnr.21118>
- Ando, Y., Coelho, T., Berk, J. L., Cruz, M. W., Ericzon, B. G., Ikeda, S. I., ... Salvi, F. (2013). Guideline of transthyretin-related hereditary amyloidosis for clinicians. *Orphanet Journal of Rare Diseases*, 8(1), 1–18. <https://doi.org/10.1186/1750-1172-8-31>
- Argyros, O., Wong, S.-P., & Harbottle, R. P. (2011). Non-viral episomal modification of cells using S/MAR elements. *Expert Opinion on Biological Therapy*, 11(9), 1177–1191. <https://doi.org/10.1517/14712598.2011.582035>
- Armbruster, N., Lattanzi, A., Jeavons, M., Van Wittenberghe, L., Gjata, B., Marais, T., ... Buj-Bello, A. (2016). Efficacy and biodistribution analysis of intracerebroventricular

- administration of an optimized scAAV9-SMN1 vector in a mouse model of spinal muscular atrophy. *Molecular Therapy - Methods and Clinical Development*, 3(July), 16060. <https://doi.org/10.1038/mtm.2016.60>
- Arnaud, E., Zenker, J., de Preux Charles, A.-S., Stendel, C., Roos, A., Medard, J.-J., ... Chrast. (2009). SH3TC2/KIAA1985 protein is required for proper myelination and the integrity of the node of Ranvier in the peripheral nervous system. *Proc. Natl. Acad. Sci.*, 106(41), 17528–17533. <https://doi.org/10.1073/pnas.1011320107>
- Arroyo, E. J., & Scherer, S. S. (2000). On the molecular architecture of myelinated fibers. *Histochemistry and Cell Biology*, 113(1), 0001. <https://doi.org/10.1007/s004180050001>
- Atkins, E. J., Bruce, B. B., Newman, N. J., & Biouesse, V. (2010). Treatment of Nonarteritic Anterior Ischemic Optic Neuropathy. *Survey of Ophthalmology*, 55(1), 47–63. <https://doi.org/10.1016/j.survophthal.2009.06.008>
- Attarian, S., Vallat, J.-M., Magy, L., Funalot, B., Gonnaud, P.-M., Lacour, A., ... Cohen, D. (2016). An exploratory randomised double-blind and placebo-controlled phase 2 study of a combination of baclofen, naltrexone and sorbitol (PXT3003) in patients with Charcot-Marie-Tooth disease type 1A. *Orphanet Journal of Rare Diseases*, 11(1), 92. <https://doi.org/10.1186/s13023-016-0463-6>
- Auricchio, A. (2003). Pseudotyped AAV vectors for constitutive and regulated gene expression in the eye. In *Vision Research* (Vol. 43, pp. 913–918). [https://doi.org/10.1016/S0042-6989\(02\)00676-4](https://doi.org/10.1016/S0042-6989(02)00676-4)
- Ayciriex, S., Djelti, F., Alves, S., Regazzetti, A., Gaudin, M., Varin, J., ... Cartier, N. (2017). Neuronal Cholesterol Accumulation Induced by Cyp46a1 Down-Regulation in Mouse Hippocampus Disrupts Brain Lipid Homeostasis. *Frontiers in Molecular Neuroscience*, 10, 211. <https://doi.org/10.3389/fnmol.2017.00211>
- Baechner, D., Liehr, T., Hameister, H., Altenberger, H., Grehl, H., Suter, U., & Rautenstrauss, B. (1995). Widespread expression of the peripheral myelin protein-22 gene (pmp22) in neural and non-neural tissues during murine development. *Journal of Neuroscience Research*, 42(6), 733–741. <https://doi.org/10.1002/jnr.490420602>

- Balaji, S., King, A., Dhamija, Y., Le, L. D., Shaaban, A. F., Crombleholme, T. M., & Keswani, S. G. (2013). Pseudotyped adeno-associated viral vectors for gene transfer in dermal fibroblasts: Implications for wound-healing applications. *Journal of Surgical Research*, 184(1), 691–698. <https://doi.org/10.1016/j.jss.2013.03.051>
- Bartlett, J. S., Samulski, R. J., & McCown, T. J. (1998). Selective and rapid uptake of adeno-associated virus type 2 in brain. *Human Gene Therapy*, 9(8), 1181–1186. <https://doi.org/10.1089/hum.1998.9.8-1181>
- Bartlett, J. S., Wilcher, R., & Samulski, R. J. (2000). Infectious Entry Pathway of Adeno-Associated Virus and Adeno-Associated Virus Vectors. *Journal Of Virology*, 74(6), 2777–2785.
- Barton, G. M., Kagan, J. C., & Medzhitov, R. (2006). Intracellular localization of Toll-like receptor 9 prevents recognition of self DNA but facilitates access to viral DNA. *Nature Immunology*, 7(1), 49–56. <https://doi.org/10.1038/ni1280>
- Batka, R. J., Brown, T. J., Mcmillan, K. P., Meadows, R. M., Jones, K. J., & Haulcomb, M. M. (2014). The need for speed in rodent locomotion analyses. *Anatomical Record*, 297(10), 1839–1864. <https://doi.org/10.1002/ar.22955>
- Baumgärtner, U., Magerl, W., Klein, T., Hopf, H. C., & Treede, R. D. (2002). Neurogenic hyperalgesia versus painful hypoalgesia: Two distinct mechanisms of neuropathic pain. *Pain*, 96(1–2), 141–151. [https://doi.org/10.1016/S0304-3959\(01\)00438-9](https://doi.org/10.1016/S0304-3959(01)00438-9)
- Baxter, R. V., Othmane, K. Ben, Rochelle, J. M., Stajich, J. E., Hulette, C., Dew-Knight, S., ... Vance, J. M. (2002). Ganglioside-induced differentiation-associated protein-1 is mutant in Charcot-Marie-Tooth disease type 4A/8q21. *Nature Genetics*, 30(1), 21–22. <https://doi.org/10.1038/ng796>
- Bell, P., Wang, L., Gao, G., Haskins, M. E., Tarantal, A. F., McCarter, R. J., ... Wilson, J. M. (2011). Inverse zonation of hepatocyte transduction with AAV vectors between mice and non-human primates. *Molecular Genetics and Metabolism*, 104(3), 395–403. <https://doi.org/10.1016/j.ymgme.2011.06.002>

- Bennett, C. F., Baker, B. F., Pham, N., Swayze, E., & Geary, R. S. (2017). Pharmacology of Antisense Drugs. *Annu. Rev. Pharmacol. Toxicol.*, 57, 81–105. <https://doi.org/10.1146/annurev-pharmtox-010716-104846>
- Bennett, C. F., & Swayze, E. E. (2010). RNA Targeting Therapeutics: Molecular Mechanisms of Antisense Oligonucleotides as a Therapeutic Platform. *Annual Review of Pharmacology and Toxicology*, 50(1), 259–293. <https://doi.org/10.1146/annurev.pharmtox.010909.105654>
- Bensoussan, L., Jouvion, A., Kerzoncuf, M., Delarque, A., Theodoridou, E., Milhe De Bovis, V., ... Viton, J. M. (2016). Orthopaedic shoes along with physical therapy was effective in Charcot-Marie-Tooth patient over 10 years. *Prosthetics and Orthotics International*, 40(5), 636–642. <https://doi.org/10.1177/0309364615584657>
- Berns, K. I. (1990). Parvovirus replication. *Microbiological Reviews*, 54(3), 316–29. <http://www.ncbi.nlm.nih.gov/pubmed/2215424>
- Berns, K. I., & Linden, R. M. (1995). The cryptic life style of adenoassociated virus. *BioEssays*, 17(3), 237–245. <https://doi.org/10.1002/bies.950170310>
- Bernstein, E., Caudy, A. A., Hammond, S. M., & Hannon, G. J. (2001). Role for bidentate ribonuclease in the initiation site of RNA interference. *Nature*, 409(6818), 363–366. <https://doi.org/10.1038/35053110>
- Beutler, E. (2001). The Cline affair. *Molecular Therapy*, 4(5), 396–397. <https://doi.org/10.1006/mthe.2001.0486>
- Birchmeier, C., & Nave, K. A. (2008). Neuregulin-1, a key axonal signal that drives schwann cell growth and differentiation. *Glia*, 56(14), 1491–1497. <https://doi.org/10.1002/glia.20753>
- Braathén, G. J. (2012). Genetic epidemiology of Charcot-Marie-Tooth disease. *Acta Neurologica Scandinavica. Supplementum*, 126(193), iv-22. <https://doi.org/10.1111/ane.12013>
- Brennan, K. M., Bai, Y., & Shy, M. E. (2015). Demyelinating CMT-what's known, what's new and what's in store? *Neuroscience Letters*, 596, 14–26. <https://doi.org/10.1016/j.neulet.2015.01.059>

- Brizzi, K. T., & Lyons, J. L. (2014). Peripheral Nervous System Manifestations of Infectious Diseases. *The Neurohospitalist*, 4(4), 230–240. <https://doi.org/10.1177/1941874414535215>
- Buchlis, G., Podsakoff, G. M., Radu, A., Hawk, S. M., Flake, A. W., Mingozzi, F., & High, K. A. (2012). Factor IX expression in skeletal muscle of a severe hemophilia B patient 10 years after AAV-mediated gene transfer. *Blood*, 119(13), 3038–41. <https://doi.org/10.1182/blood>
- Burger, C., Gorbatyuk, O. S., Velardo, M. J., Peden, C. S., Williams, P., Zolotukhin, S., ... Muzyczka, N. (2004). Recombinant AAV viral vectors pseudotyped with viral capsids from serotypes 1, 2, and 5 display differential efficiency and cell tropism after delivery to different regions of the central nervous system. *Molecular Therapy*, 10(2), 302–317. <https://doi.org/10.1016/j.ymthe.2004.05.024>
- Burlot, M.-A., Braudeau, J., Michaelsen-Preusse, K., Potier, B., Ayciriex, S., Varin, J., ... Cartier, N. (2015). Cholesterol 24-hydroxylase defect is implicated in memory impairments associated with Alzheimer-like Tau pathology. *Human Molecular Genetics*, 24(21), 5965–5976. <https://doi.org/10.1093/hmg/ddv268>
- Burnett, J. C., Rossi, J. J., & Tiemann, K. (2011). Current progress of siRNA/shRNA therapeutics in clinical trials. *Biotechnology Journal*, 6(9), 1130–1146. <https://doi.org/10.1002/biot.201100054>
- Burns, J., Ouvrier, R., Estilow, T., Shy, R., Laurá, M., Pallant, J. F., ... Finkel, R. S. (2012). Validation of the Charcot-Marie-Tooth disease pediatric scale as an outcome measure of disability. *Annals of Neurology*, 71(5), 642–652. <https://doi.org/10.1002/ana.23572>
- Carter, B. J. (2004). Adeno-associated virus and the development of adeno-associated virus vectors: A historical perspective. *Molecular Therapy*, 10(6), 981–989. <https://doi.org/10.1016/j.ymthe.2004.09.011>
- Chamcheu, J., Adhami, V., Siddiqui, I., & Mukhtar, H. (2015). Cutaneous Cell- and Gene-Based Therapies for Inherited and Acquired Skin Disorders. *Gene and Cell Therapy*, 1091–1122. Smyth Templeton, N. (Ed.). Boca Raton: CRC Press. <https://doi.org/10.1201/b18002-52>
- Chance, P. F., Kathryn Alderson, M., Leppig, K. A., William Lensch, se M., Matsunami, N.,

- Smith, B., ... Bird, T. D. (1993). DNA n Associated with Neuropathy with LiaMity to P. *Cell*, 72, 143–151.
- Chen, S., Kapturczak, M., Loiler, S. A., & Zolotukhin, S. (2005). Efficient Transduction of Vascular Endothelial Cells with Recombinant Adeno-Associated Virus Serotype 1 and 5 Vectors, *Human gene therapy*, 16(2), 235-47. <https://doi.org/10.1002/humu.21462>.New
- Chetlin, R. D., Gutmann, L., Tarnopolsky, M. A., Ullrich, I. H., & Yeater, R. A. (2004). Resistance training exercise and creatine in patients with Charcot-Marie-Tooth disease. *Muscle and Nerve*, 30(1), 69–76. <https://doi.org/10.1002/mus.20078>
- Chirmule, N., Xiao, W., Truneh, A., Schnell, M. A., Hughes, J. V, Zoltick, P., & Wilson, J. M. (2000). Humoral Immunity to Adeno-Associated Virus Type 2 Vectors following Administration to Murine and Nonhuman Primate Muscle. *Journal Of Virology*, 74(5), 3.
- Chumakov, I., Milet, A., Cholet, N., Primas, G., Boucard, A., Pereira, Y., ... Cohen, D. (2014). Polytherapy with a combination of three repurposed drugs (PXT3003) down-regulates Pmp22 over-expression and improves myelination, axonal and functional parameters in models of CMT1A neuropathy. *Orphanet Journal of Rare Diseases*, 9(1), 1–16. <https://doi.org/10.1186/s13023-014-0201-x>
- Ciron, C., Cressant, A., Raoul, S., Cherel, Y., Hantraye, P., & De, N. (2009). Human a -Iduronidase Gene Transfer Mediated of Nonhuman Primates : Vector Diffusion and Biodistribution. *Human Gene Therapy*, 20(4), 350–360. <https://doi.org/10.1089/hum.2008.155>
- Coleman, M. P., Conforti, L., Buckmaster, E. A., Tarlton, A., Ewing, R. M., Brown, M. C., ... Perry, V. H. (1998). An 85-kb tandem triplication in the slow Wallerian degeneration (Wlds) mouse. *Proceedings of the National Academy of Sciences of the United States of America*, 95(17), 9985–90. <https://doi.org/10.1073/pnas.95.17.9985>
- Colle, M. A., Piguet, F., Bertrand, L., Raoul, S., Bieche, I., Dubreil, L., ... Sevin, C. (2009). Efficient intracerebral delivery of AAV5 vector encoding human ARSA in non-human primate. *Human Molecular Genetics*, 19(1), 147–158. <https://doi.org/10.1093/hmg/ddp475>
- Colle, M. A., Piguet, F., Bertrand, L., Raoul, S., Bieche, I., Dubreil, L., ... Sevin, C. (2010).

- Efficient intracerebral delivery of AAV5 vector encoding human ARSA in non-human primate. *Human Molecular Genetics*, 19(1), 147–158. <https://doi.org/10.1093/hmg/ddp475>
- Conceição, I., González-Duarte, A., Obici, L., Schmidt, H. H. J., Simoneau, D., Ong, M. L., & Amass, L. (2016). Red-flag symptom clusters in transthyretin familial amyloid polyneuropathy. *Journal of the Peripheral Nervous System*, 21(1), 5–9. <https://doi.org/10.1111/jns.12153>
- Cornbrooks, C. J., Carey, D. J., McDonald, J. A., Timpl, R., & Bunge, R. P. (1983). In vivo and in vitro observations on laminin production by Schwann cells. *Proc. Natl Acad. Sci. USA*, 80, 3850–3854.
- Cornett, K. M. D., Menezes, M. P., Shy, R. R., Moroni, I., Pagliano, E., Pareyson, D., ... Burns, J. (2017). Natural history of Charcot-Marie-Tooth disease during childhood. *Annals of Neurology*, 82(3), 353–359. <https://doi.org/10.1002/ana.25009>
- Cotter, L., Ozcelik, M., Jacob, C., Pereira, J. A., Locher, V., Baumann, R., ... Tricaud, N. (2010). Dlg1-PTEN Interaction Regulates Myelin Thickness to Prevent Damaging Peripheral Nerve Overmyelination. *Science*, 328(June), 1415–1418. <https://doi.org/10.1126/science.1187735>
- Coulthard, P., Pleuvry, B. J., Brewster, M., Wilson, K. L., & Macfarlane, T. V. (2002). Gait analysis as an objective measure in a chronic pain model. *Journal of Neuroscience Methods*, 116(2), 197–213.
- Crystal, R. G., Sondhi, D., Hackett, N. R., Kaminsky, S. M., Worgall, S., Stieg, P., ... Voss, H. (2004). Clinical protocol. Administration of a replication-deficient adeno-associated virus gene transfer vector expressing the human CLN2 cDNA to the brain of children with late infantile neuronal ceroid lipofuscinosis. *Human Gene Therapy*, 15(11), 1131–1154. <https://doi.org/10.1089/hum.2004.15.1131>
- D’Urso, D., Schmalenbach, C., Zoidl, G., Prior, R., & Müller, H. W. (1997). Studies on the effects of altered PMP22 expression during myelination in vitro. *Journal of Neuroscience Research*, 48(1), 31–42.
- Daya, S., & Berns, K. I. (2008). Gene therapy using adeno-associated virus vectors. *Clinical*

- Microbiology Reviews*, 21(4), 583–593. <https://doi.org/10.1128/CMR.00008-08>
- de Carvalho Alcantara, M., Nogueira-Barbosa, M. H., Fernandes, R. M. F., da Silva, G. A., Lourenco, C. M., Sander, H. H., & Marques Junior, W. (2015). Respiratory dysfunction in Charcot-Marie-Tooth disease type 1A. *Journal of Neurology*, 262(5), 1164–1171. <https://doi.org/10.1007/s00415-015-7677-8>
- de Leon, M., Nahin, R. L., Mendoza, M. E., & Ruda, M. A. (1994). SR13 / PMP-22 expression in rat nervous system, in PC12 cells, and C6 glial cell lines. *Journal of Neuroscience Research*, 38(2), 167–181.
- Deffieux, T., Demene, C., Pernot, M., & Tanter, M. (2018). Functional ultrasound neuroimaging: a review of the preclinical and clinical state of the art. *Current Opinion in Neurobiology*, 50, 128–135. <https://doi.org/10.1016/j.conb.2018.02.001>
- Deng, Y., Man, L., Wu, N., Bai, S., Zhao, C., Wang, H., ... Lu, & Q. R. (2017). A reciprocal regulatory loop between TAZ/YAP and G-protein Gas regulates Schwann cell proliferation and myelination. *Nature Communications*, 8, 15161. <https://doi.org/10.1038/ncomms15161>
- Désarnaud, F., Bidichandani, S., Patel, P. I., Baulieu, E. E., & Schumacher, M. (2000). Glucocorticosteroids stimulate the activity of the promoters of peripheral myelin protein-22 and protein zero genes in Schwann cells. *Brain Research*, 865(1), 12–16. [https://doi.org/10.1016/S0006-8993\(00\)02130-2](https://doi.org/10.1016/S0006-8993(00)02130-2)
- Dimachkie, M. M., & Barohn, R. J. (2015). *Peripheral Neuropathies. Nerves and Nerve Injuries* (Vol. 2). Edited by Tubbs, R.S., Rizk, E., Shoja, M. M., Loukas, M., Barbaro, N., Spinner, R.J. Elsevier Ltd. <https://doi.org/10.1016/B978-0-12-802653-3.00104-4>
- Ding, W., Zhang, L., Yan, Z., & Engelhardt, J. F. (2005). Intracellular trafficking of adeno-associated viral vectors. *Gene Therapy*, 12(11), 873–880. <https://doi.org/10.1038/sj.gt.3302527>
- Djelti, F., Braudeau, J., Hudry, E., Dhenain, M., Varin, J., Bièche, I., ... Cartier, N. (2015). CYP46A1 inhibition, brain cholesterol accumulation and neurodegeneration pave the way for Alzheimer's disease. *Brain*, 138(8), 2383–2398. <https://doi.org/10.1093/brain/awv166>

- Donsante, A., Vogler, C., Muzyczka, N., Crawford, J. M., Barker, J., Flotte, T., ... Sands, M. S. (2001). Observed incidence of tumorigenesis in long-term rodent studies of rAAV vectors. *Gene Therapy*, 8(17), 1343–1346. <https://doi.org/10.1038/sj.gt.3301541>
- Dowling, J., Gonorazky, H. D., & Cohn, R. D. (2018). Treating pediatric neuromuscular disorders: The future is now. *American Journal of Medical Genetics*, 176, 804–841.
- Dunbar, C. E., High, K. A., Joung, J. K., Kohn, D. B., Ozawa, K., & Sadelain, M. (2018). Gene therapy comes of age. *Science*, 359(6372). <https://doi.org/10.1126/science.aan4672>
- Evers, M. M., Toonen, L. J. A., & van Roon-Mom, W. M. C. (2015). Antisense oligonucleotides in therapy for neurodegenerative disorders. *Advanced Drug Delivery Reviews*, 87, 90–103. <https://doi.org/10.1016/j.addr.2015.03.008>
- Fabbretti, E., Edomi, P., Brancolini, C., & Schneider, C. (1995). Apoptotic phenotype induced by overexpression of wild-type gas3/PMP22: its relation to the demyelinating peripheral neuropathy CMT1A. *Genes & Development*, 9, 1846–1856.
- Falls, D. L. (2003). Neuregulins: Functions, forms, and signaling strategies. *Experimental Cell Research*, 284, 14–30. <https://doi.org/10.1016/B978-012160281-9/50003-7>
- Fannon, A. M., Sherman, D. L., Ilyina-Gragerova, G., Brophy, P. J., Friedrich, V. L., & Colman, D. R. (1995). Novel E-cadherin-mediated adhesion in peripheral nerve: Schwann cell architecture is stabilized by autotypic adherens junctions. *Journal of Cell Biology*, 129(1), 189–202. <https://doi.org/10.1083/jcb.129.1.189>
- Fattal, E., & Bochot, A. (2006). Ocular delivery of nucleic acids: antisense oligonucleotides, aptamers and siRNA. *Advanced Drug Delivery Reviews*, 58(11), 1203–1223. <https://doi.org/10.1016/j.addr.2006.07.020>
- Fehse, B., & Roeder, I. (2008). Insertional mutagenesis and clonal dominance: Biological and statistical considerations. *Gene Therapy*, 15(2), 143–153. <https://doi.org/10.1038/sj.gt.3303052>
- Fenwick, N., Griffin, G., & Gauthier, C. (2009). Animal Welfare Bien-être des animaux. *Canadian Veterinary Journal*, 50 (5), 523-530.

- Fernando, R. N., Cotter, L., Perrin-Tricaud, C., Berthelot, J., Bartolami, S., Pereira, J. A., ... Tricaud, N. (2016). Optimal myelin elongation relies on YAP activation by axonal growth and inhibition by Crb3/Hippo pathway. *Nature Communications*, 7, 1–14. <https://doi.org/10.1038/ncomms12186>
- Ferrarin, M., Lencioni, T., Rabuffetti, M., Moroni, I., Pagliano, E., & Pareyson, D. (2013). Changes of gait pattern in children with Charcot-Marie-Tooth disease type 1A: a 18 months follow-up study. *Journal of NeuroEngineering and Rehabilitation*, 10(1), 65. <https://doi.org/10.1186/1743-0003-10-65>
- Ferreira, V., Petry, H., & Salmon, F. (2014). Immune responses to AAV-vectors, The Glybera example from bench to bedside. *Frontiers in Immunology*, 5, 82. <https://doi.org/10.3389/fimmu.2014.00082>
- Ferreira, V., Twisk, J., Kwikkers, K., Aronica, E., Brisson, D., Methot, J., ... Gaudet, D. (2014). Immune Responses to Intramuscular Administration of Alipogene Tiparvovec (AAV1-LPL^{S447X}) in a Phase II Clinical Trial of Lipoprotein Lipase Deficiency Gene Therapy. *Human Gene Therapy*, 25(3), 180–188.
- Fields, R. D., & Stevens, B. (2000). ATP: an extracellular signaling molecule between neurons and glia. *Trends in Neuroscience*, 23(12), 625–633.
- Finkel, R. S., Mercuri, E., Darras, B. T., Connolly, A. M., Kuntz, N. L., Kirschner, J., ... De Vivo, D. C. (2017). Nusinersen versus Sham Control in Infantile-Onset Spinal Muscular Atrophy. *New England Journal of Medicine*, 377(18), 1723–1732. <https://doi.org/10.1056/NEJMoa1702752>
- Fisher, K. J., Gao, G. P., Weitzman, M. D., DeMatteo, R., Burda, J. F., & Wilson, J. M. (1996). Transduction with recombinant adeno-associated virus for gene therapy is limited by leading-strand synthesis. *Journal of Virology*, 70(1), 520–532.
- Fledrich, R., Mannil, M., Leha, andreas, ehbrecht, caroline, solari, alessandra, pelayo-Negro, ana L., ... sereda, M. W. (2017). Biomarkers predict outcome in Charcot-Marie-Tooth disease 1A. *J Neurol Neurosurg Psychiatry*, 88(11), 941-952. <https://doi.org/10.1136/jnnp-2017-315721>

- Fledrich, R., Schlotter-Weigel, B., Schnizer, T. J., Wichert, S. P., Stassart, R. M., Meyer Zu Hörste, G., ... Sereda, M. W. (2012). A rat model of Charcot-Marie-Tooth disease 1A recapitulates disease variability and supplies biomarkers of axonal loss in patients. *Brain*, 135(1), 72–87. <https://doi.org/10.1093/brain/awr322>
- Fledrich, R., Stassart, R. M., Klink, A., Rasch, L. M., Prukop, T., Haag, L., ... Sereda, M. W. (2014). Soluble neuregulin-1 modulates disease pathogenesis in rodent models of Charcot-Marie-Tooth disease 1A. *Nature Medicine*, 20(9), 1055–1061. <https://doi.org/10.1038/nm.3664>
- Fledrich, R., Stassart, R. M., & Sereda, M. W. (2012). Murine therapeutic models for Charcot-Marie-Tooth (CMT) disease. *British Medical Bulletin*, 102(1), 89–113. <https://doi.org/10.1093/bmb/lds010>
- Flotte, T. R., Trapnell, B. C., Humphries, M., Carey, B., Calcedo, R., Rouhani, F., ... Chulay, J. D. (2011). Phase 2 Clinical Trial of a Recombinant Adeno-Associated Viral Vector Expressing a 1-Antitrypsin: Interim Results. *Human Gene Therapy*, 22(10), 1239–1247. <https://doi.org/10.1089/hum.2011.053>
- Fortun, J., Go, J. C., Li, J., Amici, S. A., Dunn, W. A., & Notterpek, L. (2006). Alterations in degradative pathways and protein aggregation in a neuropathy model based on PMP22 overexpression. *Neurobiology of Disease*, 22(1), 153–164. <https://doi.org/10.1016/j.nbd.2005.10.010>
- Foust, K. D., Nurre, E., Montgomery, C. L., Hernandez, A., Curtis, M., & Kaspar, B. K. (2009). Intravascular AAV9 preferentially targets neonatal neurons and adult astrocytes, *Nature biotechnology*, 27(1), 59–65. <https://doi.org/10.1038/nbt.1515>.
- Fricker, F. R., & Bennett, D. L. (2011). The role of neuregulin-1 in the response to nerve injury. *Future Neurology*, 6(6):809–822. <https://doi.org/10.2217/fnl.11.45>
- Fricker, F. R., Lago, N., Balarajah, S., Tsantoulas, C., Tanna, S., Zhu, N., ... Bennett, D. L. H. (2011). Development/Plasticity/Repair Axonally Derived Neuregulin-1 Is Required for Remyelination and Regeneration after Nerve Injury in Adulthood. *The Journal of Neuroscience*, 31(9), 3225–3233. <https://doi.org/10.1523/JNEUROSCI.2568-10.2011>

- Friedmann, T. (2000). Principles for Human Gene Therapy Studies. *Science*, 287 (5461) 2163-2165. doi: 10.1126/science.287.5461.2163
- Friedmann, T., & Roblin, R. (1972). Gene therapy for human genetic disease? *Science*, 175 (4025), 949–55. <https://doi.org/10.1126/science.175.4025.949>
- Frostick, S. P., Yin, Q., & Kemp, G. J. (1998). Schwann cells, neurotrophic factors, and peripheral nerve regeneration. *Microsurgery*, 18, 397–405. [https://doi.org/10.1002/\(SICI\)1098-2752\(1998\)18:7<397::AID-MICR2>3.0.CO;2-F](https://doi.org/10.1002/(SICI)1098-2752(1998)18:7<397::AID-MICR2>3.0.CO;2-F) [pii]
- Gabreëls-Festen, A. A. W. M., Bolhuis, P. A., Hoogendijk, J. E., Valentijn, L. J., Eshuis, E. J. H. M., & Gabreëls, F. J. M. (1995). Charcot-Marie-Tooth disease type 1A: morphological phenotype of the 17p duplication versus PMP22 point mutations. *Acta Neuropathologica*, 90(6), 645–649. <https://doi.org/10.1007/BF00318579>
- Gabreëls-Festen, A., & Van de Wetering, R. (1999). Human Nerve Pathology Caused by different Mutational Mechanisms of the PMP22 Gene. *Annals of New York Academy of Sciences*, 883, 336–343.
- Gambarotta, G., Fregnan, F., Gnani, S., & Perroteau, I. (2013). *Neuregulin 1 role in schwann cell regulation and potential applications to promote peripheral nerve regeneration. International Review of Neurobiology*, 108, 223-256. <https://doi.org/10.1016/B978-0-12-410499-0.00009-5>
- Gambarotta, G., Ronchi, G., Geuna, S., & Perroteau, I. (2014). Neuregulin 1 isoforms could be an effective therapeutic candidate to promote peripheral nerve regeneration. *Neural Regeneration Research*, 9(12), 1183–1185. <https://doi.org/10.4103/1673-5374.135324>
- Gao, C., Zhang, R., Zheng, N., & Wang, C. (2018). Adeno-associated virus type 2-mediated gene transfer of a short hairpin-RNA targeting human IGFBP-2 suppresses the proliferation and invasion of MDA-MB-468 cells. *Molecular Medicine Reports*, 17, 4383–4391. <https://doi.org/10.3892/mmr.2018.8434>
- Gao, G.-P., Alvira, M. R., Wang, L., Calcedo, R., Johnston, J., & Wilson, J. M. (2002). Novel adeno-associated viruses from rhesus monkeys as vectors for human gene therapy. *Proceedings of the National Academy of Sciences*, 99(18), 11854–11859. <https://doi.org/10.1073/pnas.182412299>

- Garbay, B., Heape, A. M., Sargueil, F., & Cassagne, C. (2000). Myelin synthesis in the peripheral nervous system. *Progress in Neurobiology*, 61(3), 267–304. [https://doi.org/10.1016/S0301-0082\(99\)00049-0](https://doi.org/10.1016/S0301-0082(99)00049-0)
- Gaudet, D., Méthot, J., & Kastelein, J. (2012). Gene therapy for lipoprotein lipase deficiency. *Current Opinion in Lipidology*, 23(4), 310–320. <https://doi.org/10.1097/MOL.0b013e3283555a7e>
- Ghabriel, M. N., & Allt, G. (1981). Incisures of Schmidt-Lanterman. *Progress in Neurobiology*, 17(1–2), 25–58. [https://doi.org/10.1016/0301-0082\(81\)90003-4](https://doi.org/10.1016/0301-0082(81)90003-4)
- Giacca, M., & Zacchigna, S. (2012). Virus-mediated gene delivery for human gene therapy. *Journal of Controlled Release*, 161(2), 377–388. <https://doi.org/10.1016/j.jconrel.2012.04.008>
- Giambonini-Brugnoli, G., Buchstaller, J., Sommer, L., Suter, U., & Mantei, N. (2005). Distinct disease mechanisms in peripheral neuropathies due to altered peripheral myelin protein 22 gene dosage or a Pmp22 point mutation. *Neurobiology of Disease*, 18(3), 656–668. <https://doi.org/10.1016/j.nbd.2004.10.023>
- Gill, D. R., Pringle, I. A., & Hyde, S. C. (2009). Progress and Prospects: The design and production of plasmid vectors. *Gene Therapy*, 16(2), 165–171. <https://doi.org/10.1038/gt.2008.183>
- Girod, A., Wobus, C. E., Zádori, Z., Ried, M., Leike, K., Tijssen, P., ... Hallek, M. (2002). The VP1 capsid protein of adeno-associated virus type 2 is carrying a phospholipase A2 domain required for virus infectivity. *Journal of General Virology*, 83(5), 973–978. <https://doi.org/10.1099/0022-1317-83-5-973>
- Glasser, C. E., Gartner, M. R., Wilson, D., Miller, B., Sherman, M. L., & Attie, K. M. (2018). Locally acting ACE-083 increases muscle volume in healthy volunteers. *Muscle & Nerve*, 57(6), 921–926. <https://doi.org/10.1002/mus.26113>
- Glatzel, M., Flechsig, E., Navarro, B., Klein, M. A., Paterna, J. C., Büeler, H., & Aguzzi, A. (2000). Adenoviral and adeno-associated viral transfer of genes to the peripheral nervous system. *Proceedings of the National Academy of Sciences of the United States of America*, 97(1),

442–7. <https://doi.org/10.1073/pnas.97.1.442>

- Gonzalez, S., Fernando, R. N., Perrin-Tricaud, C., & Tricaud, N. (2014). In vivo introduction of transgenes into mouse sciatic nerve cells in situ using viral vectors. *Nature Protocols*, 9(5), 1160–1169. <https://doi.org/10.1038/nprot.2014.073>
- Grandis, M., Leandri, M., Vigo, T., Cilli, M., Sereda, M. W., Gherardi, G., ... Schenone, A. (2004). Early abnormalities in sciatic nerve function and structure in a rat model of Charcot-Marie-Tooth type 1A disease. *Experimental Neurology*, 190(1), 213–223. <https://doi.org/10.1016/j.expneurol.2004.07.008>
- Grandis, M., & Shy, M. E. (2005). Current therapy for Charcot-Marie-Tooth disease. *Current Treatment Options in Neurology*, 7(1), 23–31. <https://doi.org/10.1007/s11940-005-0003-5>
- Gray, S. J., Blake, B. L., Criswell, H. E., Nicolson, S. C., Samulski, R. J., & McCown, T. J. (2010). Directed evolution of a novel adeno-associated virus (AAV) vector that crosses the seizure-compromised blood-brain barrier (BBB). *Molecular Therapy*, 18(3), 570–578. <https://doi.org/10.1038/mt.2009.292>
- Gregson, N. A., Zhang, G., Pritchard, J., Wang, A., Sanvito, L., Hayday, A. C., & Hughes, R. A. (2007). Characterization of a monoclonal antibody specific for human peripheral myelin protein 22 and its use in immunohistochemical studies of the fetal and adult nervous system. *J Peripher Nerv Syst*, 12(1), 2–10. <https://doi.org/10.1007/JNS112> [pii]r10.1111/j.1529-8027.2007.00112.x
- Grieger, J. C., & Samulski, R. J. (2012). Adeno-associated virus vectorology, manufacturing, and clinical applications. *Methods in Enzymology*, 507, 229–54. <https://doi.org/10.1016/B978-0-12-386509-0.00012-0>
- Grishok, A., Pasquinelli, A. E., Conte, D., Li, N., Parrish, S., Ha, I., ... Mello, C. C. (2001). Genes and mechanisms related to RNA interference regulate expression of the small temporal RNAs that control *C. elegans* developmental timing. *Cell*, 106(1), 23–34. [https://doi.org/10.1016/S0092-8674\(01\)00431-7](https://doi.org/10.1016/S0092-8674(01)00431-7)
- Grove, M., Kim, H., Santerre, M., Krupka, A. J., Han, S. B., Zhai, J., ... Son, Y. J. (2017).

- YAP/TAZ initiate and maintain schwann cell myelination. *eLife*, 6, e20982. <https://doi.org/10.7554/eLife.20982>
- Grover, V. P. B., Tognarelli, J. M., Crossey, M. M. E., Cox, I. J., Taylor-Robinson, S. D., & McPhail, M. J. W. (2015). Magnetic Resonance Imaging: Principles and Techniques: Lessons for Clinicians. *Journal of Clinical and Experimental Hepatology*, 5(3), 246–255. <https://doi.org/10.1016/j.jceh.2015.08.001>
- Hacein-Bey-Abina, S., Hauer, J., Lim, A., Picard, C., Wang, G. P., Berry, C. C., ... Cavazzana-Calvo, M. (2010). Efficacy of Gene Therapy for X-Linked Severe Combined Immunodeficiency. *New England Journal of Medicine*, 363(4), 355–364. <https://doi.org/10.1056/NEJMoa1000164>
- Hacein-Bey-Abina, S., Pai, S. ., Gaspar, H. ., Armant, M., Berry, C. ., Blanche, S. J., & Leesing, J. (2014). A Modified γ -Retrovirus Vector for X-Linked Severe Combined Immunodeficiency. *New England Journal of Medicine*, 371(15), 1407–1417. <https://doi.org/10.1111/j.1743-6109.2008.01122.x>.Endothelial
- Halbert, C. L., Allen, J. M., & Miller, A. D. (2001). Adeno-Associated Virus Type 6 (AAV6) Vectors Mediate Efficient Transduction of Airway Epithelial Cells in Mouse Lungs Compared to That of AAV2 Vectors. *Journal Of Virology*, 75(14), 6615–6624. <https://doi.org/10.1128/JVI.75.14.6615-6624.2001>
- Haltia, M., & Goebel, H. H. (2013). The neuronal ceroid-lipofuscinoses: A historical introduction *Molecular Basis of Disease, 1832, 1795–1800*. <https://doi.org/10.1016/j.bbadis.2012.08.012>
- Hamers, F. P. T., Koopmans, G. C., & Joosten, E. A. J. (2006). CatWalk-Assisted Gait Analysis in the Assessment of Spinal Cord Injury. *Journal of Neurotrauma*, 23(3–4), 537–548. <https://doi.org/10.1089/neu.2006.23.537>
- Hammond, S. M., Bernstein, E., Beach, D., & Hannon, G. J. (2000). An RNA-directed nuclease mediates post-transcriptional gene silencing in *Drosophila* cells. *Nature*, 404, 293–296. <https://doi.org/10.1038/35005107>
- Han, H., Myllykoski, M., Ruskamo, S., Wang, C., & Kursula, P. (2013). Myelin-specific proteins:

- A structurally diverse group of membrane-interacting molecules. *BioFactors*, 39(3), 233–241. <https://doi.org/10.1002/biof.1076>
- Hanemann, C. O., Gabreëls-Festen, A. A. W. M., Stoll, G., & Müller, H. W. (1997). Schwann cell differentiation in Charcot-Marie-Tooth disease type 1A (CMT1A): Normal number of myelinating Schwann cells in young CMT1A patients and neural cell adhesion molecule expression in onion bulbs. *Acta Neuropathologica*, 94(4), 310–315. <https://doi.org/10.1007/s004010050712>
- Hanemann, C. O., Rosenbaum, C., Kupfer, S., Wosch, S., Stoegbauer, F., & Müller, H. W. (1998). Improved culture methods to expand schwann cells with altered growth behaviour from CMT1a patients. *Glia*, 23(2), 89–98. [https://doi.org/10.1002/\(SICI\)1098-1136\(199806\)23:2<89::AID-GLIA1>3.0.CO;2-Z](https://doi.org/10.1002/(SICI)1098-1136(199806)23:2<89::AID-GLIA1>3.0.CO;2-Z)
- Harding, A., & Thomas, P. (1980). The clinical features of hereditary motor and sensory neuropathy types I and II. *Brain: A Journal of Neurology*, 17(2), 259–280. <https://doi.org/10.1136/jmg.17.5.329>
- Hasse, B., Bosse, F., Hanenberg, H., & Werner Müller, H. (2004). Peripheral myelin protein 22 kDa and protein zero: Domain specific trans-interactions. *Molecular and Cellular Neuroscience*, 27(4), 370–378. <https://doi.org/10.1016/j.mcn.2004.06.009>
- Haurigot, V., Marcó, S., Ribera, A., Garcia, M., Ruzo, A., Villacampa, P., ... Bosch, F. (2013). Whole body correction of mucopolysaccharidosis IIIA by intracerebrospinal fluid gene therapy. *Journal of Clinical Investigation*, 123(8), 3254–3271. <https://doi.org/10.1172/JCI66778>
- Hawkins, P. N., Ando, Y., Dispenzeri, A., Gonzalez-Duarte, A., Adams, D., & Suhr, O. B. (2015). Evolving landscape in the management of transthyretin amyloidosis. *Annals of Medicine*, 47(8), 625–638. <https://doi.org/10.3109/07853890.2015.1068949>
- Hayasaka', K., Himoro', M., Nanao', K., Sato', W., Miura', M., Uyemura', K., ... Takada', G. (1992). Isolation And Sequence Determination Of Cdna Encoding PMP-22 (PAS-H/SRW/GAS-3) Of Human Peripheral Myelin, *Biochemical and Biophysical Research Communications*, 186(2), 827-831. <https://ac-els-cdn->

com.gate2.inist.fr/0006291X9290820B/1-s2.0-0006291X9290820B-main.pdf?_tid=a23f157a-c6d5-49e5-9c19-99d768654ea0&acdnat=1531499164_c656f40b0260cfe781807f82325c1a28

- He, B., Liu, S.-Q., Chen, Q., Li, H.-H., Ding, W.-J., & Deng, M. (2011). Neuropharmacology and Analgesia Carboxymethylated chitosan stimulates proliferation of Schwann cells in vitro via the activation of the ERK and Akt signaling pathways. *European Journal of Pharmacology*, 667, 195–201. <https://doi.org/10.1016/j.ejphar.2011.06.001>
- Heckel, A., Weiler, M., Xia, A., Ruetters, M., Pham, M., Bendszus, M., ... Baeumer, P. (2015). Peripheral Nerve Diffusion Tensor Imaging: Assessment of Axon and Myelin Sheath Integrity. *Plos One*, 10(6), e0130833. <https://doi.org/10.1371/journal.pone.0130833>
- Hedman, M., Muona, K., Hedman, A., Kivelä, A., Syväne, M., Eränen, J., ... Ylä-Herttuala, S. (2009). Eight-year safety follow-up of coronary artery disease patients after local intracoronary VEGF gene transfer. *Gene Therapy*, 16(5), 629–634. <https://doi.org/10.1038/gt.2009.4>
- Herzog, R. W., Cao, O., & Srivastava, A. (2010). Two decades of clinical gene therapy--success is finally mounting. *Discovery Medicine*, 9(45), 105–111.
- Hirsch, M. L., Li, C., Bellon, I., Yin, C., Chavala, S., Pryadkina, M., ... Samulski, R. J. (2013). Oversized AAV transduction is mediated via a DNA-PKcs-independent, Rad51C-dependent repair pathway. *Molecular Therapy*, 21(12), 2205–2216. <https://doi.org/10.1038/mt.2013.184>
- Homs, J., Ariza, L., Pagè, G., Udina, E., Navarro, X., Chilló, M., & Bosch, A. (2011). Schwann cell targeting via intrasciatic injection of AAV8 as gene therapy strategy for peripheral nerve regeneration. *Gene Therapy*, 18, 622–630. <https://doi.org/10.1038/gt.2011.7>
- Horton, J. D., Goldstein, J. L., & Brown, M. S. (2002). SREBPs: activators of the complete program of cholesterol and fatty acid synthesis in the liver, *Journal of Clinical Investigation*, 109(9), 1125–1131. <https://doi.org/10.1172/JCI200215593>
- Hu, X., He, W., Diaconu, C., Tang, X., Kidd, G. J., Macklin, W. B., ... Yan, R. (2008a). Genetic

- deletion of BACE1 in mice affects remyelination of sciatic nerves. *The FASEB Journal*, 22(8), 2970–2980. <https://doi.org/10.1096/fj.08-106666>
- Hughes, R. A., & Cornblath, D. R. (2005). Guillain-Barré syndrome. *The Lancet*, 366(9497), 1653–1666. [https://doi.org/10.1016/S0140-6736\(05\)67665-9](https://doi.org/10.1016/S0140-6736(05)67665-9)
- Hutvagner, G., Simard, M. J., Mello, C. C., & Zamore, P. D. (2004). Sequence-specific inhibition of small RNA function. *PLoS Biology*, 2(4), 465–475. <https://doi.org/10.1371/journal.pbio.0020098>
- Huxley, C., Passage, E., Manson, A., Putzu, G., Figarella-Branger, D., Pellissier, J. F., & Fontés, M. (1996). Construction of a mouse model of Charcot-Marie-Tooth disease type 1A by pronuclear injection of human YAC DNA. *Human Molecular Genetics*, 5(5), 563–569. <https://doi.org/10.1093/hmg/5.5.563>
- Huxley, C., Passage, E., Robertson, A. M., Youl, B., Huston, S., Manson, A., ... Fontés, M. (1998). Correlation between varying levels of PMP22 expression and the degree of demyelination and reduction in nerve conduction velocity in transgenic mice. *Human Molecular Genetics*, 7(3), 449–458. <https://doi.org/10.1093/hmg/7.3.449>
- Inouye, H., & Kirschner, D. A. (1988). Membrane interactions in nerve myelin: II. Determination of surface charge from biochemical data. *Biophysical Journal*, 53(2), 247–260. [https://doi.org/10.1016/S0006-3495\(88\)83086-8](https://doi.org/10.1016/S0006-3495(88)83086-8)
- Jabbour, A., Hayward, C. S., Keogh, A. M., Kotlyar, E., McCrohon, J. A., England, J. F., ... MacDonald, P. S. (2011). Parenteral administration of recombinant human neuregulin-1 to patients with stable chronic heart failure produces favourable acute and chronic haemodynamic responses. *European Journal of Heart Failure*, 13(1), 83–92. <https://doi.org/10.1093/eurjhf/hfq152>
- Jacob, C., Christen, C. N., Pereira, J. A., Somandin, C., Baggiolini, A., Lötscher, P., ... Suter, U. (2011). HDAC1 and HDAC2 control the transcriptional program of myelination and the survival of Schwann cells. *Nature Neuroscience*, 14(4), 429–436. <https://doi.org/10.1038/nn.2762>

- Jacobs, J. M., & Love, S. (1985). Qualitative and quantitative morphology of human sural nerve at different ages. *Brain: A Journal of Neurology*, 108 (4), 897–924. <https://doi.org/10.1093/brain/108.4.897>
- Jaegle, M., & Meijer, D. (1998). Role of Oct-6 in Schwann cell differentiation. *Microscopy Research and Technique*, 41(5), 372–378. [https://doi.org/10.1002/\(SICI\)1097-0029\(19980601\)41:5<372::AID-JEMT4>3.0.CO;2-S](https://doi.org/10.1002/(SICI)1097-0029(19980601)41:5<372::AID-JEMT4>3.0.CO;2-S)
- Janson, C., McPhee, S., Bilaniuk, L., Haselgrove, J., Testaiuti, M., Freese, A., ... Leone, P. (2002). Gene Therapy of Canavan Disease: AAV-2 Vector for Neurosurgical Delivery of Aspartoacylase Gene (*ASPA*) to the Human Brain. *Human Gene Therapy*, 13(11), 1391–1412. <https://doi.org/10.1089/104303402760128612>
- Jerath, N. U., & Shy, M. E. (2017). Charcot–Marie–Tooth Disease Type 1A: Influence of Body Mass Index on Nerve Conduction Studies and on the Charcot–Marie–Tooth Examination Score. *Journal of Clinical Neurophysiology*, 34(6):508-511. <https://doi.org/10.1097/WNP.0000000000000415>
- Jetten, A. M., & Suter, U. (2000). The Peripheral Myelin Protein 22 and Epithelial Membrane Protein Family. *Progress in Nucleic Acid and Research Molecular Biology*, 64, 97-129.
- Jiang, H., Couto, L. B., Patarroyo-white, S., Liu, T., Nagy, D., Joseph, A., ... Vargas, J. A. (2006). Effects of transient immunosuppression on adenoassociated , virus-mediated , liver-directed gene transfer in rhesus macaques and implications for human gene therapy. *Blood*, 108(10), 3321–3328. <https://doi.org/10.1182/blood-2006-04-017913>
- Jin, L., Zeng, X., Liu, M., Deng, Y., & He, N. (2014). Current progress in gene delivery technology based on chemical methods and nano-carriers. *Theranostics*, 4(3), 240–255. <https://doi.org/10.7150/thno.6914>
- Kagiava, A., Sargiannidou, I., Theophilidis, G., Karaiskos, C., Richter, J., Bashiardes, S., ... Kleopa, K. A. (2016). Intrathecal gene therapy rescues a model of demyelinating peripheral neuropathy. *Proceedings of the National Academy of Sciences*, 113(17), E2421–E2429. <https://doi.org/10.1073/pnas.1522202113>

- Kenis-Coskun, O., & Matthews, D. J. (2016). Rehabilitation issues in Charcot-Marie-Tooth disease. *Journal of Pediatric Rehabilitation Medicine*, 9(1), 31–34. <https://doi.org/10.3233/PRM-160359>
- Kennedy, R. A., Carroll, K., & McGinley, J. L. (2016). Gait in children and adolescents with Charcot-Marie-Tooth disease: a systematic review. *Journal of the Peripheral Nervous System : JPNS*, 21(4), 317–328. <https://doi.org/10.1111/jns.12183>
- Kinter, J., Lazzati, T., Schmid, D., Zeis, T., Erne, B., Lützel Schwab, R., ... Schaeren-Wiemers, N. (2013). An essential role of MAG in mediating axon-myelin attachment in Charcot-Marie-Tooth 1A disease. *Neurobiology of Disease*, 49(1), 221–231. <https://doi.org/10.1016/j.nbd.2012.08.009>
- Kloos, A. D., Fisher, L. C., Detloff, M. R., Hassenzahl, D. L., & Basso, D. M. (2005). Stepwise motor and all-or-none sensory recovery is associated with nonlinear sparing after incremental spinal cord injury in rats. *Experimental Neurology*, 191(2), 251–265. <https://doi.org/10.1016/j.expneurol.2004.09.016>
- Kobsar, I., Hasenpusch-Theil, K., Wessig, C., Müller, H. W., & Martini, R. (2005). Evidence for macrophage-mediated myelin disruption in an animal model for Charcot-Marie-Tooth neuropathy type 1A. *Journal of Neuroscience Research*, 81(6), 857–864. <https://doi.org/10.1002/jnr.20601>
- Koczot, F. J., Carter, B. J., Garon, C. F., & Rose, J. A. (1973). Self-complementarity of terminal sequences within plus or minus strands of adenovirus-associated virus DNA. *Proceedings of the National Academy of Sciences of the United States of America*, 70(1), 215–219. <https://doi.org/10.1073/pnas.70.1.215>
- Koeberl, D. D., Alexander, I. E., Halbert, C. L., Russell, D. W., & Miller, A. D. (1997). Persistent expression of human clotting factor IX from mouse liver after intravenous injection of adeno-associated virus vectors. *Proceedings of the National Academy of Sciences of the United States of America*, 94(4), 1426–1431. <https://doi.org/10.1073/pnas.94.4.1426>
- Landon, David Neil. (1976). *The peripheral nerve*. London : Chapman and Hall

- Lee, J. S., Chang, E. H., Koo, O. J., Jwa, D. H., Mo, W. M., Kwak, G., ... Choi, B. O. (2017). Pmp22 mutant allele-specific siRNA alleviates demyelinating neuropathic phenotype in vivo. *Neurobiology of Disease*, 100, 99–107. <https://doi.org/10.1016/j.nbd.2017.01.006>
- Lee, S., Bazick, H., Chittoor-Vinod, V., Al Salihi, M. O., Xia, G., & Notterpek, L. (2018). Elevated Peripheral Myelin Protein 22, Reduced Mitotic Potential, and Proteasome Impairment in Dermal Fibroblasts from Charcot-Marie-Tooth Disease Type 1A Patients. *American Journal of Pathology*, 188(3), 728–738. <https://doi.org/10.1016/j.ajpath.2017.10.021>
- Lee, Y., Ahn, C., Han, J., Choi, H., Kim, J., Yim, J., ... Kim, V. N. (2003). The nuclear RNase III Drosha initiates microRNA processing. *Nature*, 425(6956), 415–419. <https://doi.org/10.1038/nature01957>
- Le Guiner, C. Le, Moullier, P., & Arruda, V. R. (2011). Adeno-Associated Virus, *Methods and Protocols*, 807(4), 339–359. Editors: Snyder, R.O.; Moullier, P. *Humana Press*. <https://doi.org/10.1007/978-1-61779-370-7>
- Lehrman, S. (1999). Virus treatment questioned after gene therapy death. *Nature*, 401(6753), 517–518. <https://doi.org/10.1038/43977>
- Lemke, G. (1988). Unwrapping the genes of myelin. *Neuron*, 1(7), 535–543. [https://doi.org/10.1016/0896-6273\(88\)90103-1](https://doi.org/10.1016/0896-6273(88)90103-1)
- Lencioni, T., Piscosquito, G., Rabuffetti, M., Bovi, G., Calabrese, D., Aiello, A., ... Ferrarin, M. (2015). The influence of somatosensory and muscular deficits on postural stabilization: Insights from an instrumented analysis of subjects affected by different types of Charcot-Marie-Tooth disease. *Neuromuscular Disorders*, 25(8), 640–645. <https://doi.org/10.1016/j.nmd.2015.05.003>
- Lencioni, T., Piscosquito, G., Rabuffetti, M., Bovi, G., Di Sipio, E., Diverio, M., ... Ferrarin, M. (2017). Responsiveness of gait analysis parameters in a cohort of 71 CMT subjects. *Neuromuscular Disorders* 27(11), 1029–1037. <https://doi.org/10.1016/j.nmd.2017.07.003>
- Lencioni, T., Rabuffetti, M., Piscosquito, G., Pareyson, D., Aiello, A., Di Sipio, E., ... Ferrarin, M. (2014). Postural stabilization and balance assessment in Charcot-Marie-Tooth 1A

- subjects. *Gait and Posture*, 40(4), 481–486. <https://doi.org/10.1016/j.gaitpost.2014.07.006>
- Lewis, R. A., McDermott, M. P., Herrmann, D. N., Hoke, A., Clawson, L. L., Siskind, C., ... Shy, M. E. (2013). High-dosage ascorbic acid treatment in charcot-marie-tooth disease type 1A results of a randomized, double-masked, controlled trial. *JAMA Neurology*, 70(8), 981–987. <https://doi.org/10.1001/jamaneurol.2013.3178>
- Li, J. (2015). Molecular Regulators of Nerve Conduction - Lessons from Inherited Neuropathies and Rodent Genetic Models. *Anal Chem.*, 267, 209–218. <https://doi.org/10.1016/j.cogdev.2010.08.003>
- Li, J. (2017). Caveats in the Established Understanding of CMT1A. *Annals of Clinical and Translational Neurology*, 4(8), 601–607. <https://doi.org/10.1002/acn3.432>
- Li, J., Parker, B., Martyn, C., Natarajan, C., & Guo, J. (2013). The PMP22 gene and its related diseases. *Molecular Neurobiology*, 47(2), 673–698. <https://doi.org/10.1007/s12035-012-8370-x>
- Lombardo, A., Genovese, P., Beausejour, C. M., Colleoni, S., Lee, Y. L., Kim, K. A., ... Naldini, L. (2007). Gene editing in human stem cells using zinc finger nucleases and integrase-defective lentiviral vector delivery. *Nature Biotechnology*, 25(11), 1298–1306. <https://doi.org/10.1038/nbt1353>
- Louis Jeune, V., Joergensen, J. A., Hajjar, R. J., & Weber, T. (n.d.). Pre-existing Anti-Adeno-Associated Virus Antibodies as a Challenge in AAV Gene Therapy. *Human Gene Therapy Methods*, 24(2):59-67. <https://doi.org/10.1089/hgtb.2012.243>
- Lunn, M. P. T., & Sheikh, K. A. (2014). Chapter 53: Peripheral Neuropathies. *The Autoimmune Diseases: Fifth Edition*. Editors: Rose, N. R., Mackay, I. R. Academic Press, 757-776 <https://doi.org/10.1016/B978-0-12-384929-8.00053-8>
- Lupski, J. R., de Oca-Luna, R. M., Slaugenhaupt, S., Pentao, L., Guzzetta, V., Trask, B. J., ... Patel, P. I. (1991). DNA duplication associated with Charcot-Marie-Tooth disease type 1A. *Cell*, 66(2), 219–232. [https://doi.org/10.1016/0092-8674\(91\)90613-4](https://doi.org/10.1016/0092-8674(91)90613-4)
- Ma, Z., Wang, J., Song, F., & Loeb, J. A. (2011). Critical period of axoglial signaling between

- neuregulin-1 and brain-derived neurotrophic factor required for early Schwann cell survival and differentiation. *The Journal of Neuroscience : The Official Journal of the Society for Neuroscience*, 31(26), 9630–9640. <https://doi.org/10.1523/JNEUROSCI.1659-11.2011>
- Mack, D. L., Poulard, K., Goddard, M. A., Latournerie, V., Snyder, J. M., Grange, R. W., ... Childers, M. K. (2017). Systemic AAV8-Mediated Gene Therapy Drives Whole-Body Correction of Myotubular Myopathy in Dogs. *Molecular Therapy*, 25(4), 839–854. <https://doi.org/10.1016/j.ymthe.2017.02.004>
- Mack, T. G., Reiner, M., Beirowski, B., Mi, W., Emanuelli, M., Wagner, D., ... Coleman, M. P. (2001). Wallerian degeneration of injured axons and synapses is delayed by a Ube4b/Nmnat chimeric gene. *Nature Neuroscience*, 4(12), 1199–1206. <https://doi.org/10.1038/nn770>
- Mager, G. M., Ward, R. M., Srinivasan, R., Jang, S. W., Wrabetz, L., & Svaren, J. (2008). Active gene repression by the Egr2·NAB complex during peripheral nerve myelination. *Journal of Biological Chemistry*, 283(26), 18187–18197. <https://doi.org/10.1074/jbc.M803330200>
- Magy, L., Mathis, S., Le Masson, G., Goizet, C., Tazir, M., & Vallat, J.-M. (2018). Updating the classification of inherited neuropathies. *Neurology*, 90(10), e870–e876. <https://doi.org/10.1212/WNL.0000000000005074>
- Magyar, J. P., Martini, R., Ruelicke, T., Aguzzi, a, Adlkofer, K., Dembic, Z., ... Suter, U. (1996). Impaired differentiation of Schwann cells in transgenic mice with increased PMP22 gene dosage. *The Journal of Neuroscience : The Official Journal of the Society for Neuroscience*, 16(17), 5351–5360.
- Mandel, J., Bertrand, V., Leher, P., Attarian, S., Magy, L., Micallef, J., ... Cohen, D. (2015). A meta-analysis of randomized double-blind clinical trials in CMT1A to assess the change from baseline in CMTNS and ONLS scales after one year of treatment. *Orphanet Journal of Rare Diseases*, 10(1), 1–4. <https://doi.org/10.1186/s13023-015-0293-y>
- Manganelli, F., Pisciotto, C., Reilly, M. M., Tozza, S., Schenone, A., Fabrizi, G. M., ... Blake, J. (2016). Nerve conduction velocity in CMT1A: what else can we tell? *European Journal of Neurology*, 23(10), 1566–1571. <https://doi.org/10.1111/ene.13079>

- Manno, C. S., Chew, A. J., Hutchison, S., Larson, P. J., Herzog, R. W., Arruda, V. R., ... Glader, B. (2003). AAV-mediated factor IX gene transfer to skeletal muscle in patients with severe hemophilia B. *Analgesia*, 101(8), 2963–2972. <https://doi.org/10.1182/blood-2002-10-3296>.Supported
- Manservigi, R., Argnani, R., & Marconi, P. (2010). HSV Recombinant Vectors for Gene Therapy. *The Open Virology Journal*, 4(3), 123–156. <https://doi.org/10.2174/1874357901004030123>
- Marca, R. La, Cerri, F., Horiuchi, K., Bachi, A., Feltri, M. L., Wrabetz, L., ... Salzer, J. L., Taveggia, C (2011). TACE (ADAM17) inhibits Schwann cell myelination. *Nature Neuroscience*, 14(7), 857–865. <https://doi.org/10.1038/nn.2849>
- Marcaida, M. J., Muñoz, I. G., Blanco, F. J., Prieto, J., & Montoya, G. (2010). Homing endonucleases: From basics to therapeutic applications. *Cellular and Molecular Life Sciences*, 67(5), 727–748. <https://doi.org/10.1007/s00018-009-0188-y>
- Masia, F., Pope, I., Watson, P., Langbein, W., & Borri, P. (2018). Bessel-Beam Hyperspectral CARS Microscopy with Sparse Sampling: Enabling High-Content High-Throughput Label-Free Quantitative Chemical Imaging. *Analytical Chemistry*, 90(6), 3775–3785. <https://doi.org/10.1021/acs.analchem.7b04039>
- Masocha, W., & Parvarthy, S. S. (2009). Assessment of weight bearing changes and pharmacological antinociception in mice with LPS-induced monoarthritis using the Catwalk gait analysis system. *Life Science*, 18, 85(11-12), 462-469. <https://doi.org/10.1016/j.lfs.2009.07.015>
- McCarthy, D. M. (2008). Self-complementary AAV Vectors; Advances and Applications, *Molecular Therapy*. 16(10), 1648–1656. <https://doi.org/10.1038/mt.2008.171>
- McKee, K. K., Yang, D.-H., Patel, R., Chen, Z.-L., Strickland, S., Takagi, J., ... Yurchenco, P. D. (2012). Schwann cell myelination requires integration of laminin activities. *Journal of Cell Science*, 125(19), 4609–4619. <https://doi.org/10.1242/jcs.107995>
- McPhee, S. W. J., Janson, C. G., Li, C., Samulski, R. J., Camp, A. S., Francis, J., ... Leone, P. (2006). Immune responses to AAV in a phase I study for Canavan disease. *Journal of Gene*

- Medicine*, 8(5), 577–588. <https://doi.org/10.1002/jgm.885>
- Mei, L., & Xiong Wen-Cheng. (2008). Neuregulin 1 in neural development, synaptic plasticity and schizophrenia. *Nature Review Neuroscience*, 9(6), 437–452. <https://doi.org/10.1038/nrn2392>.
- Meier, C., Parmantier, E., Brennan, A., Mirsky, R., & Jessen, K. R. (1999). Developing Schwann cells acquire the ability to survive without axons by establishing an autocrine circuit involving insulin-like growth factor, neurotrophin-3, and platelet-derived growth factor-BB. *The Journal of Neuroscience*, 19(10), 3847–3859. Retrieved from <http://www.jneurosci.org.gate2.inist.fr/content/jneuro/19/10/3847.full.pdf>
- Mendell, J. R., Al-Zaidy, S., Shell, R., Arnold, W. D., Rodino-Klapac, L. R., Prior, T. W., ... Kaspar, B. K. (2017). Single-Dose Gene-Replacement Therapy for Spinal Muscular Atrophy. *New England Journal of Medicine*, 377(18), 1713–1722. <https://doi.org/10.1056/NEJMoa1706198>
- Menotti, F., Laudani, L., Damiani, A., Mignogna, T., & Macaluso, A. (2014). An anterior ankle-foot orthosis improves walking economy in Charcot-Marie-Tooth type 1A patients. *Prosthetics and Orthotics International*, 38(5), 387–392. <https://doi.org/10.1177/0309364613506250>
- Meyer-Franke, A., & Barres, B. (1994). Axon Myelination: Myelination without myelin-associated glycoprotein. *Current Biology*, 4(9), 847–850. [https://doi.org/10.1016/S0960-9822\(00\)00190-1](https://doi.org/10.1016/S0960-9822(00)00190-1)
- Meyer zu Horste, G., Miesbach, T. A., Muller, J. I., Fledrich, R., Stassart, R. M., Kieseier, B. C., ... Sereda, M. W. (2011). The Wlds transgene reduces axon loss in a Charcot-Marie-Tooth disease 1A rat model and nicotinamide delays post-traumatic axonal degeneration. *Neurobiology of Disease*, 42(1), 1–8. <https://doi.org/10.1016/j.nbd.2010.12.006>
- Michailov, G. V., Sereda, M. W., Brinkmann, B. G., Fischer, T. H., Haug, B., Birchmeier, C., ... Nave, K. A. (2004). Axonal Neuregulin-1 Regulates Myelin Sheath Thickness. *Science*, 304(5671), 700–703. <https://doi.org/10.1126/science.1095862>

- Mirsky, R., Jessen, K. R., Brennan, A., Parkinson, D., Dong, Z., Meier, C., ... Lawson, D. (2002). Schwann cells as regulators of nerve development. In *Journal of Physiology Paris*, 96, 17–24. [https://doi.org/10.1016/S0928-4257\(01\)00076-6](https://doi.org/10.1016/S0928-4257(01)00076-6)
- Mittendorf, K. F., Marinko, J. T., Hampton, C. M., Ke, Z., Hadziselimovic, A., Schleich, J. P., ... Ohi, M. D. (2017). Peripheral myelin protein 22 alters membrane architecture. *Science Advances*, 3(7), 1–12. <https://doi.org/10.1126/sciadv.1700220>
- Monahan, P. E., Lothrop, C. D., Sun, J., Hirsch, M. L., Kafri, T., Kantor, B., ... Samulski, R. J. (2010). Proteasome inhibitors enhance gene delivery by AAV virus vectors expressing large genomes in hemophilia mouse and dog models: A strategy for broad clinical application. *Molecular Therapy*, 18(11), 1907–1916. <https://doi.org/10.1038/mt.2010.170>
- Monia, B. P., Lesnik, E. A., Gonzalez, C., Lima, W. F., McGee, D., Guinosso, C. J., ... Freier, S. M. (1993). Evaluation of 2'-modified oligonucleotides containing 2'-deoxy gaps as antisense inhibitors of gene expression. *Journal of Biological Chemistry*, 268(19), 14514–14522.
- Monteilhet, V., Veron, P., Leborgne, C., & Benveniste, O. (2010). Prevalence of Serum IgG and Neutralizing Factors and 9 in the Healthy Population : Implications for Gene Therapy Using AAV Vectors. *Human Gene Therapy*, 712, 704–712.
- Moore, C. B., Guthrie, E. H., Tze-, M., Huang, H., & Taxman, D. J. (2010). Short Hairpin RNA (shRNA): Design, Delivery, and Assessment of Gene Knockdown, *Methods in Molecular Biology*, 629, 141–158. https://doi.org/10.1007/978-1-60761-657-3_10
- Morrison, B., & Chaudhry, V. (2012). Medication, toxic, and vitamin-related neuropathies. *CONTINUUM Lifelong Learning in Neurology*, 18(1), 139-160. <https://doi.org/10.1212/01.CON.0000411565.49332.84>
- Morrison, C. (2018). Alnylam prepares to land first RNAi drug approval. *Nature Reviews Drug Discovery*, 17(3), 156–157. <https://doi.org/10.1038/nrd.2018.20>
- Mountney, A., Leung, L. Y., Pedersen, R., Shear, D., & Tortella, F. (2013). Longitudinal assessment of gait abnormalities following penetrating ballistic-like brain injury in rats. *Journal of Neuroscience Methods*, 212(1), 1–16.

<https://doi.org/10.1016/j.jneumeth.2012.08.025>

- Muona, K., Mäkinen, K., Hedman, M., Manninen, H., & Ylä-Herttuala, S. (2012). 10-Year safety follow-up in patients with local VEGF gene transfer to ischemic lower limb. *Gene Therapy*, 19(4), 392–395. <https://doi.org/10.1038/gt.2011.109>
- Murphy, S. M., Laura, M., Fawcett, K., Pandraud, A., Liu, Y. T., Davidson, G. L., ... Reilly, M. M. (2012). Charcot-Marie-Tooth disease: Frequency of genetic subtypes and guidelines for genetic testing. *Journal of Neurology, Neurosurgery and Psychiatry*, 83(7), 706–710. <https://doi.org/10.1136/jnnp-2012-302451>
- Mussolino, C., & Cathomen, T. (2012). TALE nucleases: Tailored genome engineering made easy. *Current Opinion in Biotechnology*, 23(5), 644–650. <https://doi.org/10.1016/j.copbio.2012.01.013>
- Mustonen, E. K., Palomäki, T., & Pasanen, M. (2017). Oligonucleotide-based pharmaceuticals: Non-clinical and clinical safety signals and non-clinical testing strategies. *Regulatory Toxicology and Pharmacology*, 90, 328–341. <https://doi.org/10.1016/j.yrtph.2017.09.028>
- Naldini, L. (2015). Gene therapy returns to centre stage. *Nature*, 526(7573), 351–360. <https://doi.org/10.1038/nature15818>
- Nathwani, A. C., Gray, J. T., McIntosh, J., Ng, C. Y. C., Zhou, J., Spence, Y., ... Davidoff, A. M. (2007). Safe and efficient transduction of the liver after peripheral vein infusion of self-complementary AAV vector results in stable therapeutic expression of human FIX in nonhuman primates. *Blood*, 109(4), 1414–1421. <https://doi.org/10.1182/blood-2006-03-010181>
- Nave, K. A., & Salzer, J. L. (2006). Axonal regulation of myelination by neuregulin 1. *Current Opinion in Neurobiology*, 16(5), 492–500. <https://doi.org/10.1016/j.conb.2006.08.008>
- Nayak, R., & Pintel, D. J. (2007). Adeno-associated viruses can induce phosphorylation of eIF2alpha via PKR activation, which can be overcome by helper adenovirus type 5 virus-associated RNA. *Journal of Virology*, 81(21), 11908–16. <https://doi.org/10.1128/JVI.01132-07>

- Niemann, S., Sereda, M., Rossner, M., Stewart, H., Suter, U., & Meinck, H. M. (1999). The CMT rat peripheral neuropathy and dysmyelination caused by transgenic overexpression of PMP22. *Annals of New York Academy of Sciences*, 883, 254-261.
- Nietupski, J. B., Hurlbut, G. D., Ziegler, R. J., Chu, Q., Hodges, B. L., Ashe, K. M., ... Scheule, R. K. (2011). Systemic administration of AAV8- α -galactosidase a induces humoral tolerance in nonhuman primates despite low hepatic expression. *Molecular Therapy*, 19(11), 1999–2011. <https://doi.org/10.1038/mt.2011.119>
- Nobbio, L., Sturla, L., Fiorese, F., Usai, C., Basile, G., Moreschi, I., ... Bruzzone, S. (2009). P2X7-mediated increased intracellular calcium causes functional derangement in Schwann cells from rats with CMT1A neuropathy. *The Journal of Biological Chemistry*, 284(34), 23146–58. <https://doi.org/10.1074/jbc.M109.027128>
- Noldus Information Technology (2015). CatWalk XT 10.6 Reference Manual.
- Norreel, J. C., Jamon, M., Riviere, G., Passage, E., Fontes, M., & Clarac, F. (2001). Behavioural profiling of a murine Charcot-Marie-Tooth disease type 1A model. *European Journal of Neuroscience*, 13(8), 1625–1634. <https://doi.org/10.1046/j.0953-816x.2001.01535.x>
- Noto, Y. I., Shiga, K., Tsuji, Y., Mizuta, I., Higuchi, Y., Hashiguchi, A., ... Mizuno, T. (2015). Nerve ultrasound depicts peripheral nerve enlargement in patients with genetically distinct Charcot-Marie-Tooth disease. *Journal of Neurology, Neurosurgery and Psychiatry*, 86(4), 378–384. <https://doi.org/10.1136/jnnp-2014-308211>
- Notterpek, L., Roux, K. J., Amici, S. A., Yazdanpour, A., Rahner, C., & Fletcher, B. S. (2001). Peripheral myelin protein 22 is a constituent of intercellular junctions in epithelia. *Proceedings of the National Academy of Sciences*, 98(25), 14404–14409. <https://doi.org/10.1073/pnas.251548398>
- Notterpek, L., Ryan, M. C., Tobler, A. R., & Shooter, E. M. (1999). PMP22 accumulation in aggresomes: Implications for CMT1A pathology. *Neurobiology of Disease*, 6(5), 450–460. <https://doi.org/10.1006/nbdi.1999.0274>
- Nykänen, A., Haley, B., & Zamore, P. D. (2001). ATP requirements and small interfering RNA

structure in the RNA interference pathway. *Cell*, 107(3), 309–321. [https://doi.org/10.1016/S0092-8674\(01\)00547-5](https://doi.org/10.1016/S0092-8674(01)00547-5)

Ohsawa, Y., Murakami, T., Miyazaki, Y., Shirabe, T., & Sunada, Y. (2006). Peripheral myelin protein 22 is expressed in human central nervous system. *Journal of the Neurological Sciences*, 247(1), 11–15. <https://doi.org/10.1016/j.jns.2006.03.004>

Okada, T. (2013). Chapter 17 Efficient AAV Vector Production System: Towards Gene Therapy For Duchenne Muscular Dystrophy. *Gene Therapy - Tools and Potential Applications*. Edited by Martin, F. <https://doi.org/10.5772/53023>

Öunpuu, S., Garibay, E., Solomito, M., Bell, K., Pierz, K., Thomson, J., ... DeLuca, P. (2013). A comprehensive evaluation of the variation in ankle function during gait in children and youth with Charcot-Marie-Tooth disease. *Gait and Posture*, 38(4), 900–906. <https://doi.org/10.1016/j.gaitpost.2013.04.016>

Ozcelik, M., Cotter, L., Jacob, C., Pereira, J. A., Relvas, J. B., Suter, U., & Tricaud, N. (2010). Pals1 Is a Major Regulator of the Epithelial-Like Polarization and the Extension of the Myelin Sheath in Peripheral Nerves. *Journal of Neuroscience*, 30(11), 4120–4131. <https://doi.org/10.1523/JNEUROSCI.5185-09.2010>

Paasen, B. W. van, Van Der Kooi, A. J., Van Spaendonck-Zwarts, K. Y., Verhamme, C., Baas, F., & de Visser, M. (2014). PMP22 related neuropathies: Charcot-Marie-Tooth disease type 1A and Hereditary Neuropathy with liability to Pressure Palsies. *Orphanet Journal of Rare Diseases*, 19 (9), 38. doi: 10.1186/1750-1172-9-38.

Padua, L., Coraci, D., Lucchetta, M., Paolasso, I., Pazzaglia, C., Granata, G., ... Briani, C. (2017). Different nerve ultrasound patterns in charcot-marie-tooth types and hereditary neuropathy with liability to pressure palsies. *Muscle and Nerve*, 57(1), E18–E23. <https://doi.org/10.1002/mus.25766>

Palumbo, C., Massa, R., Panico, M. B., Di Muzio, A., Sinibaldi, P., Bernardi, G., & Modesti, A. (2002). Peripheral nerve extracellular matrix remodeling in Charcot-Marie-Tooth type I disease. *Acta Neuropathologica*, 104(3), 287–296. <https://doi.org/10.1007/s00401-002-0558-0>

- Pareyson, D., & Marchesi, C. (2009). Diagnosis, natural history, and management of Charcot-Marie-Tooth disease. *The Lancet Neurology*, 8(7), 654–667. [https://doi.org/10.1016/S1474-4422\(09\)70110-3](https://doi.org/10.1016/S1474-4422(09)70110-3)
- Pareyson, D., Reilly, M. M., Schenone, A., Fabrizi, G. M., Cavallaro, T., Manganeli, L., ... Sereda, M. (2011). Ascorbic acid in charcot-marie-tooth disease type 1A (CMTTRIAL and CMT-TRAUK): A double-blind randomised trial. *The Lancet Neurology*, 10(4), 320–328. [https://doi.org/10.1016/S1474-4422\(11\)70025-4](https://doi.org/10.1016/S1474-4422(11)70025-4)
- Pareyson, D., Saveri, P., & Pisciotto, C. (2017). New developments in Charcot-Marie-Tooth neuropathy and related diseases. *Current Opinion in Neurology*, 30(5), 471–480. <https://doi.org/10.1097/WCO.0000000000000474>
- Pareyson, D., Saveri, P., Sagnelli, A., & Piscosquito, G. (2015). Mitochondrial dynamics and inherited peripheral nerve diseases. *Neuroscience Letters*, 596, 66–77. <https://doi.org/10.1016/j.neulet.2015.04.001>
- Parkinson, D. B., Bhaskaran, A., Arthur-Farraj, P., Noon, L. A., Woodhoo, A., Lloyd, A. C., ... Jessen, K. R. (2008). c-Jun is a negative regulator of myelination. *Journal of Cell Biology*, 181(4), 625–637. <https://doi.org/10.1083/jcb.200803013>
- Parmantier, E., Cabon, F., Braun, C., D’Urso, D., Müller, H. W., & Zalc, B. (1995). Peripheral myelin protein-22 is expressed in rat and mouse brain and spinal cord motoneurons. *The European Journal of Neuroscience*, 7(5), 1080–1088.
- Passage, E., Norreel, J. C., Noack-Fraissignes, P., Sanguedolce, V., Pizant, J., Thirion, X., ... Fontés, M. (2004). Ascorbic acid treatment corrects the phenotype of a mouse model of Charcot-Marie-Tooth disease. *Nature Medicine*, 10(4), 396–401. <https://doi.org/10.1038/nm1023>
- Patel, K., Kilfoil, G., Wyles, D. L., Naggie, S., Lawitz, E., Bradley, S., ... Suhy, D. (2016). 258. Phase I/IIa Study of TT-034, a DNA-Directed RNA Interference (ddRNAi) Agent Delivered as a Single Administration for the Treatment of Subjects with Chronic Hepatitis C Virus (HCV). *Molecular Therapy*, 24, S102. [https://doi.org/10.1016/S1525-0016\(16\)33067-2](https://doi.org/10.1016/S1525-0016(16)33067-2)

- Pazzaglia, C., Camerota, F., Germanotta, M., Di Sipio, E., Celletti, C., & Padua, L. (2016). Efficacy of focal mechanic vibration treatment on balance in Charcot-Marie-Tooth 1A disease: a pilot study. *Journal of Neurology*, 263(7), 1434–1441. <https://doi.org/10.1007/s00415-016-8157-5>
- Pentao, L., Wise, C. A., Chinault, A. C., Patel, P. I., & Lupski, J. R. (1992). Charcot-Marie-Tooth type 1A duplication appears to arise from recombination at repeat sequences flanking the 1.5 Mb monomer unit. *Nature Genetics*, 2(4), 292–300. <https://doi.org/10.1038/ng1292-292>
- Perea, J., Robertson, a, Tolmachova, T., Muddle, J., King, R. H., Ponsford, S., ... Huxley, C. (2001). Induced myelination and demyelination in a conditional mouse model of Charcot-Marie-Tooth disease type 1A. *Human Molecular Genetics*, 10(10), 1007–1018. <https://doi.org/10.1093/hmg/10.10.1007>
- Pereira, D. J., McCarty, D. M., & Muzyczka, N. (1997). The adeno-associated virus (AAV) Rep protein acts as both a repressor and an activator to regulate AAV transcription during a productive infection. *J Virol*, 71(2), 1079–1088.
- Pereira, J. A., Benninger, Y., Baumann, R., Gonçalves, A. F., Özçelik, M., Thurnherr, T., ... Relvas, J. B. (2009). Integrin-linked kinase is required for radial sorting of axons and schwann cell remyelination in the peripheral nervous system. *Journal of Cell Biology*, 185(1), 147–161. <https://doi.org/10.1083/jcb.200809008>
- Perrin-Tricaud, C., Rutishauser, U., & Tricaud, N. (2007). P120 catenin is required for thickening of Schwann cell myelin. *Molecular and Cellular Neuroscience*, 35(1), 120–129. <https://doi.org/10.1016/j.mcn.2007.02.010>
- Peters, A., & Palay SL. (1991). In *The Fine Structure of the Nervous System*, 3rd edn, Published by *Oxford University Press*, 212–272.
- Pfaffl, M. W., Horgan, G. W., & Dempfle, L. (2002). Relative expression software tool (REST) for group-wise comparison and statistical analysis of relative expression results in real-time PCR. *Nucleic Acids Research*, 30(9), e36.
- Piguet, F., Alves, S., & Cartier, N. (2017). Clinical Gene Therapy for Neurodegenerative Diseases:

- Past, Present, and Future. *Human Gene Therapy*, 28(11), 988–1003.
<https://doi.org/10.1089/hum.2017.160>
- Pirmohamed, M. (2018). Nucleic acid based therapies: developing frontier for precision medicine. *Bmj*, 223, k223. <https://doi.org/10.1136/bmj.k223>
- Pisciotta, C., & Shy, M. E. (2018). Neuropathy. *Handbook of Clinical Neurology*, 148, 653–665.
<https://doi.org/10.1016/B978-0-444-64076-5.00042-9>
- Poitelon, Y., Lopez-Anido, C., Catignas, K., Berti, C., Palmisano, M., Williamson, C., ... Feltri, M. L. (2016). YAP and TAZ control peripheral myelination and the expression of laminin receptors in Schwann cells, *Nature Neuroscience*, 19(7), 879–887.
<https://doi.org/10.1038/nn.4316>
- Provasi, E., Genovese, P., Lombardo, A., Magnani, Z., Liu, P. Q., Reik, A., ... Bonini, C. (2012). Editing T cell specificity towards leukemia by zinc finger nucleases and lentiviral gene transfer. *Nature Medicine*, 18(5), 807–815. <https://doi.org/10.1038/nm.2700>
- Pushparaj, P. N., Aarthi, J. J., Manikandan, J., & Kumar, S. D. (2008). siRNA, miRNA, and shRNA: in vivo Applications. *Journal of Dental Research*, 87(11), 992–1003.
<https://doi.org/10.1177/154405910808701109>
- Qiu, J., & Pintel, D. (2008). Processing of adeno-associated virus RNA. *Frontiers in Bioscience : A Journal and Virtual Library*, 13(4), 3101–3115.
- Quarles, R. H., Macklin, W. B., & Morell, P. (2006). Myelin Formation, Structure, and Biochemistry. *Basic Neurochemistry 6th Edition: Molecular, Cellular and Medical Aspects*, 51–71. Siegel GJ, Agranoff BW, Albers RW, et al., editors.
- Rabinowitz, J. E., Bowles, D. E., Faust, S. M., Ledford, J. G., Cunningham, S. E., & Samulski, R. J. (2004). Cross-Dressing the Virion: the Transcapsidation of Adeno-Associated Virus Serotypes Functionally Defines Subgroups. *Journal Of Virology*, 78(9), 4421–4432.
<https://doi.org/10.1128/JVI.78.9.4421-4432.2004>
- Raeymaekers, P., Timmerman, V., Nelis, E., De Jonghe, P., Hoogendijk, J. E., Baas, F., ... Bolhuis, P. A. (1991). Duplication in chromosome 17p11.2 in Charcot-Marie-Tooth

- neuropathy type 1a (CMT 1a). The HMSN Collaborative Research Group. *Neuromuscular Disorders : NMD*, 1(2), 93–7.
- Raine C.S. (1977) Morphology of Myelin and Myelinationm 1-49. In: Morell P. (eds) *Myelin*. Springer, Boston, MA. https://doi.org/10.1007/978-1-4757-1830-0_1
- Ramachandran, P. S., Keiser, M. S., & Davidson, B. L. (2013). Recent Advances in RNA Interference Therapeutics for CNS Diseases. *Neurotherapeutics*, 10(3):473-85. <https://doi.org/10.1007/s13311-013-0183-8>
- Ramdharay, G. M., Day, B. L., Reilly, M. M., & Marsden, J. F. (2012). Foot drop splints improve proximal as well as distal leg control during gait in Charcot-Marie-Tooth Disease. *Muscle and Nerve*, 46(4), 512–519. <https://doi.org/10.1002/mus.23348>
- Rangaraju, S., & Notterpek, L. (2011). Autophagy aids membrane expansion by neuropathic Schwann cells. *Autophagy*, 7(2), 238–239. <https://doi.org/10.4161/auto.7.2.14278>
- Rao, D. D., Vorhies, J. S., Senzer, N., & Nemunaitis, J. (2009). siRNA vs. shRNA: Similarities and differences. *Advanced Drug Delivery Review*, 61(9), 746-759. <https://doi.org/10.1016/j.addr.2009.04.004>
- Raper, S. E., Chirmule, N., Lee, F. S., Wivel, N. A., Bagg, A., Gao, G. P., ... Batshaw, M. L. (2003). Fatal systemic inflammatory response syndrome in a ornithine transcarbamylase deficient patient following adenoviral gene transfer. *Molecular Genetics and Metabolism*, 80(1–2), 148–158. <https://doi.org/10.1016/j.ymgme.2003.08.016>
- Rapti, K., Louis-Jeune, V., Kohlbrenner, E., Ishikawa, K., Ladage, D., Zolotukhin, S., ... Weber, T. (2012). Neutralizing antibodies against AAV serotypes 1, 2, 6, and 9 in sera of commonly used animal models. *Molecular Therapy*, 20(1), 73–83. <https://doi.org/10.1038/mt.2011.177>
- Reynolds, A., Leake, D., Boese, Q., Scaringe, S., Marshall, W. S., & Khvorova, A. (2004). Rational siRNA design for RNA interference. *Nature Biotechnology*, 22(3), 326–330. <https://doi.org/10.1038/nbt936>
- Ribiere, C., Bernardin, M., Sacconi, S., Delmont, E., Fournier-Mehouas, M., Rauscent, H., ... Desnuelle, C. (2012). Pain assessment in Charcot-Marie-Tooth (CMT) disease. *Annals of*

- Physical and Rehabilitation Medicine*, 55(3), 160–173.
<https://doi.org/10.1016/j.rehab.2012.02.005>
- Richter, M., Iwata, A., Nyhuis, J., Nitta, Y., Miller, A. D., Halbert, C. L., & Allen, M. D. (2000). Adeno-associated virus vector transduction of vascular smooth muscle cells in vivo. *Physiological Genomics*, 2(3), 117–27.
<https://doi.org/10.1152/physiolgenomics.2000.2.3.117>
- Rinaldi, C., & A Wood, M. J. (2017). Antisense oligonucleotides: the next frontier for treatment of neurological disorders. *Nature Reviews Neurology*, 14(1), 9–21.
<https://doi.org/10.1038/nrneurol.2017.148>
- Robertson, A. M., Huxley, C., King, R. H. M., & Thomas, P. K. (1999). Development of early postnatal peripheral nerve abnormalities in Trembler-J and PMP22 transgenic mice. *J. Anat*, 195, 331–339.
- Robertson, A. M., Perea, J., McGuigan, A., King, R. H. M., Muddle, J. R., Gabreëls-Festen, A. A., ... Huxley, C. (2002). Comparison of a new pmp22 transgenic mouse line with other mouse models and human patients with CMT1A. *J. Anat*, 200, 377–390.
- Rossor, A. M., Carr, A. S., Devine, H., Chandrashekar, H., Pelayo-Negro, A. L., Pareyson, D., ... Reilly, M. M. (2017). Peripheral neuropathy in complex inherited diseases: An approach to diagnosis. *Journal of Neurology, Neurosurgery and Psychiatry*, 88(10), 846–863.
<https://doi.org/10.1136/jnnp-2016-313960>
- Ruberg, F. L., & Berk, J. L. (2012). Transthyretin (TTR) cardiac amyloidosis. *Circulation*, 126(10), 1286–1300. <https://doi.org/10.1161/CIRCULATIONAHA.111.078915>
- Rushton, W. A. H. (1951). A theory of the effects of fibre size in medullated nerve. *The Journal of Physiology*, 115(1), 101–122. <https://doi.org/10.1113/jphysiol.1951.sp004655>
- Sahenk, Z., Galloway, G., Clark, K. R., Malik, V., Rodino-Klapac, L. R., Kaspar, B. K., ... Mendell, J. R. (2014). AAV1.NT-3 gene therapy for charcot-marie-tooth neuropathy. *Molecular Therapy*, 22(3), 511–521. <https://doi.org/10.1038/mt.2013.250>
- Sahenk, Z., Nagaraja, H. N., McCracken, B. S., King, W. M., Freimer, M. L., Cedarbaum, J. M.,

- & Mendell, J. R. (2005). NT-3 promotes nerve regeneration and sensory improvement in CMT1A mouse models and in patients. *Neurology*, 65(5), 681–689. <https://doi.org/10.1212/01.WNL.0000171978.70849.c5>
- Saher, G., Quintes, S., Mobius, W., Wehr, M. C., Kramer-Albers, E.-M., Brugger, B., & Nave, K.-A. (2009). Cholesterol Regulates the Endoplasmic Reticulum Exit of the Major Membrane Protein P0 Required for Peripheral Myelin Compaction. *Journal of Neuroscience*, 29(19), 6094–6104. <https://doi.org/10.1523/JNEUROSCI.0686-09.2009>
- Sakakura, Y., Shimano, H., Sone, H., Takahashi, A., Inoue, K., Toyoshima, H., ... Yamada, N. (2001). Sterol regulatory element-binding proteins induce an entire pathway of cholesterol synthesis. *Biochemical and Biophysical Research Communications*, 286(1), 176–183. <https://doi.org/10.1006/bbrc.2001.5375>
- Sakuma, T., Barry, M. A., & Ikeda, Y. (2012). Lentiviral vectors: basic to translational. *Biochemical Journal*, 443(3), 603–618. <https://doi.org/10.1042/BJ20120146>
- Samulski, R. J., & Shenk, T. (1988). Adenovirus E1B 55-Mr polypeptide facilitates timely cytoplasmic accumulation of adeno-associated virus mRNAs. *Journal of Virology*, 62(1), 206–10.
- Sancho, S., Magyar, J. P., Aguzzi, A., & Suter, U. (1999). Distal axonopathy in peripheral nerves of PMP22-mutant mice. *Brain*, 122, 1563–1577.
- Sancho, S., Young, P., & Suter, U. (2001). Regulation of Schwann cell proliferation and apoptosis in PMP22-deficient mice and mouse models of Charcot-Marie-Tooth disease type 1A. *Brain*, 124(11), 2177–2187. <https://doi.org/10.1093/brain/124.11.2177>
- Saporta, A. S. D., Sottile, S. L., Miller, L. J., Shawna, M. E., Siskind, C. E., & Shy, M. E. (2011). Charcot Marie Tooth (CMT) Subtypes and Genetic Testing Strategies, *Annals of Neurology* 69(1), 22–33. <https://doi.org/10.1002/ana.22166>
- Saporta, M. A., Katona, I., Lewis, R. A., Masse, S., Shy, M. E., & Li, J. (2009). Shortened internodal length of dermal myelinated nerve fibres in Charcot-Marie-Tooth disease type 1A. *Brain*, 132(12), 3263–3273. <https://doi.org/10.1093/brain/awp274>

- Saporta, M. A., & Shy, M. E. (2015). Peripheral Neuropathies. *Neurobiology of Brain Disorders: Biological Basis of Neurological and Psychiatric Disorders*, 167–188. <https://doi.org/10.1016/B978-0-12-398270-4.00012-4>
- Schain, A. J., Hill, R. A., & Grutzendler, J. (2014). Label-free in vivo imaging of myelinated axons in health and disease with spectral confocal reflectance microscopy. *Nature Medicine*, 20(4), 443–449. <https://doi.org/10.1038/nm.3495>
- Schenone, A., Nobbio, L., Bragadin, M. M., Ursino, G., & Grandis, M. (2011). Inherited neuropathies. *Current Treatment Options in Neurology*, 13(2), 160–179. <https://doi.org/10.1007/s11940-011-0115-z>
- Schmalbruch, H. (1986). Fiber composition of the rat sciatic nerve. *The Anatomical Record*, 215, 71–81. <https://doi.org/10.1002/ar.1092150111>
- Schmidt, W. M., Rutledge, S. L., Schüle, R., Mayerhofer, B., Züchner, S., Boltshauser, E., & Bittner, R. E. (2015). Disruptive SCYL1 Mutations Underlie a Syndrome Characterized by Recurrent Episodes of Liver Failure, Peripheral Neuropathy, Cerebellar Atrophy, and Ataxia. *American Journal of Human Genetics*, 97(6), 855–861. <https://doi.org/10.1016/j.ajhg.2015.10.011>
- Schuster, D. J., Dykstra, J. A., Riedl, M. S., Kitto, K. F., Belur, L. R., McIvor, R. S., ... Vulchanova, L. (2014). Biodistribution of adeno-associated virus serotype 9 (AAV9) vector after intrathecal and intravenous delivery in mouse. *Frontiers in Neuroanatomy*, 8, 1–14. <https://doi.org/10.3389/fnana.2014.00042>
- Sereda, M., Griffiths, I., Pühlhofer, A., Stewart, H., Rossner, M. J., Zimmerman, F., ... Nave, K. A. (1996). A transgenic rat model of Charcot-Marie-Tooth disease. *Neuron*, 16 (5), 1049–60.. [https://doi.org/10.1016/S0896-6273\(00\)80128-2](https://doi.org/10.1016/S0896-6273(00)80128-2)
- Sereda, M. W. (1999). Altered protein synthesis in SN by TG overexpressio of PMP22 in the CMT rat. *Annals New York Academy of Sciences*, 883(1), 530–532. doi: 10.1111/j.1749-6632.1999.tb08629.x.
- Sereda, M. W., Meyer Zu Hörste, G., Suter, U., Uzma, N., & Nave, K. A. (2003). Therapeutic

- administration of progesterone antagonist in a model of Charcot-Marie-Tooth disease (CMT-1A). *Nature Medicine*, 9(12), 1533–1537. <https://doi.org/10.1038/nm957>
- Sherman, D. L., & Brophy, P. J. (2018). A murine model of Charcot-Marie-Tooth disease 4F reveals a role for the C-terminus of periaxin in the formation and stabilization of Cajal bands. *Wellcome Open Research*, 3, 20. <https://doi.org/10.12688/wellcomeopenres.13673.1>
- Sheth, S., Francies, K., Siskind, C. E., Feely, S. M. E., Lewis, R. a, & Shy, M. E. (2008). Diabetes mellitus exacerbates motor and sensory impairment in CMT1A. *Journal of the Peripheral Nervous System : JPNS*, 13(4), 299–304. <https://doi.org/10.1111/j.1529-8027.2008.00196.x>
- Shinowara, N. L., Beutel, W. B., & Revel, J. P. (1980). Comparative analysis of junctions in the myelin sheath of central and peripheral axons of fish, amphibians and mammals: A freeze-fracture study using complementary replicas. *Journal of Neurocytology*, 9(1), 15–38. <https://doi.org/10.1007/BF01205225>
- Sierakowska, H., Sambade, M. J., Agrawal, S., & Kole, R. (1996). Repair of thalassemic human beta-globin mRNA in mammalian cells by antisense oligonucleotides. *Proceedings of the National Academy of Sciences of the United States of America*, 93(23), 12840–4. <https://doi.org/10.1073/pnas.93.23.12840>
- Sleeman, M. W., Anderson, K. D., Lambert, P. D., Yancopoulos, G. D., & Wiegand, S. J. (2000). The ciliary neurotrophic factor and its receptor, CNTFR α . *Pharmacochemistry Library*, 31(C), 265–272. [https://doi.org/10.1016/S0165-7208\(00\)80028-8](https://doi.org/10.1016/S0165-7208(00)80028-8)
- Smith, K. J., & Hall, S. M. (1988). Peripheral demyelination and remyelination initiated by the calcium-selective ionophore ionomycin: In vivo observations. *Journal of the Neurological Sciences*, 83(1), 37–53. [https://doi.org/10.1016/0022-510X\(88\)90018-4](https://doi.org/10.1016/0022-510X(88)90018-4)
- Smith, R. H. (2008). Adeno-associated virus integration: Virus versus vector. *Gene Therapy*, 15(11), 817–822. <https://doi.org/10.1038/gt.2008.55>
- Snipes, G. J., & Suter, U. (1995). Molecular anatomy and genetics of myelin proteins in the peripheral nervous system. *Journal of Anatomy*, 186 (3), 483–494.
- Snipes, G. J., Suter, U., Welcher, A. A., & Shooter, E. M. (1992). Characterization of a novel

- peripheral nervous system myelin protein (PMP-22/SR13). *The Journal of Cell Biology*, 117(1), 225–38. <https://doi.org/10.1083/jcb.117.1.225>
- Sociali, G., Visigalli, D., Prukop, T., Cervellini, I., Mannino, E., Venturi, C., ... Schenone, A. (2016). Tolerability and efficacy study of P2X7 inhibition in experimental Charcot-Marie-Tooth type 1A (CMT1A) neuropathy. *Neurobiology of Disease*, 95, 145–157. <https://doi.org/10.1016/j.nbd.2016.07.017>
- Sondhi, D., Peterson, D. A., Giannaris, E. L., Sanders, C. T., Mendez, B. S., De, B., ... Crystal, R. G. (2005). AAV2-mediated CLN2 gene transfer to rodent and non-human primate brain results in long-term TPP-I expression compatible with therapy for LINCL. *Gene Therapy*, 12(22), 1618–1632. <https://doi.org/10.1038/sj.gt.3302549>
- Srivastava, A. (2008). Adeno-associated virus-mediated gene transfer. *Journal of Cell Biochemistry*, 105(1), 17–24. <https://doi.org/10.1111/j.1743-6109.2008.01122.x> Endothelial
- Stankoff, B., Aigrot, M.-S. P., Dé Ric Noë, F., Lie Wattilliaux, A., Zalc, B., & Lubetzki, C. (2002). Ciliary Neurotrophic Factor (CNTF) Enhances Myelin Formation: A Novel Role for CNTF and CNTF-Related Molecules. *Journal of Neurosciences*, 22(21):9221-7.
- Stassart, R. M., Fledrich, R., Velanac, V., Brinkmann, B. G., Schwab, M. H., Meijer, D., ... Nave, K. A. (2013). A role for Schwann cell-derived neuregulin-1 in remyelination. *Nature Neuroscience*, 16(1), 48–54. <https://doi.org/10.1038/nn.3281>
- Stein, C. A., Subasinghe, C., Shinozuka, K., & Cohen, J. S. (1988). Physicochemical properties of phosphorothioate oligodeoxynucleotides. *Nucleic Acids Research*, 16(8), 3209–3221. <https://doi.org/10.1093/nar/16.5.2269>
- Stroes, E. S., Nierman, M. C., Meulenberg, J. J., Franssen, R., Twisk, J., Henny, C. P., ... Kuivenhoven, J. A. (2008). Intramuscular administration of AAV1-lipoprotein lipaseS447Xlowers triglycerides in lipoprotein lipase-deficient patients. *Arteriosclerosis, Thrombosis, and Vascular Biology*, 28(12), 2303–2304. <https://doi.org/10.1161/ATVBAHA.108.175620>
- Sun, Y. T., Tzeng, S. F., Lin, T. S., Hsu, K. Sen, Delpire, E., & Shen, M. R. (2016). KCC3

- deficiency-induced disruption of paranodal loops and impairment of axonal excitability in the peripheral nervous system. *Neuroscience*, 335, 91–102. <https://doi.org/10.1016/j.neuroscience.2016.08.031>
- Suter, U., & Snipes, G. J. (1995). Peripheral myelin protein 22: Facts and hypotheses. *Journal of Neuroscience Research*, 40(2), 145–151. <https://doi.org/10.1002/jnr.490400202>
- Suter, U., Welcher, A. A., Özcelik, T., Snipes, G. J., Kosaras, B., Francke, U., ... Shooter, E. M. (1992). Trembler mouse carries a point mutation in a myelin gene. *Nature*, 356(6366), 241–244. <https://doi.org/10.1038/356241a0>
- Svaren, J., & Meijer, D. (2008). The molecular machinery of myelin gene transcription in schwann cells. *Glia*, 56(14), 1541–1551. <https://doi.org/10.1002/glia.20767>
- Syed, N., & Kim, H. A. (2010). Soluble Neuregulin and Schwann Cell Myelination: a Therapeutic Potential for Improving Remyelination of Adult Axons. *Molecular Cell Pharmacology*, 2(4), 161–167. <https://doi.org/10.4255/mcpharmacol.10.22.Soluble>
- Tachi, N., Sasaki, K., Kusano, T., Wakai, S., Nagaoka, M., Annaka, S., ... Imamura, S. (1988). Peripheral Neuropathy in Four Cases of Group A Xeroderma Pigmentosum. *Journal of Child Neurology*, 3(2):114-119. <http://journals.sagepub.com/gate2.inist.fr/doi/pdf/10.1177/088307388800300207>
- Taneri, B., Asilmaz, E., & Gaasterland, T. (2012). Biomedical Impact of Splicing Mutations Revealed through Exome Sequencing. *Molecular Medicine*, 18, 314–319. <https://doi.org/10.2119/molmed.2011.00126>
- Taveggia C, Zanazzi G, Petrylak A, Yano H, Rosenbluth J, Einheber S, Xu X, Esper RM, Loeb JA, Shrager P, Chao MV, Falls DL, Role L, Salzer JL (2005). Neuregulin-1 type III determines the ensheathment fate of axons. *Neuron*, 47, 681–694
- Taveggia, C., Feltri, M. L., & Wrabetz, L. (2010). Signals to promote myelin formation and repair. *Nature Review Neurology*, 276–287. <https://doi.org/10.1038/nrneurol.2010.37>
- Taxman, D. J., Moore, C. B., Guthrie, E. H., & Huang, M. T.-H. (2010). Short Hairpin RNA (shRNA): Design, Delivery, and Assessment of Gene Knockdown. In *Methods in molecular*

- biology (Clifton, N.J.)* (Vol. 629, pp. 139–156). https://doi.org/10.1007/978-1-60761-657-3_10
- Tazir, M., Hamadouche, T., Nouioua, S., Mathis, S., & Vallat, J. M. (2014). Hereditary motor and sensory neuropathies or Charcot-Marie-Tooth diseases: An update. *Journal of the Neurological Sciences*, 347(1–2), 14–22. <https://doi.org/10.1016/j.jns.2014.10.013>
- Thomas PK, Berthold C-H, O. J. (1993). Microscopic anatomy of the peripheral nervous system. In *Peripheral Neuropathy*, pp. 28–91. <https://doi.org/10.1016/B978-0-7216-9491-7.50126-5>
- Timmons, L., Tabara, H., Mello, C. C., & Fire, A. Z. (2003). Inducible Systemic RNA Silencing in *Caenorhabditis elegans*. *Molecular Biology of the Cell*, 14, 2972–2983. <https://doi.org/10.1091/mbc.E03>
- Tooth, H. (1886). *On the peroneal type of progressive muscular atrophy*. H.K. Lewis and Co.: London.
- Tourbah, A., Gout, O., Vighetto, A., Deburghgraeve, V., Pelletier, J., Papeix, C., ... Arndt, C. (2018). MD1003 (High-Dose Pharmaceutical-Grade Biotin) for the Treatment of Chronic Visual Loss Related to Optic Neuritis in Multiple Sclerosis: A Randomized, Double-Blind, Placebo-Controlled Study. *CNS Drugs*, 1003, 1–12. <https://doi.org/10.1007/s40263-018-0528-2>
- Trapp, B. D. (1990). Myelin- Associated Glycoprotein Location and Potential Functions. *Annals of New York Academy of Sciences*, 29–43.
- Tricaud, N. (2005). Adherens Junctions in Myelinating Schwann Cells Stabilize Schmidt-Lanterman Incisures via Recruitment of p120 Catenin to E-Cadherin. *Journal of Neuroscience*, 25(13), 3259–3269. <https://doi.org/10.1523/JNEUROSCI.5168-04.2005>
- Tyson, J., Ellis, D., Fairbrother, U., King, R. H., Muntoni, F., Jacobs, J., ... Thomas, P. K. (1997). Hereditary demyelinating neuropathy of infancy. A genetically complex syndrome. *Brain : A Journal of Neurology*, 120 (1), 47–63.
- Urnov, F. D., Rebar, E. J., Holmes, M. C., Zhang, H. S., & Gregory, P. D. (2010). Genome editing with engineered zinc finger nucleases. *Nature Reviews Genetics*, 11(9), 636–646.

<https://doi.org/10.1038/nrg2842>

- Use of minicircle plasmids for gene therapy. (2009). *Mayrhofer P Schleef M Jechlinger W.*, 542, 87–104. <https://doi.org/10.1007/978-1-59745-561-9>
- Valleix, S., Gillmore, J. D., Bridoux, F., Mangione, P. P., Dogan, A., Nedelec, B., ... Bellotti, V. (2012). Hereditary Systemic Amyloidosis Due to Asp76Asn Variant β 2 -Microglobulin. *New England Journal of Medicine*, 366(24), 2276–2283. <https://doi.org/10.1056/NEJMoa1201356>
- van Deutekom, J. C. T. (2001). Antisense-induced exon skipping restores dystrophin expression in DMD patient derived muscle cells. *Human Molecular Genetics*, 10(15), 1547–1554. <https://doi.org/10.1093/hmg/10.15.1547>
- van Roon-Mom, W. M. C., Roos, R. A. C., & de Bot, S. T. (2018). Dose-Dependent Lowering of Mutant Huntingtin Using Antisense Oligonucleotides in Huntington Disease Patients. *Nucleic Acid Therapeutics*, 28(2), 59–62. <https://doi.org/10.1089/nat.2018.0720>
- Vandamme, C., ADJALI, O., & Mingozzi, F. (2017). Unraveling the complex story of immune responses to AAV vectors trial after trial. *Human Gene Therapy*, 28(11), hum.2017.150. <https://doi.org/10.1089/hum.2017.150>
- Vannucci, L., Lai, M., Chiuppesi, F., Ceccherini-nelli, L., & Pistello, M. (2013). Viral vectors : a look back and ahead on gene transfer technology. *New Microbiologica*, 36, 1–22.
- Vattemi, E., & Claudio, P. P. (2009). The feasibility of gene therapy in the treatment of head and neck cancer. *Head & Neck Oncology*, 1, 3. <https://doi.org/10.1186/1758-3284-1-3>
- Verhamme, C., King, R. H. M., ten Asbroek, A. L. M. A., Muddle, J. R., Nourallah, M., Wolterman, R., ... van Schaik, I. N. (2011). Myelin and Axon Pathology in a Long-Term Study of *PMP22* -Overexpressing Mice. *Journal of Neuropathology & Experimental Neurology*, 70(5), 386–398. <https://doi.org/10.1097/NEN.0b013e318217eba0>
- Vigo, T., Nobbio, L., Van Hummelen, P., Abbruzzese, M., Mancardi, G., Verpoorten, N., ... Schenone, A. (2005). Experimental Charcot-Marie-Tooth type 1A: A cDNA microarrays analysis. *Molecular and Cellular Neuroscience*, 28(4), 703–714.

<https://doi.org/10.1016/j.mcn.2004.11.016>

- Vijay, S., Chiu, M., Dacks, J. B., & Roberts, R. C. (2016). Exclusive expression of the Rab11 effector SH3TC2 in Schwann cells links integrin- α 6 and myelin maintenance to Charcot-Marie-Tooth disease type 4C. *Biochimica et Biophysica Acta - Molecular Basis of Disease*, 1862(7), 1279–1290. <https://doi.org/10.1016/j.bbadis.2016.04.003>
- Vincent, M., Gao, G., & Jacobson, L. (2014). Comparison of the efficacy of five adeno-associated virus vectors for transducing dorsal raphe nucleus cells in the mouse. *Journal of Neuroscience Methods*, 235, 189–192. <https://doi.org/10.1016/j.jneumeth.2014.07.005>
- Visigalli, D., Castagnola, P., Capodivento, G., Geroldi, A., Bellone, E., Mancardi, G., ... Nobbio, L. (2016). Alternative Splicing in the Human PMP22 Gene: Implications in CMT1A Neuropathy. *Human Mutation*, 37(1), 98–109. <https://doi.org/10.1002/humu.22921>
- von Boxberg, Y., Soares, S., Féréol, S., Fodil, R., Bartolami, S., Taxi, J., ... Nothias, F. (2014). Giant scaffolding protein AHNAK1 interacts with β -dystroglycan and controls motility and mechanical properties of schwann cells. *Glia*, 62(9), 1392–1406. <https://doi.org/10.1002/glia.22685>
- Vrinten, D. H., & Hamers, F. F. . (2003). “CatWalk” automated quantitative gait analysis as a novel method to assess mechanical allodynia in the rat; a comparison with von Frey testing. *Pain*, 102(1–2), 203–209. [https://doi.org/10.1016/s0304-3959\(02\)00382-2](https://doi.org/10.1016/s0304-3959(02)00382-2)
- Wang, D., & Gao, Guangping. (2014). State-of-the-Art Human Gene Therapy: Part I. Gene Delivery Technologies, 18(97), 1–21. <https://doi.org/10.1021/acschemneuro.5b00094>. Serotonin
- Wang, D., & Gao, G. (2014). State-Of-The-Art Human Gene Therapy: Part II. Gene Therapy Strategies And Applications. *Discovery Medicine*, 18(98), 151–161. <https://doi.org/10.1016/j.cogdev.2010.08.003>
- Wang, L., Bell, P., Lin, J., Calcedo, R., Tarantal, A. F., & Wilson, J. M. (2011). AAV8-mediated hepatic gene transfer in infant rhesus monkeys (macaca mulatta). *Molecular Therapy*, 19(11), 2012–2020. <https://doi.org/10.1038/mt.2011.151>

- Wang, L., Calcedo, R., Wang, H., Bell, P., Grant, R., Vandenberghe, L. H., ... Wilson, J. M. (2010). The pleiotropic effects of natural AAV infections on liver-directed gene transfer in macaques. *Molecular Therapy*, 18(1), 126–134. <https://doi.org/10.1038/mt.2009.245>
- Wang, W., Li, W., Ma, N., & Steinhoff, G. (2013). Non-viral gene delivery methods. *Current Pharmaceutical Biotechnology*, 14, 46–60. <https://doi.org/10.2174/1389201011314010008>
- Ward, P., Dean, F. B., Donnell, M. E. O., & Berns, K. I. (1998). Role of the Adenovirus DNA-Binding Protein in In Vitro Adeno-Associated Virus DNA Replication, *Journal of Virology* 72(1), 420–427.
- Welcher, A. A., Suter, U., De Leon, M., Snipes, G. J., & Shooter, E. M. (1991). A myelin protein is encoded by the homologue of a growth arrest-specific gene. *Proceedings of the National Academy of Sciences of the United States of America*, 88(16), 7195–9. <https://doi.org/10.1073/pnas.88.16.7195>
- Wiley, C. A., & Ellisman, M. H. (1980). Rows of dimeric-particles within the axolemma and juxtaposed particles within glia, incorporated into a new model for the paranodal glial-axonal junction at the node of ranvier. *Journal of Cell Biology*, 84(2), 261–280. <https://doi.org/10.1083/jcb.84.2.261>
- Willem, M., Garratt, A. N., Novak, B., Citron, M., Kaufmann, S., Rittger, A., ... Haass, C. (2006). Control of peripheral nerve myelination by the beta-secretase BACE1. *Science (New York, N.Y.)*, 314(5799), 664–666. <https://doi.org/10.1126/science.1132341>
- Wirth, T., Parker, N., & Ylä-Herttuala, S. (2013). History of gene therapy. *Gene*, 525(2), 162–169. <https://doi.org/10.1016/j.gene.2013.03.137>
- Woodhoo, A., Alonso, M. B. D., Droggiti, A., Turmaine, M., D’Antonio, M., Parkinson, D. B., ... Jessen, K. R. (2009). Notch controls embryonic Schwann cell differentiation, postnatal myelination and adult plasticity. *Nature Neuroscience*, 12(7), 839–847. <https://doi.org/10.1038/nn.2323>
- Wu, W., Liu, Q., Liu, Y., Yu, Z., & Wang, Y. (2016). Dixdc1 targets CyclinD1 and p21 via PI3K pathway activation to promote Schwann cell proliferation after sciatic nerve crush.

- Biochemical and Biophysical Research Communications*, 478, 956–963.
<https://doi.org/10.1016/j.bbrc.2016.08.058>
- Wu, Z., Asokan, A., & Samulski, R. J. (2006). Adeno-associated Virus Serotypes: Vector Toolkit for Human Gene Therapy. *Molecular Therapy*, 14(3), 316–327.
<https://doi.org/10.1016/j.ymthe.2006.05.009>
- Wulf, P., & Suter, U. (1999). Embryonic expression of epithelial membrane protein 1 in early neurons. *Brain Research Developmental Brain Research*, 116(2), 169–180.
- Xia, H., Mao, Q., Eliason, S. L., Harper, S. Q., Martins, I. H., Orr, H. T., ... Davidson, B. L. (2004). RNAi suppresses polyglutamine-induced neurodegeneration in a model of spinocerebellar ataxia. *Nature Medicine*, 10(8), 816–820. <https://doi.org/10.1038/nm1076>
- Yalkinoglu, A. Ö., Heilbronn, R., Bürkle, A., A., A., Bärkle, A., Schlehofer, J. A., & Hausen, H. (1988). DNA Amplification of Adeno-associated Virus as a Response to Cellular Genotoxic Stress, *Cancer Research*, 48(11), 3123–3129.
- Yamazaki, T., Sabit, H., Oya, T., Ishii, Y., Hamashima, T., Tokunaga, A., ... Sasahara, M. (2009). Activation of MAP kinases, Akt and PDGF receptors in injured peripheral nerves. *Journal of the Peripheral Nervous System*, 14(3), 165–176. <https://doi.org/10.1111/j.1529-8027.2009.00228.x>
- Yáñez-Muñoz, R. J., Balaggan, K. S., MacNeil, A., Howe, S. J., Schmidt, M., Smith, A. J., ... Thrasher, A. J. (2006). Effective gene therapy with nonintegrating lentiviral vectors. *Nature Medicine*, 12(3), 348–353. <https://doi.org/10.1038/nm1365>
- Yi, R., Qin, Y., Macara, I. G., & Cullen, B. R. (2003). Exportin-5 mediates the nuclear export of pre-microRNAs and short hairpin RNAs, *Genes and Development*, 17(24), 3011–3016. <https://doi.org/10.1101/gad.1158803>
- Yiu, E. M., Burns, J., Ryan, M. M., & Ouvrier, R. a. (2008). Neurophysiologic abnormalities in children with Charcot-Marie-Tooth disease type 1A. *Journal of the Peripheral Nervous System : JPNS*, 13(3), 236–41. <https://doi.org/10.1111/j.1529-8027.2008.00182.x>
- Ylä-Herttuala, S. (2012). Endgame: Glybera finally recommended for approval as the first gene

- therapy drug in the European union. *Molecular Therapy*, 20(10), 1831–1832. <https://doi.org/10.1038/mt.2012.194>
- Young, S. M., Carty, D. M. M. C., Degtyareva, N., Carolina, N., Hill, C., & Carolina, N. (2000). Roles of Adeno-Associated Virus Rep Protein and Human Chromosome 19 in Site-Specific Recombination, *Journal of Virology*, 74(9), 3953–3966.
- Zerah, M., Piguet, F., Colle, M.-A., Raoul, S., Deschamps, J.-Y., Deniaud, J., & Gautier, B. (2015). Intracerebral gene therapy using AAVrh.10-hARSA recombinant vector to treat patients with early-onset forms of metachromatic leukodystrophy: preclinical feasibility and safety assessments in non-human primates. *Human Gene Therapy Clinical Development*, 26(2). <https://doi.org/10.2134/agronj2016.02.0085>
- Zhang, S., Zhao, B., Jiang, H., Wang, B., & Ma, B. (2007). Cationic lipids and polymers mediated vectors for delivery of siRNA. *Journal of Controlled Release*, 123(1), 1–10. <https://doi.org/10.1016/j.jconrel.2007.07.016>
- Zhang, Y., Guo, Y., & Lee, W. N. (2018). Ultrafast Ultrasound Imaging with Cascaded Dual-Polarity Waves. *IEEE Transactions on Medical Imaging*, 37(4), 906–917. <https://doi.org/10.1109/TMI.2017.2781261>
- Zhao, H. T., Damle, S., Ikeda-lee, K., Kuntz, S., Li, J., Mohan, A., ... Kordasiewicz, H. B. (2017). PMP22 antisense oligonucleotides reverse Charcot- Marie-Tooth disease type 1A features in rodent models. *The Journal of Clinical Investigation*, 128(1), 1–10. <https://doi.org/10.1172/JCI96499>
- Zincarelli, C., Soltys, S., Rengo, G., & Rabinowitz, J. E. (2008). Analysis of AAV serotypes 1-9 mediated gene expression and tropism in mice after systemic injection. *Molecular Therapy*, 16(6), 1073–1080. <https://doi.org/10.1038/mt.2008.76>
- Zoidl, G., Blass-Kampmann, S., D’Urso, D., Schmalenbach, C., & Müller, H. W. (1995). Retroviral-mediated gene transfer of the peripheral myelin protein PMP22 in Schwann cells: modulation of cell growth. *The EMBO Journal*, 14(6), 1122–8.
- Zoidl, G., D’Urso, D., Blass-Kampmann, S., Schmalenbach, C., Kuhn, R., & Müller, H. W. (1997).

Influence of elevated expression of rat wild-type PMP22 and its mutant PMP22 Trembler on cell growth of NIH3T3 fibroblasts. *Cell and Tissue Research*, 287(3), 459–470. <https://doi.org/10.1007/s004410050770>

Zoidl¹, G., Blass-Kampmann², S., D'ursol¹, D., Schmalenbach, C., Muiller¹, H. W., & Betz, H. (1995). Retroviral-mediated gene transfer of the peripheral myelin protein PMP22 in Schwann cells: modulation of cell growth. *The EMBO Journal*, 14(6), 1122–1128.

Zu Hörste, G. M., & Nave, K. A. (2006). Animal models of inherited neuropathies. *Current Opinion in Neurology*, 19(5), 464–473. <https://doi.org/10.1097/01.wco.0000245369.44199.27>

Zu Horste, G. M., Prukop, T., Liebetanz, D., Mobius, W., Nave, K. A., & Sereida, M. W. (2007). Antiprogestosterone therapy uncouples axonal loss from demyelination in a transgenic rat model of CMT1A neuropathy. *Annals of Neurology*, 61(1), 61–72. <https://doi.org/10.1002/ana.21026>

Zufferey, R., Dull, T., Mandel, R. J., Bukovsky, A., Quiroz, D., Naldini, L., & Trono, D. (1998). Self-inactivating lentivirus vector for safe and efficient in vivo gene delivery. *Journal of Virology*, 72(12), 9873–80. <https://doi.org/99030895>

Clinical trials:

<https://clinicaltrials.gov/ct2/home>